(1)

# Final Technical Report

## Growth and Doping of $Al_xGa_{1-x}N$ Films by Electron Cyclotron Resonance Assisted Molecular Beam Epitaxy

ONR Grant No. N00014-92-J-1436

(May 1, 1992-April 30, 1994)



P.I. Theodore D. Moustakas

Department of Electrical, Computer and Systems Engineering
Boston University
Boston, MA 02215
617-353-5431



Approved for Public Release; Distribution Unlimited

August 31, 1994

# REPORT DOCUMENTATION PAGE

Form Approved
OMB No 0704-0188

| | | |
|---|---|---|
| 1. AGENCY USE ONLY (Leave blank) | 2. REPORT DATE<br>August 31, 1994 | 3. REPORT TYPE AND DATES COVERED<br>Final 1 May 1992 - 30April 1994 |

| | |
|---|---|
| 4. TITLE AND SUBTITLE<br>Growth and Doping of $Al_xGa_{1-x}N$ Films by Electron Cyclotron Resonance Assisted Molecular Beam | 5. FUNDING NUMBERS<br>R& T:4145329-01<br>S.O:1114SS<br>AGO:N66017<br>CAGE: 3A817 |
| 6. AUTHOR(S)<br>Moustakas, Theodore D. | |
| 7. PERFORMING ORGANIZATION NAME(S) AND ADDRESS(ES)<br>Boston University<br>College of Engineering<br>44 Cummington St<br>Boston, MA 02215 | 8. PERFORMING ORGANIZATION REPORT NUMBER |
| 9. SPONSORING MONITORING AGENCY NAME(S) AND ADDRESS(ES)<br>Department of the Navy<br>Office of the Chief of Naval Research<br>800 North Quincy St<br>Arlington, VA 22217-5000 | 10. SPONSORING/MONITORING AGENCY REPORT NUMBER |
| 11. SUPPLEMENTARY NOTES | |
| 12a. DISTRIBUTION AVAILABILITY STATEMENT<br>Approved for Public Release; Distribution but in unlimited | 12b. DISTRIBUTION CODE |

13. ABSTRACT (Maximum 200 words)

The work focused on the heteroepitaxial growth, doping and structural and optoelectronic characterization of GaN and AlN films by the method of ECR-assisted MBE. The effect of charged species in the ECR discharge in the growth and properties of the films was investigated. Conditions were identified to grow atomically smooth films (layer-by-layer growth) in semi-insulating form(p=10exp12 ohmsxcm). Such films were doped p- and n-type with Mg and Si respectively at the level of 10exp19 cmexp-3. Reactive ion etching and metallic contacts to GaN were developed. From these studies we concluded that surface states are not present in the gap of GaN and thus dislocation should not effect the device performance. The role of hydrogen in the doping of GaN was investigated and p-n junction LED's were fabricated and tested. The defects in these materials were investigated by transport, photoluminescence and optical studies.

| | |
|---|---|
| 14. SUBJECT TERMS Gallium Nitride, Aluminum Nitride, n-doping, p-doping, Molecular Beam Epitaxy, Electron Cyclotron Resonance source, Ohmic contacts, photoluminescence, conduction electron spin, p-n junction blue LED's | 15. NUMBER OF PAGES<br><br>16. PRICE CODE |

| 17. SECURITY CLASSIFICATION OF REPORT | 18. SECURITY CLASSIFICATION OF THIS PAGE | 19. SECURITY CLASSIFICATION OF ABSTRACT | 20. LIMITATION OF ABSTRACT |
|---|---|---|---|
| UNCLAS | UNCLAS | UNCLAS | |

NSN 7540-01-280-5500

Standard Form 298 (Rev. 2-89)
Prescribed by ANSI Std. Z39-18
298-102

# Table of Contents

# Appendices

# 1. Summary of results during the funding period

During the grant period the work was focused on the heteroepitaxial growth and doping of GaN films by the method of Electron Cyclotron Resonance microwave plasma assisted Molecular Beam Epitaxy. Work was also initiated in the growth of AlN.

## 1.1 Growth of GaN by ECR-assisted MBE

High-quality GaN films have been grown on a variety of substrates by electron cyclotron resonance microwave plasma-assisted molecular beam epitaxy (ECR-MBE). The films were grown in two steps. First, a GaN-buffer was grown at low temperature and then the rest of the films was grown at higher temperatures. We found that this method of growth leads to a relatively small two-dimensional nucleation rate (~ 20 nuclei/$\mu m^2 h$) and high lateral growth rate (100 times faster than the vertical growth rate). This type of quasi-layer-by-layer growth results in a smooth surface morphology to within 100 Å. Growth on Si(100) leads to single-crystalline GaN films having the zinc-blende structure. Growth on Si(111) leads to GaN films having the wurtzitic structure with a large concentration of stacking faults. The crystallographic orientation and the surface morphology of GaN films on sapphire depends on the orientation of sapphire. To this date, the best films were grown on the basal plane of sapphire. For more details see Appendix A.

## 1.2 Growth and doping of GaN films by ECR-assisted MBE

We report on growth, doping and characterization studies of GaN films produced by the Electron Cyclotron Resonance microwave plasma assisted Molecular Beam Epitaxy. The films were grown heteroepitaxially on sapphire (0001), whose surface was converted into atomically smooth AlN by plasma nitridation. The GaN films were grown in two temperature steps, a process found to promote the layer-by-layer growth mode. ECR plasma conditions to grow either n-type autodoped or semi-insulating GaN film were identified. The structure and microstructure as well as the electrical properties of these two classes of films are discussed. A systematic dependence between electron mobility and net carrier concentration was found, which predicts that the mobility of GaN with a net carrier concentration of $10^{14}$ $cm^{-3}$ is about $10^4 cm^2/V.sec$. The insulating films were intentionally doped either p-type or n-type by incorporation of Mg or Si during film growth. Hole or electron concentrations at 300K between $10^{18}$ - $10^{19}$ $cm^{-3}$ have been obtained without requiring any post-growth treatment. For more details see Appendix B.

## 1.3 High mobility GaN films produced by ECR-assisted MBE

High electron mobility autodoped GaN films were produced by the ECR assisted MBE method. The net electron concentration was varied systematically from $2 \times 10^{19}$ to $2 \times 10^{17} cm^{-3}$ by controlling the active nitrogen overpressure. Correspondingly, the electron mobility increased from 20 to 210 $cm^2/V.sec$. The line through the experimental data also predicts the electron mobilities of GaN films produced by the CVD methods. For more details see Appendix C.

## 1.4 Electron transport mechanism in gallium nitride

The electron transport mechanism in autodoped gallium nitride films grown by electron cyclotron resonance microwave plasma-assisted molecular beam epitaxy was investigated by studying the temperature dependence of the Hall coefficient and resistivity on samples with various concentrations of autodoping centers. The Hall coefficients go through a maximum as the temperature is lowered from 300 K and then saturate at lower temperatures. The resistivities in the same temperature range initially increase exponentially and then saturate at lower temperatures. These findings are accounted for if a significant fraction of electron transport, even at room temperature, takes place in the autodoping centers and that conduction through these centers becomes dominant at lower temperatures. The activation energy of these centers was found to be on the order of 20-30 meV. When the concentration of the autodoping centers becomes smaller than that of deep compensating defects, the material becomes semi-insulating and transport by hopping in the compensating defects becomes dominant. For more details see Appendix D.

## 1.5 Metal contacts to gallium nitride

We report measurements on the nature of aluminum and gold contacts to GaN. The GaN films were deposited onto the *R*-plane of sapphire substrates by molecular beam epitaxy and are autodoped n-type. Metal contacts were deposited by evaporation and were patterned photolithographically. Current-voltage characterization shows that the as-deposited aluminum contacts are ohmic while the as-deposited gold contacts are rectifying. The gold contacts become ohmic after annealing at 575 $^{o}$C, a result attributed to gold diffusion. The specific contact resistivity of the ohmic aluminum and gold contacts were found by transfer length measurements to be of device quality ($10^{-7}$ - $10^{-8}$ $\Omega m^2$). The results of these studies suggest a direct correlation between barrier height and work function of the metal, consistent with the strong ionic character of GaN. For more details see Appendix E.

## 1.6 Heteroepitaxy, polymorphism and faulting in GaN thin films on silicon and sapphire substrates

The structure of GaN films grown by electron-cyclotron-resonance-assisted MBE on Si(111), Si(001), basal-plane sapphire, a-plane sapphire and r-plane sapphire substrates was studied with four-circle x-ray diffractometry. Phase content, domain size, inhomogeneous strain and in-plane and out-of-plane domain misorientations were measured and compared for films grown on each type of substrate. Wurtzite and zincblende polymorphs were found to coexist in films grown on Si(111). The two structures grow in the (0002) and (111) orientations respectively so that they may transform into each other via stacking faults on close-packed planes. Smaller amounts of zincblende material were also found in predominantly (0002) wurtzitic films on a-plane sapphire and (1120) wurtzitic films on r-plane sapphire. For more details see Appendix F.

## 1.7 Conduction-electron spin resonance in zinc-blende GaN thin films

We report electron-spin-resonance measurements on zinc-blende GaN. The observed resonance has and isotropic *g* value of 1.9533 0.0008 independent of temperature, a Lorentzian line shape, and a linewidth (18 G at 10 K) which depends on temperature. The spin-lattice relaxation time at 10 K was estimated to be $T_{1e} = (6 \quad 2) \times 10^{-5}$ sec. Using a five-band model a *g* value consistent with the experimental results was obtained and a conduction-electron effective mass $m^*/m_0 = 0.15 \quad 0.014$ was calculated. The observed signal, together with conductivity data, was attributed to nonlocalized electrons in a band of autodoping centers and in the conduction band. For more details see Appendix G.

## 1.8 Intensity dependence of photoluminescence in GaN thin films

We report the intensity dependence of band-gap and midgap photoluminescence in GaN films grown by electron cyclotron resonance (ECR) microwave plasma-assisted molecular beam epitaxy. We find that the band-gap luminescence depends linearly while the midgap luminescence has a nonlinear dependence on the incident light intensity. These date were compared with a simple recombination model which assumes a density of recombination centers 2.2 eV below the conduction band edge. The concentration of these centers is higher in films grown at higher microwave power in the ECR plasma. For more details see Appendix H.

## 1.9 Microstructures of GaN Films Deposited on (001) and (111) Si Using ECR-MBE

The microstructures of GaN films, grown on (001) and (111) Si substrates, by a two-step method using ECR-MBE, were studied by electron microscopy techniques. Films grown on (001) Si had a predominantly zinc-blende structure. The GaN buffer layer, grown in the first deposition step accommodated the 17% lattice mismatch between the film and substrate by a combination of misoriented domains and misfit dislocations. Beyond the buffer layer, the film consisted of highly oriented domains separated by inversion domain boundaries, with a substantial decrease in the defect density away from the interface. The majority of defects in the film were stacking faults, microtwins and localized regions having the wurtzitic structure. The structure of the GaN films grown on (111) Si was found to be primarily wurtzitic, with a substantial fraction of twinned zinc-blende phase. Occasional wurtzitic grains, misoriented by a 30° twist along the [0001] axis were also observed. For more details see Appendix I.

## 1.10 Hydrogenation of Gallium Nitride

A comparative study of the effects of hydrogen in n-type (unintentionally and Si-doped) as well as p-type (Mg-doped) MBE-grown GaN is presented. Hydrogenation above 500 °C reduces the hole concentration at room temperature in the p-type material by one order of magnitude. Three different microscopic effects of hydrogen are suggested: Passivation of deep defects and of Mg-acceptors due to formation of hydrogen-related complexes and the introduction of a hydrogen-related donor state 100 meV below the conduction band edge. New local vibrational modes in Mg-doped GaN, which was grown in high concentration of hydrogen were discovered. Based on observed selection rules, one pair at frequencies at 2168 and 2219 $cm^{-1}$ was attributed to inequivalent Mg-H complexes in the c-plane and parallel to the c-axis. The origin of a second pair of modes at 2151 and 2185 $cm^{-1}$, which is IR inactive is speculated to be due to molecular $N_2$ or $H_2$. For more details see Appendix J,K,L.

## 1.11 Reactive Ion Etching of GaN Thin Films

Reactive ion etching of GaN grown by electron-cyclotron-resonance, microwave plasma-assisted molecular beam epitaxy on (0001) sapphire substrates was investigated. A variety of reactive and inert gases such as $CCl_2F_2$, $SF_6$, $CF_4$, $H_2/CH_4$ mixtures, $CF_3Br$, $CF_3Br/Ar$ mixtures and Ar were investigated. From these studies we conclude that of the halogen radicals investigated, Cl and Br etch GaN more effectively than F. The etching rate was found to increase with decreasing pressure at a constant cathode voltage, a result attributed to larger mean free path of the reactive species. For more details see Appendix M.

## 1.12 Blue-violet Light Emitting Gallium Nitride p-n Junctions

Blue-violet light emitting GaN p-n junctions were grown and characterized. The ECR-MBE growth method was modified to minimize plasma induced defects. Contrary to similar devices grown by Metallorganic Chemical Vapor Deposition, these devices do not require any post growth annealing to activate the Mg-acceptors in the p-layer. These devices turn-on at approximately 3 volts and have a spectral emission peaking at 430 nm. See Appendix N,O for more details.

## 1.13 Optical Properties of GaN

We performed optical-absorption studies of the energy gap in various GaN samples in the temperature range from 10 up to 600 K. We investigated both bulk single crystals of GaN and an epitaxial layer grown on a sapphire substrate. The observed positions of the absorption edge vary for different samples of GaN (from 3.45 to 3.6 eV at T=20 K). We attribute this effect to different free-electron concentrations (Burstein-Moss effect) characterizing the employed samples. For the sample for which the Burstein shift is zero (low free-electron concentration) we could deduce the value of the energy gap as equal to 3.427 eV at 20 K. Samples with a different free-electron concentration exhibit differences in the temperature dependence of the absorption edge. We explain the origin of these differences by the temperature dependence of the Burstein-Moss effect.

## 1.14 Heteroepitaxial growth of AlN

The growth of AlN has not yet been optimized. In the initial studies we attempted to grow AlN on (0001) sapphire at relatively low temperatures (800 oC) so that the growth of AlN would be comparable with that of GaN. The RHEED pattern, surface morphology, and XRD of such a film are shown in figures 1,2 and 3 respectively. These data indicate that the AlN grown so far is inferior to our GaN films.

## 2. Publication List


1. "Growth of GaN by ECR-Assisted MBE" T.D. Moustakas, T. Lei and R.J. Molnar, Physica B, 185, 36 (1993)
2. "Growth and Doping of GaN Films by ECR-Assisted MBE" T.D. Moustakas and R.J. Molnar,Mat. Res. Soc. Proc., vol. 281 (1993)
3. "High Mobility GaN Films Produced by ECR-Assisted MBE" R.J. Molnar, T. Lei and T.D. Moustakas, Mat. Res. Soc. Proc., vol. 281
4. "Electron Transport Mechanism in Gallium Nitride" R.J. Molnar, T. Lei and T.D. Moustakas, Appl. Phys. Lett., 62, 72 (1993)
5. "Metal Contacts to Gallium Nitride" J.S. Foresi and T.D. Moustakas, Appl. Phys. Lett., 62, 2859 (1993)
6. "Heteroepitaxy, Polymorphism, and Faulting in GaN Thin Films on Silicon and Sapphire Substrates" T. Lei, K.F. Ludwig and T.D. Moustakas, J. Appl. Phys., 74, 4430 (1993)
7. "Conduction Electron Spin Resonance in Zinc-blende GaN Thin Films" M. Fanciulli, T. Lei and T.D. Moustakas,Phys. Rev. B, 48, 15144 (1993)
8. "Intensity Dependence of Photoluminescence in Gallium Nitride Thin Films" R. Singh, R.J. Molnar, M.S. Ünlü and T.D. Moustakas, Appl. Phys. Lett., 64, 336 (1994)
9. "Microstructures of GaN Films Deposited on (001) and (111) Si Using ECR-MBE" S.N. Basu, T. Lei and T.D. Moustakas, J. Mater. Res. 9, 2370 (1994)
10. "Hydrogenation of Gallium Nitride" M.S. Brandt, N.M. Johnson, R. Molnar, R. Singh and T.D. Moustakas, Mat. Res. Soc. Symp. Proc., accepted (1994)
11. "Hydrogenation of Gallium Nitride" M.S. Brandt, N.M. Johnson, R.J. Molnar, R. Singh and T.D. Moustakas, Appl. Phys. Lett. 64, 2264 (1994)
12. "Local Vibrational Modes in Mg-doped Gallium Nitride" M.S. Brandt, J.W. Ager III, W. Gotz, N.M. Johnson, J.S. Harris, R.J. Molnar and T.D. Moustakas, Mat. Res. Soc. Symp. Proc.
13. "Reactive Ion Etching of GaN Thin Films" M.J. Manfra, S.J. Berkowitz, R.J. Molnar, A.M. Clark, T.D. Moustakas and W.J. Skocpol, Mat. Res. Soc. Symp. Proc., 324, 477 (1994)
14. "The Growth of Gallium Nitride by ECR Plasma Assisted MBE; The role of Charged Species" R.J. Molnar and T.D. Moustakas, J. Appl. Phys. 76 (15 Oct. 1994)

15. "Blue-violet Light Emitting GaN p-n Junctions grown by Electron Cyclotron Resonance-assisted Molecular Beam Epitaxy" R.J. Molnar, R. Singh and T.D. Moustakas, Appl. Phys. Lett. (submitted)

16. "Temperature dependence of the energy gap in GaN bulk single crystals and epitaxial layer" H. Teisseyre, P. Perlin, T. Suski, I. Grzegory, S. Porowski, J. Jun, A. Pietraszko and T.D. Moustakas, J. Appl. Phys. 76, 2429 (1994)

# RHEED During Growth of AlN

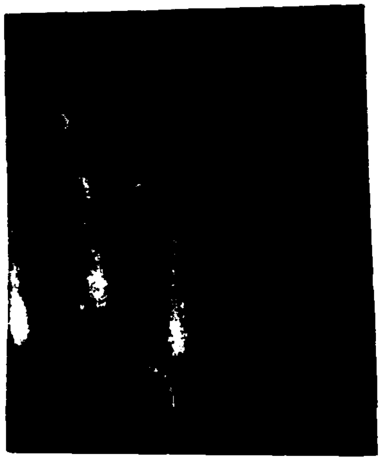

Substrate after Plasma Nitridation

5 min

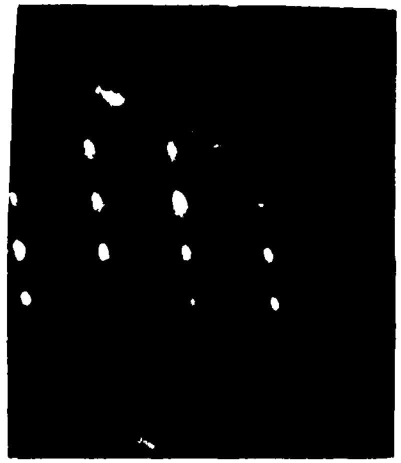

35 min

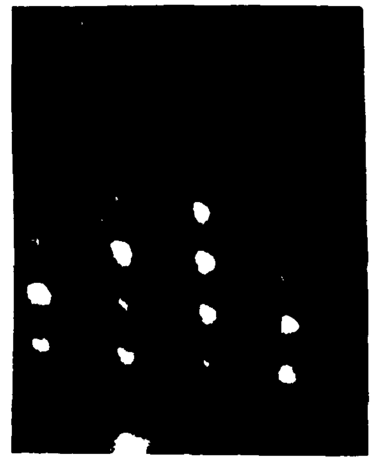

8 hr

# Surface Morphology of AlN

# $\theta/2\theta$ XRD and $\theta$-Rocking Curve for an AlN Film

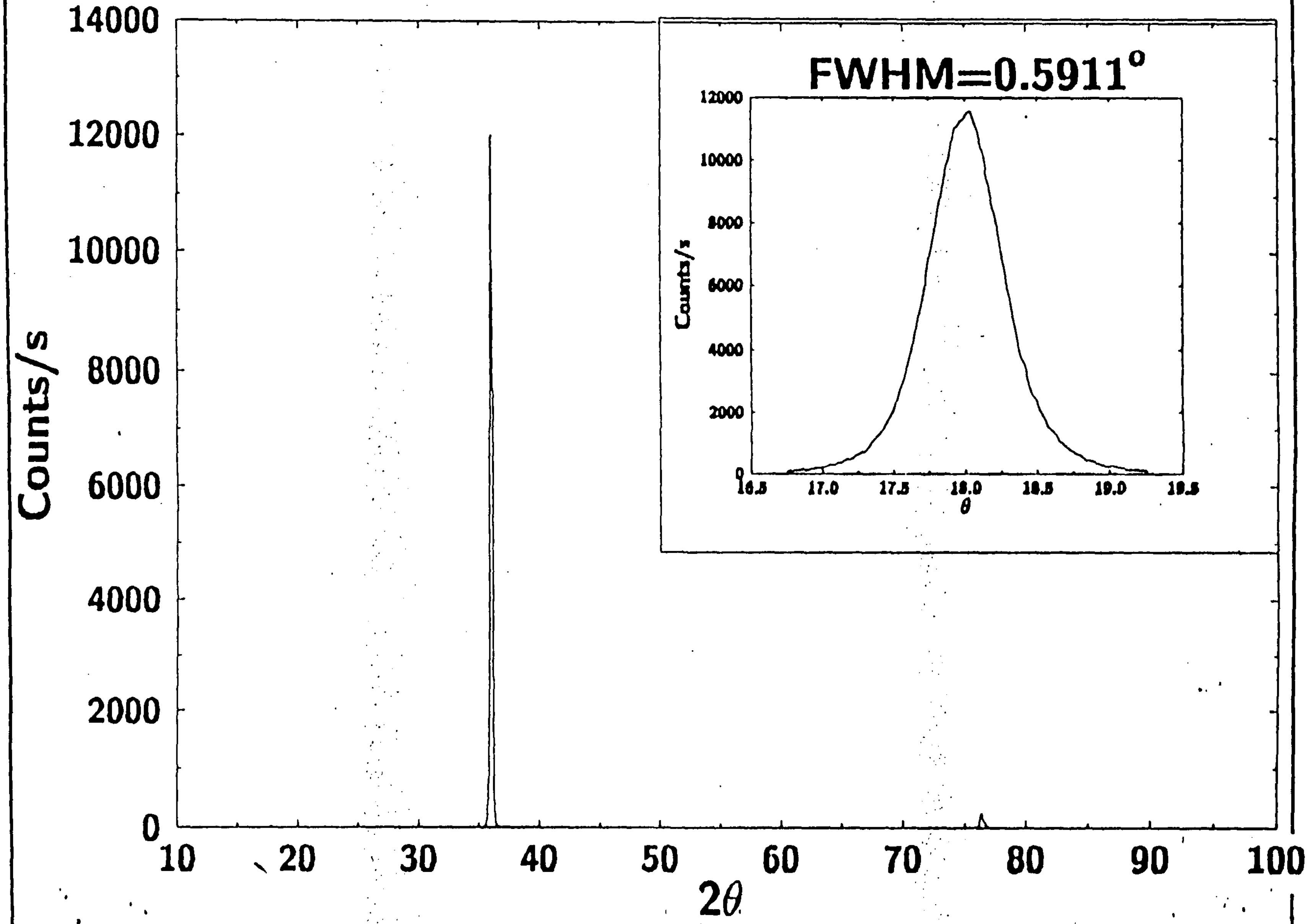

# Appendix A : "Growth of GaN by ECR-assisted MBE"

Physica B 185 (1993) 36–49
North-Holland

PHYSICA

# Growth of GaN by ECR-assisted MBE

T.D. Moustakas, T. Lei and R.J. Molnar

*Molecular Beam Epitaxy Laboratory, Department of Electrical, Computer and Systems Engineering, Boston University, MA, USA*

High-quality GaN films have been grown on a variety of substrates by electron cyclotron resonance microwave plasma-assisted molecular beam epitaxy (ECR-MBE). The films were grown in two steps. First, a GaN-buffer was grown at low temperature and then the rest of the film was grown at higher temperatures. We found that this method of growth leads to a relatively small two-dimensional nucleation rate (~20 nuclei/μm$^2$ h) and high lateral growth rate (100 times faster than the vertical growth rate). This type of quasi-layer-by-layer growth results in a smooth surface morphology to within 100 Å. Growth on Si(1 0 0) leads to single-crystalline GaN films having the zinc-blende structure. Growth on Si(1 1 1) leads to GaN films having the wurtzitic structure with a large concentration of stacking faults. The crystallographic orientation and the surface morphology of GaN films on sapphire depends on the orientation of sapphire. To this date, the best films were grown on the basal plane of sapphire.

## 1. Introduction

The family of refractory nitrides (InN, GaN and AlN), their solid solutions and heterojunctions are one of the most promising families of electronic materials. All three are direct bandgap semiconductors with their energy gaps covering the region from 1.95 eV (InN) and 3.5 eV (GaN) to 6.28 eV (AlN). Thus, the growth of high-quality crystals and successful doping of these materials should lead to applications in optoelectronic devices from the visible to the ultraviolet part of the electromagnetic spectrum, as well as in devices for high-power and high-temperature electronics [1–2]. GaN, in particular, is predicted to have a high electron drift velocity, so it should also be suitable for high-frequency and microwave devices [3].

GaN films have been grown by many growth techniques, including chemical vapor deposition [4–7], metal–organic chemical vapor deposition [8–15], molecular beam epitaxy [16–25] and a number of plasma-assisted processes [26–30]. A variety of substrates such as silicon, spinel, silicon carbide and various crystallographic orientations of sapphire have been used in these studies. Most of the films grown are wurtzitic (α-GaN) and have n-type conductivity with high carrier concentration [31], which is believed to result from nitrogen vacancies [31–32] or oxygen impurity incorporation [33]. P-type conductivity has been reported recently on Mg-doped GaN films [34–35].

Zincblende GaN (β-GaN), which is the thermodynamically metastable phase of GaN, is hoped to be more amenable to doping than the wurtzitic GaN, since all of the III–V compounds that can be efficiently doped n-type or p-type are cubic [2]. β-GaN has been epitaxially stabilized on a β-SiC and MgO(1 0 0) substrate [18–19], which are closely lattice-matched to β-GaN and on a GaAs [36–37] and Si substrate [21–25] which have significant mismatch to β-GaN.

In this paper, we review the growth of GaN films by the electron cyclotron resonance microwave plasma-assisted molecular beam epitaxy. Particular emphasis is placed on the growth of this material in two temperature steps, a method developed recently in our laboratory for the growth of GaN. [21–25,38]. Films have been

*Correspondence to:* T.D. Moustakas, Molecular Beam Epitaxy Laboratory, Department of Electrical, Computer and Systems Engineering, Boston University, Boston, MA 02215, USA.

grown on Si(1 0 0), Si(1 1 1) and various faces of sapphire.

## 2. Experimental methods

The deposition system used in this study is schematically illustrated in fig. 1. Two ECR sources were used. The first (Astex 8" model 1000) was used for the growth of GaN on Si(1 0 0) and Si(1 1 1). The second (Astex compact model) was used for the growth of GaN on sapphire. The base pressure in the overall system was $10^{-11}$ Torr. A reflection high-energy electron diffraction (RHEED) setup is an integral part of the apparatus. A conventional Knudsen effusion cell was used to evaporate gallium. Atomic and ionic nitrogen were produced by passing molecular nitrogen through the ECR source. Part of the molecular nitrogen was also introduced downstream the ECR source. Typically, 10% of the molecular nitrogen gas is converted into atomic nitrogen. Due to this high decomposition rate, a source pressure of about $10^{-4}$ Torr is sufficient for the growth of stoichiometric films. The magnetic field configuration for the 8" source under optimized conditions for the growth of GaN films is illustrated in fig. 2. The on-axis ECR condition ($H = 875$ G) is about 40 cm above the substrate. The compact ECR source fits inside an effusion cell and thus the distance from the front of the source to the substrate is only 12 cm.

The structure and microstructure of the films were studied by reflection high-energy electron diffraction (RHEED), X-ray diffraction and scanning electron microscopy (SEM). X-ray diffraction studies were performed using a diffrac-

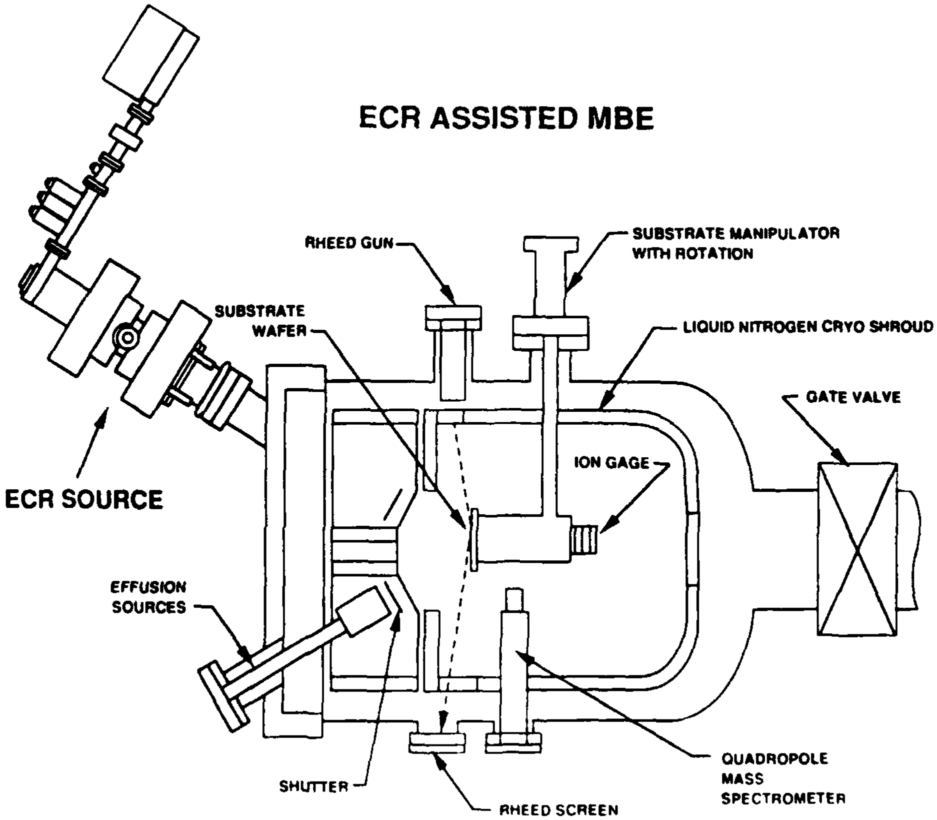


Fig. 1. Schematic of the deposition system.

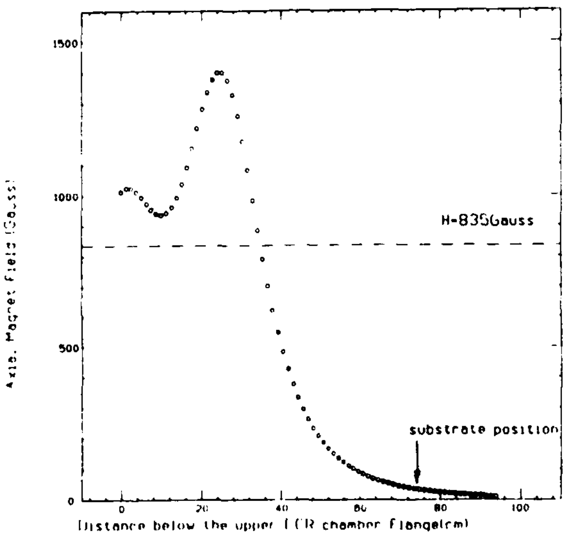


Fig. 2. Magnetic field configuration under optimized growth conditions.

tometer with four-circle geometry. This allows us to perform $\phi$-scans at a reflection peak $(h\,k\,l)$, corresponding to planes not parallel to the substrate to probe in-plane ordering. Additionally, standard $\theta$–$2\theta$ scans were performed to probe the ordering normal to the substrate.

Si(0 0 1) and Si(1 1 1) substrates (n-type, p-type or undoped) were used in these studies. They were ultrasonically degreased in solvents and etched in buffered HF to remove the oxides, prior to their introduction into the MBE unit. In the preparation chamber, the substrates were outgassed for 15 minutes at 850°C.

The sapphire substrates were subjected to the following cleaning steps prior to the growth of the GaN films. They were sequentially cleaned in ultrasonic baths of trichloroethylene, acetone and isopropanol for removal of hydrocarbon residues from the surface, etched in $H_3PO_4:H_2SO_4$ (1:3) for the removal of surface contaminants and mechanical damage due to polishing and finally rinsed in de-ionized water. After these steps, the substrates were blown dry with nitrogen, mounted on a molybdenum block and transferred to the introduction chamber of the MBE system. In the preparation chamber, the substrates were heated to 850°C for approximately half an hour and then transferred to the growth chamber where they were subjected to bombardment by nitrogen plasma for approximately half an hour at 700°C.

## 3. Experimental results

### 3.1. Growth on Si(1 0 0)

Following cleaning, the Si substrate was examined by studying its RHEED pattern in the growth chamber at 400°C. Figure 3 shows typical

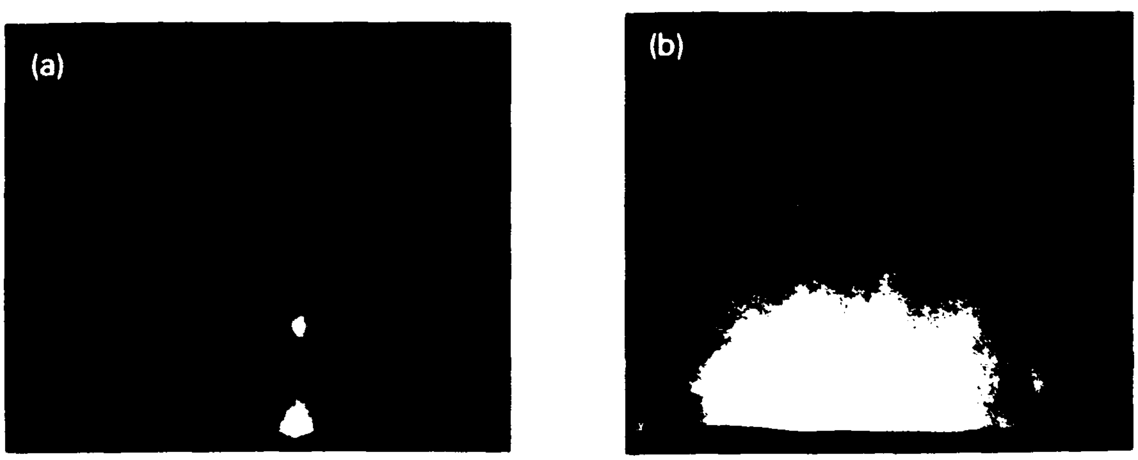


Fig. 3. RHEED patterns of Si(0 0 1) substrates after the routine preparation; (a) for [1 0 0] azimuthal incidence of the electron beam; (b) for [1 1 0] azimuthal incidence of the electron beam.

RHEED patterns of the Si substrate with the electron beam incident along the [1 0 0] and [1 1 0] directions. These results clearly indicate that the Si(0 0 1) surface is unreconstructed (i.e. 1 × 1). We find that such an unreconstructed Si(0 0 1) surface is required to epitaxially grow a single crystalline GaN-buffer. Outgassing of the Si substrate at lower temperatures, for example 600°C, leads to an irregular pattern with few diffraction spots, which we were unable to index with any reconstruction pattern. A GaN-buffer grown on such a surface would generally be polycrystalline with the wurtzitic structure. It is conceivable that epitaxy of GaN should take place on a well-ordered unreconstructed surface, but not on an irregular disordered surface.

After the substrate preparation and characterization, a GaN-buffer layer of about 300 Å to 900 Å thick was deposited at a temperature of 400°C for 10 to 30 minutes. Figure 4 shows the RHEED patterns at two azimuthal incidence angles of the electron beam for the GaN buffer layer. The diffraction spots were relatively broad, signifying that the thin buffer layer is very defective. This is expected due to the large lattice mismatch between the film and the substrate. However, the symmetry of the patterns indicates that the buffer layer has the zincblende structure with the [0 0 1] direction perpendicular to the substrate.

Following the deposition and characterization of the GaN-buffer the substrate was heated to a higher temperature, typically 600°C, and a GaN film of about 1 μm thick was grown at a growth rate about 2000 Å/h. Shown in fig. 5(a) and (b) are typical RHEED patterns of a GaN film about 1 μm thick grown on a p-type substrate for [1 0 0] and [1 1 0] azimuthal incidence of the electron beam. The results are similar when the growth takes place on undoped substrates. These results clearly indicate that the GaN film has the zincblende structure, with its (0 0 1) crystallographic planes parallel to the substate surface. The diffraction spots of this pattern are significantly sharper and elongated, which suggests that the final GaN film has a better crystalline quality and a smoother surface morphology than the GaN-buffer.

The RHEED pattern of a GaN film grown on a p-type substrate under slightly lower nitrogen pressure is shown in fig. 6. The streak-like pattern is characteristic of two-dimensional scattering, indicating that the GaN film is close to atomically smooth. Such elongated RHEED patterns were frequently observed when the growth took place on n-type substrates. This may sug-

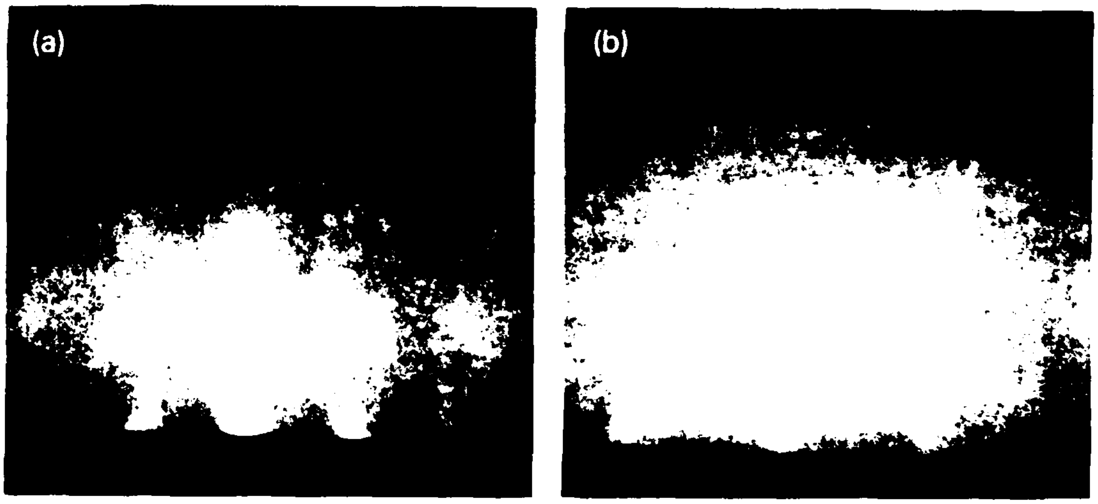


Fig. 4. RHEED patterns of GaN buffer grown at 400°C for 10 minutes; (a) for [1 0 0] azimuthal incidence of the electron beam; (b) for [1 1 0] azimuthal incidence of the electron beam.

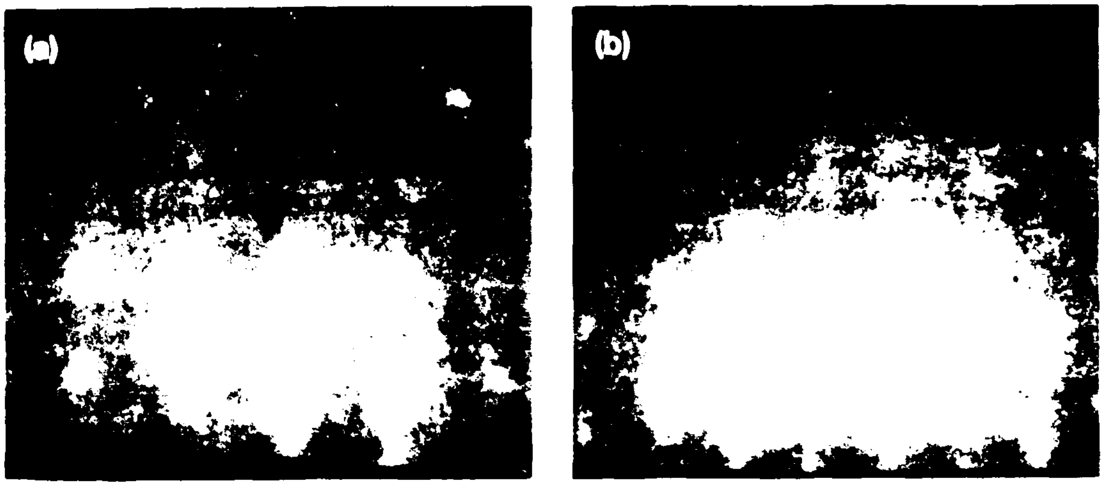


Fig. 5. Typical RHEED patterns of a GaN films on p-type or undoped substrate: (a) for [1 0 0] azimuthal incidence of the electron beam, (b) for [1 1 0] azimuthal incidence of the electron beam.

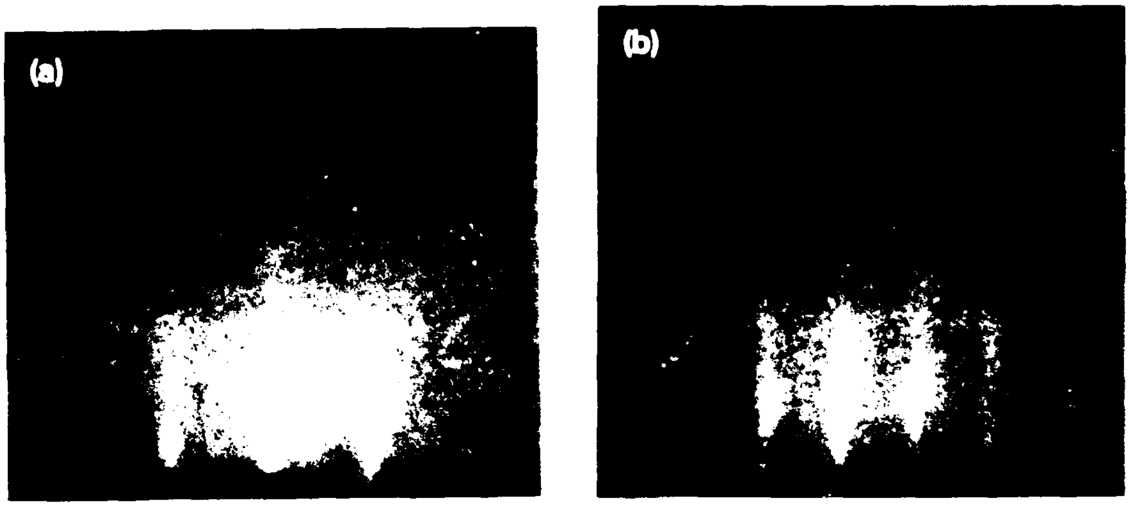


Fig. 6. The RHEED patterns of a GaN film with smooth-surface morphology, (a) for [1 0 0] azimuthal incidence of the electron beam, (b) for [1 1 0] azimuthal incidence of the electron beam.

gest that GaN wets to the n-type substrate better than the p-type substrate. Morimoto and coworkers reported that in vapor phase growth, GaN adhered to n-type silicon, but not to p-type silicon substrates.

In a few cases, the Si substrate was first bombarded with nitrogen plasma prior to the formation of the GaN buffer. The lack of a RHEED pattern indicates that either an amorphous SiN film was formed on the substrate or that the surface was disordered. The GaN buffer grown on nitrogen-plasma bombarded substrates were found to be polycrystalline having the wurtzitic structure with the (0 0 0 2) preferred orientation.

Shown in fig. 7 are the surface morphology and the cross-sectional view of a β-GaN film on a p-type silicon substrate studied by SEM. It can be seen that the film has a relatively flat surface, roughened with many well-oriented rectangular shaped "tiles", which reflect the symmetry of the β-GaN(0 0 1) surface. The cross-sectional view shows no evidence of columnar morphology, which is another indication that the film is single crystalline.

Detailed electron microscopy studies [23] have shown that the tiles in fig. 7 are oriented along the [1 1 0] and $[1\,\bar{1}\,0]$ directions. This presumably arises because the GaN surfaces corresponding to those directions are more closely packed than the [1 0 0] and [0 1 0] surfaces and therefore have lower surface energy.

Shown in fig. 8(a) is the morphology of the GaN film, whose RHEED pattern was discussed in fig. 6. The surface morphology of a film on an n-type substrate is shown in fig. 8(b). Both of these surfaces are smooth with steps approximately 100 A thick, which resulted from a layer-by-layer growth [23]. These results suggest that additional optimization of the growth process could lead to atomically smooth surfaces.

From the data of fig. 8, we can calculate the two-dimensional nucleation rate and the lateral growth rate. Let $J$ be the nucleation rate, $s$ be the average area of the plateau, $h$ the height of

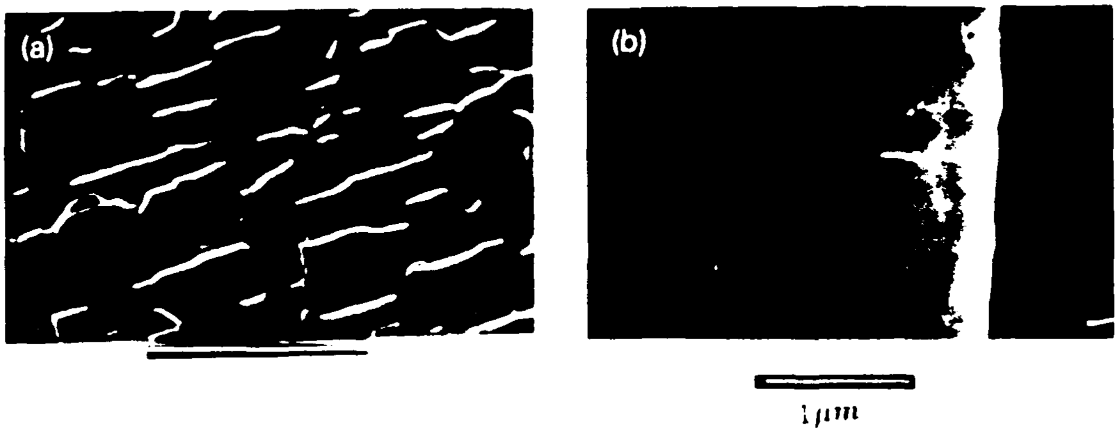


Fig. 7. Surface morphology of a GaN thin film on p-type Si substrate; (a) front view; (b) cross-sectional view.

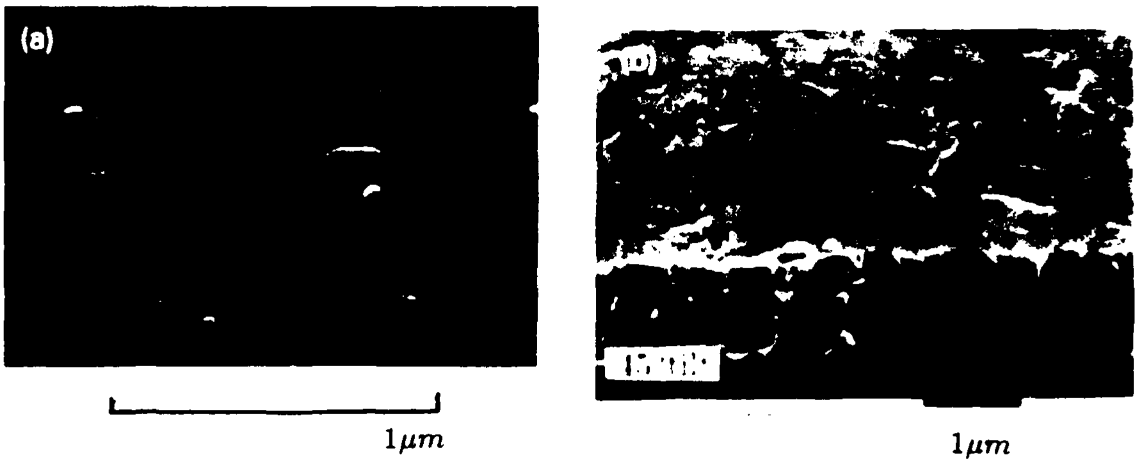


Fig. 8. SEM surface morphology of a smooth GaN thin film; (a) on a p-type substrate; (b) on an n-type substrate

the plateau, and $t$ the time for the plateau to grow, which is limited by nucleation. Then, we have

$$\sqrt{s} \simeq v_l t = \frac{v_l}{(Js)}, \quad (1)$$

$$h \simeq v_n t = \frac{v_n}{(Js)}, \quad (2)$$

where $v_l$ and $v_n$ are the lateral and vertical growth rates respectively. From the data of fig. 8, we have $\sqrt{s} = 1$ μm and $h = 100$ Å. If we use the known vertical growth rate $v_n = 2000$ Å/h, then from eqs. (1) and (2) we obtain $v_l \simeq 100V_n$ and $J \simeq 20$ nuclei/(μm$^2$ h).

These data indicate that this two-step method of film growth leads to quasi-layer-by-layer growth with a very small two-dimensional nucleation rate and high lateral growth rate.

The structure of the films was confirmed by convergent beam electron diffraction (CBED) and selected area diffraction (SAD). These studies were published elsewhere [23]. In this paper, we focus on the X-ray diffraction studies of the films.

The X-ray diffraction in fig. 9 shows a strong peak at $2\theta = 40.1$ degrees, whose $d$-spacing is 2.25 Å, which is due to the (0 0 2) reflection from β-GaN. Hence, the lattice constant to β-GaN

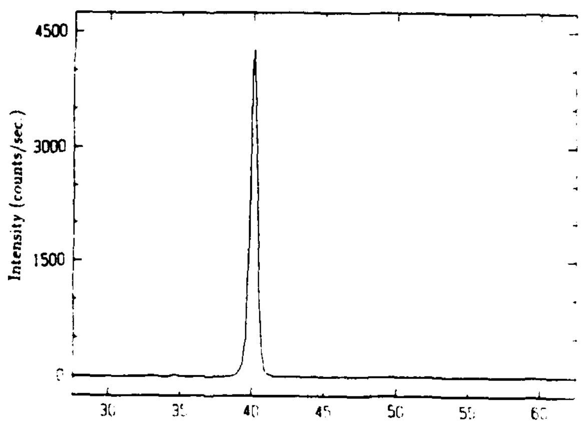


Fig. 9. X-ray diffraction using Cu-$K_\alpha$ radiation of a β-GaN film

was found to be 4.50 Å, in good agreement with the electron diffraction data [23]. A small peak was also observed at $2\theta = 34.6°$, which is due to the $d$-spacing of (1 1 1) β-GaN or (0 0 0 2) α-GaN. This suggests that the GaN film has some misoriented domains. These domains may have developed in the early stages of the buffer layer deposition as revealed by TEM imaging [39]. Similar structural faults have also been observed in the interface between GaN epitaxy on GaAs(1 0 0) [37]. We have also observed these misoriented domains in almost all of our samples. The consistent appearance of the misoriented domains in GaN–Si and GaN–GaAs heteroepitaxy is very likely to be related to the large lattice mismatch between the GaN and the substrate. Because of the large lattice mismatch, the interface of GaN and the substrate is under significant strain; therefore, it might be favorable for the system to introduce dislocations or misorientations of GaN to reduce the interfacial energies. In zincblende or wurtzitic structures, the [1 1 1] or [0 0 0 2] planes are the most closely packed, and hence have the lowest surface energies. Therefore, the introduction of [1 1 1] or [0 0 0 2] oriented GaN would lower the surface energy at the GaN–vapor interface, and would not necessarily increase the energy for the GaN–substrate interface, since it was strained significantly. However, the [1 1 1] or [0 0 0 2] oriented GaN domains would grow slower than the [0 0 1] oriented GaN grains stabilized by introduction of dislocations. As a result, they were buried in the interface region as the film grew.

The X-ray rocking curve of the [0 0 2] peak of a GaN film 4 μm thick was found to have a full width at half maximum (FWHM) of approximately 60 minutes, which measures the orientation spread perpendicular to the substrate. This is significantly narrower than that of GaN on GaAs [37], but much broader than that of β-GaN on MgO substrates [19] and α-GaN on [0 0 0 1] sapphire substrates as discussed later.

The $\phi$-scan for the zincblende GaN was performed at the [$\bar{1}$ 1 1] reflection, and is shown in fig. 10. The data clearly show that the peak repeats itself every 90 degrees, consistent with the cubic symmetry of this material. The FWHM

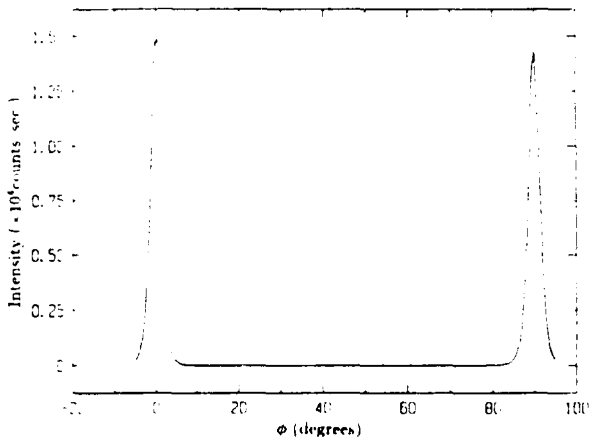


Fig. 10. $\phi$-scan at (1 1 1) for a zincblende GaN film.

of these peaks, which measures the in-plane orientation spread, was found to be 2.5 degrees.

## 3.2. Growth on Si(1 1 1)

Growth on Si(1 1 1) followed the same steps as described previously in the growth on Si(0 0 1). Figure 11 shows the RHEED pattern for a GaN film on Si(1 1 1). The data indicate that the film has the wurtzitic structure with the [0 0 0 1] planes parallel to the substrate. The sharpness of

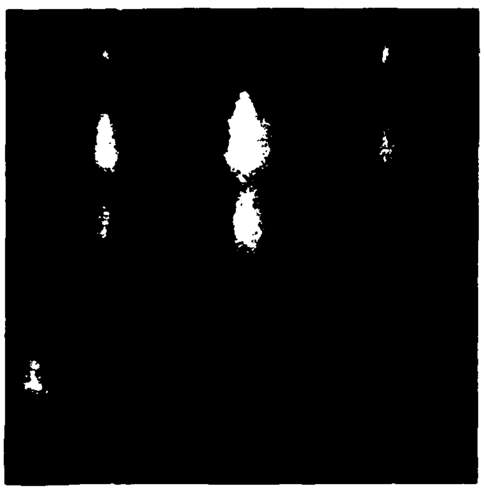

Fig. 11 RHEED patterns for a GaN film on Si(1 1 1) with [1 1 2 0] electron azimuthal incidence.

the diffraction spots indicate good crystalline quality of the film.

Figure 12 shows a $\theta-2\theta$ scan for a GaN film on Si(1 1 1). The single peak at 34.6 degrees corresponds to [0 0 0 2] reflection of the wurtzitic GaN; thus, the lattice constant in the $c$-direction is 5.18 Å.

The $\phi$-scan for the wurtzitic GaN shown in fig. 13 was performed at the [1 $\bar{1}$ 0 2] reflection. Clearly, this peak repeats every 60 degrees, consistent with the 3 mm symmetry of the rotation axis. The FWHM is found to be 1.9 degrees,

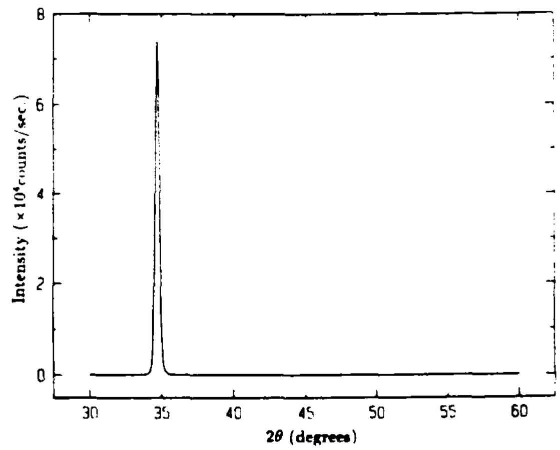


Fig. 12. $\theta-2\theta$ scans for a wurtzitic GaN film on Si(1 1 1).

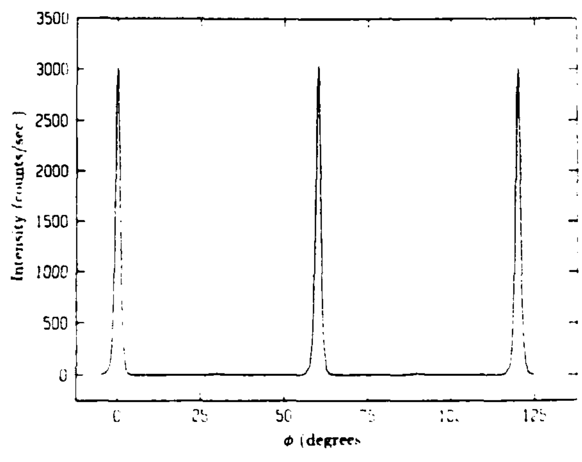


Fig. 13. $\phi$-scan for a wurtzite GaN film on Si(1 1 1)

while the FWHM of the $\theta-2\theta$ rocking curve at the [0 0 0 2] peak is found to be 0.9 degrees.

The XRD data of fig. 12 and fig. 13 appear to indicate that the α-GaN film on Si(1 1 1) is a single crystal. However, any stacking faults along the growth direction of the GaN film on Si(1 1 1) cannot be easily detected in the normal $\theta-2\theta$ scans [40]. Such stacking faults are very common defects in materials with the FCC or HCP structures growing along the [1 1 1] and [0 0 0 2] directions [40]. Such stacking faults, if they exist in the wurtzitic GaN films on Si(1 1 1), should give rise to a certain amount of cubic GaN component with the [1 1 1] planes parallel to the substrate. To explore this possibility, we rotated the sample in such a way that the X-ray diffraction corresponds to the [0 0 2] reflection of the zincblende structure, and indeed a peak was detected at $2\theta = 40$ degrees. This is shown in a $\theta-2\theta$ scan around this peak (see fig. 14).

To obtain a stronger reflection, $\phi$-scans on these cubic domains were performed at the [$\bar{1}$ 1 1] peak, which is shown in fig. 15. These data reveal a repetition every 60 degrees. Since the [1 1 1] axis in the zincblende structure is only a 3-fold rotational axis, the $\phi$-scan should show a repetition every 120 degrees instead of every 60 degrees. This can be accounted for if there are two kinds of stacking sequences, namely the ABC··· and CBA··· sequence. The fact that the peak at $\phi = 60$ degrees is of comparable intensity to the other two peaks suggests that the two types of stacking sequences occur with an equal probability, as is expected.

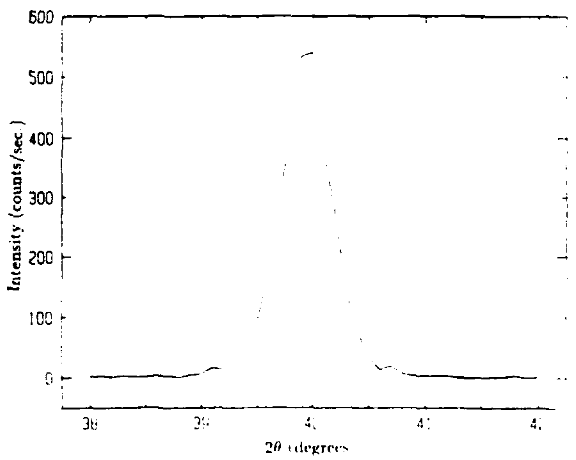


Fig. 14. $\theta-2\theta$ scan at the (0 0 2) reflection of cubic GaN grains in GaN on Si(1 1 1).

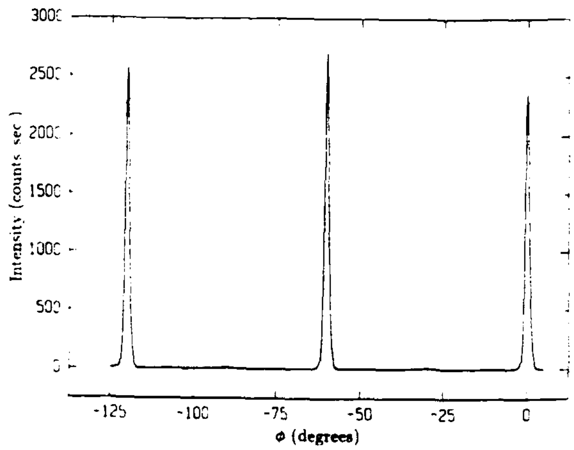


Fig. 15. $\phi$-scan at the ($\bar{1}$ 1 1) peak of cubic GaN components.

The existence of the cubic GaN domains in the wurtzite structures implies the existence of a high concentration of stacking faults. This could be due to the fact that the cohesive energies of wurtzite and zincblende GaN are comparable, so that the formation energy of a stacking fault is negligible. If this is true, then all of the [0 0 0 2] oriented GaN films have a considerable amount of stacking faults. This is currently being investigated by XRD studies of GaN on [1 1 $\bar{2}$ 0] and [0 0 0 1] sapphire substrates. However, one should not rule out that the high concentration of stacking faults in GaN on Si(1 1 1) is related to strain resulting from the large lattice mismatch between GaN and Si, which could lead to a reduction of the formation energy of stacking faults due to structural deformation.

### 3.3. *Growth on a sapphire substrate*

GaN films were also grown on the *c*-plane [0 0 0 1], *a*-plane [1 1 $\bar{2}$ 0] and *r*-plane [1 $\bar{1}$ 0 2] of sapphire. Figure 16 shows RHEED patterns of

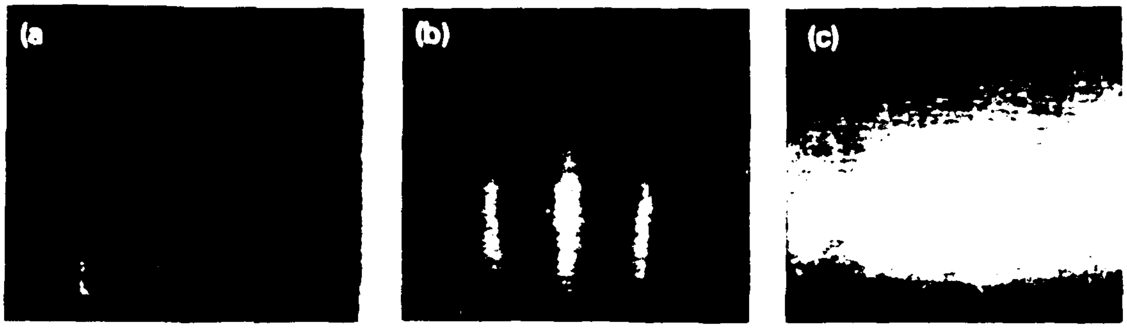


Fig. 16. RHEED patterns of the sapphire substrates after exposure to the nitrogen plasma: (a) $c$-plane, (b) $a$-plane, (c) $r$-plane.

the three types of substrates after exposure to the nitrogen plasma. The data indicate that the surface of the substrates were nitrided and from the diffraction patterns, the lattice constant of the AlN was estimated to be $a = 3.1$ Å. Furthermore, the streakiness of the diffraction patterns, in particular those of the $c$-plane and $a$-plane sapphire substrates, suggests that the AlN layers are atomically smooth.

Figure 17 shows RHEED patterns of the GaN-buffer on the three types of substrates. The data indicate that the GaN-buffer is single crystalline on all three types of substrates. The GaN films grown on the $c$-plane and $a$-plane sapphire substrates have their $c$-plane [0 0 0 1] parallel to the substrates, while the GaN films grown on the $r$-plane of sapphire have their $a$-plane $[1\,1\,\bar{2}\,0]$ parallel to the substrate. The streakiness of the diffraction patterns of the GaN-buffers on the $c$-plane and $a$-plane sapphire substrates suggests that the GaN-buffer on these substrates are atomically smooth.

Figure 18 shows RHEED patterns of the GaN films at the end of each run. These reveal the same epitaxial relationship between GaN films and the substrates as the corresponding GaN-buffers discussed in fig. 17. Also, the films on the $c$-plane and $a$-plane sapphire substrates are atomically smooth.

Figure 19 shows the surface morphology of GaN films grown on the three types of substrates. The films on the $a$-plane have the smoothest surface morphology. The surface morphology of GaN films on the $c$-plane consists of interconnected tiles several thousand angstroms in size. The GaN films grown on the $r$-plane sapphire were found to have the roughest surface morphology. The pyramidal surface morphology


Fig. 17. RHEED patterns of the GaN buffer on the various sapphire substrates: (a) $c$-plane, (b) $a$-plane, (c) $r$-plane.

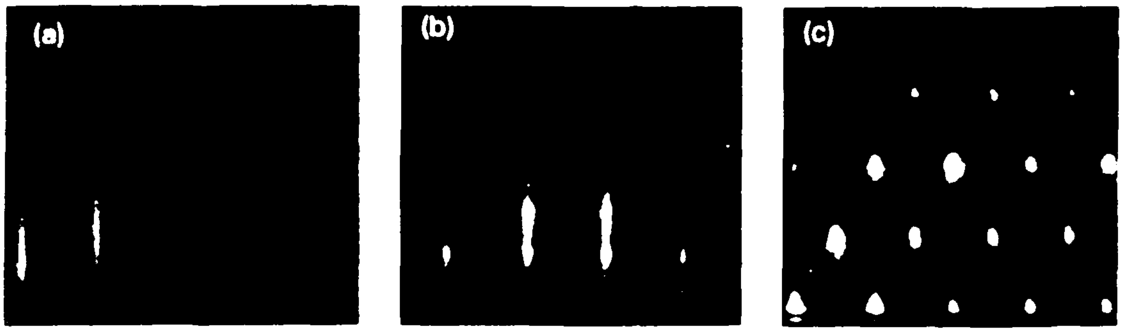


Fig. 18. RHEED patterns of the GaN films after growth on the various sapphire substrates: (a) c-plane, (b) a-plane, (c) r-plane.

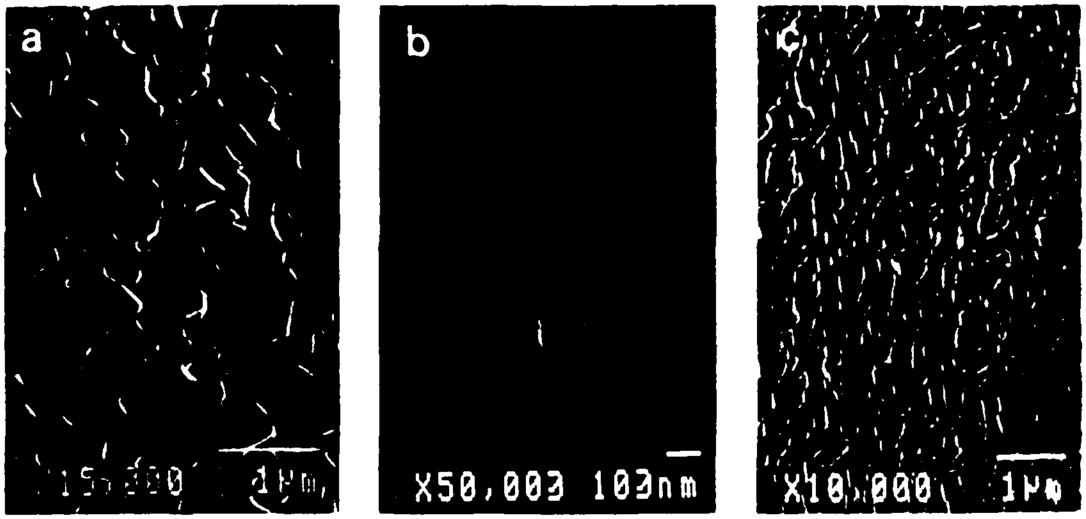


Fig. 19. SEM surface morphology of GaN films grown on various sapphire substrates: (a) c-plane, (b) a-plane, (c) r-plane.

is likely to be related to the fact that the $a$-plane of GaN is bounded by two prism planes under equilibrium growth conditions.

Figure 20 shows the $\theta$–$2\theta$ XRD and the $\theta$ rocking curve at the main reflection peak of the GaN films grown on the three types of substrates. The main reflection peak for the GaN films grown on the $c$-plane and $a$-plane sapphire occurs at $2\theta = 34.6$ degrees, corresponding to the (0002) reflection. This confirms that films were grown with their $c$-planes parallel to the substrate. The main diffraction peak of the GaN film on the $r$-plane of sapphire occurs at $2\theta = 57.8$ degrees corresponding to the GaN (11$\bar{2}$0) reflection. This confirms the RHEED study that the $a$-plane of the GaN film is parallel to the substrate. The rocking curve of the GaN film on the $c$-plane of sapphire has the smallest width (FWHM = 10 min), indicating the crystalline quality of these films to be the best. Such films were also found to have the highest electron mobility ($\mu = 200$ cm$^2$/V s) among films grown by MBE processes.

The epitaxial relationship of the GaN films to the $c$-plane of sapphire is to be expected. However, the epitaxial relationship of the GaN films

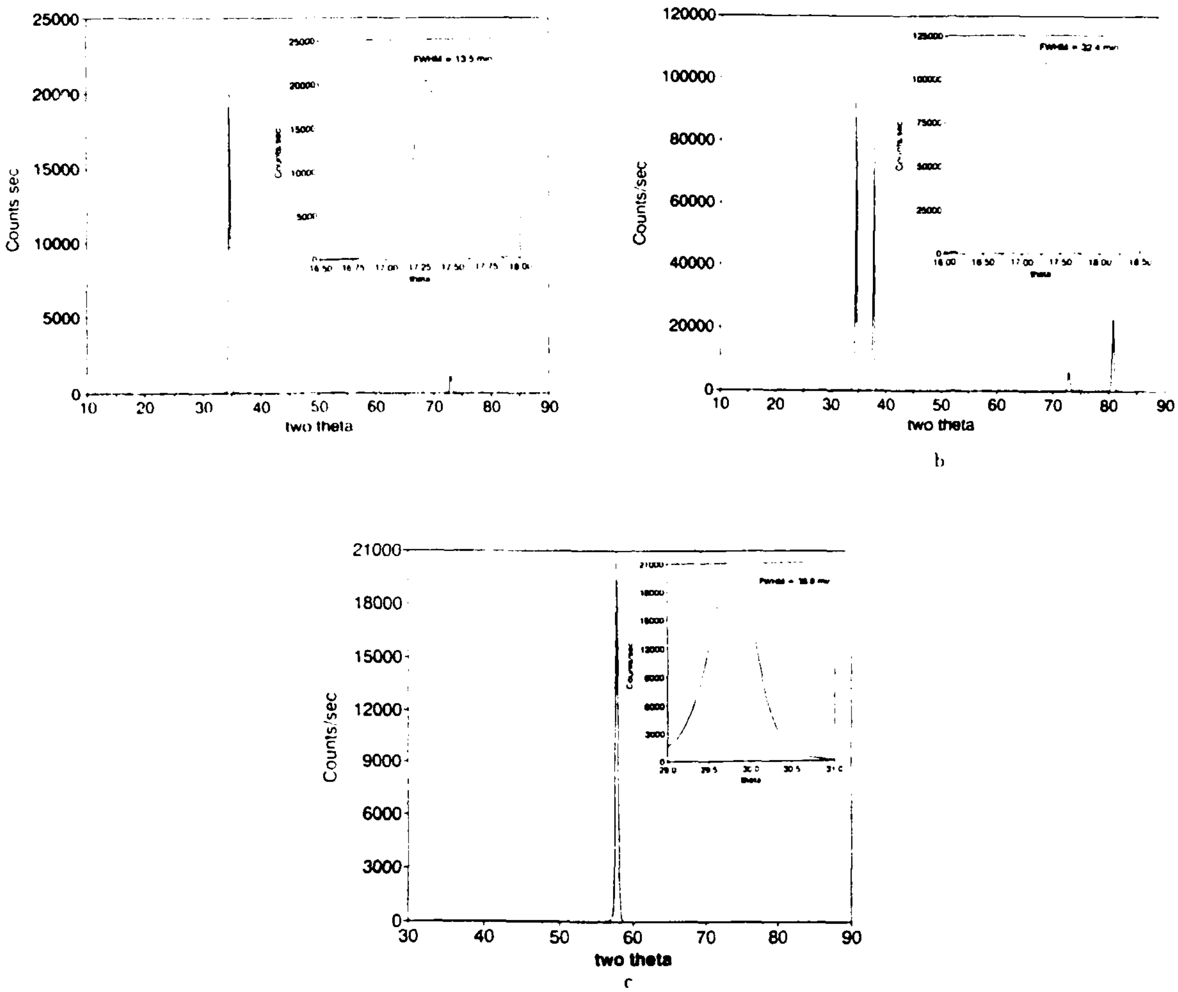


Fig. 20. $\theta$–$2\theta$ XRD of the GaN film on various sapphire substrates: (a) c-plane, (b) a-plane, (c) r-plane. The inserts show the corresponding rocking curves.

on the *a*-plane and *r*-plane of sapphire is not obvious. This epitaxial relationship can be accounted for as follows: The *a*-plane sapphire has a rectangular unit cell with dimensions 12.97 Å × 8.23 Å, two of which can accomodate a number of unit cells of GaN basal planes as illustrated in fig. 21(a). This results in 1.6% lattice mismatch along [0001] of sapphire and 0.6% along the $[1\bar{1}00]$ axis of the sapphire substrate. The *r*-plane of sapphire substrate has a unit cell with dimensions 4.75 Å × 15.34 Å, which accommodates three unit cells of the *a*-plane of GaN as illustrated in fig. 21(b). This results in 16% lattice mismatch along the $[11\bar{2}0]$ of sapphire and 1.3% along the $[1\bar{1}01]$ of sapphire.

## 4. Conclusion

In conclusion, a two-step growth process has been developed for the heteroepitaxial growth of

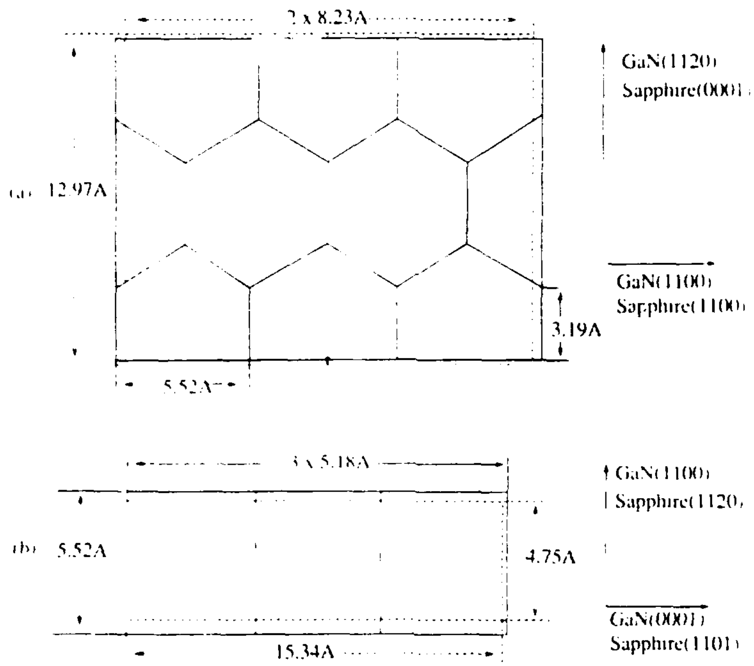


Fig. 21. Epitaxial relationship between GaN and (a) the *a*-plane of sapphire, (b) the *r*-plane of sapphire.

GaN films. This method was found to lead to films with smooth surface morphology, which we interpreted as resulting from a quasi-layer-by-layer growth. Using this process GaN films were grown on a variety of substrates by the ECR-assisted MBE method.

GaN films were successfully grown on Si(0 0 1) and (1 1 1) substrates, using this two-step process. The films on Si(0 0 1) are single-crystalline and epitaxially stabilized in the zincblende structure, while those on Si(1 1 1) have the wurtzite structure. Although RHEED suggest that the wurtzitic GaN on Si(1 1 1) is single-crystalline, a considerable amount of cubic phase was detected by XRD studies, and was attributed to a larger concentration of stacking faults along the growth direction.

GaN films were also grown on *c*-plane, *a*-plane and *r*-plane sapphire. The growth process involves the conversion of the sapphire surface into AlN by plasma nitridation. The XRD studies indicate that GaN films on *c*-plane sapphire have the best crystalline quality.


## Acknowledgements

We are grateful to Prof. Karl Ludwig for stimulating discussions and help with the XRD studies. This work was supported by the Office of Naval Research (Grant No. N00014-92-J-1436).


## References


[1] R.F. Davis, Proc. IEEE 79 (1991) 702; R.F. Davis, Z. Sitar, B.E. Williams, H.S. Kong, H.J. Kim, J.W. Palmour, J.A. Edmond, J. Ryu, J.T. Glass and C.H. Carter Jr., Mat. Sci. Eng. B 1 (1988) 77.

[2] J.I. Pankove, MRS Symp. Proc. 162 (1990) 515.

[3] P. Das and D.K. Ferry, Solid State Electron. 19 (1976) 851.

[4] H.P. Maruska and J.J. Tietjen, Appl. Phys. Lett. 15 (1969) 327.

[5] J.I. Pankove, Phys. Rev. Lett. 34 (1975) 809.

[6] R. Madar, G. Jacob, J. Hallis and R. Fruchart, J. Cryst. Growth 31 (1975) 197.

[7] B. Monemar, O. Lagerstedt and H.P. Gislason, J. Appl. Phys. 51 (1980) 625.

[8] T. Sasaki and S. Zembutsu, J. Appl. Phys. 61 (1986) 2533.
[9] M.A. Khan, R.A. Skogman, R.G. Schulze and M. Gershenzon, Appl. Phys. Lett. 42 (1983) 430.
[10] M.A. Khan, J.N. Kuznia, J.M. Van Hove, D.T. Olson, S. Krishnankutty and R.M. Kolbas, Appl. Phys. Lett. 58 (1991) 526.
[11] M.A. Khan, J.M. Hove, J.N. Kuznia and D.T. Olston, Appl. Phys. Lett. 58 (1991) 2408.
[12] M. Manasewit, F.M. Erdmann and W.I. Simpson, J. Electrochem. Soc. 118 (1971) 1864.
[13] H. Amano, N. Sawaski, I. Akasaki and Y. Toyoda, Appl. Phys. Lett. 48 (1986) 353.
[14] T. Kawabata, T. Matsuda and Susumu Koike, J. Appl. Phys. 56 (1984) 2367.
[15] T. Duffy, C.C. Wang, G.D. O'Clock Jr., S.H. McFarelane and P.I. Zanzucchig, J. Electron. Mater. 2 (1973) 359.
[16] H. Gotoh, T. Suga, H. Susuki and M. Kimata, Jpn. J. Appl. Phys. 20 (1981) L545.
[17] S. Yoshida, S. Misawa and S. Gonda, Appl. Phys. Lett. 42 (1983) 427.
[18] M.J. Paisley, Z. Sitar, J.B. Posthil and R.F. Davis, J. Vac. Sci. Technol. 7 (1989) 701.
[19] R.C. Powell, G.A. Tomasch, Y.W. Kim, J.A. Thornton and J.E. Greene, MRS Symp. Proc. 162 (1990) 525.
[20] Z. Sitar, M.J. Paisley, B. Yan and R.F. Davis, MRS Symp. Proc. 162 (1990) 537.
[21] T. Lei, M. Fanciulli, R. Molnar, Y. He, T.D. Moustakas and J. Scanlon, Bull. Am. Phys. Soc. 36 (1991) 543.
[22] T. Lei, M. Fanciulli, R.J. Molnar, T.D. Moustakas, R.J. Graham and J. Scanlon, Appl. Phys. Lett. 58 (1991) 944.
[23] T. Lei, T.D. Moustakas, R.J. Graham, Y. He and S.J. Berkowitz, J. Appl. Phys. 71 (1992) 4933.
[24] T. Lei and T.D. Moustakas, Mat. Res. Soc. Proc. 242 (1992) 433.
[25] T.D. Moustakas, R.J. Molnar, T. Lei, G. Menon and C.R. Eddy Jr., Mat. Res. Soc. Proc. 242 (1992) 427.
[26] T.P. Humphreys, C.A. Sukow, R.J. Nemanich, J.B. Posthil, R.A. Rudder, S.V. Hattangady and R.J. Markunas, MRS Symp. Proc. 162 (1990) 531.
[27] E. Lashimi, B. Mathur, A.B. Bhattacharya and V.P. Bhargava, Thin Solid Films 74 (1980) 77.
[28] S. Zembutsu and T. Sasaki, Appl. Phys. Lett. 48 (1986) 870.
[29] S. Zembutsu and M. Kobayashi, Thin Solid Films 129 (1985) 289.
[30] J. Knights and R.A. Lujan, J. Appl. Phys. 49 (1978) 129.
[31] J.I. Pankove, S. Bloom and G. Harbeke, RCA Rev. 36 (1975) 163.
[32] O. Lagerstedt and B. Monemar, J. Appl. Phys. 45 (1974) 2266.
[33] W. Seifert, R. Franzheld, E. Butter, H. Sobotta and V. Riede, Cryst. Res. Technol. 18 (1983) 383.
[34] H. Amano, M. Kito, K. Hiramatsu and I. Aksaki, Jpn. J. Appl. Phys. 28 (1989) L2112–L2114.
[35] S. Nakamura, Jpn. J. Appl. Phys. 30 (1991) L1705.
[36] M. Mizuta, S. Fujieda, Y. Matsumoto and T. Kawamura, Jpn. J. Appl. Phys. 25 (1986) L945.
[37] S. Strite, J. Ruan, Z. Li, N. Manning, A. Salvador, H. Chen, D.J. Smith, W.J. Choyke and H. Morkoc, J. Vac. Sci. Technol. B 9 (1991) 1924.
[38] G. Menon, MSc thesis, Boston University (1990).
[39] S.N. Basu, private communications.
[40] B.E. Warren, X-ray Diffraction (Addison-Welsley, New York, 1969).

Appendix B : “Growth and Doping of GaN films by ECR-Assisted MBE”

# GROWTH AND DOPING OF GaN FILMS BY ECR-ASSISTED MBE

T.D. Moustakas and R.J. Molnar
Molecular Beam Epitaxy Laboratory, Department of Electrical, Computer, and Systems Engineering, Boston University, Boston, MA 02215.

## ABSTRACT

We report on growth, doping, and characterization studies of GaN films produced by the Electron Cyclotron Resonance microwave plasma assisted Molecular Beam Epitaxy. The films were grown heteroepitaxially on sapphire (0001), whose surface was converted into atomically smooth AlN by plasma nitridation. The GaN films were grown in two temperature steps, a process found to promote the layer-by-layer growth mode. ECR plasma conditions to grow either n-type autodoped or semi-insulating GaN film were identified. The structure and microstructure as well as the electrical properties of these two classes of films are discussed. A systematic dependence between electron mobility and net carrier concentration was found, which predicts that the mobility of GaN with a net carrier concentration of $10^{14}$cm$^{-3}$ is about $10^4 cm^2/V{\cdot}s$. The insulating films were intentionally doped either p-type or n-type by incorporation of Mg or Si during film growth. Hole or electron concentrations at 300K between $10^{18}$ – $10^{19}$cm$^{-3}$ have been obtained without requiring any post-growth treatment.

## INTRODUCTION

The family of refractory nitrides (InN, GaN, AlN) is one of the most promising classes of optoelectronic materials. The three binaries are direct band-gap semiconductors and their energy gaps cover the spectral region from 1.95eV (InN) and 3.4eV (GaN) to 6.28eV (AlN). The successful development of these materials would lead to devices such as light emitting diodes, lasers, and light detectors, operating in the spectral region from the visible to ultraviolet. Due to their unique physical properties (high energy gap, high thermal conductivity, high saturation velocity), these materials are also expected to be used in the fabrication of devices for high temperature, high power, and high frequency applications. Heterojunctions, quantum wells, and superlattices based on these materials are expected to show novel low dimensional electronic behavior due both to the strong quantum confinement and to the lack of defects associated with the transition from direct to indirect semiconductors, a problem common in GaAs / $Al_xGa_{1-x}As$ structures.

The majority of the published work deals mostly with the synthesis and characterization of these materials. Early work dealing primarily with bulk growth is reviewed in "Refractory Semiconductor Materials" (1) and recent results were presented in the MRS symposium on "Wide Band-Gap Semiconductors" (2) as well as in reviews by Pankove (3) and Davis (4).

The synthesis of bulk crystals of GaN and AlN by equilibrium processes (1) has led only to the growth of milimeter size single crystals. Vapor phase synthesis of III-V nitrides has focused on heteropitaxial growth, primarily on (0001) sapphire. The most important recent development is the discovery that AlN (5-8) and GaN (9-12) buffers lead to lateral growth which significantly improves the surface morphology as well as the optical and electrical properties of the films. Another recent significant development was the epitaxial stabilization of cubic-GaN of selective substrates, including $\beta$-SiC (13), GaAs (14), MgO (15), and Si (10,11).

GaN films have been grown by many growth techniques, including CVD (16), MOCVD (17), and MBE (18). All these methods produced n-type GaN films, a result attributed to nitrogen vacancies due to thermal decomposition of GaN at the high growth temperature. To reduce the growth temperature, plasma assisted deposition methods were developed (9-11,13-15) which lead to the growth of semi-insulating GaN films. The early effort at p-type doping were unsucessful (19) due to compensation by n-type defects. With improvements in film quality, recent reports indicate the possibility of p-type doping and the resulting fabrication of efficient light emitting devices (7,20).

In this paper, we report our progress in the growth, doping, and characterization of GaN films by the Electron Cyclotron Resonance microwave plasma assisted Molecular Beam Epitaxy (ECR-MBE).

## EXPERIMENTAL METHODS

The deposition system used in this study is schematically illustrated in Figure 1. It consists of a Varian GenII MBE unit with an ASTeX compact ECR source inserted into one of the effusion cell ports. The pressure in the overall system is $10^{-11}$Torr. A Reflection High Energy Electron Diffraction (RHEED) setup is an integral part of the apparatus. Ga and dopant elements (Si and Mg) are evaporated from conventional Knudsen effusion cells, while active nitrogen is produced by passing molecular nitrogen through the ECR source at a total pressure of $10^{-4}$Torr. The growth rate of the GaN films is controlled by varying the flux of Ga. The stoichiometry of the films is controlled by varying the microwave power in the ECR discharge, which affects the flux of the active nitrogen. Generally, microwave power of 35 Watts or higher was found to lead to semi-insulating GaN films (stoichiometric) for growth rates up to 6500Å/h. For higher growth rates or smaller microwave power in the discharge, the flux of active nitrogen is insufficient for the growth of stoichiometric films and excess gallium in the films is phase separated in the form of Ga droplets (21). The films discussed in this paper were grown at growth rates of 2000-2500Å/h, and microwave power levels appropriate for the growth of conducting or insulating films. n-type and p-type doping of GaN films was accomplished by subliming Si or Mg respectively during the growth process.

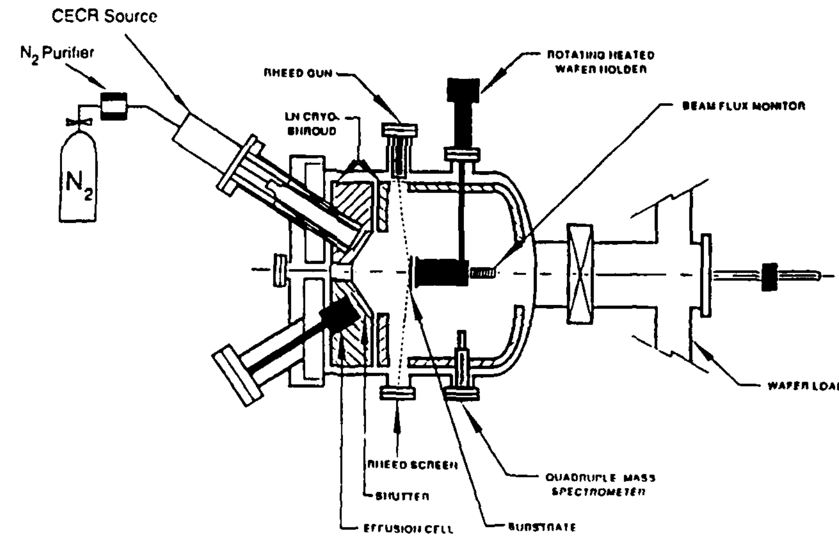


*Figure 1. ECR-MBE growth chamber.*

The GaN films were grown on the c-plane (0001) of sapphire. The substrates were degreased and etched in $H_3PO_4 : H_2SO_4(1:3)$ for the removal of surface contaminants and mechanical damage due to polishing, and finally were rinsed in de-ionized water. After these steps, the substrates were blown dry with nitrogen, mounted on a BN block and transferred to the introduction chamber of the MBE system. In the preparation chamber, the substrates were heated to 850°C for approximately half an hour and then transferred to the growth chamber where they were subjected to bombardment by nitrogen plasma for approximately half an hour at 800°C.

The structure and microstructure of the films were studied by RHEED, XRD, and SEM. To measure the transport coefficients, the samples were abrasively etched into Van der Pauw lamillas and electrical contacts were formed by soldering gold wires with indium.

## EXPERIMENTAL RESULTS AND DISCUSSION

### A. Film Growth

We found that exposure of the substrate to a nitrogen plasma results in nitridation of the surface of the substrate and its conversion into AlN. The AlN thin film was found to be a single crystal and its RHEED pattern is illustrated in Figure 2a. The streakiness of the diffraction pattern suggests that the AlN film is atomically smooth. Similar nitridation has also been observed when the $\alpha$-plane $(11\bar{2}0)$ and the r-plane$(1\bar{1}02)$ of sapphire were exposed to a nitrogen plasma (22,23).

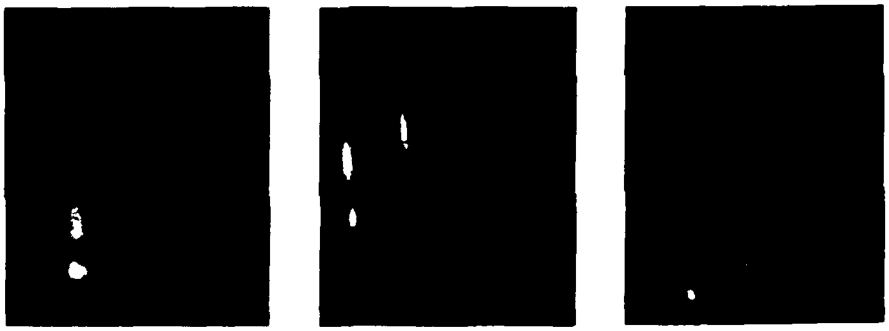

a b c

*Figure 2. RHEED patterns taken at various steps during growth: (a) substrate after plasma nitridation (b) after the growth of the GaN buffer (c) after growth at high temperature.*

The GaN film was grown on the previously formed AlN film following a two temperature step process developed in our laboratories over the past few years (9-11, 22-24). In this process a GaN-buffer, approximately 200Å thick, is grown first at a relatively low temperature (500°C) followed by a higher temperature growth (800°C) of the rest of the film. Figures 2b and 2c show the RHEED patterns of the GaN buffer and the GaN film after the completion of the growth. The streakiness of these diffraction patterns also indicate that both the thin GaN-buffer as well as the thick GaN film are atomically smooth. The diffraction pattern of Figure 2c tends to be spotty under deposition conditions which lead to semi-insulating GaN films. This is consistent with the surface morphology of these films as discussed later. This method of film growth, using a GaN-buffer, has also been used for the growth of GaN films by the MOCVD method (12) and the reports indicate significant improvements in the quality of such films as well.

## B. Surface Morphology

The surface morpholgy of GaN films was found to depend strongly on the ECR plasmas. In low power plasmas, which lead to n-type autodoped GaN films, the surface morphology is flat as shown in Figure 3a. These data are in agreement with the RHEED data of Figure 2c. Furthermore, the cross-sectional view shows no evidence of columnar morphology. These findings suggest that lateral growth in these films is significantly higher than the vertical growth. In a similar study on the growth of GaN on Si(100), we were able to resolve steps of approximately 100Å on the top of the plateaus and by comparing this with the area of the plateus, we concluded that the lateral growth rate is larger than the vertical growth rate by a approximately a factor of 100, and that the two dimensional nucleation rate was found to be 20 nuclei/$\mu m^2$h (11,23). Based on these findings, we characterized the growth on Si(100) as quasi layer-by-layer growth. The evidence from the data presented in here is that growth on (0001) sapphire proceeds via the layer-by-layer mode.

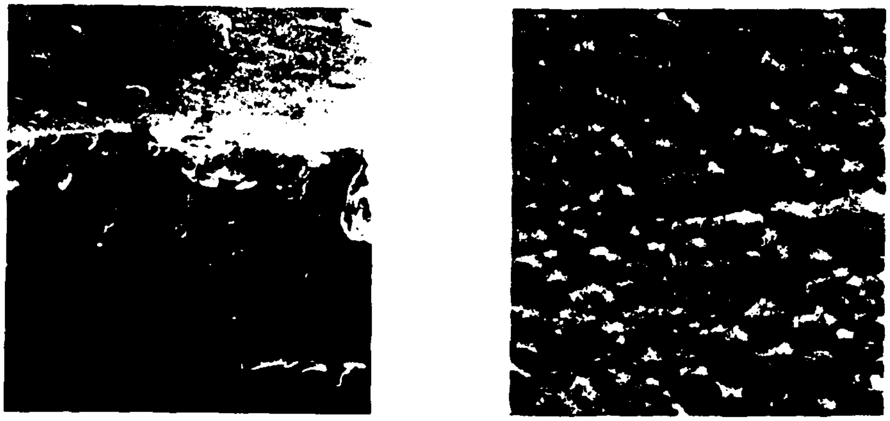

a 1$\mu$m b

*Figure 3. SEM surface morphologies (a) conducting film (b) insulating film*

Higher power plasmas, which lead to semi-insulating films, result to some degree of surface roughening. The surface morphology of such a film is shown in Figure 3b. At this moment, we do not know whether the change in growth mode, under the two plasma conditions, is related to the change in surface mobility of the absorbed atoms or to the kinetics of growth due to the change in concentration of active nitrogen at the growing surface.

## C. Film Structure

A comprehensive study on the structure of GaN films on silicon and sapphire substrates has been published elsewhere (25). Here, we present data on GaN films grown on (0001) sapphire substrates and discuss only $\theta - 2\theta$ scans and rocking curves around the main diffraction peak.

Figure 4 shows the $\theta - 2\theta$ scan and the $\theta$-rocking curve at the main reflection peak for a GaN film grown under lower power plasma conditions (conducting films). There are two peaks in the $\theta - 2\theta$ scans, one at $2\theta = 34.6°$ corresponding to the (0002) reflection, and the second at $2\theta = 72°$ which is the second order harmonic. The $\theta$-rocking curve of the (0002) peak, shown in the insert of Figure 4, has a FWHM of 10 minutes, which is comparable to the best reported in the literature (26) for films grown by other deposition methods. These data confirm that the

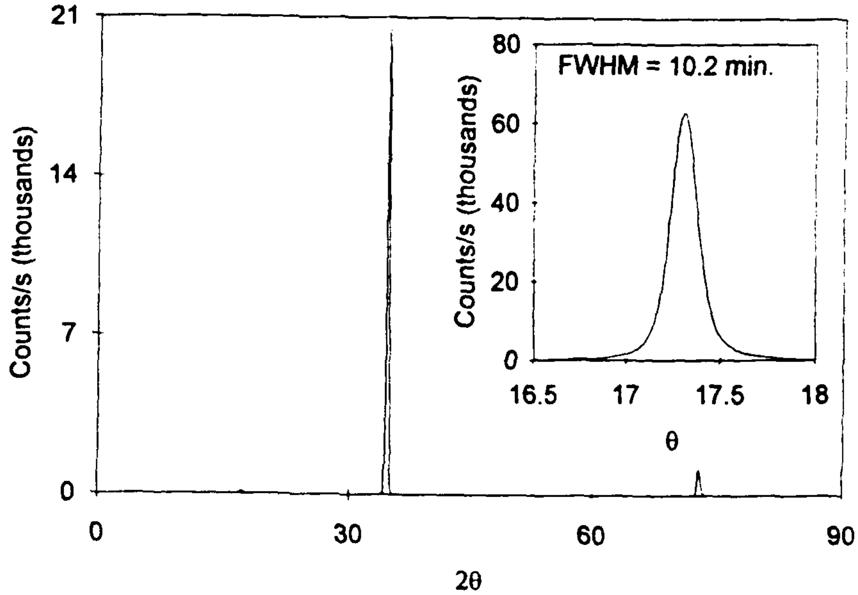


*Figure 4. XRD of a conducting GaN film. The insert shows the rocking curve around the main peak.*

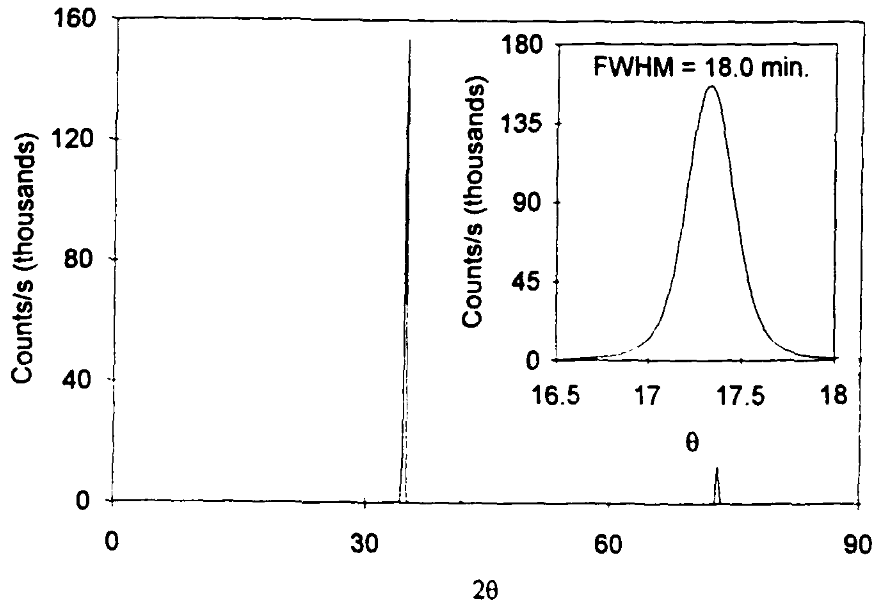


*Figure 5. XRD of a semi-insulating GaN film. The insert shows the rocking curve around the main peak.*

GaN films were grown with their c-plane parallel to the substrate. The epitaxial relationship between GaN and (0001) sapphire was discussed by Lee *et. al.* (25). The GaN basal unit cell is oriented 30° away from the sapphire unit cell in epitaxial relationship with a smaller hexagonal unit cell consisting of the Al atoms in the sapphire substrate.

Figure 5 shows a $\theta - 2\theta$ scan and the $\theta$-rocking curve for a GaN film grown under higher power plasma conditions (insulating films).

## D. Electrical Properties

GaN films grown by various methods were generally found to be heavily doped n-type ($10^{18} - 10^{20} cm^{-3}$). Recently, GaN films grown by the MOCVD method with either an AlN-buffer (7) or with a GaN-buffer (12) were found to have carrier concentrations in the range of $10^{16} - 10^{17} cm^{-3}$ and electron mobilities as high as 900 $cm^2/V \cdot s$.

As discussed earlier, GaN films grown by the ECR method can be made either conducting or insulating by choosing the power level in the ECR discharge. Films grown at relatively low power levels (< 35 Watts) were found to be autodoped with n-type conductivity, while those grown at higher power levels in the ECR discharge were found to be insulating. Since the power in the ECR discharge controls the amount of active nitrogen, the observed trend in the electrical behavior together with the presence of phase separated gallium in the conducting films, suggest that the origin of autodoping centers in GaN is indeed due to N-vacancies. In the following, we review the electrical properties of both conducting and insulating GaN films. Details on these studies were published elsewhere (27,28).

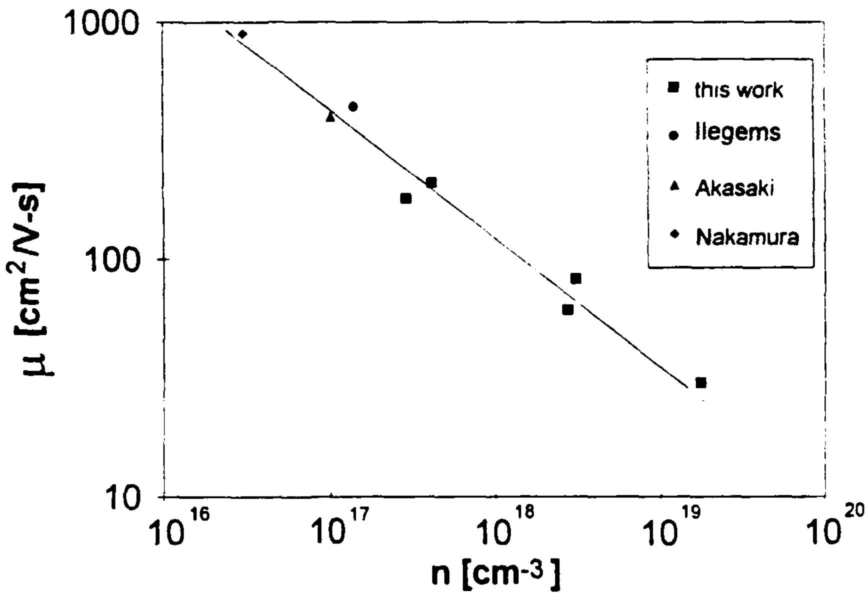


***Figure 6. Electron mobilities vs. electron concentration for a number of GaN films.***

A number of n-type GaN films were produced by keeping the power in the ECR discharge constant (active nitrogen overpressure fixed) and gradually reducing the flux of the Ga-beam. The electron mobility vs net carrier concentration at 300K for these films is shown in Figure 6. Shown in the same Figure are also the results reported for GaN films produced by various

CVD methods (7,29,30). It is important to note that all data follow the same trend which can be extrapolated to predict the electron mobility of relatively pure and defect free GaN films. For example, films with carrier concentrations of $10^{14}cm^{-3}$ are predicted to have a mobility of $10^4 cm^2/V \cdot s$, which is comparable with that of GaAs.

The electron transport mechanism in our films was investigated by studying the temperature dependence of the Hall coefficient and of the resistivity (27,28). The analysis of these data indicate that the ionization energy of the autodoping centers is 20 to 30 meV. These autodoping centers form a band when their concentration is larger than $10^{17}cm^{-3}$ and conduction in this band was found to dominate the transport at low temperatures. In fact for heavily autodoped films ($5 \times 10^{18}cm^{-3}$), transport in this band dominates even at room temperature.

GaN films with net carrier concentrations less than $10^{16}cm^{-3}$ were also produced. Paradoxically, such films were found to have low electron mobilities ($\leq 1cm^2/V \cdot s$). This result can be accounted for as follows: When the concentration of the autodoping centers becomes less than the concentration of the deep defects, the material becomes fully compensated and thus conduction is dominated by hopping transport in the deep compensating defects. This suggests that the concentration of deep defects in our films is of the order of $10^{16}cm^{-3}$. This may also be true for films grown by the MOCVD methods, since the best films grown by this method have net carrier concentrations of $3 \times 10^{16}cm^{-3}$ (30). These deep defects are probably related to heteropitaxial growth, such as dislocations.

## E. Doping

Early efforts to dope GaN films with Zn or other group II-elements led to compensated films. Recently, Akasaki and co-workers (7) reproted that Mg compensated GaN films can be converted to p-type when irradiated with a beam of low energy electrons (LEEBI). Subsequently, Nakamura and co-workers (31) demonstrated that similar results can be obtained by thermal annealing in a nitrogen atmosphere and attributed the acceptor activation to thermal removal of $H_2$ which ties up the Mg in the form of Mg-H complexes.

GaN films produced by the ECR-MBE methods were doped p- or n-type by incorporation of Mg or Si respectively during film growth. Hall effect measurements on Mg-doped films indicate that the films are p-type and that carrier concentrations at 300K between $10^{18} - 10^{19}cm^{-3}$ have been obtained without requiring any post growth annealing treatment (32). These films have electrical conductivities of between 0.1 to 1.0 $\Omega^{-1}cm^{-1}$. The magnitude of the hole mobility at room temperature was found to be 0.6 $cm^2/V \cdot s$ and was not strongly dependent on temperature. The carrier concentration vs inverse temperature for one of the samples is shown in Figure 7. We believe that the scatter in the data is due to difficulties in measuring the Hall coefficient of a low mobility material. The conductivity measurements, which are far more consistent, are shown in Figure 8. Since the electron mobility, at this level of doping, was found to be temperature independent, we can use the conductivity data to extract the activation energy for the carrier concentration. From the high temperature data of Figure 8. (>150K), an activation energy for the conductivity of $\Delta E$=0.15eV was calculated. This is in agreement with the results of Akasaki (33) for LEEBI activated Mg-doped GaN films grown by the MOCVD method. The low temperature data in Figures 7 and 8 are consistent of impurity conduction (34).

The concentration of holes in a semiconductor with an acceptor concentration $N_A$ and donor concentration $N_D$ ($N_A > N_D$) is given by the expression (35):

$$\frac{p(N_D + p)}{N_A - N_D - p} = 2N_V \exp\left[-\frac{(E_A - E_V)}{kT}\right] \tag{1}$$

where $N_V$ is the effective density of states at the valence band

$$N_V = 2\left(\frac{m_h^* kT}{2\pi\hbar^2}\right)^{3/2} \tag{2}$$

Equation (1) has two approximations. If $p << N_D$, Eq. (1) takes the form

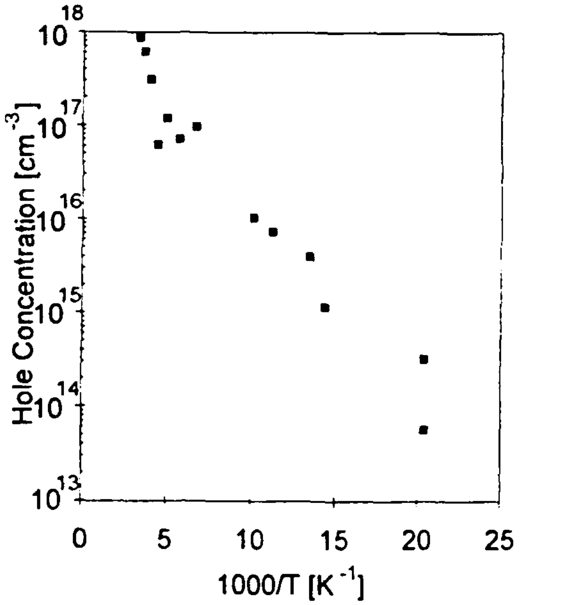


*Figure 7. Hole concentration vs 1/T for a Mg-doped GaN film.*

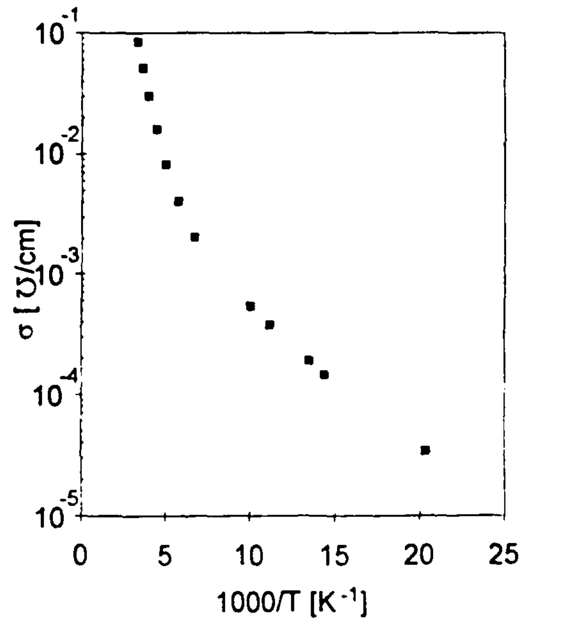


*Figure 8. Conductivity vs 1/T for the same GaN film discussed in in Figure 7.*

$$p = 2N_v \frac{(N_A - N_D)}{N_D} \exp\left[-\frac{(E_A - E_V)}{kT}\right] \tag{3}$$

In this case the plot of $\ln\left(pT^{-3/2}\right)$ vs inverse temperature should have a slope equal to the ionization energy of acceptors ($E_A - E_V$).

If $p >> N_D$, then Equation (1) takes the form

$$p = (2N_V N_A)^{1/2} \exp\left[-\frac{(E_A - E_V)}{2kT}\right] \tag{4}$$

In this case, the exponential involves only half of the ionization energy.

The evidence suggests that N-vacancies in GaN act as donors and their concentration depends on the overpressure of active nitrogen during film growth. The films in this study were grown under high N-overpressure and thus $N_D$ should be very low. If this is true, Equation (4) should be applicable in the high temperature region of the experimental data and $E_A - E_V$=0.30eV. However, one cannot rule out that the kinetics of the formation of N-vacancies is modified in the presence of Mg, and that $N_D >> p$ in the investigated temperature range. If this is true, then Equation (3) is applicable and $E_A - E_V$=0.15eV. Further studies are required to determine the ionization energy of Mg in GaN.

The activation of Mg-acceptors without any post-growth annealing is not inconsistent with Nakamura's proposal for the formation of Mg-H complexes in GaN:Mg films grown by the MOCVD method (36), since the concentration of $H_2$ is low in MBE growth. However, one should not rule out the possibilty of ion assisted doping phenomena present in our method.

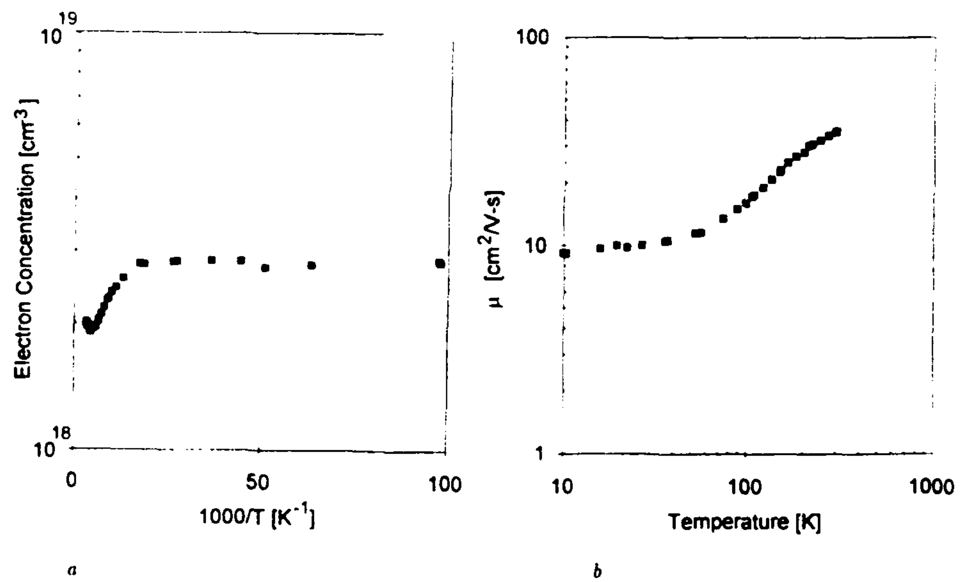


*Figure 9. (a) Electron concentration vs 1/T and (b) electron mobility vs T for a GaN film doped with Si.*

Hall effect measurements on Si doped films indicate that the films are n-type. Net carrier concentration at 300K between $10^{18} - 10^{19}$cm$^{-3}$ have been obtained. The temperature dependence of the carrier concentration and electron mobility for one of the Si-doped films is shown in

Figures 9a and 9b. The carrier concentration was computed from the measured values of the Hall coefficient, $R_H$, using the equation

$$n = \frac{1}{eR_H} \tag{5}$$

Equation (5) assumes electron conduction in one band. However, as discussed previously (27), the data of Figure 9 are consistent with two-band conduction (conduction and impurity bands).

## CONCLUSIONS

We discussed the growth of GaN on sapphire (0001). The surface of the substrate was first converted to atomically smooth AlN by plasma nitridation and the GaN film was grown on the top of this AlN-buffe. .sing a two temperature step process. It was shown that this process promotes growth in the layer-by-layer mode. Plasma conditions to grow either conducting or insulating films were identified and the effect of these conditions on the structure, microstructure, and electrical properties were discussed. The insulating films were doped p-type or n-type by incorporating Mg or Si respectively. Carrier concentrations in the range of $10^{18} - 10^{19}cm^{-3}$ were obtained without requiring any post growth annealing.

## ACKNOWLEDGEMENTS

This work was supported by the office of Naval Research (grant number N0014-92-j-1436) We are grateful to Karl Ludwig for collaboration in XRD, and to Max Yoder for discussions and encouragement.

## REFERENCES

1. Refractory Semiconductor Materials, edited by N.A. Garjunaova and D.N. Nasledov (Consultant Bureau, New York, 1966)

2. Wide Band-Gap Semiconductors, Mat. Res. Soc. Symp. Proc., Vol. 242, edited by T.D. Moustakas, J.I. Pankove, and Y. Hamakura (1992).

3. J.I. Pankove, Mat. Res. Soc. Proc., Vol. 162, 516 (1990)

4. R.F. Davis, Proc. of the IEEE, 79, 702 (1991)

5. H. Amano, N. Sawaki, I. Akasaki, and Y. Toyoda, Appl. Phys. Lett., 48 , 353 (1986)

6. H. Amano, I. Akasaki, H. Hiramatsu, N. Koide, and N. Sawaki, Thin Solid Films, 163, 415 (1988)

7. J. Akasaki and H. Amano, reference 2, p. 383

8. M. Asif Khan, J.N. Kuznia, J.M. Van Hove, D.T. Olson, S. Krishnankutty, R.M. Kolba, Appl. Phys. Lett. 58, 526 (1991)

9. G. Menon, Master Thesis, Boston University (1990); G. Menon, R. Molnar, S.J. Berkowitz, and T.D. Moustakas, Bull. APS 36, 544 (1991)

10. T. Lei, M. Fanciulli, R.J. Molnar, T.D. Moustakas, R.J. Graham, and J. Scanlon, Appl. Phys. Lett., 59, 944 (1991)

11. T. Lei, T.D. Moustakas, R.J. Graham, T. He, and S.R. Berkowitz, J. Appl. Phys., 71, 4933 (1992)

12. S. Nakamura, Jpn. J. Appl. Phys. 30, L1705 (1991)

13. M.J. Paisley, Z. Sitar, J.B. Posthill, and R.F. Davis, J. Vac. Sci. and Technol., A7, 701 (1989)

14. G. Martin, S. Strite, J. Thornston, and H. Morkoc, Appl. Phys. Lett., 58, 2375 (1991)

15. R.C. Powell, G.A. Tomasch, Y.W. Kim, J.A. Thornton and J.E. Greene, MRS Symp. Proc 162, 525 (1990)

16. H.P. Maruska and J.J. Tietjen, Appl. Phys. Lett. 15, 327 (1969)

17. H.M. Manasevit, F.M. Erdmann, and W.I. Simpson, J. Electochem. Soc. 118, 1864 (1971)

18. S. Yoshida, S. Misawa, Y. Fujii, S.Tanaka, S. Hayakawa, S. Gonda, and A. Itoh, J. Vac. Sci. Technol., 16, 990 (1979)

19. J.I. Pankove, J.E. Berkeyheiser and E.A. Miller, J. Appl. Phys., 45 1280 (1974)

20. S. Nakamura, T. Mukai,and M. Senoh, Jpn. J. Appl. Phys. L1998 (1991)

21. C.R. Eddy Jr., T.D. Moustakas, and J. Scanlon, J. Appl. Phys. 73 (Jan. 1993)

22. T.D. Moustakas, R.J. Molnar, T. Lei, G. Menon, and C.R. Eddy Jr., Reference 2, p 427

23. T.D. Moustakas, T. Lei, and R.J. Molnar, Physica B: Condensed Matter (1993)

24. T. Lei and T.D. Moustakas, Reference 2, p. 433

25. T. Lei, K.F. Ludwig, and T.D. Moustakas, J. Appl. Phys. (submitted for publication)

26. T. Sasaki and S. Zembutsu, J. Appl. Phys. 61, 2533 (1987)

27. R.J. Molnar, T. Lei, and T.D. Moustakas, Appl. Phys. Lett. 62 (Jan. 1993).

28. R.J. Molnar, T. Lei, and T.D. Moustakas (this volume)

29. M. Ilegems, J. Cryst. Growth 13/14, 360 (1972)

30. S. Nakamura, T. Mukai, and M. Senoh, J. Appl. Phys. 71, 5543 (1992)

31. S. Nakamura, M. Senoh, and T. Makai, Jpn. J. Appl. Phys., L1708 (1992)

32. R.J. Molnar and T.D. Moustakas, Appl. Phys. Lett. (submitted for publication)

33. I. Akasaki, H. Amano, N. Koide, M. Kotaki, and K. Mannabe (to be published)

34. N.F. Mott, T.D. Twose, Advances in Physics 10, 107 (1961)

35. N.B. Hannay, Semiconductors (Reinhold Publishing Corp., New York, 1960)

36. S. Nakamura, N. Iwasa, M.Senoh, and T. Mukai, Jpn. J. Appl. Phys., 31 (1992)

Appendix C : "High Mobility GaN Films Produced by ECR-Assisted MBE"

# HIGH MOBILITY GaN FILMS PRODUCED BY ECR-ASSISTED MBE

R.J. Molnar, T. Lei, and T.D. Moustakas
Molecular Beam Epitaxy Laboratory, Department of Electrical, Computer, and Systems Engineering, Boston University, Boston, MA 02215

## ABSTRACT

High electron mobility autodoped GaN films were produced by the ECR assisted MBE method. The net electron concentration was varied systematically from $2 \times 10^{19}$ to $2 \times 10^{17} cm^{-3}$ by controlling the active nitrogen overpressure. Correspondingly, the electron mobility increased from 20 to 210 $cm^2V^{-1}sec^{-1}$. The line through the experimental data also predicts the electron mobilities of GaN films produced by the CVD methods.

## INTRODUCTION

GaN films, produced by a variety of vapor phase methods, are autodoped n-type, a result attributed to the formation of nitrogen vacancies during film growth. In general, the net carrier concentration in such films was reported to be in the range of $10^{18} - 10^{20} cm^{-3}$ (1). Recently, GaN films grown by the MOCVD method either with an AlN-buffer (2), or with a GaN-buffer (3) were found to have carrier concentrations of between $10^{16} - 10^{17} cm^{-3}$ and electron mobilities as high as 900 $cm^2V^{-1}sec^{-1}$.

In this paper, we report for the first time the growth of high mobility autodoped GaN films by Electron Cyclotron Resonance assisted Molecular Beam Epitaxy (ECR-MBE). The transport mechanism in these films was investigated by studying the temperature dependence of the Hall constant and resistivity.

## EXPERIMENTAL METHODS

The thin film deposition system used in this study consists of a Varian GenII MBE unit with an ASTeX compact ECR source inserted in one of the effusion cell ports. A conventional Knudsen effusion cell was used to evaporate Ga, while active nitrogen was provided by passing molecular nitrogen through the ECR source.

The GaN films were grown on the c-plane (0001) of sapphire. The substrates were degreased and etched in $H_3PO_4 : H_2SO_4(1:3)$ for the removal of surface contaminants and mechanical damage due to polishing and finally rinsed in de-ionized water. After these steps, the substrates were blown dry with nitrogen, mounted on a BN block, and transferred to the introduction chamber of the MBE system. In the preparation chamber, the substrates were heated to 850°C for approximately half an hour and then transferred to the growth chamber where they were subjected to bombardment by nitrogen plasma for approximately half an hour at 800°C. As discussed elsewhere (4,5), this resulted in the formation of an atomically smooth AlN layer. The GaN film was grown on the top of this AlN-buffer in two temperature steps as described elsewhere(4,5). First, a thin (~200Å) GaN-buffer was grown at 500°C and the rest of the film, typically 2$\mu$m thick, was grown at 800°C. This two step process leads to quasi layer-by-layer growth.(5)

The samples were abrasively etched into Van der Pauw lamilla and electrical contacts were formed by soldering gold wires with indium. The samples' conductivities and Hall constants were measured as a function of temperature.

## RESULTS AND DISCUSSION

Although the films were not intentionally doped, Hall effect measurements indicate that they have n-type conductivity. The magnitude of the electron mobility vs. the net electron concentration at 300K for the investigated films is shown in Figure 1. Also shown in the same figure are the results reported for GaN films produced by CVD methods (2,3,6). It is important to note that all data follow the same trend, which can be extrapolated to predict the electron mobility of relatively pure and defect free GaN-films. For example, a GaN film with net carrier concentration of $10^{14}cm^{-3}$ is predicted from this graph to have an electron mobility of about $10^4 cm^2V^{-1}sec^{-1}$, which is comparable with that of GaAs.

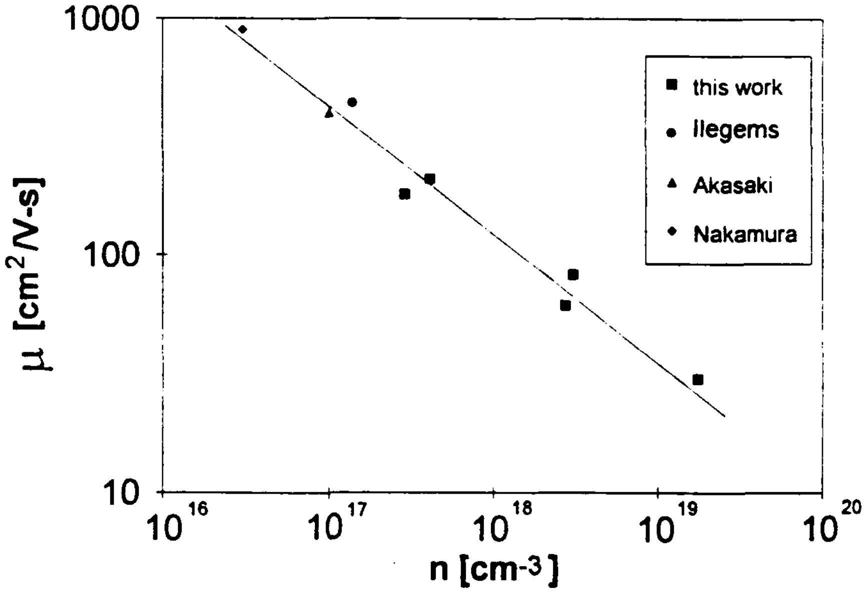


*Figure 1. Electron mobility vs. net carrier concentration at 300K for a number of GaN films.*

The electron concentrations in Figure 1 were calculated from the expression

$$n = \frac{1}{eR_H} \tag{1}$$

where $R_H$ is the Hall constant. Equation (1) assumes electron conduction in one band. As discussed previously (7), this assumption is valid at 300K, but at lower temperatures, conduction in the autodoping centers (presumably nitrogen vacancies) becomes dominant. This is illustrated in Figures 2 and 3, where we plot the Hall coefficient and resistivity of the most insulating of our films vs 1/T. As discussed previously (7), these data indicate that at about 100K, the transport switches from the conduction band to the band of the autodoping centers. Thus, in general, the Hall constant and resistivity of these films should be described by two band expressions:

$$R_H = \frac{n_c\mu_c^2 + n_d\mu_d^2}{(n_c\mu_c + n_d\mu_d)^2 e} \tag{2}$$

$$\rho = \frac{1}{n_c e\mu_c + n_d e\mu_d} \tag{3}$$

where $n_c$ and $n_d$ are the concentrations of conducting carriers in the conduction band and the band of the autodoping centers respectively; $\mu_c$ and $\mu_d$ are their corresponding mobilities. Equations (2) and (3) can account for the experimental behavior of Figures 2 and 3. Similar behavior was reported also by Ilegems (6) and Akasaki (2) for the GaN films grown by CVD methods. Nakamura (3), on the other hand, who produced GaN films with the smallest carrier concentration ($3 \times 10^{16}cm^{-3}$) sees only transport in the conduction band down to 40K.

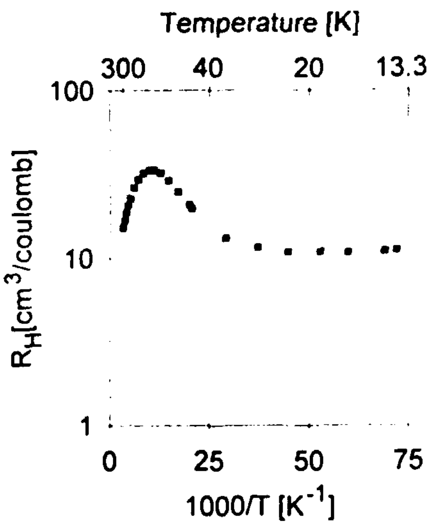


*Figure 2. Hall Constant vs. 1/T for our higest mobiltiy GaN Film*

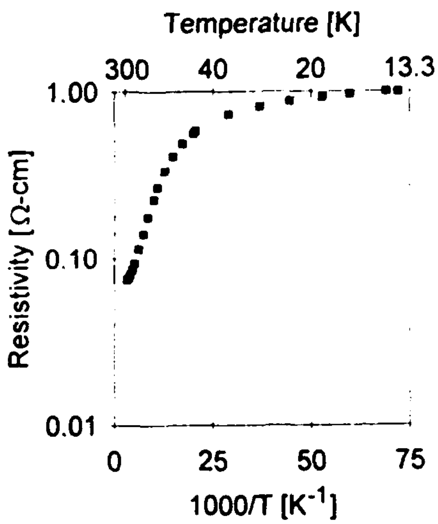


*Figure 3. Resistivity vs. 1/T for the same GaN film discussed in Figure 2.*

The temperature dependence of the electron mobility for the film discussed in Figures 2 and 3 is shown in Figure 4. The high temperaure data in this Figure are characteristic of transport in the conduction band, while the low temperature correspond to transport in the band of the autodoping centers.

## CONCLUSIONS

We have demonstrated the growth of high mobility GaN-films grown by the method of Electron Cyclotron Resonance assisted Molecular Beam Epitaxy. The relation between mobility and net carrier concentration also predicts the results on GaN films grown by CVD methods as well as anticipates the values of electron mobility for purer and relatively defect free GaN films. For GaN films with carrier concentrations larger than $10^{17}cm^{-3}$, transport in the autodoping center becomes dominant at temperatures below 300K.

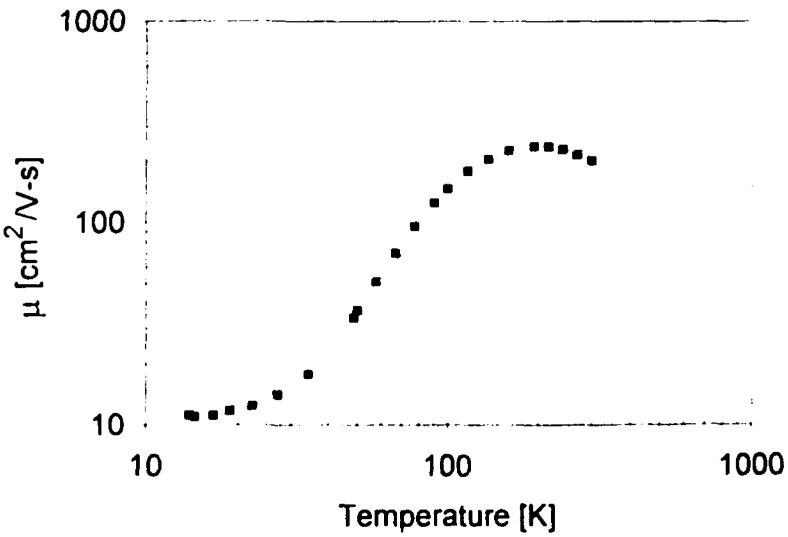


*Figure 4. Temperature dependence of the electron mobility for the film discussed in Figures 2 and 3*

**Acknowledgements**

This work was supported by the Office of Naval Research (Grant Number N00014-92-J-1436). We acknowledge the collaboration with Olga Razumovsky and James Foresi.

**REFERENCES**

1. J.I. Pankove, Mat. Res. Soc. Symp. Proc., vol. 162, 515 (1990).

2. I. Akasaki and H. Amano, Mat. Res. Soc. Symp. Proc., vol. 242, 383 (1992).

3. S. Nakamura, T. Mukai, and M. Senoh, J. Appl. Phys., 71, 5543 (1992).

4. T.D. Moustakas, R.J. Molnar, T. Lei, G. Menon, and C.R. Eddy Jr., Mat. Res. Soc. Proc., vol. 242, 427 (1992).

5. T.D. Moustakas, T. Lei, and R.J. Molnar, Physica B: Condensed Matter (accepted for publication).

6. M. Ilegems, J. Crystal Growth, 13/14, 360 (1972).

7. R.J. Molnar, T.Lei, and T.D. Moustakas, Appl. Phys. Lett., 62 (Jan. 1993).

# Appendix D : "Electron Transport Mechanism in Gallium Nitride"

# Electron transport mechanism in gallium nitride

R. J. Molnar, T. Lei, and T. D. Moustakas
*Molecular Beam Epitaxy Laboratory, Department of Electrical Computer and Systems Engineering, Boston University, Boston, Massachusetts 02215*

(Received 23 July 1992; accepted for publication 20 October 1992)

The electron transport mechanism in autodoped gallium nitride films grown by electron cyclotron resonance microwave plasma-assisted molecular beam epitaxy was investigated by studying the temperature dependence of the Hall coefficient and resistivity on samples with various concentrations of autodoping centers. The Hall coefficients go through a maximum as the temperature is lowered from 300 K and then saturate at lower temperatures. The resistivities in the same temperature range initially increase exponentially and then saturate at lower temperatures. These findings are accounted for if a significant fraction of electron transport, even at room temperature, takes place in the autodoping centers and that conduction through these centers becomes dominant at lower temperatures. The activation energy of these centers was found to be on the order of 20–30 meV. When the concentration of the autodoping centers becomes smaller than that of deep compensating defects, the material becomes semi-insulating and transport by hopping in the compensating defects becomes dominant.

Gallium nitride (GaN) is one of the most promising wide-band-gap semiconductors for the development of high efficiency UV-vis photonic devices due to its direct band gap. The majority of reported work indicates that the GaN films are autodoped *n*-type, a result generally attributed to nitrogen vacancies.[1,2] In general, the defect structure of GaN films is poorly understood and very difficult to control experimentally, resulting in difficulties in doping this material *p*-type.[2,3]

GaN films produced by a variety of deposition methods were generally found to have low electron mobilities ($<100$ cm$^2$/V s) and high carrier concentration ($>10^{18}$ cm$^{-3}$),[2,3] although there have been reports[4,5] of mobilities $\sim 600$ cm$^2$/V s and carrier concentration $\sim 10^{16}$ cm$^{-3}$. Some other workers[6,7] reported semi-insulating films. One would expect that more lightly doped films would have higher Hall mobilities. However, such films generally do not have measurable Hall coefficients, suggesting low carrier mobilities,[6,7] while highly conductive (even degenerate) samples readily have mobilities $>20$ cm$^2$/V s. This anomaly has not yet been accounted for.

In this letter, we report on Hall measurements performed on a number of GaN thin films grown on the (0001) plane of sapphire by the electron cyclotron resonance microwave plasma assisted molecular beam epitaxy (ECR-MBE) method. The data is analyzed by taking into account that conduction through defects makes a significant contribution to the electrical transport. The proposed model also accounts for the low mobility in the semi-insulating films.

The films were deposited by the two-step growth process in which a GaN buffer is grown first at relatively low temperatures and the rest of the film is grown at higher temperatures.[7-12] This method is capable of producing either conductive or insulating films. The conductive films, which are reported here, are generally grown under conditions (high substrate temperature, low nitrogen overpressure) which are believed to lead to the introduction of nitrogen vacancies.[1,2] These films tend to be covered at the end of the run with microscopic Ga droplets, due to phase separation of excess Ga in the GaN films. To study the transport properties in these films the Ga droplets are etched by emersing them in concentrated HCl. The insulating films, which are grown at high nitrogen overpressure are free of Ga droplets.

The structure and surface morphology of these films were reported elsewhere.[10] X-ray diffraction studies indicate that the films are high-quality single crystals with full width at the half-maximum of the $\theta$-rocking curves found to be $\sim$10-20 min.

The films were grown at a deposition rate of 0.2 $\mu$m/h and were 1–2-$\mu$m thick. The samples were abrasively etched into Van der Pauw lamilla and ohmic contacts were made by annealing indium pads. The transport coefficients were measured from 10 to 300 K in a closed loop helium cryostat. The magnitude of the magnetic field was varied up to 7 kG and the current through the sample was varied from $10^{-5}$ to $10^{-3}$ A.

The resistivities of the investigated samples at 300 K are shown in Table I. All the samples are *n*-type and their room temperature resistivities vary from 0.01 to 0.12 $\Omega$ cm. Figure 1 shows the Hall coefficient vs $1/T$ for the investigated samples. For the more resistive samples (118, 119, 110, 115) the Hall coefficient goes through a maximum. The temperature at which this maximum occurs is higher for samples with lower resistivity. The Hall coefficients for all the samples saturate to constant values at low temperatures. The resistivity vs $1/T$ of the investigated films is shown in Fig. 2. In all samples the resistivity initially increases as the temperature is lowered and then saturates to a constant value.

The observed decrease in the Hall coefficient at low temperatures is not typical for semiconductors.[illegible] Similar behavior has been observed for GaN films grown by chemical vapor deposition.[14,15] The data of Figs. 1 and 2 bear resemblance to behavior observed in *p*-type and *n*-type Ge,[illegible] where a model involving transport in both the defect centers and the conduction band was introduced to explain

TABLE I. Room temperature resistivities of the investigated samples.

| Sample | Thickness [μm] | Type | Resistivity at 300 K [Ω cm] |
|---|---|---|---|
| 118 | 1.9 | *n* | 0.121 |
| 119 | 1.7 | *n* | 0.074 |
| 110 | 1.8 | *n* | 0.038 |
| 115 | 1.8 | *n* | 0.025 |
| 114 | 1.1 | *n* | 0.012 |

the phenomenon. The conduction in the defect centers may be either diffusive, due to the small but finite overlap of the localized electron wave functions of the defect centers or hopping.[17] Therefore the defect band mobility is expected to be small compared to the conduction band mobility, and defect band conduction only becomes dominant when carriers in the conduction band become negligible.

The results of Figs. 1 and 2 can be fitted to such a two-band model in order to determine the relative concentration and the corresponding mobilities of electrons in the autodoping centers and the conduction band. Let us assume that the donor concentration in our films is $N_d$, with an activation energy $\Delta E_d$, and that the concentration of deep compensating centers (due to defects such as dislocations) is $N_a$. At a given temperature, a portion of the net carrier concentration $(N_d - N_a)$ is excited into the conduction band and has mobility $\mu_c$ and concentration $n_c$. The unexcited carriers remain in the defect states with a much lower mobility $\mu_d$ and concentration $n_d$. The net carrier concentration of the conducting carrier is

$$N_0 = n_c + n_d = N_d - N_a. \tag{1}$$

Taking both these contributions into account, the Hall coefficient, $R_H$ can be expressed as[16]

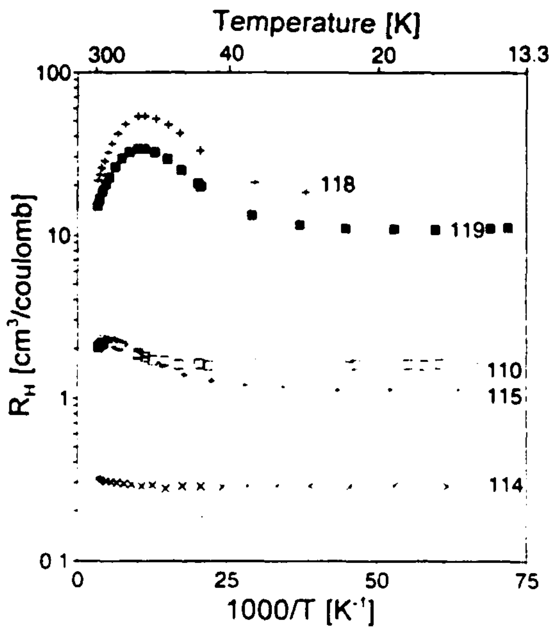


FIG. 1. Hall coefficient vs $1/T$.

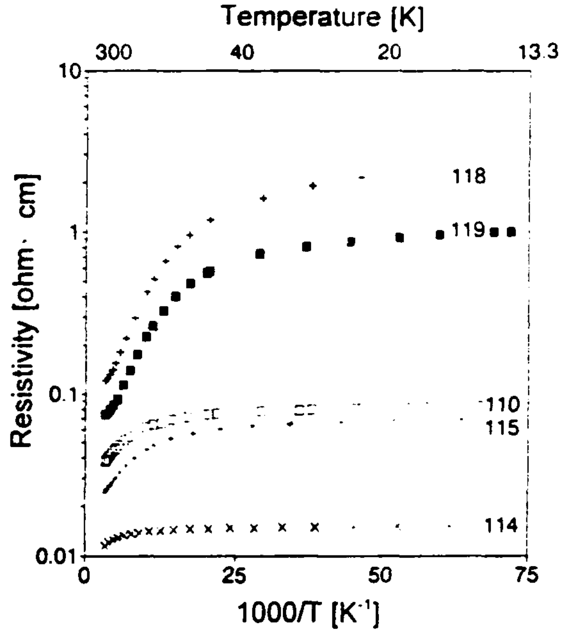


FIG. 2. Resistivity vs $1/T$.

$$R_H = \frac{n_c \mu_c^2 + (N_0 - n_c)\mu_d^2}{[n_c \mu_c + (N_0 - n_c)\mu_d]^2 e} \tag{2}$$

and the measured resistivity is

$$\rho = \frac{1}{\sigma} = \frac{1}{n_c e \mu_c + (N_0 - n_c) e \mu_d}. \tag{3}$$

Letting $b = \mu_d / \mu_c$, we have

$$eR_H = \frac{(1-b^2) n_c + N_0 b^2}{[(1-b) n_c + N_0 b]^2}, \tag{4}$$

$$\rho = \frac{1}{\mu_c [(1-b) n_c + N_0 b] e}. \tag{5}$$

Note that if $n_c$ is much larger than $n_d$ (the high temperature limit), the expression for $R_H$ reduces to the expression used for one-band conduction. However, for $\mu_d \neq 0$, as the temperature is lowered the carriers in the conduction band will decrease to the point where conduction through the defect states will dominate. It is also apparent from Eq. (4) that $eR_H$ at both temperature limits is the same and equal to $1/N_0$. If $b$ is not a strong function of temperature, it can be shown that $eR_H$ in Eq. (4) has a maximum

$$eR_{H_{max}} = \frac{(1+b)^2}{4 N_0 b}, \tag{6}$$

when

$$n_c = \frac{N_0 b}{(1+b)}. \tag{7}$$

Then the expression of $R_H$ in Eq. (4) qualitatively predicts the shape of the experimental curves shown in Fig. 1.

The parameters $\mu_d$, $\mu_c$, $n_c$, and $n_d$ are related to $R_H$ and $\rho$ by Eqs. (4) and (5). However, at each temperature, there are three unknowns for the two equations. Hung

TABLE II. Values of $N_0$ and $\Delta E_d$ for samples studied.

| Sample | $N_0$ [carrier/cm$^3$] | $\Delta E_D$ [meV] |
|---|---|---|
| 118 | $4.75\times 10^{17}$ | 19.09 |
| 119 | $5.80\times 10^{17}$ | 18.82 |
| 110 | $4.00\times 10^{18}$ | 32.16 |
| 115 | $5.56\times 10^{18}$ | 31.31 |
| 114 | $2.19\times 10^{19}$ | ··· |

*et al.*[16] analyzed the Ge data by assuming that the measurements at high temperatures were dominated by the conduction band electrons and extrapolated the carrier concentration curve to low temperatures to predict $n_c$ at low temperatures. However, we found that in our case, the defect band conduction is not negligible even at room temperature and therefore we did not adopt this approach.

In the case of a well-defined activation energy $\Delta E_d$, the carrier concentration in the conduction band is expected to change exponentially with temperature. The parameters $N_0$, $\Delta E_d$, and $\mu_c$, $\mu_d$ at each temperature can be extracted using Eqs. (4)–(7).[12] The extracted values of $N_0$ and $\Delta E_d$ for each of the samples are listed in Table II.

Figure 3 shows the temperature dependence of $\mu_c$ and $\mu_d$ calculated for sample No. 119. The temperature dependence of $\mu_c$ is typical of semiconductors. The scattering is dominated at low temperatures by ionized impurities and at high temperatures by phonon scattering. Figure 4 shows the temperature dependence of $n_c$ and $n_d$ calculated for the same sample (119).

If the concentration of donors is smaller than the deep defects known to exist in GaN films, the material will be fully compensated with its Fermi level pinned by these defects. In such a material, transport is dominated by hopping in the compensating centers leading to low electron mobilities.

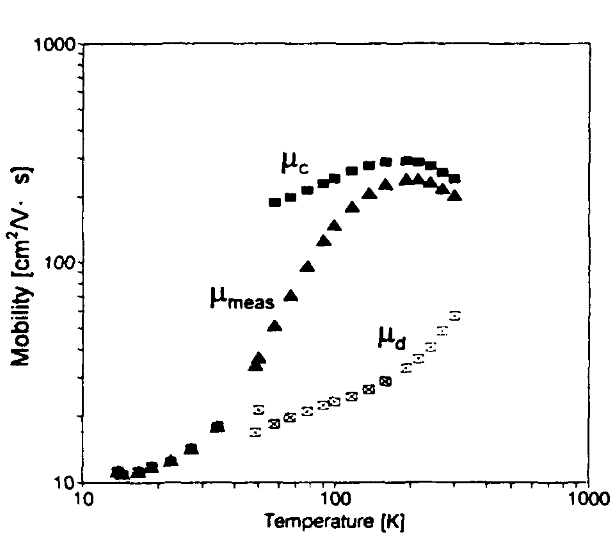


FIG. 3. Temperature dependence of $\mu_{meas}$, $\mu_c$, and $\mu_d$.

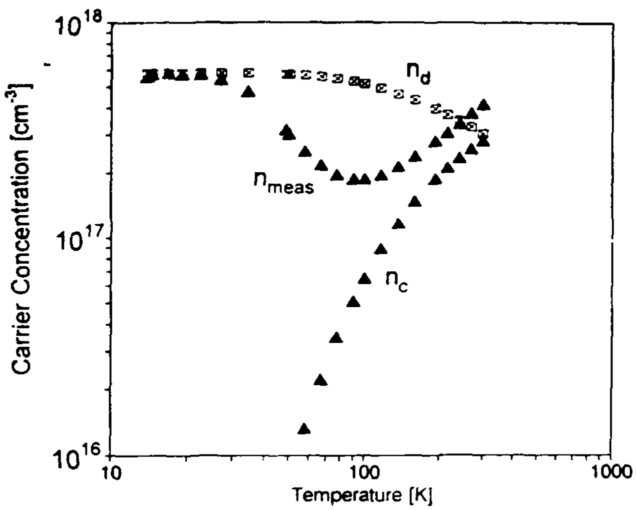


FIG. 4. Temperature dependence of $n_{meas}$, $n_c$, and $n_d$.

In conclusion, we studied the transport mechanism of a number of GaN films produced by the ECR-MBE method. The experimental results were accounted for by invoking conduction both through the conduction band and the autodoping centers at 20–30 meV below the conduction band. When the concentration of the autodoping centers becomes smaller than the deep compensating defects, the material becomes semi-insulating and the transport is determined by electron hopping through the deep compensating defects. This accounts for the low electron mobility of the semi-insulating GaN films. The nature of the autodoping centers is assumed to be nitrogen vacancies, and their energy levels are found to be 20–30 meV.


We would like to thank M. Yoder for his encouragement in this effort. This work was supported by the Office of Naval Research (Grant No. N00014-92-J-1436).



[1] H. P. Maruska and J. J. Tietjen, Appl. Phys. Lett. **15**, 327 (1969).
[2] J. I. Pankove, Mater. Res. Symp. Proc. **162**, 515 (1990).
[3] R. F. Davis, Proc. IEEE **79**, 702 (1991).
[4] M. Ilegems, J. Cryst. Growth **13/14**, 360 (1972).
[5] S. Nakamura, Jpn. J. Appl. Phys. **30**, L1705 (1991).
[6] R. C. Powell, G. A. Tomasch, Y. W. Kim, J. A. Thornton, and J. E. Greene, Mater. Res. Symp. Proc. **162**, 525 (1990).
[7] G. Menon, M. S. thesis, Boston University, 1990.
[8] T. Lei, M. Fanciulli, R. J. Molnar, T. D. Moustakas, R. J. Graham, and J. Scanlon, Appl. Phys. Lett. **59**, 944 (1991).
[9] T. Lei, T. D. Moustakas, R. J. Graham, Y. He, and S. J. Berkowitz, J. Appl. Phys. **71**, 4933 (1992).
[10] T. D. Moustakas, T. Lei, R. J. Molnar, Phys. B (to be published).
[11] T. D. Moustakas, R. J. Molnar, T. Lei, G. Menon, and C. R. Eddy, Jr., Mater. Res. Symp. Proc. **242**, 427 (1992).
[12] T. Lei, Ph.D. dissertation, Boston University, 1992.
[13] C. Kittel, *Introduction to Solid State Physics*, 6th ed. (Wiley, New York, 1986).
[14] M. Ilegems and H. C. Montgomery, J. Phys. Chem. Solids **34**, 885 (1973).
[15] I. Akasaki and H. Amano, Mater. Res. Symp. Proc. **242**, 383 (1991).
[16] C. S. Hung and J. R. Gliessman, Phys. Rev. **96**, 1226 (1954).
[17] N. F. Mott and T. D. Twose, Adv. Phys. **10**, 107 (1961).
[18] T. L. Tansley and R. J. Egan, Mater. Res. Symp. Proc. **242**, 395 (1992).

# Appendix E : “Metal Contacts to Gallium Nitride”

# Metal contacts to gallium nitride

J. S. Foresi and T. D. Moustakas
*Molecular Beam Epitaxy Laboratory, Department of Electrical, Computer, and Systems Engineering, Boston University, Boston, Massachusetts 02215*

(Received 19 October 1992; accepted for publication 9 March 1993)

We report measurements on the nature of aluminum and gold contacts to GaN. The GaN films were deposited onto the *R*-plane of sapphire substrates by molecular beam epitaxy and are autodoped *n*-type. Metal contacts were deposited by evaporation and were patterned photolithographically. Current-voltage characterization shows that the as-deposited aluminum contacts are ohmic while the as-deposited gold contacts are rectifying. The gold contacts become ohmic after annealing at 575 °C, a result attributed to gold diffusion. The specific contact resistivity of the ohmic aluminum and gold contacts were found by transfer length measurements to be of device quality ($10^{-7}$–$10^{-8}$ $\Omega$ m$^2$). The results of these studies suggest a direct correlation between barrier height and work function of the metal, consistent with the strong ionic character of GaN.

Gallium nitride (GaN) is a direct, wide band-gap semiconductor ($E_g \simeq 3.4$ eV) whose conduction band structure allows for a high saturation velocity ($3\times 10^7$ cm/s).[1,2] Due to these unique properties GaN is expected to find applications in optical devices (LEDs, lasers, detectors) operating in the spectral region from the blue to near-UV and in electronic devices such as high temperature, high power, and high frequency transistors.

GaN films are generally *n*-type[3] with carrier concentrations between $10^{18}$ and $10^{20}$ cm$^{-3}$ and electron mobilities of about 20 cm$^2$/V s. The *n*-type autodoping is attributed to nitrogen vacancies. The most important recent development is the discovery that AlN[4] and GaN[5–10] buffers lead to lateral growth which significantly improves the surface morphology and the electrical properties of the films.

In this letter, we report our initial investigation of metal/GaN contacts. Metals investigated include Al and Au. Current-voltage (*I-V*) measurements and transfer length measurements (TLM) of the specific contact resistivity are presented.

The GaN films used in this study were grown by the ECR-MBE method without a GaN buffer layer.[11,12] All films were deposited on sapphire substrates with *R*-plane orientation. X-ray diffraction studies show that the films have the wurtzitic crystal structure with $(11\bar{2}0)$ orientation, which leads to a faceted surface morphology.[12] The faceted surface makes these films unsuitable for planar devices, however, the metal contact results presented in this letter should be applicable to GaN films grown on other substrates and orientations. The transport coefficients were determined by Hall effect measurements using the Van der Pauw configuration. The investigated films were *n*-type with resistivities of about $10^{-1}$ $\Omega$ cm, carrier concentration of $3\times 10^{18}$ cm$^{-3}$ and Hall mobilities of about 20 cm$^2$/V s. The thickness of the films was 1.6 $\mu$m.

The Au and Al contacts were deposited on the GaN films by thermal evaporation and patterned using photolithography and liftoff techniques.[13] The base pressure of the evaporation unit was $10^{-7}$ Torr and the system was cryopumped to keep the chamber oil-free. Tungsten evaporation boats were used to evaporate 99.999% pure Al and Au. The substrates were kept at room temperature during the evaporation. Prior to photolithography, the samples were degreased. Following metal deposition, the metals were patterned using liftoff techniques which consisted of ultrasonic baths in acetone and methanol. The contacts were patterned in TLM structures which consist of three square contacts separated by known distances [see Fig. 1(a)]. The same contacts were also used in pairs to evaluate the rectifying nature of the metal/semiconductor interface by *I-V* characterization. Because these pairs of contacts were deposited on the surface of the GaN films, they constituted back-to-back Schottky barrier systems.

*I-V* characterization was carried out by injecting up to $\pm 20$ mA with a current source and measuring the voltage across the same contacts with an electrometer. *I-V* characterization was performed on both as-deposited metal contacts and metal contacts which had been annealed in a reducing atmosphere for 10 min at 575 °C. All of the measurements were made in atmosphere at room temperature.

Measurements of the specific contact resistivity were made using the TLM method which is employed widely in the characterization of ohmic contacts to semiconductors.[14–16] The technique requires the formation of contacts

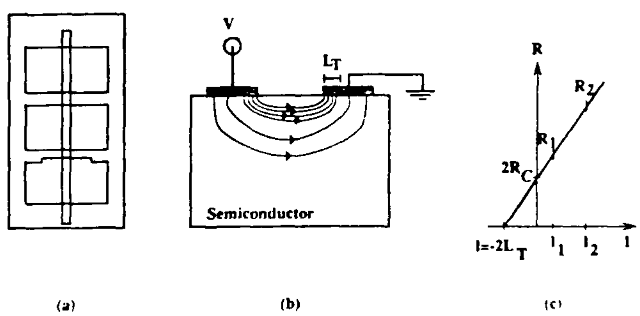


FIG. 1. (a) Sample configuration for *I-V* and TLM characterization. The thin vertical stripe is a 10 $\mu$m wide area of exposed GaN. The three wide rectangles are metal contacts separated by 20 and 15 $\mu$m. (b) Schematic of current flow through planar contacts. Nearly all of the current flows through one transfer length, $L_t$, of the contacts' front edges. (c) Plot of the measured resistance against the contact separation.

  

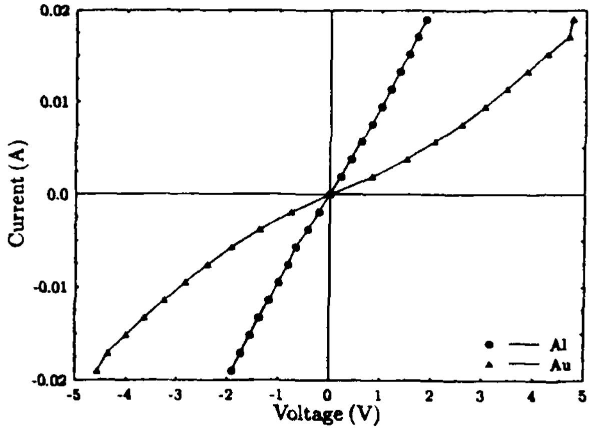


FIG. 2. $I$-$V$ characteristics of as-deposited Al/$n$-GaN and Au/$n$-GaN structures.

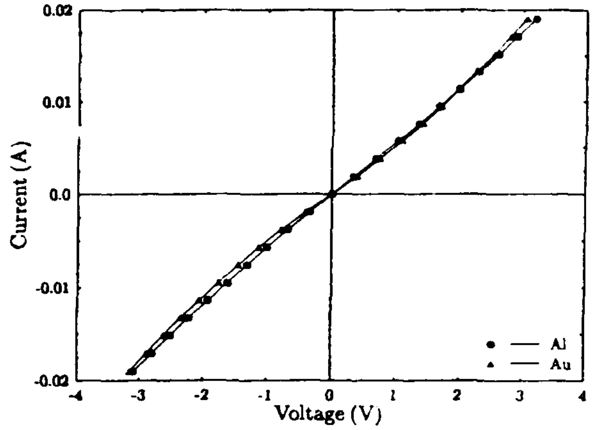


FIG. 3. $I$-$V$ characteristics of annealed Al/$n$-GaN and Au/$n$-GaN structures.

with controlled geometry and evaluates the difference in resistance between equally sized pairs of contacts separated by different distances. The specific contact resistivity ($\rho_c$) is calculated from a measurement of the effective contact resistance ($R_c$), the contact width ($W$), and the transfer length ($L_T$):

$$\rho_c = R_c W L_T. \tag{1}$$

The effective contact resistance is given by:

$$2R_c = \frac{R_2 l_1 - R_1 l_2}{l_1 - l_2}, \tag{2}$$

where $R_1$ is the resistance measured between contacts spaced $l_1$ apart and $R_2$ is the resistance measured between contacts spaced $l_2$ apart. In a planar contact configuration, nearly all of the current enters the semiconductor through a small area at the edge of the contact.[17] The parameter $L_T$ is the length of this area as indicated in Fig. 1(b). This quantity is estimated by plotting the resistance of two pairs of contacts against the distance separating the individual contacts within each pair. The line connecting the points $R_1$ and $R_2$ crosses the resistance axis at the $2R_c$ point and intersects the distance axis at the $-2L_T$ point [see Fig. 1(c)].

The TLM technique relies on the assumption that the semiconductor material under the contact has not been doped differently than the bulk material, and the accuracy of the method depends on the ability to control the separation between the contacts. Due to the faceted surface morphology in our films, the determination of the contact areas was difficult and limited the accuracy of the specific contact resistivity to within an order of magnitude.

The $I$-$V$ characteristics of the as-deposited Al and Au contacts are shown in Fig. 2. For both metals the $I$-$V$ curves are symmetric about the origin as is expected for back-to-back Schottky barriers where the characteristic is that of a reverse-biased barrier irrespective of the current polarity.[17] The Al contact $I$-$V$ characteristics are linear indicating that the contact is ohmic with no apparent barrier to current flow. In contrast, the $I$-$V$ characteristics of the Au contact exhibit curvature associated with the formation of a Schottky barrier. This Schottky barrier is leaky due to tunneling effects arising from the high carrier concentration of the films and the possible existence of an interfacial native oxide layer.[13] These results indicate that the barrier height depends on the metal used.

The $I$-$V$ curves for the same contacts after annealing, shown in Fig. 3, suggest that both the Al and Au contacts have changed during annealing. The $I$-$V$ curves of the Al contacts acquired a slight curvature and the calculated resistance increased by about 50%. These changes may be attributable to the formation of an interfacial AlN layer during the annealing process. No experimental work was performed to confirm the existence of such a layer. The $I$-$V$ curves of the Au contacts became practically linear. A similar result has been observed in Au contacts to GaAs and attributed to Au diffusion in GaAs.[18] Analytic measurements and electron microscopy have not been performed to confirm Au diffusion. The GaN material, however, has $10^{18}$–$10^{19}$ cm$^{-3}$ nitrogen vacancies which should facilitate the Au diffusion even though the material is tightly bonded.

The specific contact resistivities of Al and Au contacts were measured by the TLM method after annealing. The results in Table I show specific contact resistivities measured for a number of contact pairs on a single GaN sample. The variations in the contact resistivities can be attributed to the nonuniformity of the film. All of the contacts measured have specific contact resistances in the $10^{-7}$–$10^{-8}$ $\Omega$ m$^2$ range. The lowest specific contact resistivities

TABLE I. Specific contact resistivities for Au/$n$-GaN and Al/$n$-GaN after annealing. Measurements correspond to different TLM studies of a single sample.

| Metal | Specific contact resistivity ($10^{-7}$ $\Omega$ m$^2$) | Metal | Specific contact resistivity (10 [illegible] $\Omega$ m$^2$) |
|---|---|---|---|
| Au | 1.6 | Al | 0.12 |
| | 2.0 | | 4.4 |
| | 3.1 | | 1.3 |
| | 3.0 | | |

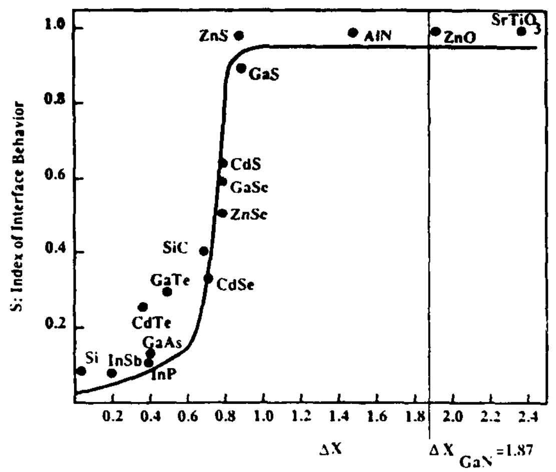


FIG. 4. Dependence of $S=d\phi_b/d\chi_m$ (change in barrier height over the change in metal work function) on the electronegativity difference between the components of the compound (after Ref. 20).

reported for GaAs are $\simeq 10^{-9}\ \Omega\,\mathrm{m}^2$ for high quality AuGeNi contacts.[18]

The simplest considerations of Schottky barrier formation between metals and semiconductors rely on the difference in work functions of the two materials to predict the barrier height. For a large number of important semiconductors, Si and GaAs included, the dependence of barrier height on work function difference has not been observed, a result attributed to the existence of surface states which pin the Fermi level at the interface.[19] The dependence of the barrier height on the work function difference has been correlated to the ionicity of the semiconductor by Kurtin and co-workers[20] as shown in Fig. 4. In this figure, the vertical axis is a parameter $S$ which is defined as the change in barrier height over the change in metal work function ($d\phi_b/dx_m$) and the horizontal axis is the electronegativity difference between the components of a compound which is a measure of the compound's ionicity. The direct dependence of the barrier height on the work function for the semiconductors with large electronegativity differences results from the bunching of surface states near the band edges where they have less effect on the surface Fermi level position.[17]

The electronegativity difference for GaN is 1.87 eV.[21,22] This puts GaN above the knee of the curve implying that Schottky barriers on GaN should have barrier heights which depend directly on the work function difference between the metal and GaN. The work function of GaN has been measured to be 4.1 eV.[23] Therefore, any metal with a work function equal to or lower than that of GaN should form essentially ohmic contacts to $n$-type GaN and any metal with a work function higher should form a rectifying contact to $n$-type GaN. The work function of Al is 4.08 eV (Ref. 22) putting Al in the ohmic category. The work function of Au is 4.82 eV (Ref. 22) which puts it in the rectifying category. Our results on Al and Au contacts to $n$-GaN are in agreement with the predictions of this model.

Based on these findings a variety of metals can be chosen to form either ohmic or Schottky barriers to $n$- or $p$-type GaN. For example, Al can form ohmic contacts to $n$-type GaN and Au can form ohmic contacts to $p$-type GaN. Other factors may also play a role in choosing the proper metals for contacts to GaN. For example, Au appears to diffuse upon annealing in the GaN. Thus, the use of Au as a contact to GaN requires a thin interlayer of Ti or Cr as a diffusion barrier.[15] Also, annealing of Al contacts may result in the formation of a thin insulating AlN interlayer, which will increase its contact resistance.

In conclusion, the nature of Al and Au contacts to $n$-GaN were investigated. It was found that the as-deposited Al- and Au-contacts are ohmic and rectifying, respectively. This result is in direct agreement with data indicating that ionic materials do not suffer from Fermi level pinning at metal/semiconductor interfaces. The lack of Fermi level pinning greatly reduces the complication of creating ohmic contacts to GaN as it is only necessary to determine metals with appropriate wor! functions. Measurements of the specific contact resistivities of Al and Au annealed contacts on GaN give values in the range of $10^{-7}$–$10^{-8}\ \Omega\,\mathrm{m}^2$ which are of device quality.

The authors benefited from collaborations with R. Molnar, W. Choi, and E. DeObaldia. Suggestions and discussions with Max Yoder and Scott Dunham are greatly appreciated. The work was supported by the Office of Naval Research (Grant No. N00014-92-J-1436).


[1] J. I. Pankove, MRS Symp. Proc. **162**, 515 (1990).
[2] P. Das and D. K. Ferry, Solid-State Electron. **19**, 76 (1976).
[3] R. F. Davis, Proc. IEEE **79**, 702 (1991).
[4] I. Akasaki and H. Amano, MRS Symp. Proc. **242**, 383 (1992).
[5] G. Menon, M. S. thesis, Boston University, 1990.
[6] T. Lei, M. Fanciuli, R. J. Molnar, T. D. Moustakas, R. J. Graham, and J. Scanlon Appl. Phys. Lett. **58**, 944 (1991).
[7] T. Lei, T. D. Moustakas, R. J. Graham, T. He, and J. Berkowitz, J. Appl. Phys. **71**, 4933 (1992).
[8] T. D. Moustakas, T. Lei, and R. J. Molnar, Physica B **185**, (1993).
[9] S. Nakamura, Jpn. J. Appl. Phys. **30**, L1705 (1991).
[10] R. J. Molnar, T. Lei, and T. D. Moustakas, Appl. Phys. Lett. **62**, 72 (1993).
[11] C. R. Eddy Jr., M. S. thesis, Boston University, 1990.
[12] C. R. Eddy, Jr., T. D. Moustakas, and J. Scanlon, J. Appl. Phys. **73**, 448 (1993).
[13] J. Foresi, M.S. thesis, Boston University, 1992.
[14] B. L. Sharma, *Metal-Semiconductor Schottky Barrier Junctions and Their Applications* (Plenum, New York, 1984).
[15] G. N. Maracas, *Gallium Arsenide Technology*, edited by D. K. Ferry (Howard W. Sams, Carmel, IN, 1989), Vol. 2.
[16] G. Stareev and A. Urrbach, J. Electron. Mater. **20**, 1059 (1991).
[17] H. K. Henisch, *Semiconductor Contacts* (Clarendon, Oxford, 1984).
[18] E. H. Rhoderick and R. H. Williams, *Metal-Semiconductor Contacts* (Clarendon, Oxford, 1988).
[19] J. Bardeen, Phys. Rev. **71**, 717 (1947).
[20] S. Kurtin, T. C. McGill, and C. A. Mead, Phys. Rev. Lett. **22**, 1433 (1969).
[21] C. M. Wolfe, N. Holonyak, Jr., and G. E. Stillman, *Physical Properties of Semiconductors* (Prentice Hall, Englewood Cliffs, NJ, 1989).
[22] K. W. Böer, *Survey of Semiconductor Physics* (Van Nostrand, New York, 1990).
[23] J. I. Pankove and H. E. P. Schade, Appl. Phys. Lett. **25**, 53 (1974).

# Appendix F : "Heteroepitaxy, Polymorphism, and Faulting in GaN Thin Films on Silicon and Sapphire Substrates"

# Heteroepitaxy, polymorphism, and faulting in GaN thin films on silicon and sapphire substrates

T. Lei and K. F. Ludwig,, Jr.
*Department of Physics, Boston University, Boston, Massachusetts 02215*

T. D. Moustakas
*Department of Physics, Boston University, Boston, Massachusetts 02215*
*and Department of Electrical Engineering, Boston University; Boston, Massachusetts 02215*

(Received 13 November 1992; accepted for publication 13 June 1993)

The structure of GaN films grown by electron-cyclotron-resonance-assisted molecular beam epitaxy on Si(111), Si(001), basal-plane sapphire, *a*-plane sapphire, and *r*-plane sapphire substrates was studied with four-circle x-ray diffractometry. Phase content, domain size, inhomogeneous strain, and in-plane and out-of-plane domain misorientations were measured and compared for films grown on each type of substrate. Wurtzite and zinc blende polymorphs were found to coexist in films grown on Si(111). The two structures grow in the (0002) and (111) orientations, respectively, so that they may transform into each other via stacking faults on close-packed planes. Smaller amounts of zinc blende material were also found in predominately (0002) wurtzitic films on *a*-plane sapphire and $(11\bar{2}0)$ wurtzitic films on *r*-plane sapphire.

## I. INTRODUCTION

The growth and properties of GaN films have been under extensive investigation because of their potential applications as light-emitting devices in the blue, violet, and near-ultraviolet spectra.[1,2] It is known that GaN exists in two polymorphs: wurtzite and zinc blende structures with direct band gaps of 3.4 and 3.2 eV, respectively. The two are analogous to hcp and fcc structures, respectively, in their stacking sequences. Since bulk GaN substrates are not available, films must be grown by heteroepitaxy on foreign substrates. The majority of GaN films reported have grown in the wurtzite structure, most commonly with the basal planes parallel to the substrate. However, epitaxial stabilization of the zinc blende phase has been obtained on GaAs, MgO, SiC, and Si substrates (see the citations in Ref. 1). All substrates used have a large mismatch to GaN films.

Despite the critical role which substrate symmetry and unit cell size must play in the formation of heteroepitaxial GaN films, relatively little detailed comparative structural work has been performed. While reflective high-energy electron diffraction (RHEED) is often used to characterize films *in situ*,[3–6] it probes only the surface structure of the growing film. Transmission electron microscopy (TEM) studies provide important information about the film microstructure and epitaxial orientation,[7,8] but they cannot quantitatively examine the degree of orientational order between film domains or reliably detect small phase components. In contrast, x-ray diffraction examines the structure of the bulk of the film, can quantify the degree of film orientational order, and can determine oriented minor phase content down to the $10^{-4}$ level. However, x-ray diffraction measurements limited to Bragg peaks from planes parallel to the substrate have significant limitations. Because the wurtzite and zinc blende structures simply differ in their packing sequences (ABAB and ABCABC, respectively), the wurtzite (0002) and zinc blende (111) stacking planes have the same lattice spacing. The wurtzite $(11\bar{2}0)$ and zinc blende (110) lattice spacings are also equal to each other. Standard $\theta$–$2\theta$ x-ray diffraction scans measure only the lattice plane spacings parallel to the film surface and therefore cannot distinguish between the zinc blende and wurtzite polymorphs if they have one of the above orientations. Moreover, rocking curves of these "on-axis" Bragg peaks (peaks due to lattice planes parallel to the surface)[9] show only the orientational order perpendicular to the substrate—they yield no information on the orientational order of film domains in the plane.

We report here a comprehensive x-ray diffraction study examining both the in-plane and out-of-plane structures of GaN films grown by electron-cyclotron-resonance-assisted molecular beam epitaxy on two of the most important substrates for technological applications—silicon and sapphire. Silicon substrates were of (111) and (001) orientation. Sapphire substrates were of (0001) (basal-plane), $(11\bar{2}0)$ (*a*-plane), and $(1\bar{1}02)$ (*r*-plane) orientations. The details of the growth process have been previously reported along with brief descriptions of some of the x-ray results.[10–13] All films studied here were approximately 1 $\mu$m thick and included a thin (~200 Å) GaN buffer layer at the substrate interface. We have found that wurtzite and zinc blende GaN polymorphs often coexist in these materials. This may explain the variable optical and transport measurements sometimes observed in GaN films.[14]

## II. EXPERIMENTAL METHODS

The x-ray diffraction measurements reported here used Cu $K\alpha$ radiation in conjunction with a sagitally focusing graphite (002) monochromator crystal and Soller slits for low resolution measurements and a Ge (111) crystal for high resolution determination of peak widths. The higher

  

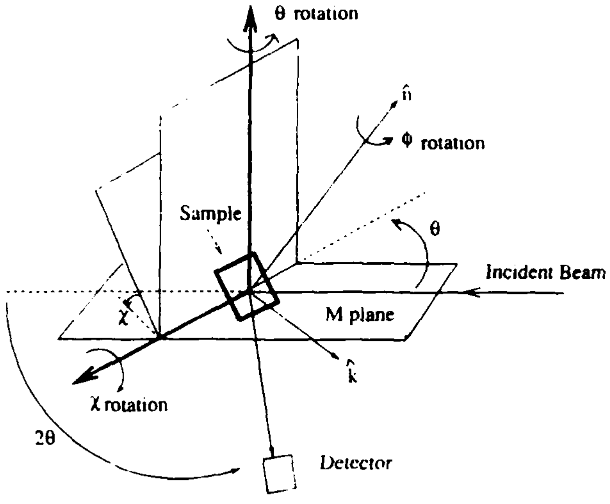


FIG. 1. Schematic of the Eulerian four-circle diffraction geometry.

flux graphite configuration was used for scans covering a wide range of angles and to examine weak peaks; its angular resolution is approximately 0.1°. The low flux of the Ge crystal configuration limited its application to relatively strong Bragg peaks; its angular resolution is approximately 0.01°, which is much smaller than the diffraction widths of the peaks observed from the GaN. Since most of the line shapes observed could be fit to a Lorentzian function, the instrumental resolution could be subtracted directly from the measured peak widths to yield the net peak width values cited throughout the rest of the paper.

The experiments utilized a four-circle diffractometer which allowed access to a large volume of reciprocal space.[15] A schematic of the four-circle geometry is shown in Fig. 1. The horizontal plane $M$ is defined by the incident and reflected beams; $\chi$ is defined as the angle between the sample surface and plane $M$ and $\chi=0$ when they are parallel. The angle $\phi$ measures the rotation around the surface normal of the substrate and $2\theta$ is defined as the angle between the incident and reflected beam. The angle $\theta$ measures the sample rotation around the axis perpendicular to the $M$ plane.

Several different types of scans were utilized to characterize the thin films. The simplest, $\theta$-$2\theta$ scans, measure the film structure along the surface normal $\hat{\mathbf{n}}$, giving information on phase presence and orientation. Homogeneous strain in the film due to uniform stress or nonstoichiometric composition is reflected in Bragg peak shifts relative to those expected from measured GaN lattice constants. Inhomogeneous strain and finite domain sizes act to broaden the $\theta$–$2\theta$ Bragg peaks. The full width at half-maximum (FWHM) of a Bragg peak in a $\theta$–$2\theta$ scan includes both effects[16]

$$\delta\theta=\frac{\lambda}{2D\cos\theta}+\epsilon_{\rm in}\tan\theta, \tag{1}$$

or, in reciprocal space

$$\delta k=\frac{2\pi}{D}+\epsilon_{\rm in}k. \tag{2}$$

Here $D$ is the average domain size, $\epsilon_{\rm in}$ is the inhomogeneous strain, i.e., the FWHM variation of the interplanar spacing $d$ through the film $\delta d/d$, and we assume that the finite domain size and inhomogeneous strain contributions lead to Lorentzian peak shapes. The different angular dependencies of the inhomogeneous strain and the domain size allow them to be separately determined from measurements of two or more diffraction peaks. Various factors can contribute to $\epsilon_{\rm in}$, including local stresses due to dislocations and mismatch as well as "stress-free" strain due to varying chemical stoichiometry through the film.

As mentioned in the introduction above, in many cases $\theta$–$2\theta$ measurements do not uniquely determine phase presence and orientation in GaN films. Because the wurtzite and zinc blende structures are based on a simple stacking sequence analogous to hcp and fcc packings, the (0002) and $(11\bar{2}0)$ planes of wurtzitic GaN films have identical spacings and structure factors as do the (111) and (220) planes of zinc blende GaN, respectively. Thus if a film grown in one of these orientations, $\theta$–$2\theta$ diffraction scans of these peaks cannot distinguish between the two polymorphs. However, the periodicities of the two structures are fundamentally different—the stacking sequence repeats every two planes in wurtzite; every three in zinc blende. Thus there are "off-axis" diffraction peaks from planes inclined relative to the substrate which unambiguously belong to either the zinc blende or the wurtzite structure. We have examined these to determine the phase contents of the films in this study.

We have also performed measurements to examine the orientational quality of the thin films. Rocking curves of $\theta$ around the on-axis Bragg peaks were used to examine the orientational spread of the film parallel to the surface normal. The spread of in-plane orientations as well as the epitaxial relationship between substrate and film axes in the plane were determined with $\phi$ scans, in which the sample was rotated about its normal while $\theta$, $2\theta$, and $\chi$ were held fixed at the peak position.

## III. EXPERIMENTAL RESULTS

### A. GaN on Si

#### 1. GaN on Si(111)

X-ray $\theta$–$2\theta$ scans of films on Si(111) show only two peaks which are indexed as the wurtzite (0002) and/or zinc blende (111) and their harmonic. The peak positions yield a $d$ spacing of 2.59 Å, which is consistent with previous lattice constant measurements.[1] No other peaks were observed, ruling out the existence of other epitaxial orientations down to the 0.1% level. Since data from only two peaks are available, the separation of the peak widths into domain size and inhomogeneous strain broadening using Eq. (1) has limited accuracy. However the theta FWHM of the fundamental peak and its harmonic are 0.08° and 0.19°, respectively, implying that the dominant contribution to the widths comes from an inhomogeneous strain of

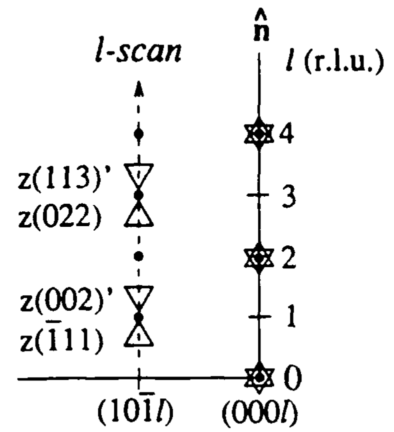


FIG. 2. Schematic of reciprocal space showing a scan along the $[10\bar{1}l]$ direction. The dots are allowed wurtzite reflections and the triangles show the allowed zinc blende reflections for each of the two twins (primed and unprimed). The off-axis zinc blende reflections are labeled with respect to the cubic cell, but the graph units are wurtzite reciprocal lattice units (r.l.u.).

approximately 0.2%. The grain size estimated from the peak widths is resolution limited, so that the coherent domain size must be larger than approximately 1500 Å.

In order to better investigate the polymorph content of the film, separate diffraction scans were performed in the [0001] direction through the wurtzite $(10\bar{1}l)$, $(1\bar{1}0l)$, and $(11\bar{2}l)$ reciprocal lattice points [Figs. 2 and 3 show the scan through the $(10\bar{1}l$ peaks]. The scans show that there are significant components of both wurtzite and zinc blende phases in the materials. The zinc blende further exists equally in its two twins corresponding to AB-CABC... and CBACBA...packing. The relative heights of the zinc blende and wurtzite peaks suggests that approximately 25% of the film is zinc blende and the remainder is wurtzite. The in-plane orientation between the two polymorphs is wurtzite $[10\bar{1}0]||$zinc blende $[1\bar{1}0]$, which is the orientation required in order for the close-packed planes of the two polymorphs to be in registry. It is noteworthy that

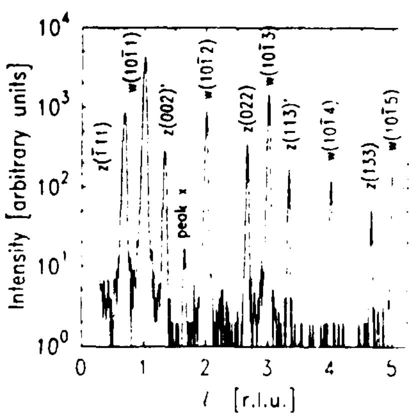


FIG. 3. A diffraction scan along the wurtzite $[10\bar{1}l]$ direction. The $l$ reciprocal lattice unit values refer to the wurtzite $c$ axis and the wurtzite and zinc blende peaks are labeled. The origin of the small peak at 2.66 r.l.u. is unclear.

earlier reports[17] of wurtzite formation on Si (111) could not distinguish between wurtzite and zinc blende structures, so that similar polymorph coexistence may have been present there as well.

It is possible that the zinc blende and wurtzite phases nucleate independently on the substrate. However, in cobalt and silicon carbide[18] it is known that the two analogous hcp and fcc polymorphs can nucleate each other at stacking faults on the close-packed planes. Moreover, twinning in metallic crystals as well as in CdTe[19] films can occur in the same way. It is therefore possible that the coexistence of the two polymorphs and of the two zinc blende twins in the GaN films may be related to the presence of stacking faults. While it is difficult to definitively confirm this with x-ray diffraction, TEM studies[21] performed after out initial reports of these results[22] have shown conclusively that wurtzite and zinc blende polymorphs do nucleate each other at stacking faults in InN films.

*Within* each of the two phases, however, the occurrence of stacking faults *can* be examined with x-ray diffraction.[20] The faults formed during the growth process here occur mostly on the close-packed plane parallel to the substrate, i.e., the growth plane of wurtzite (0002) and zinc blende (111). Therefore the on-axis wurtzite (0002) and zinc blende (111) peaks themselves are insensitive to stacking faults since they represent Fourier density components perpendicular to the stacking planes. However, faults do affect certain off-axis diffraction peaks from planes inclined relative to the surface.[20] In the wurtzite structure, those diffraction peaks $(hk.l)$ with $(h-k)\neq 3n$, where $n$ is an integer, are broadened by faulting so that the FWHM of a Bragg peak for diffraction scans along the [0001] diffraction is

$$\delta k=\frac{2\pi}{D}+\epsilon_{\rm in}k+\frac{2(3\alpha+3\beta)}{c} \tag{3}$$

for even $l$ and

$$\delta k=\frac{2\pi}{D}+\epsilon_{\rm in}k+\frac{2(3\alpha+\beta)}{c} \tag{4}$$

for odd $l$. Here we assume that the predominant faults in the material are deformation faults (...ABAB|CACA...) and growth faults (...ABAB|CBCB...) with probabilities $\alpha$ and $\beta$ of occurring in a given plane, respectively, and $c$ is the $c$-axis lattice constant. Measurements of the peak widths of the $(10\bar{1}3)$ and $(10\bar{1}4)$ peaks show that they both have an excess width associated with faulting of approximately 0.007 reciprocal lattice units $(2\pi/c)$. Thus the dominant faults appear to be the deformation faults with $\alpha\sim 0.007$ and the distance between faults is approximately $c/\alpha\sim 800$ Å.

It is more difficult to measure faulting densities accurately from the lower intensity zinc blende peaks. Those diffraction peaks $(hkl)$ with $(-h+2k-l)\neq 6n$ would be broadened and shifted by faulting.[20] If we assume that the predominant faults are deformation faults (...ABC|BCA...) with probability $\gamma$ on a given plane and

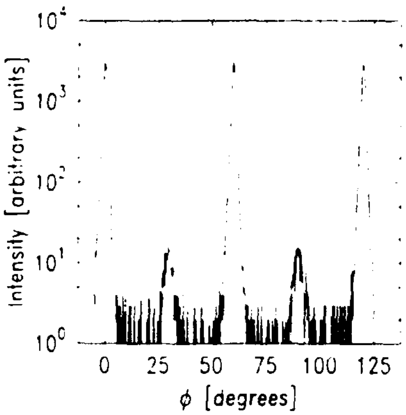


FIG. 4. A $\phi$ scan at the wurtzite $(1\bar{1}02)$ peak for a film on Si(111).

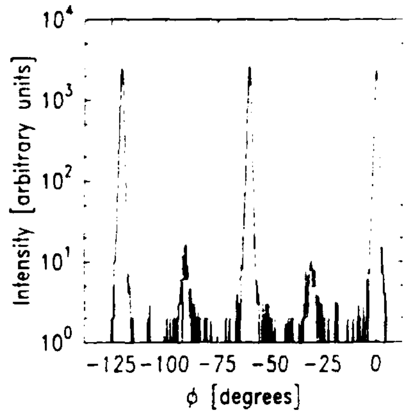


FIG. 5. A $\phi$ scan at the zinc blende $(\bar{1}11)$ peak for a film on Si(111).

twin faults (...ABCBA...) with probability $\zeta$, then the FWHM of a Bragg peak affected by faulting for scans in the [0001] direction is

$$\delta k=\frac{2\pi}{D}+\epsilon_{in}k+\frac{\sqrt{3}(3\gamma+2\zeta)}{a}. \tag{5}$$

Peak positions are shifted by $\pm 3\gamma/4\pi$ reciprocal lattice units $(2\pi/a)$, where $a$ is the cubic lattice constant. The lack of shifting and excess broadening in the zinc blende peaks measured with the high flux low resolution graphite monochromator limits the faulting probabilities to $\gamma$, $\zeta<0.005$. The distance between faults must therefore be greater than 600 Å in the zinc blende material.

In addition to the peaks which can be indexed to the wurtzite and zinc blende structures, there is a very small peak not belonging to these two phases in the $(11\bar{2}l)$ and $(1\bar{1}0l)$ scans at $l=1.66$ reciprocal lattice units. The position of a peak at a nonintegral $l$ value suggests that it could be due to a larger superstructure. Polytypes with long repeat periods are well known in the silicon carbide system.[18] However, no other peaks attributable to a long-period polytype are observed and calculations suggest that polytypes would not have a strong reflection at this position. The origin of the peak therefore remains unclear.

The orientational quality of the films normal to the substrate was examined with $\theta$ rocking curves at the wurtzite (0002)/zinc blende (111) peak. The FWHM of the rocking curve, which is a direct measure of the orientational spread of grains around the surface normal, is 0.9°. The orientational quality parallel to the substrate was measured with $\phi$ scans at the wurtzite $(1\bar{1}02)$ and zinc blende $(\bar{1}11)$ reflections. The dominant peak in the wurtzite $(1\bar{1}02)$ scan has the six fold symmetry expected from the hexagonal structure (see Fig. 4). However, very small peaks with slightly less than 1% of the intensity of the dominant peaks were observed at $\phi=30°$ and $\phi=90°$. These indicate that a small fraction of the domains have an in-plane orientation which differs by 30° from the bulk of the wurtzite component. Phi scans of the zinc blende $(\bar{1}11)$ show that these 30° misoriented domains exist in that polymorph as well (see Fig. 5). The in-plane orientational spread of the wurtzite film component is 1.9°, twice as large as the out-of-plane orientational spread. The epitaxial in-plane orientation is GaN$[11\bar{2}0]||$Si$[\bar{1}10]$. This is the same orientation as found in earlier growth studies.[17]

### 2. GaN on Si(001)

We have previously reported the results of $\theta$–$2\theta$ scans and rocking curves of GaN films on Si(001) substrates.[11,12] The dominant peaks in the $\theta$–$2\theta$ scans are indexed to zinc blende (002) and (004). The large widths of the two peaks, 0.40° and 0.72°, respectively, indicate a higher inhomogeneous strain and a smaller domain size than occurs on the Si(111) substrate. Application of Eq. (1) yields an approximate inhomogeneous strain of 0.6% and an effective domain size of 500 Å.

In addition to the dominant zinc blende (002) peak and its harmonic, the $\theta$–$2\theta$ scan shows a small peak at the position corresponding to zinc blende (111) and/or wurtzite (0002) orientations. Thus approximately 1% of the film has this orientation. TEM has shown that this component develops in the early stage of the buffer layer deposition.

The rocking curve of the (002) peak is 1.6° wide—much broader than that of GaN on Si(111). The in-plane orientational order of the dominant zinc blende (001) phase was examined with a $\phi$ scan of the (111) reflection. It shows a fourfold rotational symmetry with a spread of approximately 2.5° about the maxima. The $\phi$ scans show also that the epitaxial relationship between film and substrate is GaN (100) $||$Si(100).

In order to explore the existence of wurtzite and of stacking faults in the films, we have also performed a series of scans in the [111] and equivalent close-packed directions. Figure 6 shows such a scan from the (002) reciprocal lattice point to the (111) point. The size of the wurtzite peaks indicates that approximately 10% of the material is in that phase. However, twinning of the zinc blende in the film is quite small—approximately 1% of the zinc blende material is in the minor twin orientation. This suggests that one twin grows preferentially at the substrate interface and its orientation is maintained throughout the bulk of the film.

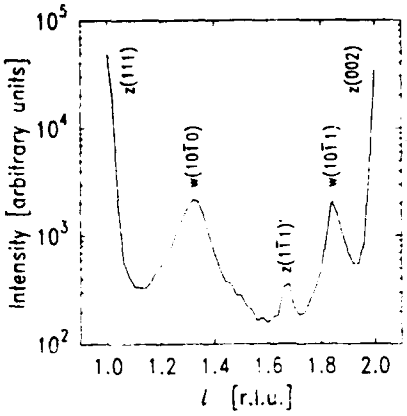


FIG. 6. A scan along the [11$\bar{1}$] direction from the (002) peak to the (111) peak for a film grown on Si(100). The stacking fault density is sufficiently high that the Bragg peak intensity is smeared into a streak in this direction (the background to the streak is approximately 2 on this scale). The $x$ axis refers to the $l$ component of the scan and is in reciprocal lattice units referenced to the zinc blende lattice constant. Peaks due to the two zinc blende twins (primed and unprimed) and to the wurtzite polymorph are indicated.

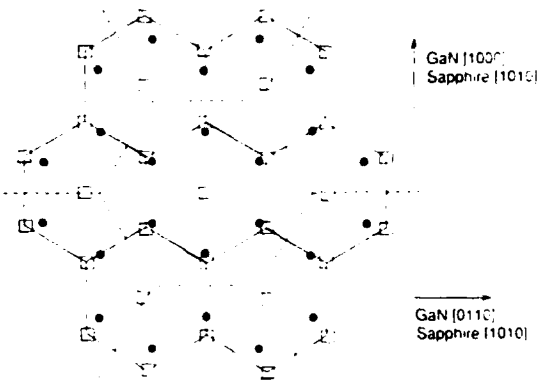


FIG. 7. Projection of bulk basal-plane sapphire and GaN cation positions for the observed epitaxial growth orientation. The dots mark aluminum atom positions and the dashed lines show the sapphire basal-plane unit cells. The open squares mark gallium atom positions and the solid lines show the GaN basal-plane unit cells. The aluminum atoms on the sapphire plane sit at positions approximately 0.5 Å above and below the plane position.

Together, Fig. 6 and scans perpendicular to it show that the faulting density in the film is so high that the Bragg peak intensities are spread into a streak along the close-packed direction; the background on which this streak sits is only two on the scale of the figure. Scans along the other three equivalent [111] cubic directions show a similar behavior. Thus the material has a very high density of stacking faults on all four sets of zinc blende close-packed planes, which are inclined at 54.74° relative to the growth plane of (001). In Fig. 6, the wurtzite (10$\bar{1}$0) peak has approximately twice the width (0.19 wurtzite reciprocal lattice units) of the (10$\bar{1}$1) peak (0.095 wurtzite reciprocal lattice units). If we assume that the average domain size of the wurtzite is much larger than the distance between stacking faults, then application of Eqs. (3) and (4) yields values of $\alpha \sim 0.05$ and $\beta \sim 0.15$. Thus the wurtzite material is indeed highly faulted—there are stacking faults every few unit cells! As Fig. 6 shows, the zinc blende peaks are all much narrower than the wurtzite peaks. Their small width implies that the distance between stacking faults in the zinc blende polymorph is at least 500 Å.

### B. GaN on sapphire substrates

#### 1. GaN on basal-plane sapphire

As was the case with the Si(111) substrate, the $\theta$–$2\theta$ scan of the GaN film on basal-plane sapphire shows two dominant peaks which correspond to wurtzite (0002) and/or to zinc blende (111) and their harmonic. The widths of the two peaks are 0.06° and 0.11°, from which the grain size is estimated to be greater than 1500 Å and the homogeneous strain to be approximately 0.8%.

In order to further examine the polymorph content of the film, we also searched for ($\bar{1}$11) reflections of (111) oriented zinc blende grains. In contrast to the case for GaN grown on Si(111), however, there is no zinc blende (111) intensity down to the $10^{-4}$ level.

The $\theta$-rocking curve of the film (0002) peak has a FWHM of 0.4°. This is comparable to that observed by Sasaki and Zembutsu[22] in films grown with metalorganic chemical vapor deposition (MOCVD) and by Shintani *et al.*[23] using HVPE, but significantly smaller than that in MOCVD films grown on AlN buffers by Amano *et al.*[9] Phi scans at the off-axis (1$\bar{1}$02) wurtzite reflection of GaN display the dominant reflection peak as $\phi$ rotates every 60°, a result of the 6/m symmetry of the rotation axis, as is in the case on Si(111). However, here no in-plane misoriented domains were observed. The in-plane orientational spread is 0.8°, about twice as large as the out-of-plane orientational spread. The in-plane orientation of the film is found to be GaN (11$\bar{2}$0)||sapphire (1$\bar{1}$00). This is in agreement with previous reports on GaN films on basal-plane sapphire grown by a variety of techniques.[3–6,24] The lattice mismatch between GaN and the basal plane of the sapphire hexagonal unit cell is over 30%. However, as noted by Kosicki and Kahng,[4] the mismatch is significantly less ($\sim$15%) between the wurtzite basal plane unit cell and a smaller hexagonal cell within the sapphire unit cell. The smaller cell of Al atoms on the basal-plane sapphire is oriented 30° away from the larger sapphire unit cell, in agreement with the GaN orientation found experimentally. Figure 7 shows that this epitaxial orientation gives relatively good agreement between the bulk atomic positions of Al atoms in the sapphire and Ga atoms in the film.

#### 2. GaN on a-plane sapphire

As is the case for GaN grown on Si(111) and basal-plane sapphire, $\theta$–$2\theta$ scans of GaN film on a-plane sapphire show peaks corresponding well to previously published values of the wurtzite (0002) interplanar spacing. The FWHM of the two peaks are 0.06° and 0.11°, the same as those for GaN on $c$-plane sapphire, so that the grain size and inhomogeneous stress are similar. The off-axis zinc blende ($\bar{1}$11) peak was examined to measure the percent-

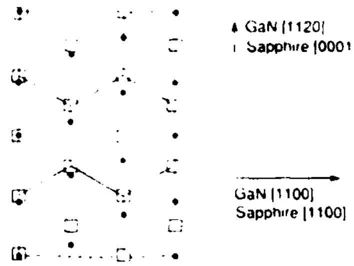


FIG. 8. Projection of bulk $a$-plane sapphire and basal-plane GaN cation positions for the observed epitaxial growth orientation. The dots mark aluminum atom positions and the dashed lines show the sapphire $a$-plane unit cell. The open squares mark gallium atom positions and the solid lines show the GaN basal-plane unit cells.

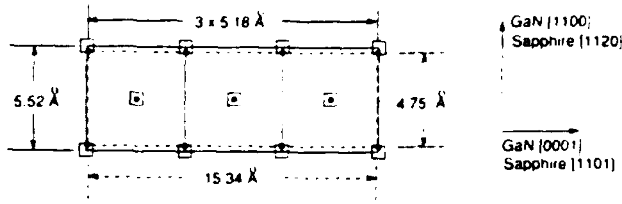


FIG. 9. Projection of bulk $r$-plane sapphire and $a$-plane GaN cation positions for the observed epitaxial growth orientation. The dots mark aluminum atom positions and the dashed lines show the sapphire $r$-plane unit cell. The open squares mark gallium atom positions and the solid lines show the GaN $a$-plane unit cells.

age of (111) oriented cubic phase present. The peak's intensity suggests that approximately 1% of the material has the zinc blende structure. A previous examination by Wickenden *et al.*[24] of GaN films deposited by vapor phase epitaxy had reported only the growth of wurtzitic material. It is unclear, however, that the study could distinguish between the wurtzite and zinc blende polymorphs.

Although the domain size and inhomogeneous strains of the GaN films grown on $a$-plane sapphire are similar to those for films grown on basal-plane sapphire, the $\theta$-rocking curve of the film on $a$-plane sapphire has a FWHM of 0.6°, 50% larger than that of GaN on basal-plane material. Phi scans at the off-axis wurtzite $(1\bar{1}02)$ reflection show no in-plane misoriented domains, as is the case with basal-plane sapphire. However, the in-plane orientational spread here is significantly larger—1.4°. The in-plane epitaxial relationship was found to be GaN $[11\bar{2}0]$||sapphire $[1\bar{1}00]$. As Wickenden *et al.*[24] point out, in this orientation the bulk positions of the substrate and film cations lie along lines in the sapphire [0001] direction (see Fig. 8). The mismatch between the substrate and film row spacings is only ~0.7%, although many of the substrate and film cation positions do not show a good correspondence.

### 3. GaN on r-plane sapphire

When $\theta$ was aligned with respect to the GaN reflection, $\theta$–$2\theta$ scans from films grown on $r$-plane sapphire showed only a peak which can be indexed to the wurtzite $(11\bar{2}0)$ or zinc blende (110) reflections. No peak from the sapphire substrate was observed. However, when $\theta$ was aligned with respect to the substrate reflection, the scan showed only the sapphire $(2\bar{2}04)$ peak. Thus the film planes are not exactly parallel to the $(1\bar{1}02)$ planes of the sapphire substrate. By varying $\phi$, it was found that the misorientation is approximately 1.5° and is along the GaN [0001] direction. In order to better measure the phase content of the films, we examined the zinc blende (111) off-axis peak. From its peak intensity, we estimate that only ~1% of the material is in the zinc blende phase; the majority is wurtzite. Again, previous studies have reported only the growth of wurtzitic GaN on $r$-plane sapphire,[3,5,22] but it is unclear that they had the ability to distinguish between the two polymorphs.

The FWHM of the $\theta$ rocking curve at the on-axis peak is 0.6°. This is comparable to values reported by Sasaki and Zembutsu[22] on films grown by MOCVD. In order to examine the in-plane orientation, a $\phi$ scan was performed at the wurtzite $(1\bar{1}00)$ reflection. The scan shows a repetition every 180° in $\phi$, which is a result of the twofold symmetry of $a$-plane GaN. The in-plane orientational spread is 6.7°, the largest for all of the GaN films. Phi scans show that the in-plane orientations between the two film polymorphs and the substrate are wurtzite (0002)|| sapphire $(1\bar{1}01)$|| zinc blende $(1\bar{1}\bar{1})$. The wurtzite epitaxial orientation is the same as that found in previous reports of films grown on $r$-plane sapphire.[3,5,22] Surface studies have found that corundum $r$-plane surfaces are quite stable and evidently do not significantly reconstruct.[26] It is therefore interesting to note the good agreement between bulk substrate and film cation positions in the experimental epitaxial orientation, as Fig. 9 shows. The lattice mismatch is only 1.3% in the sapphire $[\bar{1}101]$ direction, although it is ~15% in the $[11\bar{2}0]$ direction. The particularly small mismatch in the sapphire $[\bar{1}101]$ direction may be responsible for the small tilt between the GaN planes in the film and the substrate planes. Since the film axis in this direction is slightly longer than that of the substrate, the film planes may tilt up slightly in order to better match the projection of the GaN unit cells onto the interface with the sapphire unit cells below. Because of the twofold rotational symmetry of the sapphire $r$-plane unit cell, however, it is unclear why film domains grow with a misalignment in only one of the two possible directions. An alternate possibility is that the film tilt is related to a miscut of the substrate wafer. However, the tilt was observed in several films and was always oriented along the sapphire $[\bar{1}101]$ direction.

## IV. DISCUSSION AND CONCLUSIONS

The results of our four-circle x-ray diffractometry suggest that the coexistence of wurtzite and zinc blende polymorphs in GaN thin films may be widespread. As discussed above, most previous studies would not have been able to distinguish between the two, especially if one polymorph exists only at the 1% level. Since the two have different band gaps and possibly different doping capabilities, it is imperative that future investigators interested in optical and transport properties also evaluate their films' phase content. For this purpose x-ray or electron diffraction measurements of off-axis Bragg peaks are both suitable, but x-ray diffraction may have somewhat greater sensitivity to small volume fractions and it requires no sample thinning.

To our knowledge, these are the first experiments which have examined the orientational quality of GaN films in the film plane. On all of the films, the range of orientation angles in the plane is 1.5 to 10 times larger than along the film normal. In-plane misorientations between domains may therefore be the more important in creating domain boundary recombination sites due to broken bonds.

It is noteworthy that the measured film lattice constants in this work are all equal to accepted literature values to within experimental error. Since the lattice parameter is sensitive to the nitrogen concentration,[27] this implies that the films' compositions are not too far off stoichiometry. We have, however, observed significant variations in GaN lattice parameters with varying growth temperature which we attribute partly to the formation of large numbers of nitrogen vacancies.[28] It is widely believed that such nitrogen vacancies autodope films $n$ type.[1] The agreement between previously reported lattice constants and those observed here also suggests that the interfacial strain in the films relaxes on length scales significantly smaller than the film thickness. Given the large mismatches present between substrate and film, this is not surprising. For GaN on Si(111) and Si(001) substrates the lattice mismatch is $\delta=21\%$. As Figs. 7–9 show, however, films grown on sapphire orient themselves to match the bulk atomic positions of the film and substrate and decrease the effective lattice mismatch below the values for epitaxy on silicon. We note that, in fact, the GaN films do not grow directly on the sapphire substrate surfaces, but rather on very thin AlN layers which grow during the substrate $N_2$ plasma cleaning process.[13] However, the AlN lattice constant is quite close to that of GaN (3.11 vs 3.19 Å) and our RHEED measurements indicate that the AlN has the same orientation as does the GaN film which grows on top of it. Unfortunately, the detailed structure of the interface is unknown so the importance of matching bulk atomic positions in the early stages of film growth is unclear. Despite the reasonably good match of cation positions in the GaN films grown on $r$-plane sapphire, the orientational spread in the film plane is quite large. Clearly a better understanding of the early growth kinetics and of the interfacial structure would be quite helpful in explaining the epitaxial relationship between film and substrate.

The dominant mechanisms causing the inhomogeneous strains measured in these materials is unclear. Since the films appear to relax quickly to their bulk lattice parameter and are relatively thick, it is unlikely that $\epsilon_{in}$ could be dominated by misfit stresses from the substrate interface. However, dislocations introduced to relieve the lattice mismatch could create microstresses which would cause local variations in the lattice constant. While we know of no experimental work relating the GaN band gap to the lattice parameter, LCAO calculations suggest that the energy matrix elements $V$ which determine the band gap vary as the inverse square of the separation between atoms.[29] Therefore $\delta V/V=2\delta d/d$, and a 1% inhomogeneous strain would lead to approximately a 2% variation of the band gap. This then could be a significant source of band tailing. Nitrogen vacancies would presumably be the principal mechanism contributing "stress-free" strain due to composition inhomogeneity. While a decrease in nitrogen stoichiometry significantly decreases the wurtzite lattice parameters,[27] we know of no quantitative data relating stoichiometry and lattice constants which would allow us to interpret the inhomogeneous strain in terms of nitrogen deficiencies.

All of the films except those on Si(001) have domain sizes along the surface normal which are larger than our instrumental resolution. The very large stacking fault density in GaN films on Si(001) along with their large spread of in- and out-of-plane orientation angles and relatively large inhomogeneous strain suggest that, structurally, these are the worst films overall. The very large spread of in-plane orientations in the films on $r$-plane sapphire also implies that there are domain boundaries within the film with a relatively large angle of mismatch. In terms of orientation quality and domain size, then, the best films appear to be those which grow on their closed-packed planes. The films on sapphire (0002) substrates are the best of these, with relatively small in- and out-of-plane misorientation and little secondary phase. Despite their orientational quality, however, it appears likely that stacking faults are common in all of the GaN films. The impact of stacking faults on carrier mobility is unclear. Away from fault edges, their main effect will likely be to cause a local variation in the band gap. At the fault edges, however, bonds will be broken, producing deep states in the gap. Clearly significant work is required in order to examine the relationship between stacking fault density and electrical properties and to develop approaches which minimize the formation of faults in the growth process.

## ACKNOWLEDGMENTS

We would like to thank G. Morales and Y. Xie for their help with the x-ray measurements. This work was supported by the Office of Naval Research (Grant No. N00014-92-J-1436).

[1] R. F. Davis, Proc. IEEE 79, 702 (1991); R.F. Davis, Z. Sitar, B. E. Williams, H. S. Kong, H. J. Kim, J. W. Palmour, J. A. Edmond, J. Ryu, J. T. Glass, and C. H. Carter, Jr., Mater. Sci. Eng. B 1, 77 (1988).
[2] J. I. Pankove, Mater. Res. Soc. Symp. Proc. 162, 515 (1990).
[3] M. Sano and M. Aoki, Jpn. J. Appl. Phys. 15, 1943 (1976).
[4] B. B. Kosicki and D. Kahng, J. Vac. Sci. Technol. 6, 593 (1969).
[5] S. Yoshida, S. Misawa, and S. Gonda, J. Appl. Phys. 53, 6844 (1982).
[6] S. Yoshida, S. Misawa, and S. Gonda, Appl. Phys. Lett. 42, 427 (1983).
[7] Z. Sita, M. J. Paisley, B. Yan, and R. F. Davis, Mater. Res. Soc. Symp. Proc. 162, 531 (1990).
[8] T. P. Humphreys, C. A. Sukow, R. J. Nemanich, J. B. Posthill, R. A. Rudder, S. V. Hatangady, and R. J. Markunas, Mater. Res. Soc. Symp. Proc. 162, 531 (1990).

[9] H. Amano, N. Sawaki, I. Akasaki, and Y. Toyoda, Appl. Phys. Lett. **48**, 353 (1986); I. Akasaki and H. Amano, Mater. Res. Soc. Symp. Proc. **242**, 383 (1992).
[10] T. Lei, M. Fanciulli, R. J. Molnar, T. D. Moustakas, R. J. Graham, and J. Scanlon, Appl. Phys. Lett. **59**, 944 (1991).
[11] T. Lei, T. D. Moustakas, R. J. Graham, S. J. Berkowitz, and Y. He, J. Appl. Phys. **71**, 4933 (1992).
[12] T. Lei, T. D. Moustakas, Mater. Res. Soc. Symp. Proc. **242**, 433 (1992).
[13] T. D. Moustakas, R. J. Molnar, T. Lei, G. Menon, and C. R. Eddy, Jr., Mater. Res. Soc. Symp. Proc. **242**, 427 (1992).
[14] T. Lei and T. Moustakas (unpublished).
[15] W. R. Busing and H. A. Levy, Acta Cryst. **22**, 457 (1967).
[16] R. W. Vook, in *Epitaxial Growth*, edited by J. W. Matthews (Academic, New York, 1975), p. 339.
[17] Y. Morimoto, K. Uchiho, and S. Ushio, J. Electrochem. Soc. Solid-State Sci. Technol. **120**, 1783 (1973).
[18] R. W. G. Wyckoff, *Crystal Structures* (Interscience, New York, 1963), Vol. 1, p. 111.
[19] R. D. Horning and J.-L. Staudenmann, Appl. Phys. Lett. **49**, 1590 (1986).
[20] B. E. Warren, *X-ray Diffraction* (Addison–Wesley, Reading, 1969).
[21] S. Strite, D. Chandrasekhar, D. J. Smith, J. Sariel, H. Chen, N. Teraguchi, and H. Morkoc (preprint).
[22] T. D. Moustakas, T. Lei, and R. J. Molnar, Physica B **185**, 36 (1993).
[23] T. Sasaki and S. Zembutsu, J. Appl. Phys. **61**, 2533 (1987).
[24] H. Shintane, Y. Takano, S. Minagawa, and M. Mari, J. Electrochem. Soc. **125**, 2076 (1978).
[25] D. K. Wickenden, K. R. Faulkner, R. W. Brander, and B. J. Isherwood, J. Cryst. Growth **9**, 158 (1971).
[26] V. E. Henrich, Rep. Prog. Phys. **48**, 1481 (1985).
[27] O. Lagerstedt and B. Monemar, Phys. Rev. B **19**, 3064 (1979).
[28] C. R. Eddy, Jr., T. D. Moustakas, and J. Scanlon, J. Appl. Phys. **73**, 448 (1993).
[29] W. A. Harrison, *Electronic Structure and the Properties of Solids* (Freeman, San Francisco, 1980), p. 149.

Appendix G : “Conduction-electron spin resonance in zinc-blende GaN thin films”

# Appendix H : "Intensity dependence of photoluminescence in GaN thin films"

# Conduction-electron spin resonance in zinc-blende GaN thin films

M. Fanciulli and T. Lei
*Department of Physics, Boston University, Boston, Massachusetts 02215*

T. D. Moustakas
*Department of Physics and Department of Electrical, Computer and Systems Engineering, Boston University, Boston, Massachusetts 02215*
(Received 8 July 1993)

We report electron-spin-resonance measurements on zinc-blende GaN. The observed resonance has an isotropic $g$ value of $1.9533\pm0.0008$ independent of temperature, a Lorentzian line shape, and a linewidth (18 G at 10 K) which depends on temperature. The spin-lattice relaxation time at 10 K was estimated to be $T_{1e}=(6\pm2)\times10^{-5}$ sec. Using a five-band model a $g$ value consistent with the experimental results was obtained and a conduction-electron effective mass $m^*/m_0=0.15\pm0.01$ was calculated. The observed signal, together with conductivity data, was attributed to nonlocalized electrons in a band of autodoping centers and in the conduction band.

## I. INTRODUCTION

Gallium nitride is a wide-band-gap semiconductor which is anticipated to find applications for optical devices (light-emitting diodes, lasers, detectors) in the near uv region of the electromagnetic spectrum and electronic devices for high-power, high-frequency, and high-temperature applications. GaN was found to exist in two allotropic forms. The wurtzite structure is the thermodynamically stable phase and has an optical gap of 3.5 eV,[1,2] while the zinc-blende structure is a metastable phase which can be formed by epitaxial stabilization[3,4] and has an optical gap of 3.2 eV.[4] In both cases the material is found to be heavily autodoped $n$ type, a result attributed to nitrogen vacancies.[5] In general, the electron concentration is in the range of $10^{17}-10^{20}$ cm$^{-3}$.

In this paper we report electron-spin-resonance (ESR) studies in autodoped $n$-type zinc-blende GaN thin films. The data were correlated with electrical conductivity measurements and from their analysis the nature of the resonance was determined. The measured $g$ value was found to be in agreement with theoretical predictions based on a five-band model $\mathbf{k}\cdot\mathbf{p}$ calculation. The same calculation was also used to predict the electron effective mass.

## II. EXPERIMENTAL RESULTS AND DISCUSSION

The GaN films were grown by electron-cyclotron-resonance microwave plasma-assisted molecular-beam-epitaxy (MBE). Epitaxial stabilization of the zinc-blende structure was accomplished by using a two-temperature step process on Si(100). In this process a 200-Å GaN buffer was grown at 400 °C and the rest of the film, 4 μm thick, was grown at 600 °C. Both heavily autodoped and semi-insulating GaN films were fabricated and investigated. Transport studies in these films[6] show that the conductivity is dominated by the high-quality top layer rather than by the GaN buffer. Details on the growth are given elsewhere.[3,4] Structural studies (reflection high-energy electron diffraction, electron diffraction, and x-ray diffraction) show that the films are single crystals having the zinc-blende structure with lattice constant 4.5 Å.[3,4]

To conduct optical, transport, and spin-resonance measurements, self-standing GaN flakes were obtained by dissolving the Si substrate with a solution of $HNO_3$ and HF. The optical gap of the films was determined by transmission measurements and found to be 3.2 eV.[4] The electrical conductivity of one of the investigated films, determined by four probe measurements using sputtered Al contacts, is shown as a function of $1/T$ in Fig. 1. The data fit the expression

$$\sigma=\sigma_1\exp(-\varepsilon_1/kT)+\sigma_3\exp(-\varepsilon_3/kT)\ , \qquad (1)$$

where the activation energies $\varepsilon_1$ and $\varepsilon_3$ are 25 and 0.5 meV, respectively.

Hall-effect measurements show that the films are $n$ type; however, we were unable to perform accurate measurements of the carrier concentration on these self-standing GaN flakes. Based on our studies of wurtzite GaN films,[6] we anticipate that the investigated films have room-temperature carrier concentration of the order of $10^{17}-10^{18}$ cm$^{-3}$. The data of Fig. 1 are consistent with transport in the conduction band at temperatures higher than about 50 K and transport in a band of shallow donors at lower temperatures.[7]

The nature of these shallow donors is still controversial. They have been observed in GaN films produced by various deposition methods and attributed by early workers to nitrogen vacancies.[5] Our thin-film growth studies support this hypothesis. Since our films are grown at temperatures below the decomposition temperature of GaN, their stoichiometry can be controlled by varying the nitrogen overpressure during growth. At low active nitrogen overpressure we find that the films are $n$ type with carrier concentration between $10^{18}-10^{20}$ cm$^{-3}$. Such films tend also to be decorated with gallium drop-

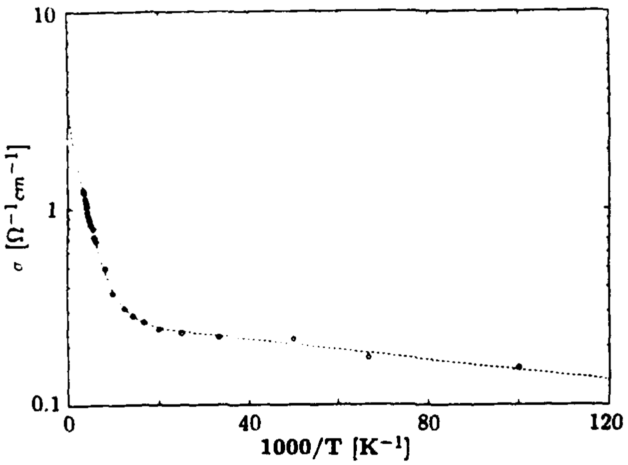


FIG. 1. Conductivity of GaN as a function of $1000/T$.

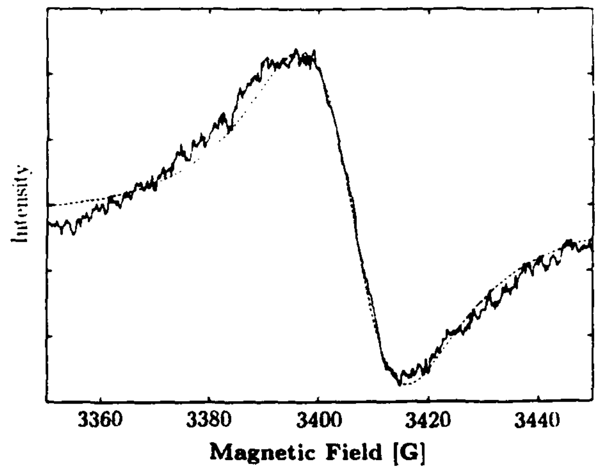


FIG. 2. First derivative absorption resonance line at 10 K and Lorentzian best fit.

lets, a result which we attribute to phase separation of excess gallium, presumably due to the narrow existence phase diagram of GaN. On the contrary, films produced under high nitrogen overpressure have carrier concentration between $10^{18}-10^{13}$ cm$^{-3}$ and their surface is free of gallium droplets. This trend is consistent with the formation of nitrogen vacancies during growth and, if their concentration is very high, some gallium is phase separated in order for the material to maintain the stoichiometry allowed by its phase diagram. The samples investigated in this paper were free of any gallium droplets. Additionally, there is also theoretical support that the nitrogen vacancy in GaN is a shallow donor. Tight-binding calculations by Jenkins and Dow[8] have shown that the neutral unrelaxed N vacancy is a shallow donor with its singly occupied $p$-like level ($T_2$) in the conduction band and its doubly occupied $s$-like level ($A_1$) in the band gap close to the conduction-band edge. It is anticipated that lattice relaxation should shift the singly occupied level in the energy gap.

ESR measurements were performed at different temperatures in a Varian E9 spectrometer at 9.3 GHz, 100-kHz modulation frequency, and 0.5–1.0-G modulation amplitude. An $\alpha,\alpha'$-diphenyl-$\beta$-picrylhydrazyl reference was used to evaluate the $g$ value. Figure 2 shows the ESR spectrum at 10 K of the same sample discussed in Fig. 1. This resonance has an isotropic $g$ value of $1.9533\pm0.0008$ independent of temperature. The shape of the line is Lorentzian and the peak-to-peak linewidth ($\Delta H_{pp}=18\pm1$ G at 10 K) has a temperature dependence shown in Fig. 3. The broadening of the line with the increase in temperature prevented us from observing the resonance at temperatures higher than 110 K. The temperature dependence of the electron-paramagnetic-resonance (EPR) intensity is shown in Fig. 4.

From the saturation behavior of the resonance we estimated a spin-lattice relaxation time, at 10 K, of $(6\pm2)\times10^{-5}$ sec. No ESR signal was observed in semi-insulating GaN films.

To discuss the nature of the observed resonance we should first rule out that such a signal is not due to either plasma resonance or cyclotron resonance. Plasma resonance is ruled out based on the prediction of Dresselhaus,

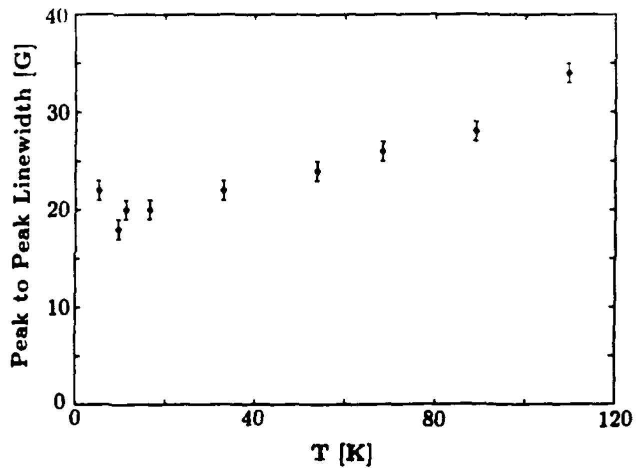


FIG. 3. Peak to peak linewidth $\Delta H_{pp}$ as a function of temperature.

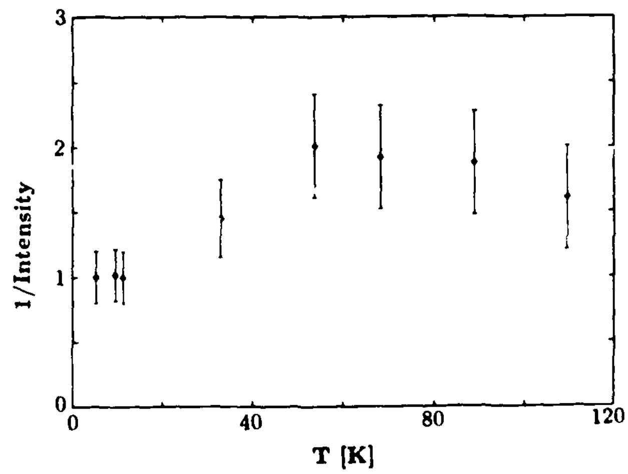


FIG. 4. Intensity of the EPR signal as a function of temperature (normalized to the value obtained at 5 K).

Kip, and Kittel[9] that the resonance moves to lower magnetic field as the frequency is increased. To test this we varied the microwave frequency in our experiment from 9.3 to 9.5 GHz and observed that the resonance moved to higher magnetic field instead. Electron cyclotron resonance also is ruled out since, assuming an effective mass similar to that of wurtzite GaN ($m^*/m_0=0.20\pm0.02$) (Ref. 10) the resonance should occur at a magnetic field $\sim5$ times smaller than it was actually observed; moreover, a mobility three orders of magnitude larger than the value reported in similarly prepared GaN films[6] would be required to obtain a distinctive signal in the $X$ band.

The observed resonance is therefore related to the ESR signal whose origin is due either to deep localized defects (intrinsic or impurities), or to delocalized electrons due to the shallow donors discussed earlier. However, the temperature dependence of the EPR intensity, shown in Fig. 4, does not follow the Curie-Weiss law suggesting that the electrons responsible for the observed resonance are not localized in deep defects. Additional arguments in favor of this conclusion are the lack of hyperfine or superhyperfine structure, expected for localized electrons in intrinsic defects of III-V semiconductors, and the lack of ESR signal in highly resistive films. The observed temperature dependence of the resonance intensity is not consistent with either a Curie or a Pauli paramagnetism. We can only speculate that the observed intermediate regime is related to the fact that the concentration of carriers in the band of the shallow donors as well as in the conduction band depend on temperature.

These findings, together with the conductivity data, suggest that the observed EPR signal at temperatures less than 50 K is due to delocalized electrons in the band of the previously discussed shallow donors and at temperatures higher than 50 K to electrons thermally activated into the conduction band. The fact that we did not observe a change in the $g$ value as a function of temperature suggests that, to within the experimental accuracy, the $g$ value is the same in both bands.

It is interesting to compare our experimental result of the electron $g$ value with theoretical predictions based on the five-band model $\mathbf{k}\cdot\mathbf{p}$ calculation[11-14] and estimate the electron effective mass. According to this model the $g$ value and the electron effective mass are given by the expressions

$$\frac{g^*}{g_e}-1=-\frac{P^2}{3}\left[\frac{\Delta_0}{E_0(E_0+\Delta_0)}+\lambda^2\frac{\Delta_0'}{(E_0'-E_0)(E_0'-E_0-\Delta_0')}\right], \quad (2)$$

$$\frac{m_0}{m^*}-1=\frac{P^2}{3}\left[\frac{3E_0+2\Delta_0}{E_0(E_0+\Delta_0)}-\lambda^2\frac{3(E_0'-E_0)-2\Delta_0'}{(E_0'-E_0)(E_0'-E_0-\Delta_0')}\right], \quad (3)$$

where $\Delta_0=\Gamma_{8v}-\Gamma_{7v}$, $\Delta_0'=\Gamma_{8c}-\Gamma_{7c}$, $E_0'=\Gamma_{8c}-\Gamma_{8v}$, and according to Chadi, Clark, and Burnham[13]

$$\lambda^2P^2=\frac{2}{m_0}|\langle\Gamma_{1c}\,p_x\,|\Gamma_{5c,x}\rangle|^2, \quad (4)$$

$$P^2=\frac{2}{m_0}|\langle\Gamma_{1c}\,|p_x|\Gamma_{5v,x}\rangle|^2. \quad (5)$$

Hermann and Weisbuch[14] presented an estimate of $P^2$ based on simplified linear combination of atomic orbitals,

$$P_{\rm est}^2=\frac{\hbar^2\eta^2}{a^2m_0}\left[\frac{(1-\alpha_p^2)^{1/2}-S}{2(1-S^2)}\right]^2, \quad (6)$$

where $\alpha_p$ is the polarity and $S$ is the overlap term[15] and $\eta$ is a best-fit parameter $\eta=(1.04\pm0.07)\times10^3$.[14] From this expression, with $\alpha_p=0.62$ (Ref. 15) and $S=0.5$,[14] one obtains for GaN $P_{\rm est}^2=28\pm2$ eV. With the following values $E_0=3.2$ eV, $\Delta_0=0.009-0.016$ eV,[16] $\Delta_0'=0.06-0.1$ eV,[17] $E_0'=8.7\pm0.3$ eV,[18] $\lambda^2=0.4$,[13] we obtained $g^*=1.95\pm0.01$ in agreement with our experimental result. The electron effective-mass calculation yields a value of $m^*/m_0=0.15\pm0.01$, a value close to that measured experimentally for GaN films having the wurtzite structure [$m^*/m_0=0.20\pm0.02$ (Ref. 10)].

A brief comment on the utilized values for $\Delta_0$, $S$, and $\lambda^2$ is necessary in order to put the previous calculation in the right perspective. Since the number and orientation of nearest and next-nearest neighbors are the same in the wurtzite and in the zinc-blende structures, the value of the spin-orbit splitting $\Delta_0$ for zinc-blende GaN should not be significantly different from the value evaluated for the wurtzite structure. The latter is known[16] and used in our calculation. The overlap integral $S$ and the parameter $\lambda^2$ depend primarily on the ionicity of the bond. GaN is the most ionic of the III-V compounds; however, its ionicity is close to the value for InP for which researchers have used $S=0.5$ (Ref. 14) and $\lambda^2=0.4$.[13]

The possible interaction mechanisms responsible for the spin-lattice relaxation rates of conduction electrons have been discussed by several authors.[19-21] As pointed out by Yafet[21] the dominant relaxation process, at least at not too low temperatures where the spin-current interaction should dominate, is the phonon modulation of the spin-orbit coupling. This mechanism gives the following spin-lattice relaxation rate:[21]

$$T_{1e}^{-1}\sim\frac{2}{\pi^{3/2}\hbar}\frac{D^2}{\rho u^2}\left[\frac{2m^*kT}{\hbar^2}\right]^{5/2}, \quad (7)$$

where $\rho$ is the density, $u$ the sound velocity, and, for a polar semiconductor, $D\sim Cf\delta g(\hbar^2/am^*E_0)$ with $C$ being the deformation potential, $f$ the relative strength of the crystal potential that is odd under inversion, $\delta g$ the $g$ shift, $a$ a parameter of the order of the lattice constant, and $E_0$ the optical gap. Using values appropriate to cubic GaN [$\rho=6.1$ g cm$^{-3}$, $u=6.9\times10^3$ msec$^{-1}$, $C\sim13$ eV,[22] $f=1$ (Ref. 11)] we find $T_{1e}\sim9\times10^{-5}$ sec at 10 K in general agreement with our experimental result.

In the effort to qualitatively account for the data of Fig. 3 we need to discuss spin-spin relaxation mechanisms which determine $T_{2e}$ and thus the magnitude of the linewidth $\Delta H_{pp}$. The analysis of the matrix elements which contribute to $T_{2e}^{-1}$, for the relaxation mechanism previously discussed, show the same **k** and **q** dependence as the matrix elements used for $T_{1e}^{-1}$. Therefore, $T_{1e}$ and $T_{2e}$ have the same temperature dependence.[21] However Eq. (7) would predict a difference in the linewidths at 10 and 100 K by a factor $\approx 300$, in contrast with the experimental results of Fig. 4. We believe that this disagreement is due to the fact that additional spin-spin relaxation mechanisms set in at low temperatures. One relevant relaxation mechanism at low temperatures is the hopping of electrons from one site to another. Such a process was observed to be the dominant line-broadening mechanism at low temperatures in heavily doped $n$-type silicon.[23] Our conductivity data have indicated hopping conduction, in the investigated sample at temperatures below 50 K, with an activation energy $\varepsilon_3 = 0.5$ meV due to overlap of the shallow donor wave functions and the presence of compensating defects.[7] In the case of hopping motion of electrons, the linewidth is inversely proportional to the probability $p$ of the phonon-assisted transition from one center to another, $\Delta H_{pp} \propto 1/p$. This probability depends on temperature as[7,24]

$$p \propto \left| \exp\left( \frac{\varepsilon_3}{kT} \right) - 1 \right|^{-1} . \tag{8}$$

Therefore, at low temperatures, where hopping is the dominant broadening mechanism, one should observe an increase in the linewidth as the temperature decreases, as perhaps suggested by our experimental point at 5 K.

## III. CONCLUSIONS

In conclusion, we reported the observation of an electron spin resonance in zinc-blende gallium nitride thin films produced by the electron-cyclotron-resonance microwave-plasma-assisted MBE method. The EPR signal was attributed to electrons predominantly in the band of autodoping centers (N vacancies) at low temperatures and in the conduction band at higher temperatures. The electron $g$ value was found to be $1.9533 \pm 0.0008$. Using a five-band model and appropriate parameters for GaN a $g$ value $g^* = 1.95 \pm 0.01$ in agreement with the experimental value was obtained and an effective mass $m^*/m_0 = 0.15 \pm 0.01$ was calculated.

From the saturation behavior of the resonance line a spin-lattice relaxation time of the order of $10^{-5}$ sec at 10 K was estimated in general agreement with the theoretical value predicted considering the phonon modulation of the spin-orbit interaction as the relaxation mechanism. The temperature dependence of the resonance linewidth was semiqualitatively accounted considering, besides the phonon modulation of the spin-orbit interaction, the hopping process at low temperature as an additional spin-spin relaxation mechanism.

## ACKNOWLEDGMENTS

This research was supported by the Office of Naval Research (Grant No. N00014-92-J-1436). We are indebted to Professor Hans Van Willigen of the University of Massachusetts for the use of the ESR facilities.


[1] J. I. Pankove, H. P. Maruska, and J. E. Berkeyheiser, Appl. Phys. Lett. **5**, 197 (1970).

[2] J. I. Pankove, in *Diamond, Silicon Carbide, and Related Wide Bandgap Semiconductors*, edited by J. T. Glass, R. F. Messier, and N. Fujimori, MRS Symposia Proceedings No. 162 (Materials Research Society, Pittsburgh, 1990), p. 515.

[3] T. Lei, M. Fanciulli, R. Molnar, T. D. Moustakas, R. J. Graham, and J. Scanlon, Appl. Phys. Lett. **58**, 944 (1991).

[4] T. Lei, T. D. Moustakas, R. J. Graham, Y. He, and S. Berkowitz, J. Appl. Phys. **71**, 4933 (1992).

[5] J. I. Pankove, S. Bloom, and G. Harbeke, RCA Rev. **36**, 163 (1975).

[6] R. J. Molnar, T. Lei, and T. D. Moustakas, Appl. Phys. Lett. **62**, 72 (1993).

[7] N. F. Mott and W. D. Twose, Adv. Phys. **10**, 107 (1961).

[8] D. W. Jenkins and J. D. Dow, Phys. Rev. B **39**, 3317 (1989).

[9] G. Dresselhaus, A. F. Kip, and C. Kittel, Phys. Rev. **100**, 618 (1955).

[10] A. S. Barker and M. Ilegems, Phys. Rev. B **7**, 743 (1973).

[11] M. Cardona, *Semiconductors and Semimetals* (Academic, New York, 1967), Vol. 3, p. 125.

[12] L. M. Roth, B. Lax, and S. Zwerdling, Phys. Rev. **114**, 90 (1959).

[13] D. J. Chadi, A. H. Clark, and R. D. Burnham, Phys. Rev. B **13**, 4466 (1976).

[14] C. Hermann and C. Weisbuch, Phys. Rev. B **15**, 823 (1977).

[15] W. A. Harrison and S. Ciraci, Phys. Rev. B **10**, 1516 (1974).

[16] R. Dingle, D. D. Sell, S. E. Stokowki, and M. Ilegems, Phys. Rev. B **4**, 1211 (1971).

[17] Estimated from the general trend of other Ga-V compounds, close to GaP (Ref. 11) [D. J. Chadi (private communication)].

[18] S. Bloom, G. Harbeke, E. Meier, and I. B. Ortenburger, Phys. Status. Solidi **66**, 161 (1974).

[19] A. W. Overhauser, Phys. Rev. **89**, 689 (1953).

[20] R. J. Elliott, Phys. Rev. **96**, 266 (1954).

[21] Y. Yafet, in *Solid State Physics*, edited by F. Seitz and D. Turnbull (Academic, New York, 1963), Vol. 14.

[22] Estimated from the general trend of other semiconductors.

[23] B. G. Zhurkin, N. A. Penin, and P. Swarup, Fiz. Tverd. Tela (Leningrad) **8**, 3550 (1966) [Sov. Phys. Solid State **8**, 2839 (1966)].

[24] A. Miller and E. Abrahams, Phys. Rev. **120**, 745 (1960).

# Intensity dependence of photoluminescence in GaN thin films

R. Singh, R. J. Molnar, M. S. Ünlü, and T. D. Moustakas
*Molecular Beam Epitaxy Laboratory, Department of Electrical, Computer, and Systems Engineering, Boston University, Boston, Massachusetts 02215*

(Received 30 August 1993; accepted for publication 15 November 1993)

We report the intensity dependence of band-gap and midgap photoluminescence in GaN films grown by electron cyclotron resonance (ECR) microwave plasma-assisted molecular beam epitaxy. We find that the band-gap luminescence depends linearly while the midgap luminescence has a nonlinear dependence on the incident light intensity. These data were compared with a simple recombination model which assumes a density of recombination centers 2.2 eV below the conduction band edge. The concentration of these centers is higher in films grown at higher microwave power in the ECR plasma.

Gallium nitride (GaN) is a wide direct band-gap semiconductor ($E_g = 3.4$ eV at 300 K), which is currently being investigated in many laboratories for its potential in optical devices (light emitting diodes, lasers, detectors) operating in the blue-violet ultraviolet part of the electromagnetic spectrum.[1] The performance and reliability of such devices depends critically on the type and concentration of electronic defects, whose origin is the heteroepitaxial growth (misfit dislocations and polarity related defects), the formation of native defects (vacancies, interstitials, and antisite defects) and the incorporation of intentional and unintentional impurities.

Defects in semiconductors can be studied by a variety of techniques, principal among which is photoluminescence (PL), a method which has been used extensively for the study of GaN films.[2,3] Photoluminescence spectra of undoped GaN films generally show a sharp peak close to the energy gap of the semiconductor, attributed to excitons bound to shallow donors[3] and a broader peak centered around 2.2 eV.[4,5] Various models have been advanced to account for the high shallow donor concentration in unintentionally doped GaN. The prevailing view is that the donors are due to nitrogen vacancies[6] although there is some evidence that oxygen impurities can also act as substitutional donors.[7] The broad yellow luminescence was attributed to electron transitions from the conduction band to a band of deep acceptor states placed 860 meV above the valence band edge.[8] These authors presented arguments that such states are introduced by carbon impurities in the films while Pankove *et al.*,[4] who observed the same photoluminescence band in ion implanted GaN samples, attributed the deep states to ion implantation processes. In general, the existence and magnitude of the yellow luminescence is associated with defective GaN films and the ratio of the yellow luminescence peak to band-gap luminescence was employed as a criterion of the carbon doping effects on the films[8] or the ion implantation related damage.[4]

In this letter, we investigated the excitation intensity dependence of PL from undoped GaN films and found that the band-gap luminescence depends linearly while the yellow luminescence has a nonlinear dependence on the light intensity. Thus the use of the ratio of yellow to band-gap luminescence as a criterion of the quality of the GaN films is meaningless unless one specifies the magnitude of the employed excitation light intensity. A simple recombination model has been proposed to qualitatively account for the observed light intensity dependence of the two luminescence bands.

The GaN films used in this study were grown by the electron cyclotron resonance microwave plasma-assisted molecular beam epitaxy (ECR-MBE), which was described in detail in a number of recent papers.[9,10] Here, we present only a brief description of the growth process. All the films were deposited on (0001) sapphire substrates, whose surface after chemical cleaning and thermal outgassing, is converted to AlN by exposing it to an ECR activated nitrogen plasma.[9] The films were deposited by the two-step growth process in which a GaN buffer of about 300 Å thick is deposited at 500 °C and the rest of the film, 1 to 2 μm thick, is deposited at 800 °C. This two-step growth method was found to lead to a low two-dimensional nucleation rate and a high lateral growth rate leading to films with relatively smooth surface morphology.[9,10] Power in the ECR discharge was the main variable during the growth of the films reported in this letter. More specifically type I samples were grown at a total microwave power of 20 W while type II samples were grown at 35 W. The transport coefficients of two representative samples are shown in Table I.

The photoluminescence was excited by a pulsed $N_2$ laser as the excitation source. The laser has a photon energy of 3.678 eV (337.1 nm), pulse, width of 10 ns, repetition rate of 40 Hz and a listed peak power of 250 kW. A circular aperture was used in front of the rectangular collimated beam and the resulting output was focused on the sample using a lens. A set of neutral density filters was used to attenuate the incident laser intensity for studying the excitation dependence of PL from the sample. The sample was held on a cold finger with a colloidal suspension of graphite which also acts as a

TABLE I. Typical values for the room temperature carrier concentration and mobility for representative type I and type II samples.

| Sample | Power (W) | Carrier conc. ($cm^{-3}$) | Mobility ($cm^2 V^{-1} s^{-1}$) |
|---|---|---|---|
| Type I | 20 | $1.0\times10^{18}$ | 50 |
| Type II | 35 | $1.90\times10^{17}$ | 13.8 |

 0003-6951/94/64(3)/336/3/$6.00 

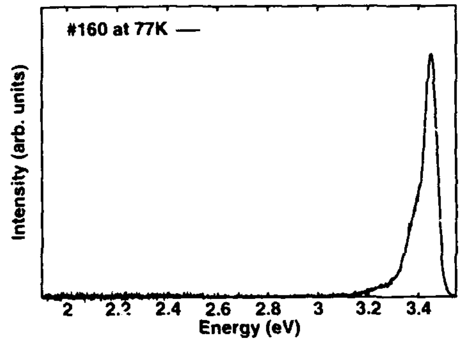


FIG. 1. PL spectra from a type I sample.

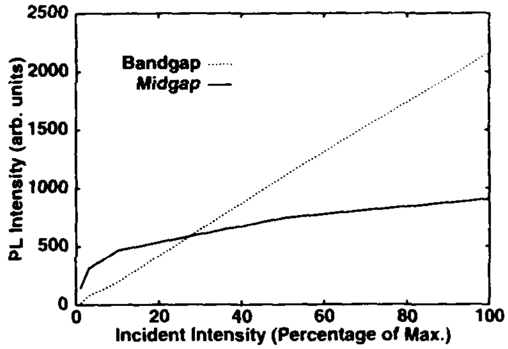


FIG. 3. Plot of the PL intensity vs the percentage excitation for the band-gap and midgap luminescence.

good heat conductor, hence preventing the sample from being heated by the laser. PL was collected by a lens and focused on the entrance slits of a 0.25-m grating spectrometer. A Hamamatsu photomultiplier (R-928) was used as the detector and its output was read by a lock-in amplifier. The spectra were not corrected for the spectral response of the system.

Figure 1 shows the photoluminescence spectrum at 77 K for a type I GaN sample. This spectrum shows only the band-gap luminescence at 3.47 eV. At the maximum excitation intensity we see no evidence of yellow luminescence, suggesting that the concentration of midgap defects is very low. The band-gap luminescence was found to vary linearly with light intensity over two orders of magnitude, a result consistent with excitonic recombination.[11]

The photoluminescence spectra of a type II GaN sample measured at 100% and 1% of the incident laser light is shown in Fig. 2. It is apparent from these data that characterizing the quality of the material by the ratio of the magnitude of the band-gap luminescence to the midgap luminescence is not correct, since the ratio depends on the excitation intensity. Thus, it is quite important to take the excitation intensity into account when analyzing any PL spectra for this material.

Figure 3 illustrates the intensity dependence of the band-gap and midgap luminescence peaks of the type II GaN sample. The band-gap luminescence depends linearly on light intensity as for type I samples. However, the midgap luminescence was found to have a light intensity dependence as shown in the figure. It initially increases with light intensity at low excitation levels and then tends to saturate as the excitation intensity is increased further.

The observed dependence on light intensity can be qualitatively accounted for in the simple recombination model illustrated in Fig. 4. We assume that the states responsible for the yellow luminescence form a broad band of a total density $N_{1\max}$. Shown in the figure are also the lifetimes for the various recombination paths and the densities $N_1$ and $N_2$ of the occupied states in the defect and conduction bands, respectively. If $G$ ($\mathrm{cm}^{-3}\,\mathrm{s}^{-1}$) is the generation rate then the rate of change of $N_1$ and $N_2$ are given by the equations

$$\frac{dN_2}{dt}=G-\frac{N_2}{\tau_{20}}-\frac{N_2}{\tau_{21}}, \quad \frac{dN_1}{dt}=\frac{N_2}{\tau_{21}}-\frac{N_1}{\tau_{10}}. \tag{1}$$

Under steady-state conditions, i.e., when the recombination lifetimes are smaller or comparable to the duration of the excitation pulse, Eqs. (1) become

$$G=\frac{N_2}{\tau_{20}}+\frac{N_2}{\tau_{21}}, \quad \frac{N_2}{\tau_{21}}=\frac{N_1}{\tau_{10}}. \tag{2}$$

The band-gap luminescence ($I_{\mathrm{gap}}$) and the midgap luminescence ($I_{\mathrm{yel}}$) are given by the expressions:

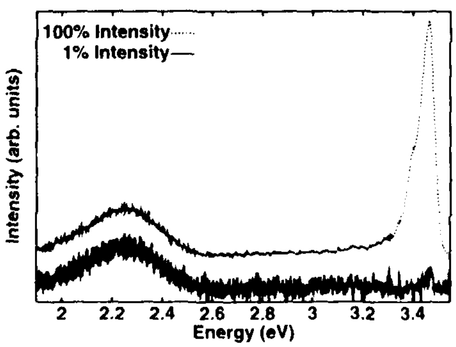


FIG. 2. PL spectra from type II samples at two different excitation levels.

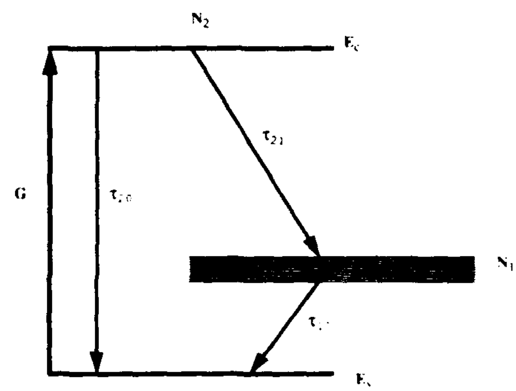


FIG. 4. Schematic of the proposed recombination model.

$$I_{gap} \propto \frac{N_2}{\tau_{20}} = \frac{G\tau_{21}}{(\tau_{21}+\tau_{20})}, \quad I_{yel} \propto \frac{N_2}{\tau_{21}} = \frac{G\tau_{20}}{(\tau_{21}+\tau_{20})}. \tag{3}$$

We assume that the recombination lifetimes $\tau_{20}$ and $\tau_{10}$ are constants while $\tau_{21}$ depends on light intensity. More specifically the value of $\tau_{21}$ can be expressed in terms of the low light intensity recombination lifetime $\tau'_{21}$ as[11]

$$\tau_{21} = \frac{N_{1\max}}{N_{1\max}-N_1}\,\tau'_{21}. \tag{4}$$

From Eqs. (3) and (4) we get

$$I_{gap} \propto \frac{GN_{1\max}\tau'_{21}}{N_{1\max}\tau'_{21}+(N_{1\max}-N_1)\tau_{20}},$$
$$I_{yel} \propto \frac{G\tau_{20}(N_{1\max}-N_1)}{N_{1\max}\tau'_{21}+\tau_{20}(N_{1\max}-N_1)}. \tag{5}$$

Case I: Low light intensity, i.e., $N_1 \ll N_{1\max}$

$$I_{gap} \propto \frac{G\tau'_{21}}{\tau_{20}+\tau'_{21}}, \quad I_{yel} \propto \frac{G\tau_{20}}{\tau_{20}+\tau'_{21}}. \tag{6}$$

Hence, in this case the yellow and the band-gap luminescence increase proportionally to the incident light intensity.

Case II: High light intensity, i.e., $N_1 \cong N_{1\max}$, the first of Eqs. (5) gives

$$I_{gap} \propto G. \tag{7a}$$

On the other hand, the yellow luminescence is governed by the recombination time, $\tau_{10}$. Thus from Eqs. (2) and (3),

$$I_{yel} \propto \frac{N_{1\max}}{\tau_{10}} \rightarrow \text{Const.} \tag{7b}$$

Equations (6) and (7) account qualitatively for the experimental results for Fig. 3.

Although this model does not take into account the change in the number of traps and recombination centers due to the shift in the quasi-Fermi levels as excitation intensity is changed,[12] it is sufficient to explain the saturation of the yellow PL from GaN. It would help further to have information about the recombination lifetimes of carriers to compute the exact number of midgap states.

In conclusion, we have determined the light intensity dependence of the band-gap and midgap luminescence in GaN films grown by electron cyclotron resonance assisted molecular beam epitaxy. As expected the band-gap luminescence varies linearly with the light intensity but the midgap luminescence initially increases and then saturates at higher light intensities. The data show the importance of relating $I_{yel}/I_{gap}$ to the generation rate employed during the measurement for the purposes of comparing samples on the basis of PL spectra. It further illustrates that samples grown at higher microwave power have higher concentration of midgap defects, which accounts for the observed compensation in the transport coefficients.

This work was supported by the Office of Naval Research (Grant No. N00014-92-J-1436).


[1] S. Strite and H. Morkoç, J. Vac. Sci. Technol. B **10**, 1237 (1992).
[2] J. I. Pankove, J. E. Berkeyheiser, H. P. Maruska, and J. Wittke, Solid State Commun. **8**, 1051 (1970).
[3] R. Dingle and M. Ilegems, Solid State Commun. **9**, 175 (1971).
[4] J. I. Pankove and J. A. Hutchby, J. Appl. Phys. **47**, 5387 (1976).
[5] I. Akasaki and H. Amano, SPIE **1361**, 138 (1990).
[6] J. I. Pankove, Mater. Res. Soc. Symp. Proc. **162**, 515 (1990).
[7] W. Wiefert, R. Fanzhelal, E. Butter, H. Sobotta, and V. Riede, Cryst. Res. Technol. **18**, 383 (1993).
[8] T. Ogino and M. Aoki, Jpn. J. Appl. Phys. **19**, 2395 (1980).
[9] T. D. Moustakas, T. Lei, and R. J. Molnar, Physica B **36**, 185 (1993).
[10] T. D. Moustakas and R. J. Molnar, Mater. Res. Soc. Proc. **281**, 753 (1993).
[11] J. I. Pankove, *Optical Processes in Semiconductors* (Dover, New York, 1975).
[12] A. Rose, *Concepts in Photoconductivity and Allied Problems* (Wiley, New York, 1963), Number 19.

# Appendix I : "Microstructures of GaN Films Deposited on (001) and (111) Si Using ECR-MBE"

# Microstructures of GaN films deposited on (001) and (111) Si substrates using electron cyclotron resonance assisted–molecular beam epitaxy

S. N. Basu
*Department of Manufacturing Engineering, Boston University, Boston, Massachusetts 02215*

T. Lei and T. D. Moustakas
*Molecular Beam Epitaxy Laboratory, Department of Electrical Engineering, Boston University, Boston, Massachusetts 02215*

(Received 17 September 1993; accepted 26 April 1994)

The microstructures of GaN films, grown on (001) and (111) Si substrates by a two-step method using Electron Cyclotron Resonance assisted–Molecular Beam Epitaxy (ECR-MBE), were studied by electron microscopy techniques. Films grown on (001) Si had a predominantly zinc-blende structure. The GaN buffer layer, grown in the first deposition step, accommodated the 17% lattice mismatch between the film and substrate by a combination of misoriented domains and misfit dislocations. Beyond the buffer layer, the film consisted of highly oriented domains separated by inversion domain boundaries, with a substantial decrease in the defect density away from the interface. The majority of defects in the film were stacking faults, microtwins, and localized regions having the wurtzite structure. The structure of the GaN films grown on (111) Si was found to be primarily wurtzite, with a substantial fraction of twinned zinc-blende phase. Occasional wurtzite grains, misoriented by a 30° twist along the [0001] axis, were also observed. A substantial diffusion of Si was seen in films grown on both substrates.

## I. INTRODUCTION

GaN films are currently being investigated in a number of laboratories because of their potential for applications in optoelectronic devices as well as high temperature and high frequency electronics.[1] These applications require the successful growth of high-quality crystals of GaN which can be intentionally doped *n*- and *p*-type.

Due to the lack of a native substrate, GaN has been grown heteroepitaxially on a variety of substrates by a number of vapor-phase methods.[2–4] Heteroepitaxy has been used successfully for the growth of semiconducting films for optoelectronic applications. A common example is GaAs on Si, in which the potential problems of misfit dislocations due to a 4% difference in the lattice parameters of the two cubic unit cells, as well as presence of anti-phase disorder due to the growth of a polar film on a nonpolar substrate, have been successfully addressed.[5]

The growth of GaN on Si, however, presents additional challenges. Unlike GaAs, which exists only in the cubic zinc-blende structure, GaN exists in two allotropic structures, wurtzite ($\alpha$) and zinc blende ($\beta$). The majority of work on the growth of GaN has been reported on sapphire substrates, where GaN is grown in its thermodynamically stable wurtzite phase. However, there is a motivation to grow the zinc-blende structure, since cubic structures of the III-V compounds have been more readily doped both *n*- and *p*-type.[6] Heteroepitaxial stabilization of $\beta$–GaN on substrates with cubic symmetry, i.e., $\beta$–SiC,[7] (001) MgO,[8] and (001) GaAs,[9] have been previously reported. This present study was undertaken to explore ways to heteroepitaxially grow GaN on Si, which is a much more technologically important substrate. The growth of $\beta$–GaN on Si is extremely challenging, since there is a huge difference of 17% in lattice parameters of the two cubic structures ($a_{Si}$ = 5.43 Å, $a_{\beta\text{-GaN}}$ = 4.52 Å).[10] Before this study, all efforts to grow $\beta$–GaN on Si led to amorphous or polycrystalline films.[11]

In this paper, we report a comprehensive TEM study of the microstructures of GaN films on (001) and (111) Si substrates, deposited by the Electron Cyclotron Resonance assisted–Molecular Beam Epitaxy (ECR-MBE) method. A comprehensive x-ray diffraction study of both films, as well as a preliminary TEM study of the films on (001) Si, have recently been reported elsewhere.[10,12]

## II. EXPERIMENTAL DETAILS

The details of the thin-film growth have been reported elsewhere.[4,10] Briefly, the GaN films were grown on *p*-type (001) and (111) Si substrates by the ECR-MBE method, using a Varian Gen-II MBE unit with an AsTeX model-1000 ECR source. Gallium was evaporated using a conventional Knudsen effusion cell, while molecular nitrogen was passed through the ECR source to produce atomic and ionic nitrogen. The films were deposited in two steps, which separated the nucleation and growth processes. Initially, a 30 nm buffer layer of GaN was deposited at 400 °C, followed by the deposition of the rest of the film at 600 °C. The deposition rate of GaN was around 250 nm/h.

The surface morphology of the films was examined using a JEOL JSM 6100 scanning electron microscope (SEM) equipped with a Kevex detector with a Be window for energy dispersive x-ray spectroscopy (EDS). The samples were also examined in plan view and cross section using a Phillips CM-30ST transmission electron microscope (TEM) having a point-to-point resolution of 0.19 nm at 300 kV acceleration voltage, as well as an Akashi EM 002B microscope with a point-to-point resolution of 0.18 nm at 200 kV acceleration voltage. The plan-view samples were thinned to perforation from the substrate side only, leading to TEM observations of the top regions of the films. Compositional analysis of the films was carried out using a VG HB5 dedicated scanning transmission electron microscope (STEM) at 100 kV with a 1 nm electron beam probe, using a Link EDS system with a windowless detector.

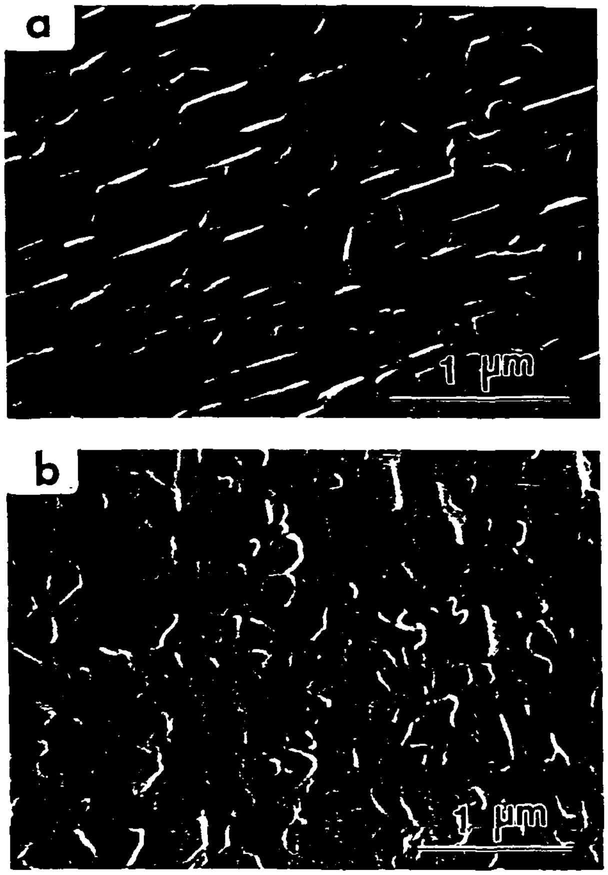


FIG. 1. SEM micrographs of the surface of GaN film deposited on (a) (001) Si and (b) (111) Si.

## III. RESULTS AND DISCUSSION

### A. GaN films on (001) Si

Figure 1(a) is a SEM micrograph of the surface of a 2 $\mu$m thick GaN film grown on (001) Si showing a tile-like morphology. It has been previously reported that the edges of the tiles are oriented along the ⟨110⟩ directions, presumably because of the lower surface energy of {110} surfaces due to a smaller density of broken bonds.[10] Figure 2(a) shows a bright-field TEM micrograph of the film in cross section. The buffer layer is marked in the figure. It appears that the film has a columnar morphology. However, the diffraction pattern of the film and substrate, shown in Fig. 2(b), confirms the epitaxial growth of GaN in the zinc-blende structure, in spite of the substantial lattice mismatch of 17%. The film actually consists of highly oriented domains. The diffraction pattern also confirms that the structure is cubic (zinc-blende). Although the wurtzite phase of GaN has a lower energy, the zinc-blende structure is stabilized by the cubic symmetry of the substrate surface. The lattice parameter of GaN was measured to be 4.5 Å, in agreement with previous reports.[7,9,10]

Another interesting feature is the presence of pits in the Si at the Si/GaN buffer interface, one of which is marked by an arrow in Fig. 2(a). These pits are crystallographic, with the side walls corresponding to {111} planes. STEM analysis showed that the pits contained GaN, indicating that these are etch pits probably formed during the cleaning process, which got filled up during film deposition.

Figure 2(a) shows that certain domains are highly faulted while others are relatively fault free. The faults also lead to streaking in the diffraction pattern perpendicular to the fault planes. Figure 3 is a higher magnification micrograph showing two domains (marked as A and B). While A is faulted throughout the thickness of the film, B is relatively fault free. The origin of the difference in fault densities of the domains is not currently understood. The two domains are separated by a boundary marked by arrows. Such boundaries have been previously reported in similar zinc-blende structures and have been identified as inversion domain boundaries (IDB).[13-15] These boundaries arise during impingement of two nuclei with different interface termination (i.e., a Ga and N layer, respectively), leading to bonding between like atoms across the boundary. Thus, the tile-like morphology, evident in Fig. 1(a), consists of highly oriented domains separated by {110} inversion domain boundaries.

In general, the domains are highly faulted near the interface, with the fault density decreasing away

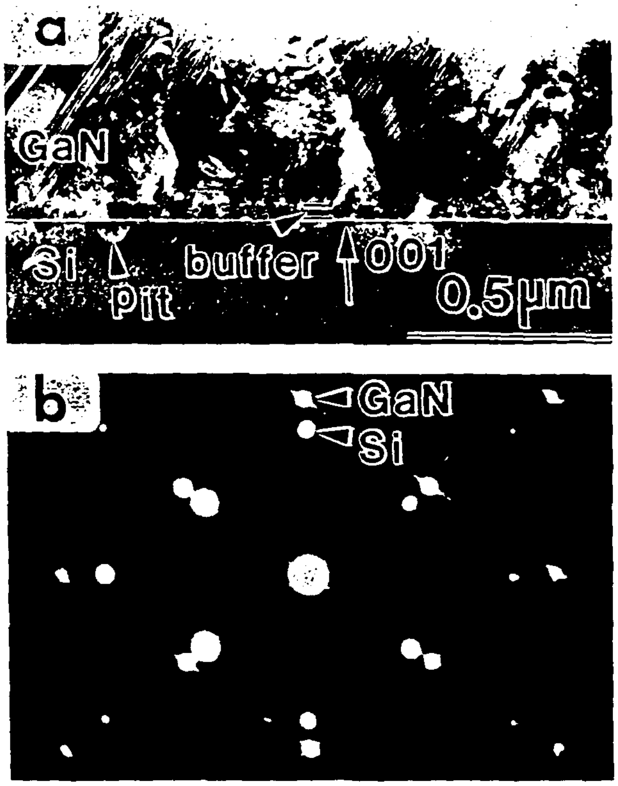


FIG. 2. (a) Bright-field TEM micrograph of GaN film grown on (001) Si in cross section. The GaN buffer layer as well as the presence of pits in the Si are marked in the figure. (b) Diffraction pattern of the interface showing the epitaxial orientation of zinc-blende GaN on (001) Si.


FIG. 3. Bright-field TEM micrograph of GaN film grown on (001) Si in cross section, showing two domains marked as A and B, separated by an inversion domain boundary marked by arrows.

from the interface. Figure 4 is a high resolution TEM micrograph of an upper region of a domain showing the various types of faults in the film. The majority of the faults away from the interface is along the {111} planes and can be identified as stacking faults (marked as S), microtwins (marked as T), and hexagonal regions (marked as H). Such faults are known to occur in fcc materials having a low stacking fault energy.[16] Since there is evidence that the cohesive energies of the two polymorphs of GaN are comparable, the formation energy of the stacking faults in this material should be small.[17] It has been previously suggested that the wurtzite structure is nucleated preferentially at stacking faults and twin boundaries of the zinc-blende structure in isostructural InN[18] and SiC.[19]

Figure 5 is a high resolution TEM micrograph of the buffer region in cross section. The figure shows the buffer layer to be highly faulted and polycrystalline, which is expected due to the large lattice mismatch and lower growth temperature. It should be noted that the thickness of the buffer layer (30 nm) is much larger than the critical thickness for strain layer epitaxy. Thus, the buffer is expected to be highly defective and free of strain. The inset diffraction pattern shows texturing along the [001] direction with a substantial number of misoriented grains. The grains in the buffer layer also exhibit a substantially larger density of stacking faults, leading to localized regions of wurtzite structure (marked as H) and twins (marked as T) in Fig. 5. The interface between the buffer layer and the Si substrate appears to be disordered. This has been reported previously[7,9] and can be attributed to a combination of damage during specimen preparation and a larger amount of disorder arising from the relatively large mismatch between the two lattices. The interfacial structure is visible in select areas; one of which, marked by a circle in Fig. 5, is shown at a higher magnification. Periodic interfacial misfit dislocations can be clearly identified in the figure. It thus appears that the misfit is accommodated in the buffer layer by a combination of misoriented grains and misfit dislocations.

The misoriented grains in the buffer layer are cut off by the oriented (001) domains away from the interface. As an example, one misoriented grain, marked as A in Fig. 5, is close to the (111) orientation. Since the (111) grain grows slower than the (001) domains, it is buried in the interface region during film growth. Figure 5 clearly shows that the film deposited in the second stage above the buffer layer is highly oriented, with a substantial decrease in the fault density.

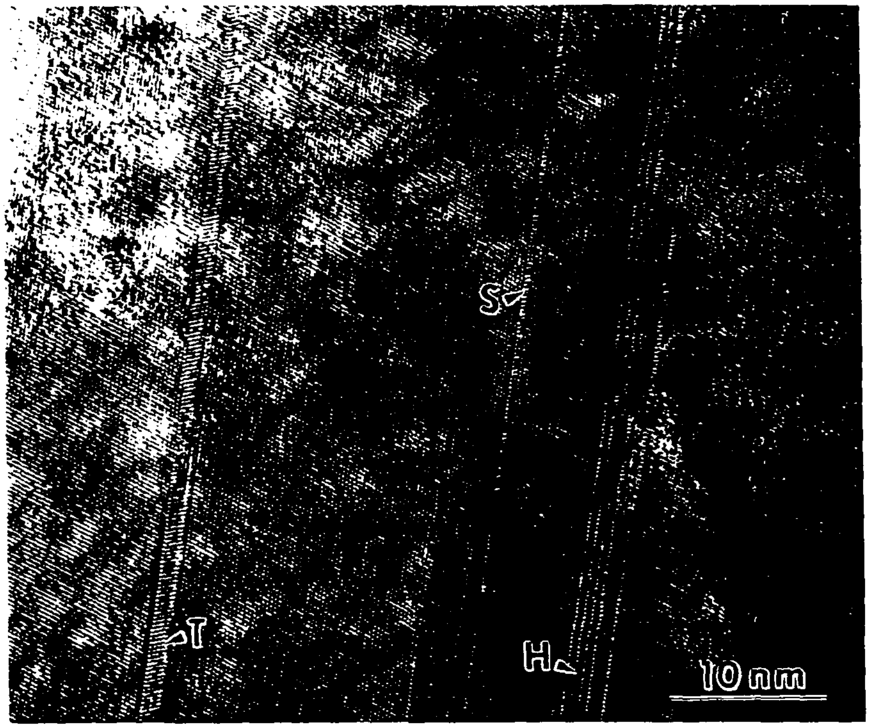


FIG. 4. High resolution TEM micrograph of the upper region of GaN film grown on (001) Si, showing a stacking fault, marked as S; a microtwin, marked as T; and a hexagonal wurtzite region, marked as H.

Compositional analysis of the film in cross section, using a 1 nm probe in the STEM, showed a substantial concentration of Si within the GaN film. Figure 6 shows a composition profile of Si in the GaN film as a function of distance from the interface. Although, to our knowledge, the solubility of Si in cubic GaN has not been studied, it is well known that the solubility of Si in isostructural GaAs is small (~0.5 at.%).[20,21] However, metastable solid solutions of much larger concentrations of Si in GaAs have been achieved by ion bombardment.[21] Figure 6 shows that the Si concentration drops sharply in the buffer layer (from 4.2 at.% at 10 nm from the interface to 0.87 at.% at 30 nm from the interface), followed by a much more gradual decrease in the profile farther into the GaN film. This suggests that the larger concentrations of Si close to the substrate are due to irradiation-assisted mixing due to bombardment of N atoms and ions produced by the ECR source, followed by a combination of thermal and irradiation-assisted diffusion farther away from the interface. Further experiments are underway to study this phenomenon in more detail. It can be conjectured that the relatively high concentration of defects (such as domain boundaries) in the film will enhance diffusivity of Si. However, no enrichment of Si at the domain boundaries was found (compared to the interior of the domains) to support this claim.

It is interesting to note that in GaN, Si can substitute for Ga as a donor and for N as an acceptor. However, a comparison of the atomic size (radius of 1.17 Å for Si, 1.26 Å for Ga, and 0.7 Å for N) suggests the Si will substitute for Ga in the film. This is supported by the electrical properties of these films, which were evaluated by dissolving the Si substrates and studying the transport coefficient of the GaN flakes by Hall effect measurements. It was found that electrical transport in these films was dominated by shallow donor states, approximately 25 meV below the conduction band,[22] consistent with the presence of Si at Ga sites in the film. Additionally, the heterojunction between GaN and Si was also investigated[23] and good rectification was observed, indicating that the films had reasonable electrical properties, in spite of the large defect density observed.

There is clearly a need to further decrease the defect density in the films. One possible way to achieve this could be by increasing the ECR power during the second stage of growth, without changing the substrate temperature. This would provide better mobility to the surface atoms for them to move to "correct" sites without enhancing thermal diffusion of Si into the film. Also, preliminary work has indicated that either a reduction in the N pressure during growth or the use of an $n$-type Si substrate leads to much smoother films.[19] This is currently being investigated.

## B. GaN films on (111) Si

Figure 1(b) shows the surface of a 1 µm thick GaN film grown on (111) Si. The tile-like morphology of the

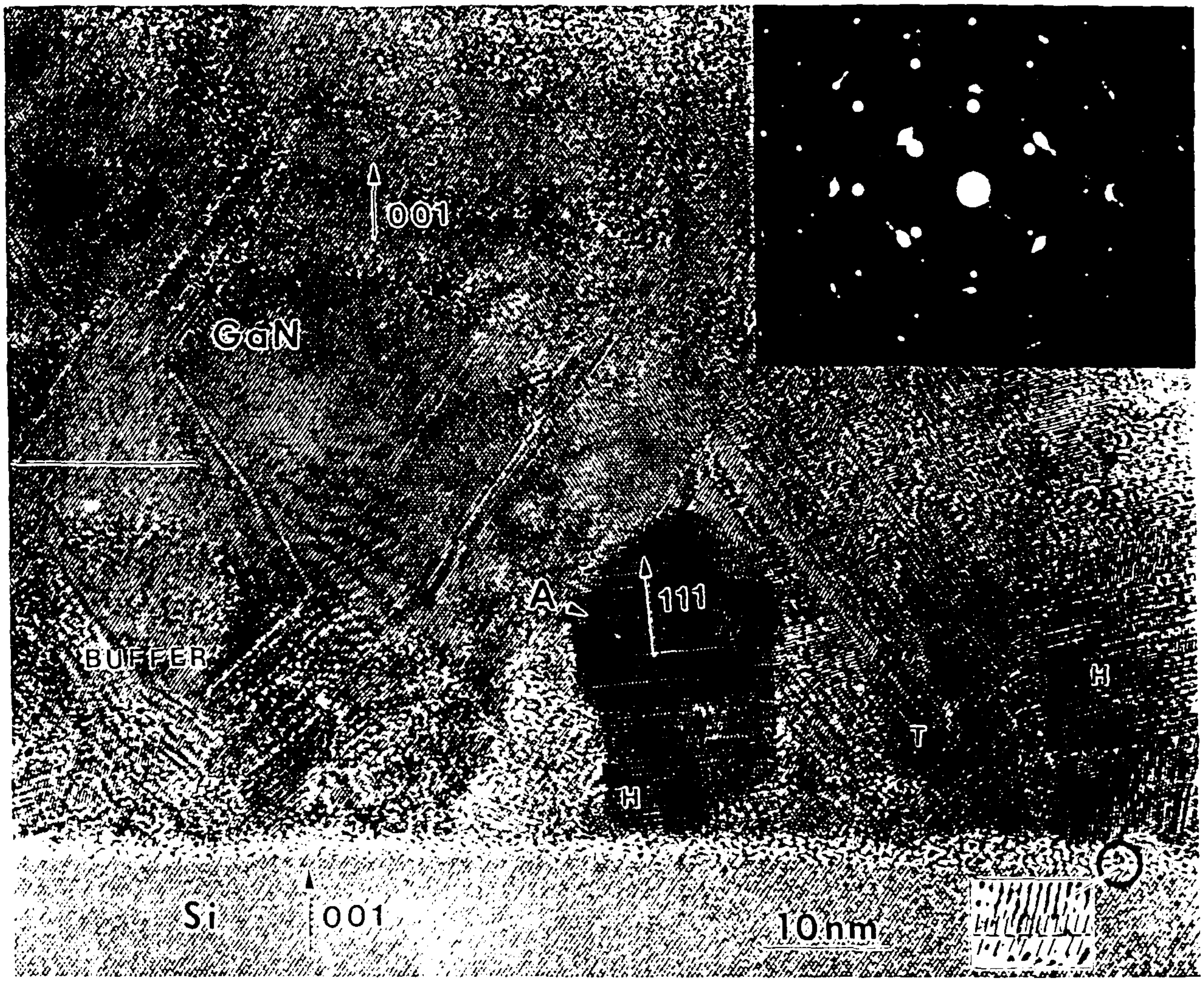


FIG. 5. High resolution TEM micrograph of the buffer region of GaN film grown on (001) Si. The inset diffraction pattern shows that although there is a (001) texturing in the buffer layer, there are a significant number of misoriented grains. The presence of wurtzite regions and microtwins is marked by H and T, respectively. Although the interface between the buffer and Si appears to be highly disordered, lattice planes can be seen up to the interface in a few areas, one of which is marked by a circle. A magnified micrograph of the circled region shows the presence of misfit dislocations at the interface.

GaN film on (001) Si is no longer evident. Figure 7 shows a plan-view bright-field TEM micrograph of the film. The figure shows the presence of domains, which are highly oriented as seen by the inset diffraction pattern. X-ray diffraction analysis showed the film to be primarily wurtzite with a substantial fraction of zinc-blende structure.[10,12] It should be noted, however, that this diffraction pattern cannot distinguish between the two phases. These domains are separated by boundaries which have been identified as inversion domain boundaries as well as stacking faults arising from the impingement of two GaN domains that are rotated by 60° around the [0001] axis. Sitar *et al.* have named these boundaries as double positioning boundaries (DPB) and have observed them in $\alpha$-GaN films on (0001) sapphire, SiC, and ZnO substrates.[13] DPB have also been studied in cubic $\beta$-SiC films on (0001) 6H-SiC substrates.[12,14]

Figure 8 shows a high resolution TEM micrograph of an inversion domain boundary, caused by different interface terminations, leading to a c/8 displacement between basal planes of adjacent domains. A more detailed analysis of the faults at the boundaries will be presented elsewhere.[15]

Figure 7 shows the presence of stacking faults in certain grains, some of which are marked as F by arrows. Stacking faults in $\alpha$-GaN lead to localized regions of zinc-blende structure in the film. Figure 9 shows a dark-field micrograph taken using only a cubic reflection, indicating the distribution of the zinc-blende structure in the GaN film. This appears to be consistent with the estimate of 25% cubic phase by x-ray diffraction analysis.[12,13] This observation has significant implications for the optical and electronic properties of such films. The optical gap of wurtzite GaN is 3.4 eV while

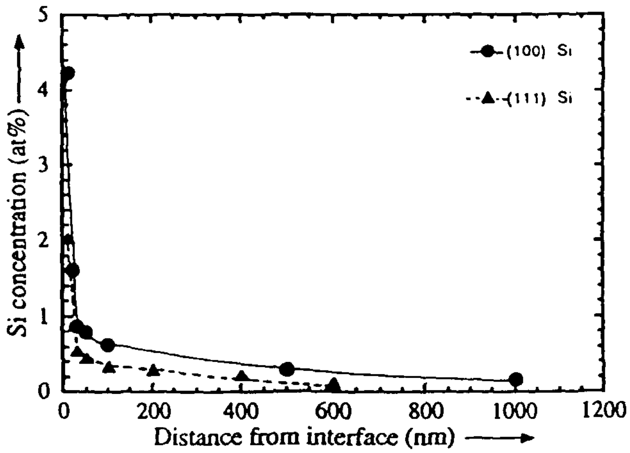


FIG. 6. Composition profile of Si (measured as a ratio of Si atoms to Ga plus Si atoms) in GaN films grown on (001) and (111) Si.

that of cubic GaN is 3.2 eV.[1,10] The incorporation of 25% of the zinc-blende phase in the wurtzite structure should affect the optical gap as well as the transport and recombination phenomena in these films. Figure 9 shows that the zinc-blende phase appears to be concentrated within certain domains and not randomly distributed throughout the film.

Figure 10(a) is a bright-field micrograph of the GaN film grown on (111) Si in cross section. The figure also shows the columnar morphology of the domains. Figure 10(b) shows the diffraction pattern obtained from the film and substrate. Figure 10(c) shows the indexed pattern (except for some double diffraction spots) showing the presence of the wurtzite (marked as H) and zinc-blende (marked as C) phases, as well as the twinned variant of the cubic zinc-blende structure (marked as T). The orientation relationships as seen from the diffraction pattern are as follows:

$$(111)\mathrm{Si} \parallel (111)\beta\text{-GaN} \parallel (0002)\alpha\text{-GaN} \quad \text{and}$$
$$[\bar{1}10]\mathrm{Si} \parallel [\bar{1}10]\beta\text{-GaN} \parallel [11\bar{2}0]\alpha\text{-GaN}\,.$$

This orientation allows the alignment of the closest-packed planes and directions of all three phases. The presence of a substantial fraction of zinc-blende structure is not surprising due to the identical symmetry of the (0002) and (111) planes in the wurtzite and zinc-blende structures, respectively, along with the small difference in the cohesive energy of the two polytypes.

Compositional analysis of this GaN film by STEM also indicated a substantial concentration of Si, as seen

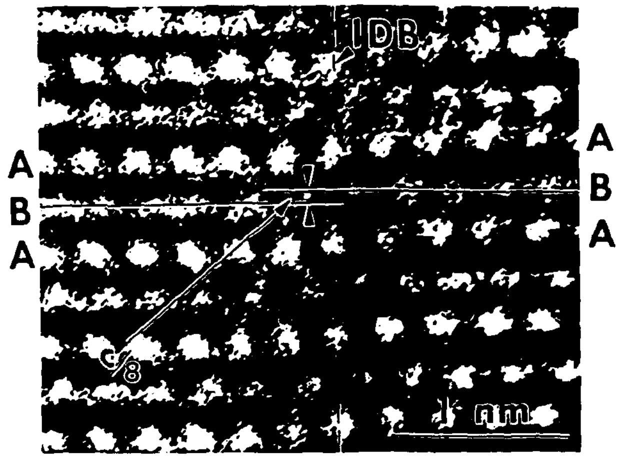


FIG. 8. High resolution TEM micrograph of an inversion domain boundary in the GaN film on (111) Si, caused by different interface terminations, leading to a $c/8$ displacement between basal planes of adjacent domains.

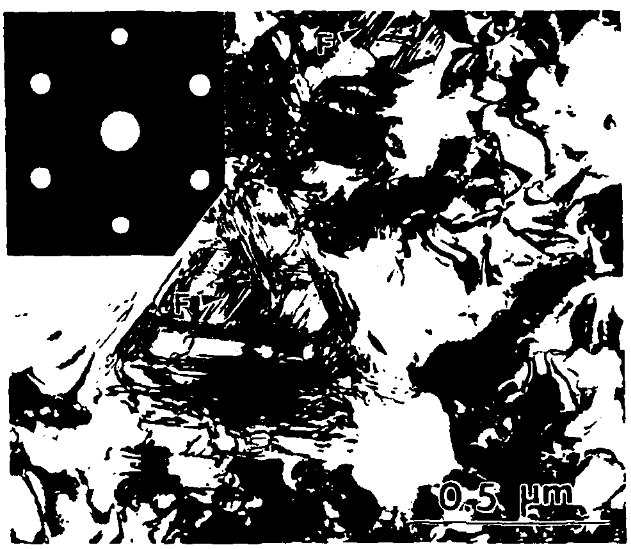


FIG. 7. Plan-view bright-field TEM micrograph of GaN film grown on (111) Si, showing the presence of domains. Some grains with stacking faults are marked as F by arrows, indicating the presence of the cubic phase. The diffraction pattern shows that the film is highly oriented and has a hexagonal symmetry common to the (0002) and (111) planes of wurtzite and zinc-blende structures.


FIG. 9. Dark-field TEM micrograph of GaN film grown on (111) Si, using a cubic reflection, highlighting the zinc-blende phase in the material.

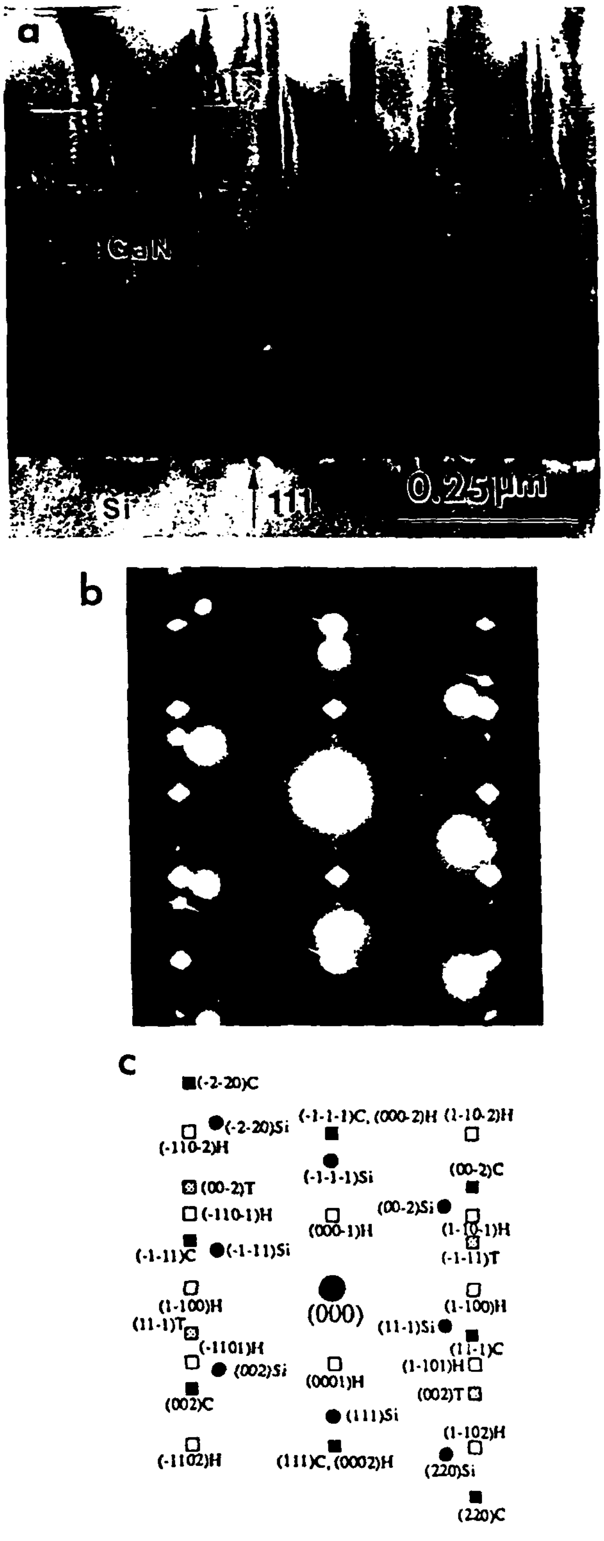


FIG. 10. (a) Bright-field TEM micrograph of GaN film grown on (111) Si in cross section, showing columnar morphology of the domains. (b) Diffraction pattern of the interface. (c) Indexed diffraction pattern showing presence of wurtzite phase (H) as well as zinc-blende phase (C) that is twinned (T), along with the reflections from the Si substrate (Si).

in Fig. 6. Although the shape of the profile is similar to that on the film grown on (001) Si, the Si concentrations for this film are lower, consistent with the fact that the processing time was lower [4 h for the films on (111) Si versus 8 h for the films on (001) Si] for this film.

Another interesting feature of these films was the presence of occasional wurtzite grains that were misoriented by a 30° twist along the [0001] axis with the rest of the wurtzite grains. Figures 11(a) and 11(b) show a bright-field TEM micrograph of such a grain and the corresponding diffraction pattern. Figure 11(c) is a dark-field micrograph highlighting the misoriented grain. Figure 12 shows the atomic positions at an unreconstructed interface between the misoriented GaN grain and the (111) Si substrate. The coincident (or near coincident) atomic positions are marked by circles. The figure shows that every fourth N (or Ga) atom is in position to directly bond with every third Si atom at the interface. This boundary would thus have a lower energy than a random boundary and could explain the presence of these misoriented GaN grains. This is an example of a near coincidence boundary between two phases, discussed by Balluffi *et al.*,[26] where $\Sigma_N$ (=4) ≠ $\Sigma_{Si}$ (=3), due to the difference in the planar atomic densities of the two phases. A hexagonal supercell formed between the two phases is marked by bold lines in the figure and has a lattice parameter of 6.5 Å.

## IV. CONCLUSIONS

The microstructures of GaN films, grown by a two-step method using ECR-MBE on (001) and (111) Si, was studied using electron microscopy techniques. The structure of films grown on (001) Si was found to be predominantly zinc-blende. The GaN buffer layer, grown in the first deposition step, was found to be highly faulted and accommodated the strain due to lattice mismatch between the substrate and film by a combination of misoriented domains and misfit dislocations. Beyond the buffer layer, the film consisted of highly oriented domains separated by inversion domain boundaries. There was a substantial decrease in the defect density away from the interface, with the majority being defects in the stacking sequence along the {111} planes, leading to stacking faults, microtwins, and localized regions having the wurtzite structure.

The structure of the GaN films grown on (111) Si was found to be primarily wurtzite. However, a substantial fraction of twinned zinc-blende structure was also identified in the films. The rest of the film consisted of highly oriented wurtzite domains separated by inversion domain and stacking faults. Occasional wurtzite grains, misoriented by a 30° twist along the [0001] axis, were also observed in the film.

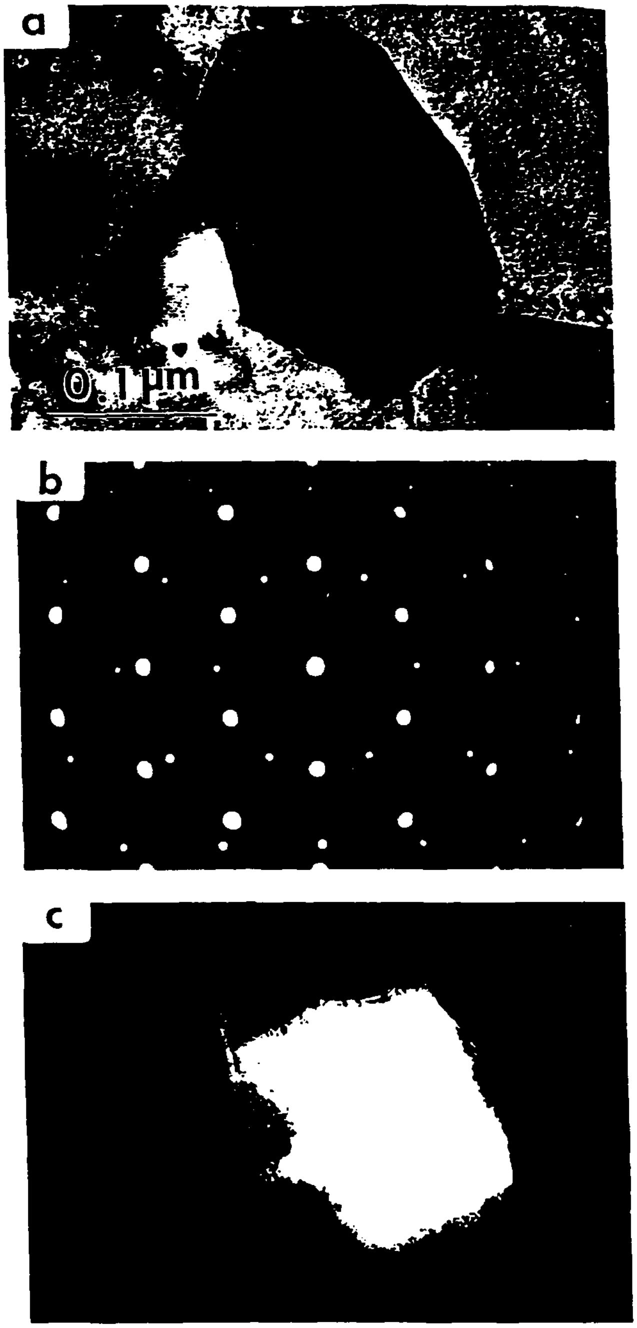


FIG. 11. (a) Bright-field TEM micrograph of a wurtzite grain in GaN film grown on (111) Si. (b) Selected area diffraction pattern, showing a 30° twist about the [0001] axis with respect to the surrounding grains. (c) Dark-field micrograph highlighting the misoriented grain.

A substantial concentration of Si was found in both GaN films, especially in the buffer layer. This is an important issue, since it leads to unintentional doping of the film. It is suggested that during the growth of the buffer layer, the microwave power of the ECR source be reduced to minimize irradiation-assisted mixing of Si from the substrate. During the growth of the film, the

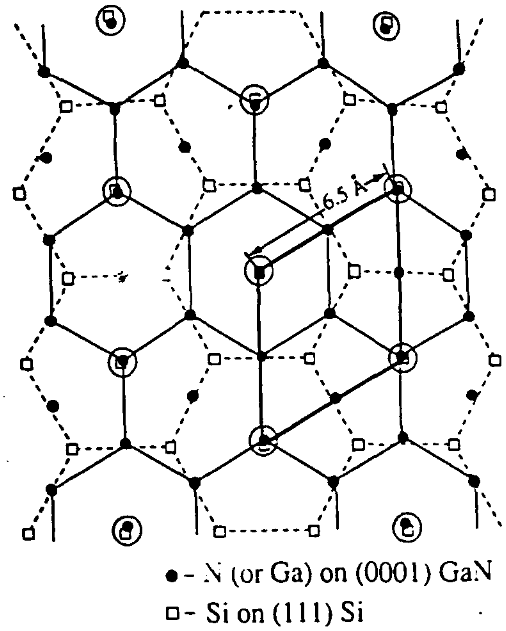


FIG. 12. Interfacial structure of the misoriented GaN grain/Si substrate. The coincident or near-coincident atomic positions at the interface are marked by circles. A hexagonal supercell with a lattice parameter of 6.5 Å is also marked by bold lines in the figure.

ECR power should be increased to reduce the defect concentration in the film.

## ACKNOWLEDGMENTS

Doctor T.E. Mitchell and Dr. K. Das Chowdhury are gratefully acknowledged for stimulating discussions. The authors would also like to thank Anlee Kruup for her help with the SEM analysis; Dr. A.J. Garratt-Reed for his assistance with the STEM analysis; and Dhruv Bhatt and Christopher McDowell for their help with TEM specimen preparation. TEM studies were carried out at the Center for Materials Science at Los Alamos National Laboratory and at the Electron Microscopy Center in the Center for Materials Science and Engineering at MIT. A portion of this work was sponsored by the Office of Naval Research (Grant No. N00014-92-J-1436).

## REFERENCES

1. R.F. Davis, Proc. IEEE **79**, 702 (1991).
2. H.P. Maruska and J.J. Tietjen, Appl. Phys. Lett. **15**, 327 (1969).
3. H.M. Manasevit, F.M. Erdmann, and W.I. Simpson, J. Electrochem. Soc. **118**, 1864 (1971).
4. T.D. Moustakas, T. Lei, and R.J. Molnar, Physica B **185**, 36 (1993).
5. J.S. Harris, Jr., S.M. Koch, and S.J. Rosner, in *Heteroepitaxy on Silicon II*, edited by J.C.C. Fan, J.M. Phillips, and B-Y. Tsaur (Mater. Res. Soc. Symp. Proc. **91**, Pittsburgh, PA, 1987), p. 3.
6. J.I. Pankove, in *Diamond, Silicon Carbide and Related Wide Bandgap Semiconductors*, edited by J.T. Glass, R. Messier, and N. Fujimori (Mater. Res. Soc. Symp. Proc. **162**, Pittsburgh, PA, 1990), p. 515.

7. M. J. Paisley, Z. Sitar, J. B. Posthill, and R. F. Davis, J. Vac. Sci. Technol. A **7**, 701 (1989).
8. R. C. Powell, G. A. Tomasch, Y. W. Kim, J. A. Thorton, and J. E. Greene, in *Diamond, Silicon Carbide and Related Wide Bandgap Semiconductors*, edited by J. T. Glass, R. Messier, and N. Fujimori (Mater. Res. Soc. Symp. Proc. **162**, Pittsburgh, PA, 1990), p. 525.
9. S. Strite, J. Ruan, Z. Li, A. Salvador, H. Chen, D. J. Smith, W. J. Choyke, and H. Morkoç, J. Vac. Sci. Technol. B **9** (4), 1924 (1991).
10. T. Lei, T. D. Moustakas, R. J. Graham, Y. He, and S. J. Berkowitz, J. Appl. Phys. **71** (10), 4933 (1992).
11. Z. Sitar, M. J. Paisley, B. Yan, and R. F. Davis, in *Diamond, Silicon Carbide and Related Wide Bandgap Semiconductors*, edited by J. T. Glass, R. Messier, and N. Fujimori (Mater. Res. Soc. Symp. Proc. **162**, Pittsburgh, PA, 1990), p. 537.
12. T. Lei, K. F. Ludwig, and T. D. Moustakas, J. Appl. Phys. **74** (7), 4430 (1993).
13. T. E. Mitchell, P. Pirouz, and A. H. Heuer, *Microbeam Analysis*, edited by R. H. Geiss (San Francisco Press, San Francisco, CA, 1987), p. 215.
14. A. Georgakilas, J. Stoemenos, K. Tsagaraki, Ph. Komninou, N. Flevaris, P. Panayotatos, and A. Christou, J. Mater. Res. **8**, 1908 (1993).
15. R. F. Davis, J. W. Palmour, and J. A. Edmond, in *Diamond, Silicon Carbide and Related Wide Bandgap Semiconductors*, edited by J. T. Glass, R. Messier, and N. Fujimori (Mater. Res. Soc. Symp. Proc. **162**, Pittsburgh, PA, 1990), p. 463.
16. P. Pirouz and Y. Yang, in *High Resolution Electron Microscopy of Defects in Materials*, edited by R. Sinclair, D. J. Smith, and U. Dahmen (Mater. Res. Soc. Symp. Proc. **183**, Pittsburgh, PA, 1990), p. 173.
17. T. Lei and T. D. Moustakas, in *Wide Band Gap Semiconductors*, edited by T. D. Moustakas, J. I. Pankove, and Y. Hamakawa (Mater. Res. Soc. Symp. Proc. **242**, Pittsburgh, PA, 1992), p. 433.
18. S. Strite, D. Chandrasekhar, D. J. Smith, J. Sariel, H. Chen, N. Teraguchi, and H. Morkoç, J. Cryst. Growth **127**, 204 (1993).
19. L. U. Ogbuji, T. E. Mitchell, A. H. Heuer, and S. Shinozaki, J. Am. Ceram. Soc. **64** (2), 100 (1981).
20. K. H. Lee, D. A. Stevenson, and M. D. Deal, J. Appl. Phys. **68** (8), 4008 (1990).
21. J. E. Greene, J. Vac. Sci. Technol. B **1** (2), 229 (1993).
22. M. Fanciulli, T. Lei, and T. D. Moustakas, Phys. Rev. B **48** (20), 1993.
23. T. Lei and T. D. Moustakas, unpublished research.
24. H. S. Hong, B. L. Jiang, J. T. Glass, G. A. Rozgonyi, and K. L. More, J. Appl. Phys. **63** (8), 2645 (1988).
25. S. N. Basu, K. Das Chowdhury, and T. D. Moustakas, unpublished research.
26. R. W. Balluffi, A. Brokman, and A. H. King, Acta Metall. **30**, 1453 (1982).

# Appendix J : “Hydrogenation of Gallium Nitride”

# HYDROGENATION OF GALLIUM NITRIDE

M. S. BRANDT,* N. M. JOHNSON,* R. J. MOLNAR,** R. SINGH,** AND T. D. MOUSTAKAS**

* Xerox Palo Alto Research Center, 3333 Coyote Hill Road, Palo Alto CA 94304
** Department of Electrical, Computer, and Systems Engineering, Boston University, Boston, MA 02215

## ABSTRACT

A comparative study of the effects of hydrogen in n-type (unintentionally and Si-doped) as well as p-type (Mg-doped) MBE-grown GaN is presented. Hydrogenation above 500°C reduces the hole concentration at room temperature in the p-type material by one order of magnitude. Three different microscopic effects of hydrogen are suggested: Passivation of deep defects and of Mg-acceptors due to formation of hydrogen-related complexes and the introduction of a hydrogen-related donor state 100 meV below the conduction band edge.

## INTRODUCTION

The effects of hydrogen on the electronic and vibrational properties of various semiconductors have been studied extensively [1]. In elemental semiconductors, one observes, e.g., the passivation of deep defects (dangling bonds) in amorphous silicon, resulting in a decrease of the subgap absorption, or the passivation of dopant atoms such as boron or phosphorous, resulting in a decrease of the carrier concentration. In recent years, these studies have been extended to compound semiconductors, but have been mostly restricted to the GaAs/AlAs system and InP. With respect to the possible effects of hydrogen wide-bandgap III-V and II-VI semiconductors like GaN and ZnSe have only recently received attention. This interest has been triggered by an intriguing difficulty to achieve p-type doping in films grown with one particular growth technique. In both the II-VI and III-V systems it is found that metal-organic chemical vapor deposition (MOCVD) is unable to produce p-type material, while molecular-beam epitaxy appears to easily grow p-type samples. This behaviour has been linked to the presence of hydrogen in the gas phase during MOCVD growth, which might lead to the formation of acceptor-hydrogen complexes. Indeed, in the case of N-doped p-type ZnSe, the observation of N-H local vibrational modes in MOCVD material strongly supports this assumption [2].

In this contribution, we report on continuing studies of the effects of hydrogen in both n-type (unintentionally doped, sometimes called autodoped, and Si-doped) and p-type (Mg-doped) GaN. In p-type samples grown by MOCVD, acceptor dopants have to be activated by either a low-energy electron beam irradiation or by a thermal annealing step [3]. Again, the formation of accceptor-hydrogen complexes under the abundant presence of hydrogen has been suggested as the origin for the necessity of a post-growth process. We therefore use MBE-grown GaN and deliberately introduce hydrogen by remote-plasma hydrogenation to study the effects of hydrogen in this III-V compound.

## SAMPLE GROWTH AND ANALYTICAL PROCEEDURES

Wurtzite GaN epilayers were grown on (0001) sapphire substrates by ECR-assisted MBE [4]. Gallium and the dopant elements (Mg and, for intentional n-type doping, Si) were evaporated



Mat. Res. Soc. Symp. Proc. Vol. 325. ©1994 Materials Research Society

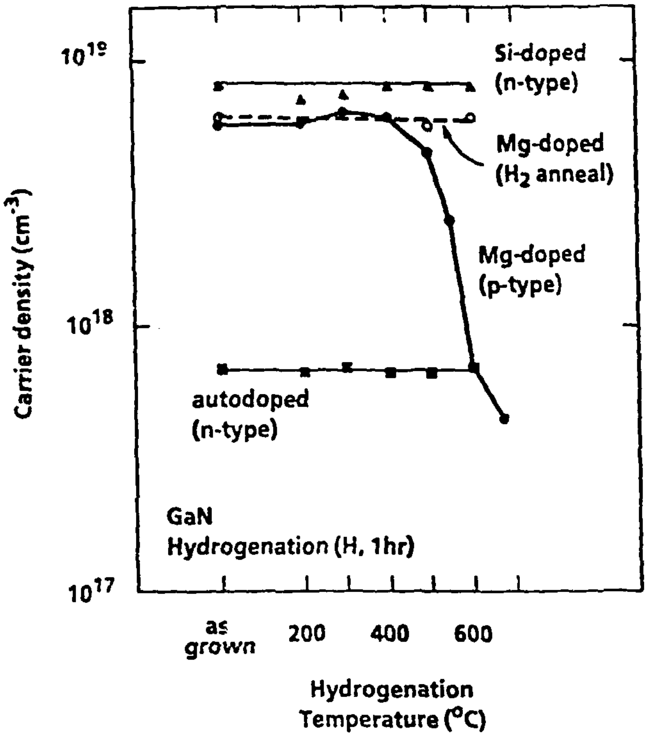


Figure 1: Dependence of the carrier concentration on hydrogenation temperature in epitaxial layers of GaN.

from conventional Knudsen cells, while nitrogen radicals were produced by passing molecular nitrogen through an ECR source at a pressure of $10^{-4}$ Torr. A microwave power of 35 W or higher was used for the growth of semi-insulating GaN films. Prior to the growth of the GaN epilayer, the substrates were exposed to the N-plasma for 30 min to form an AlN layer. A further GaN buffer layer was then grown at 500°C followed by the high-temperature growth of the actual film at 800°C at a growth rate of 200-250 nm/hr. Hydrogenation was performed with a remote microwave plasma operating at 2 Torr. This technique excludes effects due to charged particle bombardment of the sample or its illumination from the plasma. A high temperature sample holder allowed hydrogenation at temperatures up to 675°C. The films were electrically characterized in a standard Hall-effect apparatus, with the samples abrasively etched into a clover-leaf shape. For ohmic contacts Au was deposited on p-type GaN and Al on n-type material. Depth profiles were determined from secondary ion mass spectroscopy (SIMS), with a $Cs^+$ primary ion beam for the detection of hydrogen/deuterium and Si and an $O^-$ primary beam for Mg. Calibration of the SIMS data was achieved with Mg and deuterium-implanted GaN reference samples. To increase the sensitivity, the GaN samples for SIMS were treated with a plasma containing deuterium instead of hydrogen. The photoluminescence measurements were performed with a pulsed $N_2$ laser as the excitation source (3.678 eV).

## RESULTS

Figure 1 shows the carrier concentration at room temperature for three differently doped samples subjected to isochronal (1hr) hydrogenation. The n-type samples are completely uneffected by the hydrogenation, however the p-type sample shows a significant decrease in the hole concentration after hydrogenation at $T \geq 500$°C. The mobility in all three cases remained unchanged after hydrogenation at typically 50 $cm^2/Vs$ (autodoped), 10 $cm^2/Vs$ (Si-doped) and 0.3 $cm^2/Vs$ (Mg-doped). A control experiment on the p-type sample is included in Fig. 1, where the microwave plasma was switched off during the post-growth treatment demonstrating that exposure

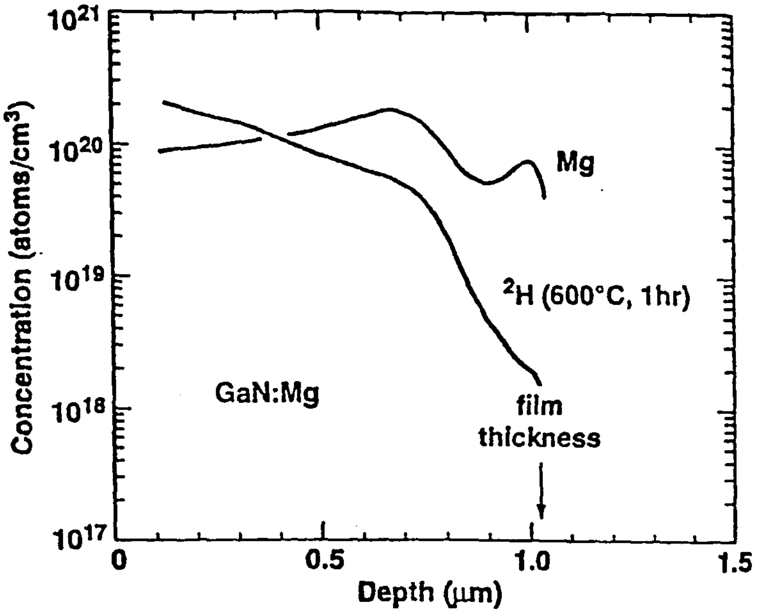


Figure 2: Depth profiles of hydrogen and magnesium in p-type GaN determined by SIMS.

to molecular hydrogen at temperatures up to 600°C does not affect the hole concentration.

Secondary-ion mass spectrosopy is used to verify the introduction of hydrogen into the material. In addition, together with the carrier concentrations determined in Fig. 1 the measurement of the dopant concentrations allows the determination of the doping efficiencies in Si- and Mg-doped GaN. Figure 2 shows the H- and Mg-depth profiled for p-type GaN. An average Mg-concentration of $10^{20}$cm$^{-3}$ is found, which indicates a very high doping efficieny of about 10%. The average hydrogen concentration is about the same as the Mg-concentration. The slight decrease in H-concentration up to a depth of 0.7$\mu$m could be due to a diffusion process. The steep decrease in the concentration, however, coincides with the doping inhomogeneity visible in the Mg-profile at 0.9$\mu$m. The high Mg-concentration at the substrate interface might be due to outdiffusion of Mg from doped GaN layers deposited on the substrate holder during previous depositions.

A similar comparison of the dopant and deuterium depth profiles is given for Si-doped n-type GaN in Fig. 3. The average Si-concentration is about $4 \times 10^{20}$cm$^{-3}$, the doping efficiency of several percent is therefore slightly lower than in the p-type material. Two hydrogen profiles are included in Fig. 3. It becomes obvious that after hydrogenation at 600°C, the hydrogen concentration levels at $2 \times 10^{20}$cm$^{-3}$, independent of the local Si concentration, which is found to vary throughout the sample.

The hydrogen concentration, after the same passivation step, incorporated in the unintentionally (autodoped) material is about one order of magnitude lower than in Si-doped material (Fig. 4), and has a constant concentration profile. Comparing the hydrogen concentrations in the three differently doped samples we find that the hydrogen incorporation is not just limited by factors like solubility, but does indeed depend on the type and concentration of the dopant present.

Further information on the effects of hydrogen in GaN were obtained from photoluminescence (PL). In Fig. 5, a comparison is shown between the photoluminescence of Mg-doped and autodoped samples, both before and after hydrogenation at 600°C. The two dominant PL-lines in the as-grown samples are the exciton line at 3.44 eV and the Mg-acceptor related line at 3.25 eV, with its two phonon replicas. After hydrogenation, these lines are still observed in the respective samples, but a quantitative comparison of signal heights is difficult. In the autodoped sample, the hydrogenation led to a complete quenching of the defect related line at 2.3 eV [5]. In addition to these known PL lines, a new PL line at 3.35 eV appears after hydrogenation in both samples, which has not been previously reported in GaN.

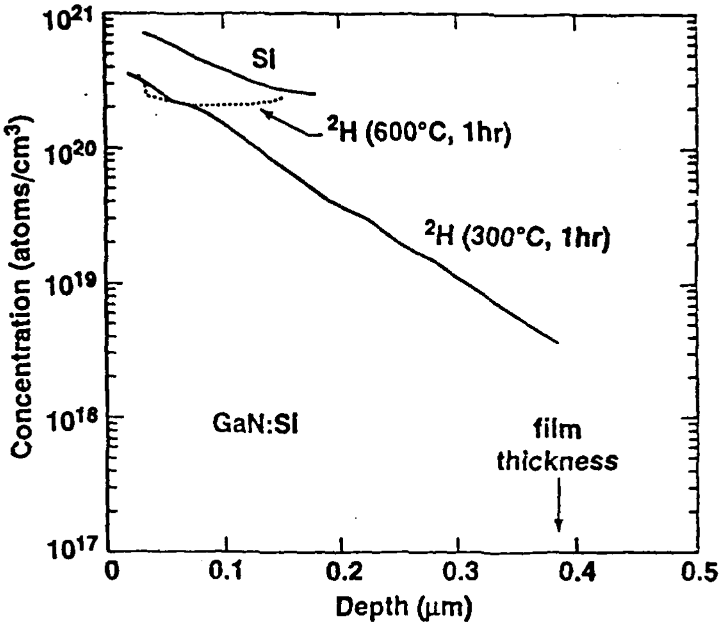


Figure 3: Depth profiles of hydrogen and silicon in n-type GaN determined by SIMS. The hydrogen profiles have been obtained on two identical samples treated at different passivation temperatures.

## DISCUSSION

A similar hydrogen-related study on p-type GaN has already been performed by Nakamura and coworkers [6]. However, there are various significant differences to the results reported here. Nakamura used MOCVD grown samples, which were LEEBI-treated to obtain p-type conductivity. In our case, the MBE gown films are p-type without any need for a post-growth treatment. Nakamura used an $NH_3$ ambient for hydrogenation and had to rely on the thermal decomposition of the molecules on the surface of the film to obtain atomic hydrogen. Our experiments, in which the atomic hydrogen is produced in a remote plasma, therefore show that the hydrogenation temperature of 500°C is indeed typical for the material, and not just for the $NH_3$ cracking process. Details of the photoluminescence results also differ. Nakamura et al. saw an increase in a possibly defect-related PL band centerd at 1.65 eV after their ammoniation treatment. No indication for such a PL line is visible in our spectra. The remote hydrogen plasma used in our hydrogenation technique therefore does not lead to defect formation detectable in PL. In fact, the quenching of the defect-related line at 2.3 eV for the n-type sample (Fig. 5) shows that hydrogen can passivate this deep defect state, most probably by a complex formation process. We can conclude that in the experiments presented here, no compensation due to deep defect formation takes place. The observed changes in the hole concentration therefore appear to arise from compensation by shallow donor states created by the incorporation of hydrogen, or by a Mg-H complex formation.

A donor-like state related to the introduction of hydrogen would indeed be consistent with both the Hall data and the photoluminescence experiments. Under this assumption, the position of the new PL line 100 meV below bandgap would indicate the energy level of this new donor state. One has then to rationalize that the introduction of hydrogen into the n-type samples does not change the effective electron concentration, as visible in Fig. 1. The SIMS data reveal about $10^{19}cm^{-3}$ and $10^{20}cm^{-3}$ hydrogen in the autodoped and in the Si-doped samples, respectively, after hydrogenation, thereby giving an upper limit for the additional donor concentration in these samples. Only 1/100 of these would be thermally activated at room temperature, leading to an added electron concentration well below the Hall concentrations measured for these samples which would be difficult to detect.

The presence of Mg-H complexes, which would passivate the acceptors in contrast to compensation as discussed above, would be shown by the observation of a local vibrational mode of such

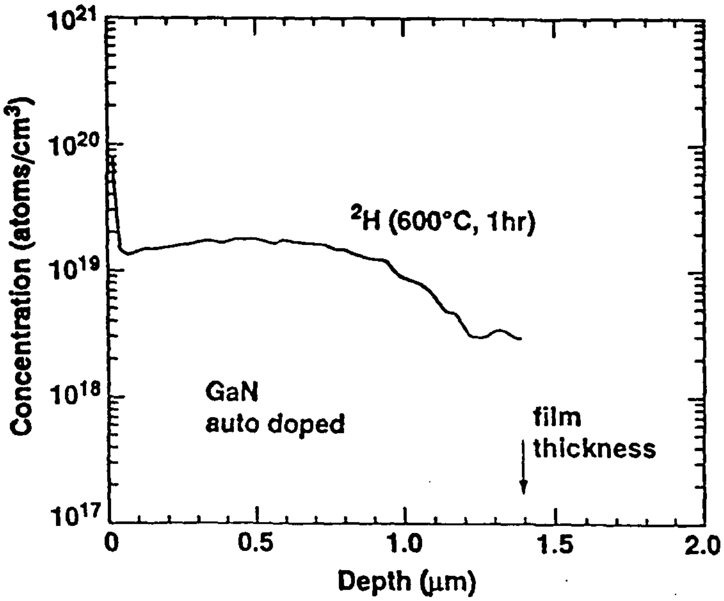


Figure 4: Depth profiles of hydrogen in unintentionally (autodoped) n-type GaN determined by SIMS.

a complex, as has been achieved for the N-H-complex in ZnSe. Preliminary Raman and infrared studies on the samples studied here indeed show such modes in the vicinity of $2200 cm^{-1}$ when Mg concentrations above $10^{19} cm^{-3}$ are present in the samples [7]. No indication for Si-H, C-H and N-H vibrational modes has been found, however. Details of these results will be subject to a future publication.

The observation of both the new PL line in n- and p-type samples and of the LVM of Mg-H complexes in p-type material suggests that hydrogen can have various effects on the properties of GaN. Indeed, in the p-type sample one has to conclude from vibrational spectroscopy and the PL measurements that both effects, the compensation and the passivation, are present, although from the relative intensities of the PL line at 3.35 eV in the p-type and autodoped samples one might expect that the hydrogen-donor state concentration is small in the p-type material. However, the chemistry of hydrogen in GaN is clearly a challenging subject [8], which will require considerably more experimental and theoretical work.

## SUMMARY

We have presented a comparative study of the effects of hydrogen in n- and p-type MBE-grown GaN. We find that the hole concentration in Mg-doped samples can be significantly reduced by hydrogenation above 500°C. The electron concentration in autodoped and Si-doped material is unaffected by hydrogenation. The observation of a new photoluminescence line at 3.35 eV in both n- and p-type samples suggests that hydrogen has a donor-like state in GaN. The defect-related PL line at 2.3 eV can be effectively quenched by hydrogenation, which indicates defect-hydrogen complex formation. As a third effect of hydrogen in GaN, Mg-H complexes are observed in vibrational spectroscopy.

## ACKNOWLEGEMENTS

The authors are pleased to acknowledge J. Ager and W. Götz for the preliminary results from Raman spectroscopy and infrared absorption spectroscopy. They also thank C. Van de Walle

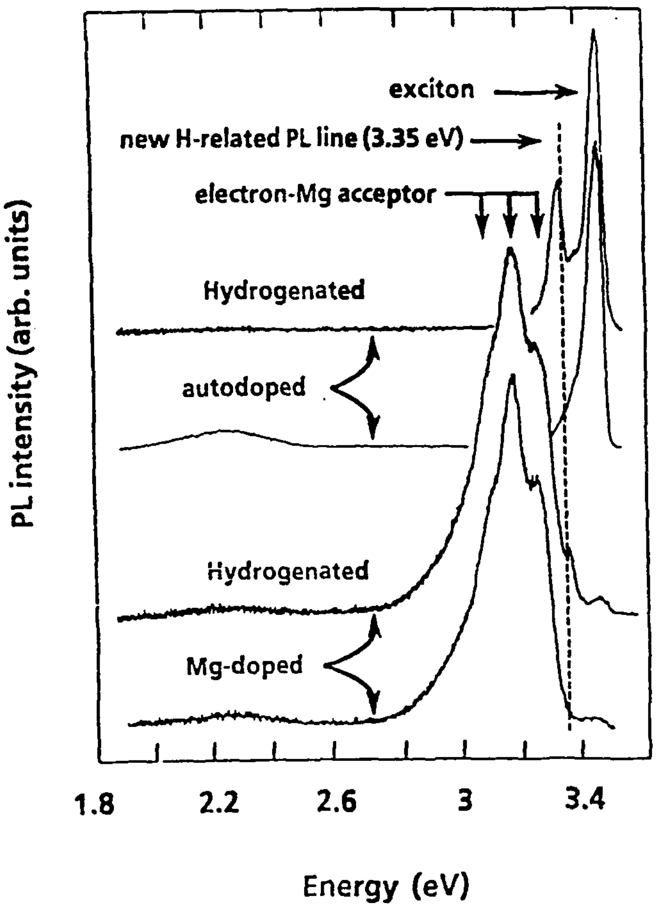


Figure 5: Photoluminescence spectra of autodoped and Mg-doped GaN, both before and after hydrogenation.

and E. E. Haller for helpful discussions and J. Walker and S. Ready for technical assistance. The work at Xerox was supported by AFOSR under contract F49620-91-C-0082 and at Boston University by ONR under contract N0014-92-j-1436. One of the authors (M.S.B.) acknowledges partial support from the Alexander von Humboldt-Stiftung.

## REFERENCES

[1] *Hydrogen in Semiconductors*, edited by J. I. Pankove and N. M. Johnson (Academic, San Diego, 1991).

[2] J. A. Wolk, J. W. Ager III, K. J. Duxstad, E. E. Haller, N. R. Taskar, D. R. Dorman, and D. J. Olego, Appl. Phys. Lett. **63**, 2756 (1993).

[3] H. Amano, M. Kito, K. Hiramatsu, and I. Akasaki, Jpn. J. Appl. Phys. **28**, L2112 (1989).

[4] T. D. Moustakas and R. J. Mclnar, Mat. Res. Soc. Conf. Proc. **281**, 753 (1993).

[5] J. I. Pankove and J. A.Hutchby, J. Appl. Phys. **47**, 5387 (1976).

[6] S. Nakamura, T. Mukai, M. Senoh, and N. Iwasa, Jpn. J. Appl. Phys. **31**, L139 (1992), S. Nakamura, N. Iwasa, M. Senoh, and T. Mukai, Jpn. J. Appl. Phys. **31**, 1258 (1992).

[7] J. Ager and W. Götz, private communication.

[8] J. A. Van Vechten, J. D. Zook, R. D. Horning, and B. Goldenberg, Jpn. J. Appl. Phys. **31**, 3662 (1992).

# Appendix K : “Hydrogenation of p-type Gallium Nitride”

# Hydrogenation of *p*-type gallium nitride

M. S. Brandt and N. M. Johnson
*Xerox Palo Alto Research Center, Palo Alto, California 94304*

R. J. Molnar, R. Singh, and T. D. Moustakas
*Department of Electrical, Computer, and Systems Engineering, Boston University, Boston, Massachusetts 02215*

(Received 29 November 1993; accepted for publication 3 February 1994)

Hole concentrations of up to $10^{19}$ $cm^{-3}$ have been reported for GaN:Mg films grown by molecular beam epitaxy without any post-growth treatment. Comparing results from Hall measurements and secondary ion mass spectrometry, we observe doping efficiencies of up to 10% at room temperatures in such *p*-type material. By hydrogenating at temperatures above 500 °C, the hole concentration can be reduced by an order of magnitude. A new photoluminescence line at 3.35 eV is observed after this treatment, both in *p*-type and unintentionally doped *n*-type material, which suggests the introduction of a hydrogen-related donor level in GaN.

Nitrogen-based III-V semiconductors are of considerable interest due to their unique electronic and mechanical properties. They are wide-band-gap semiconductors which possess a direct-gap band (e.g., GaN and AlN in the wurtzite structure have band gaps of 3.4 and 6.2 V, respectively) and high thermal stability.[1] Consequently, these materials are being developed for two different potential applications: blue/ultraviolet (UV) light-emitting diodes or lasers and high-temperature electronics. A major obstacle to the realization of these applications has been the high *n*-type background doping which is thought to arise from native *N*-vacancy defects.[2] Only recently, semi-insulating and *p*-type-doped GaN films have been obtained. In *p*-type material grown by metalorganic chemical vapor deposition (MOCVD), acceptor dopants (e.g., Mg and Zn) have been activated by either low-energy electron beam irradiation (LEEBI)[3] or thermal annealing.[4,5] On the other hand, *p*-type films can be obtained without the need of such post-growth treatments by molecular beam epitaxy (MBE) where chemically active nitrogen is generated in an electron cyclotron resonance (ECR) plasma.[6] The formation of Mg-H complexes under the abundant pressure of hydrogen during the MOCVD growth has been suggested by Nakamura[4,5] as the origin for the need to additionally activate acceptors in this material. In this letter, we report on the use of MBE-grown GaN, which as-grown displays a high acceptor concentration, to investigate the influence of intentionally introduced hydrogen on the properties of GaN. We demonstrate a substantial decrease in the hole concentration in initially *p*-type material after hydrogenation and report a new photoluminescence line at 3.35 eV after hydrogenation of both *p*-type and *n*-type material.

Wurtzite GaN epilayers were grown on (0001) sapphire substrates by ECR-assisted MBE. Gallium and the dopant elements (Mg and, for intentional *n*-type doping, Si) were evaporated from conventional Knudsen cells, while nitrogen radicals was produced by passing molecular nitrogen through an ECR source at a pressure of $10^{-4}$ Torr. A microwave power of 35 W or higher was used for the growth of semi-insulating GaN films. Prior to the growth of the GaN epilayer, the substrates were exposed to the N plasma for 30 min to form an AlN layer. A further GaN buffer layer was then grown at 500 °C followed by the high-temperature growth of the actual film at 800 °C at a growth of 200–250 nm/h. The typical thickness of the films studied here was 1 μm. In the case of *p*-type samples, an undoped buffer layer of 300 nm was first grown before the actual growth of the doped material. We have not observed any significant dependence of the crystal quality on either thickness or dopant in MBE-grown GaN.[6,7]

Hydrogenation was performed with a remote microwave plasma operating at 2 Torr. This technique excludes effects due to charged particle bombardment of the sample or its illumination from the plasma.[8] A high temperature sample holder allowed hydrogenation at temperatures up to 675 °C. No change in the surface morphology was observed after hydrogenation. The films were electrically characterized in a standard Hall-effect apparatus, with the samples abrasively etched into a clover-leaf shape. For ohmic contacts, Au was deposited on *p*-type GaN and Al on *n*-type material. Depth profiles were determined from secondary ion mass spectrometry (SIMS), with a $Cs^+$ primary ion beam for the detection of hydrogen/deuterium and an $O^-$ primary beam for Mg. Calibration of the SIMS data was achieved with Mg and deuterium-implanted GaN reference samples. To increase the sensitivity, the GaN samples for SIMS were treated with a plasma containing deuterium instead of hydrogen. The photoluminescence measurements were performed with a pulsed $N_2$ laser as the excitation source (3.678 eV). The photoluminescence was focused onto the entrance slit of a 0.25 m grating monochromator and detected with a photomultiplier read out by a lock-in amplifier.

Figure 1 shows the carrier concentration at room temperature for three different samples subjected to isochronal (1 h) hydrogenation: a Mg-doped sample exhibiting *p*-type conductivity, an unintentionally (autodoped) *n*-type sample, and a Si-doped sample exhibiting *n*-type conductivity. The latter samples were unaffected by the hydrogenation up to hydrogenation temperatures *T* of 600 °C, in contrast to recent reports on InAlN and InGaN.[9] In the *p*-type material, however, the hole concentration was reduced by over an order of magnitude by hydrogenation at T≥500 °C. The mobility, as determined by the Hall measurements, remained

 0003-6951/94/64(17)/2264/3/$6.00 

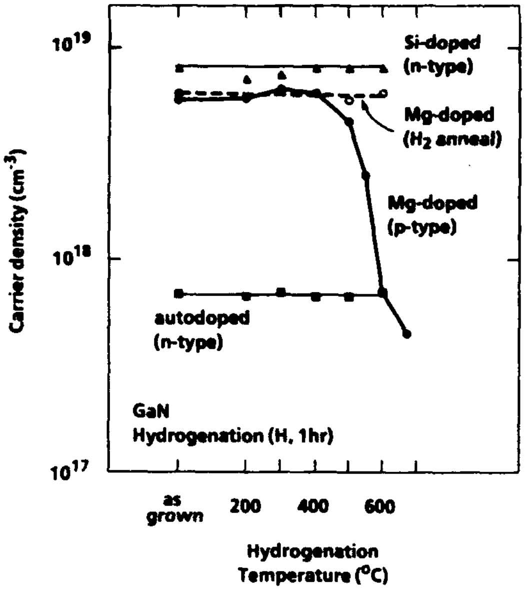


FIG. 1. Dependence of the carrier density on hydrogenation temperature in epitaxial layers of GaN. The isochronal hydrogenations were performed in a remote-plasma system.

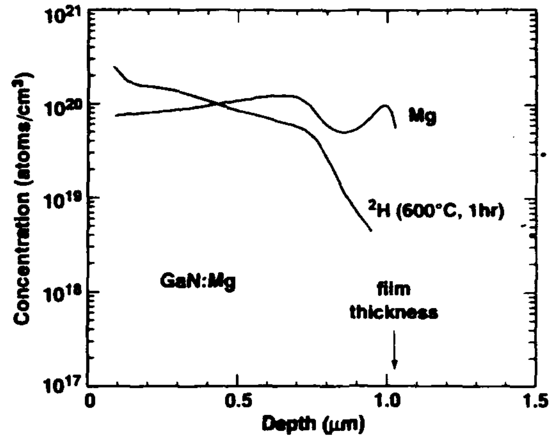


FIG. 2. Depth profiles of hydrogen and magnesium in $p$-type GaN determined by secondary ion mass spectrometry. The hole concentration before hydrogenation was $7\times10^{18}$ cm$^{-3}$.

unchanged at $\sim$0.3 cm$^2$/V s in the $p$-type samples, which suggests that the mobility is not limited by ionized dopant scattering.

A similar decrease in the hole concentration of Mg-doped GaN has been reported by Nakamura and co-workers.[4,5,10] They used MOCVD-grown material, which had been LEEBI-treated to obtain the initial dopant activation. For a source of hydrogen these authors used $NH_3$ which had to be thermally decomposed at the sample surface. The observed passivation conditions, especially the temperature, in these experiments could, therefore, be characteristic of either the GaN (e.g., diffusion process or activation energy for the formation of complexes) or rather of the $NH_3$ decomposition on the sample surface. The results presented in this letter unambiguously establish that the comparatively high temperature for the passivation is due to the bulk properties of GaN. In addition, the control experiment included in Fig. 1, where the microwave plasma was switched off during the post-growth treatment of the samples, demonstrates that exposure to molecular hydrogen at temperatures up to 600 °C does not affect the hole concentration of $p$-type GaN.

The introduction of hydrogen into the material was verified with SIMS. In Fig. 2, depth profiles are shown for both Mg and deuterium. The Mg profile together with the hole concentration quoted above permits an estimation of the doping efficiency that can be achieved with ECR-assisted MBE. For the specific sample illustrated here the efficiency is slightly less than 10% at room temperature. From photoluminescence experiments such as those discussed below, one expects the acceptor to have an ionization energy of about 150 meV. For thermal excitation into the valence band, significantly less than 1% of the acceptors should be ionized at 300 K. The considerably higher apparent ionization of 10% therefore suggests that the dominant transport process is impurity-band conductivity. This would be consistent with the high dopant concentration of $10^{20}$ cm$^{-3}$ revealed by SIMS.

With regard to the effects of hydrogenation, the SIMS profile in Fig. 2 shows that the deuterium concentration found after passivation at 600 °C for 1 h is about the same as the concentration of Mg. The gradual decrease of the deuterium concentration for depths beyond 0.7 $\mu$m coincides with the end of the intentionally Mg-doped layer, which is grown on an undoped buffer layer of 0.3 $\mu$m thickness. The SIMS data, therefore, establish that under the hydrogenation conditions which produced the observed decrease in hole concentration hydrogen is introduced into the sample to the same concentration as the Mg.

There are in principle two mechanisms which could account for the results presented in Figs. 1 and 2: the formation of Mg-H complexes, which would passivate the acceptors, or compensation due to the possible donor state induced by hydrogen in GaN. An unambiguous experiment which would show the existence of Mg-H complexes would be the observation of its local vibrational modes. Such modes have been observed in other materials such as Si and GaAs, establishing the presence of such dopant-hydrogen complexes.[11,12] With samples from the present study, preliminary Raman scattering[13] and infrared absorption[14] measurements reveal vibrational modes in the vicinity of 2200 cm$^{-1}$ in samples with very high Mg concentration and low doping efficiency. These results will be presented in a forthcoming publication. It appears that the observed reduction in the hole concentration is indeed due to the formation of hydrogen-acceptor complexes as previously suggested.[4,5]

Further information on the effects of hydrogen in GaN were obtained from photoluminescence (PL). In Fig. 3, a comparison is shown between the photoluminescence of Mg-doped and autodoped samples, both before and after hydrogenation at 600 °C. The two dominant PL lines in the as-grown samples are the exciton line at 3.44 eV and the Mg-acceptor related line at 3.25 eV, with its two phonon replicas. After hydrogenation, these lines are still observed in the respective samples, but a quantitative comparison of signal

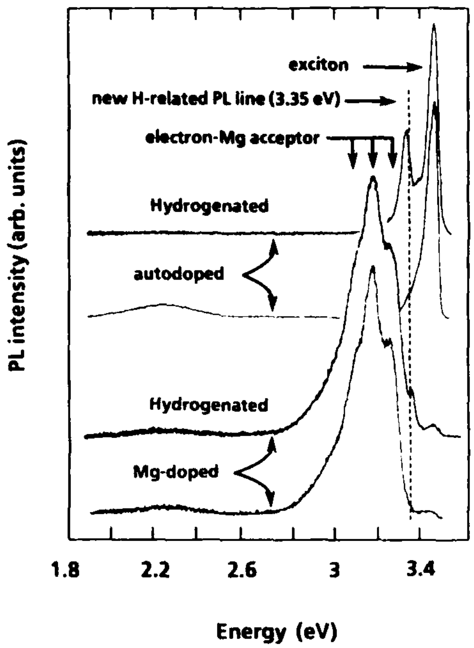


FIG. 3. Photoluminescence spectra of Mg-doped and autodoped GaN, both before and after hydrogenation.

heights is difficult. In addition to these known PL lines, a new PL line at 3.35 eV appears after hydrogenation in both samples, which has not been previously reported in GaN.

These PL results differ considerably from those reported by Nakamura and co-workers[5] on both LEEBI-treated and annealed Mg-doped GaN. The intensity of their dominant PL line, centered at 2.75 eV, is quenched by about one order of magnitude after an 800 °C treatment with $NH_3$. At the same time, the authors observed an increase of a possibly defect-related broad PL line centered at 1.65 eV. A possible explanation for the observed passivation of holes would therefore be the formation of deep defect states compensating the acceptors in their experiment. Although our PL measurements only extend down to 1.9 eV, the high-energy side of the broad defect-related PL band discussed above is clearly not observed. Our hydrogenation treatment therefore does not induce additional defects. In contrast, the defect-related PL band at 2.3 eV (Refs. 15 and 16) is completely quenched after hydrogenation of the auto-doped sample, which indicates a passivation of these defects, probably once again by complex formation.

The new PL line is located ~100 meV below the band gap after hydrogenation in both $p$-type and $n$-type GaN. From the PL data alone it is impossible to determine whether this state is adjacent to the conduction band, and therefore acting as a donor, or immediately above the valence-band maximum, and acting as an acceptor. The latter possibility seems untenable in view of the Hall data of Fig. 1, since the presence of acceptors shallower than the Mg-related level should counterbalance the observed passivation effect. On the other hand, if the state acts as a donor, there should be an effect on the electron concentration in the $n$-type samples, since the new PL line is also present in the autodoped samples. SIMS data revealed that about $10^{19}$ cm$^{-3}$ hydrogen atoms were introduced into the autodoped sample by hydrogenation, thereby giving an upper limit for the additional donor concentration. Thermal activation at room temperature of this assumed donor level deeper than the native defect related level would lead to an added electron concentration of $10^{17}$ cm$^{-3}$, significantly lower than the observed electron concentration of $8\times10^{17}$ cm$^{-3}$ due to the nitrogen deficiency. This would be consistent with the failure to observe any changes in the electron concentration of the autodoped sample in Fig. 1 and therefore be consistent with the assumption of a hydrogen-induced donor state. Another possible interpretation of the new PL line could be the formation of extended defects such as dislocations by the hydrogenation. The binding energy of such defects might be as large as the 100 meV PL shift observed. Clearly, further studies are required for the final assignment of this new PL line.

In conclusion, we have shown that by introducing hydrogen into MBE-grown $p$-type GaN the hole concentration can be substantially reduced, which suggests the formation of Mg-H complexes. No change in the electrical properties of $n$-type samples has been observed up to 600 °C. A new photoluminescence line at 3.35 eV appears after hydrogenation in both $p$- and $n$-type samples. The photoluminescence indicates that hydrogen might have a donor level in GaN.

The authors are pleased to acknowledge J. Ager and W. Götz for the preliminary results from Raman spectroscopy and infrared absorption spectroscopy. They also thank C. Van de Walle and E. E. Haller for helpful discussions and J. Walker and S. Ready for technical assistance. The work at Xerox was supported by AFOSR under Contract F49620-91-C-0082 and at Boston University by ONR under Contract N0014-92-j-1436. One of the authors (M.S.B.) acknowledges partial support from the Alexander von Humboldt-Stiftung.

[1] S. Strite and H. Morkoc, J. Vac. Sci. Technol. B **10**, 1237 (1992).
[2] J. I. Pankove, Mater. Res. Soc. Conf. Proc. **162**, 515 (1990).
[3] H. Amano, M. Kito, K. Hiramatsu, and I. Akasaki, Jpn. J. Appl. Phys. **28**, L2112 (1989).
[4] S. Nakamura, T. Mukai, M. Senoh, and N. Iwasa, Jpn. J. Appl. Phys. **31**, L139 (1992).
[5] S. Nakamura, N. Iwasa, M. Senoh, and T. Mukai, Jpn. J. Appl. Phys. **31**, 1258 (1992).
[6] T. D. Moustakas and R. J. Molnar, Mater. Res. Soc. Conf. Proc. **281**, 753 (1993).
[7] T. D. Moustakas, T. Lei, and R. J. Molnar, Physica B **185**, 36 (1993).
[8] N. M. Johnson, in *Hydrogen in Semiconductors*, edited by J. I. Pankove and N. M. Johnson (Academic, San Diego, 1991), p. 113.
[9] S. J. Pearton, C. R. Abernathy, P. W. Wisk, W. S. Hobson, and F. Ren, Appl. Phys. Lett. **63**, 1143 (1993).
[10] J. A. Van Vechten, J. D. Zook, R. D. Horning, and B. Goldenberg, Jpn. J. Appl. Phys. **31**, 3662 (1992).
[11] M. Stavola and S. J. Pearton, in *Hydrogen in Semiconductors*, edited by J. I. Pankove and N. M. Johnson (Academic, San Diego, 1991), p. 139.
[12] J. Chevallier, B. Clerjaud, and B. Pajot, in *Hydrogen in Semiconductors*, edited by J. I. Pankove and N. M. Johnson (Academic, San Diego, 1991), p. 447.
[13] J. W. Ager III (private communication).
[14] W. Götz (private communication).
[15] J. I. Pankove and J. A. Hutchby, J. Appl. Phys. **47**, 5387 (1976).
[16] R. Singh, R. J. Molnar, M. S. Ünlü and T. D. Moustakas, Appl. Phys. Lett. **64**, 336 (1994).

# Appendix L : “Local Vibrational Modes in Mg-doped Gallium Nitride”

PHYSICAL REVIEW B VOLUME 49, NUMBER 20 15 MAY 1994-II

# Local vibrational modes in Mg-doped gallium nitride

M. S. Brandt*
*Xerox Palo Alto Research Center, Palo Alto, California 94304*

J. W. Ager III
*Lawrence Berkeley Laboratory, Berkeley, California 94720*

W. Götz† and N. M. Johnson
*Xerox Palo Alto Research Center, Palo Alto, California 94304*

J. S. Harris, Jr.
*Solid State Electronics Laboratory, Stanford University, Stanford, California 94305*

R. J. Molnar and T. D. Moustakas
*Department of Electrical, Computer, and Systems Engineering, Boston University, Boston, Massachusetts 02215*

(Received 4 January 1994)

Four local vibrational modes are reported for Mg-doped wurtzite GaN. which as grown possesses high concentrations of hydrogen. The modes, studied by Raman and infrared absorption spectroscopy appear to form two pairs. Based on the observed selection rules, one pair, with room-temperature frequencies of 2168 and 2219 $cm^{-1}$ is assigned to inequivalent Mg-H complexes in the $c$ plane and parallel to the $c$ axis, respectively. The origin of the second pair of modes at 2151 and 2185 $cm^{-1}$, which are IR inactive, is speculatively linked to the presence of diatomic molecules such as $N_2$ or $H_2$.

Wide-band-gap II-VI and III-V semiconductors are receiving considerable attention due to their possible applications in ultraviolet to green-light emission devices and high-temperature electronics. A major obstacle to the realization of such devices is an apparent difficulty to obtain $p$-type doping in these materials when using growth techniques such as metal-organic chemical vapor deposition (MOCVD). This limitation has recently been overcome by the successful growth of films by molecular-beam epitaxy (MBE). The absence of hydrogen from the gas phase during MBE growth has led to the assumption that the formation of acceptor-hydrogen complexes is the reason for the low doping efficiency in MOCVD-grown material.

Dopant-hydrogen complexes in semiconductors have been studied with a variety of techniques.[1] The effect of hydrogen on the electrical activity of the dopants has been studied by temperature-dependent Hall effect measurements and the spatial extent of a passivation by capacitance-voltage measurements. A definite proof for the existence of complexes, however, can only be obtained by the observation of their local vibrational modes (LVM) with infrared (IR) or Raman spectroscopies. In silicon and gallium arsenide, where the effects of hydrogen have been most extensively studied so far, the local vibrational modes of hydrogen bound to a large variety of dopants have been identified. These include H-containing complexes with B, Al, Ga, P, As, and Sb in Si and with Si, Ge, Sn, Zn, Be, and Cd in GaAs.[2,3] By analyzing the polarization dependence of vibrational modes in IR and Raman experiments, information on the symmetry of the complexes is obtained. Calculations determining the total energy of different configurations that are compatible with the observed symmetry or measurements of the vibrational modes under uniaxial stress can then identify the microscopic structure of the complexes.

In ZnSe, a wide-band-gap compound, the observation of the vibrational modes of N-H complexes in MOCVD grown material has indeed shown that such acceptor-hydrogen complexes are formed and appear to limit the $p$-type doping efficiency.[4,5] In $p$-type GaN electrical measurements have shown that Mg acceptors can be passivated or compensated by introduction of hydrogen from a remote microwave plasma at hydrogenation temperatures above 400 °C.[6,7] A new photoluminescence line at 3.35 eV was observed after hydrogenation. which might indicate that hydrogen has a donor level in this material. On the other hand, secondary-ion mass spectrometry (SIMS) revealed that hydrogen can be introduced to the same concentrations as the Mg acceptors, which could indicate complex formation. Vibrational spectroscopy, as discussed above, should be able to establish the presence and structure of such hydrogen-dopant complexes. In this paper, we report the observation of several local vibrational modes in Mg-doped GaN epitaxial films which possess significant H concentrations. We assign a LVM pair at 2168 and 2219 $cm^{-1}$ to the stretching vibrations of two inequivalent Mg-H complexes. The origin of a second, IR inactive pair at 2151 and 2185 $cm^{-1}$ is discussed and might be due to the presence of $H_2$ or $N_2$ in the films.

Wurtzite GaN epilayers were grown on (0001) $c$-plane sapphire substrates by electron cyclotron resonance (ECR) microwave plasma assisted MBE.[8,9] Gallium and magnesium were evaporated from conventional Knudsen cells, and activated nitrogen was produced with an efficiency of about 10% by passing molecular nitrogen through the ECR source at a pressure of $10^{-4}$ Torr and a microwave power of typically 35 W in the ECR plasma. Prior to the growth of the GaN epilayer, the substrates were exposed to the N plasma for 30 min to convert the surface of the sapphire substrates to AlN. A GaN buffer layer was then grown at 500 °C followed by the high-temperature growth of the actual film at 800 °C at a growth rate of 200 to 250 nm/h. The two-temperature growth was shown to promote lateral growth and thus layer-by-layer growth. Depth profiles from SIMS typically show Mg concentrations of $10^{20}$ $cm^{-3}$. Room-temperature Hall measurements find hole concentrations of up to $10^{19}$ $cm^{-3}$ in some samples, which corresponds to a doping efficiency of $\approx$10%. However, the specific samples studied here show H concentrations above $10^{19}$ $cm^{-3}$ as determined with SIMS. The exact origin of this contamination is unknown at present, but appears correlated with the microwave power used in the ECR source and linked to the Mg doping. The ECR plasma tends to activate spurious hydrogen concentrations in the gas phase and thereby increases its incorporation probability in the films. Furthermore, there is mass-spectroscopic evidence from the outgassing Mg source that Mg tends to getter hydrogen which is then released during the Mg evaporation. The hydrogen content in the films can be minimized by carefully outgassing of the system prior to the growth of the GaN films, thereby increasing the doping efficiency. MOCVD-grown Mg-doped GaN was not available for this study.

Raman spectra were excited at room temperature by 100 mW of 488 nm laser light in a custom-built Raman microprobe based on an Olympus metallurgical microscope with a 50× objective ($NA = 0.8$). The spot size was approximately 2 $\mu$m. Spectra were detected by an imaging PMT (1024×1024) with a holographic notch filter (Kaiser Optical Systems) and a 640 nm spectrograph with a 1200 groove/mm grating. Typical collection times were between 200 and 800 s. The spectral resolution was 4 $cm^{-1}$ and the precision of the line center determinations is $\pm 1$ $cm^{-1}$. Polarized spectra were corrected for differences in grating efficiency by calibration with a white light source. Since only epilayers of typically 1 $\mu$m thickness grown on $c$-plane sapphire were available for this study, only Raman measurements in the backscattering configuration $z(xx)\bar{z}$ or $z(xy)\bar{z}$ could be performed, with the $z$ direction parallel to the $c$ axis of the wurtzite structure.

The infrared absorption measurements were conducted at temperatures of 300 K and 8 K with a Bruker IFS 113 Fourier transform spectrometer. A mid-IR globar light source, a KBr/Ge beam splitter, and an MCT detector were used. The resolution was 2 $cm^{-1}$. To avoid reduction of sensitivity due to light interference in the thin GaN layers, the light was incident on the samples at an angle of 60° from the surface normal. For an index of refraction corresponding to a relative permittivity of $\approx 9$, the infrared light propagation vector made an angle of 15° with respect to the $c$ axis. Because of the sample geometry, only transmission measurements with the propagation of the light nearly parrallel to the $c$ axis could be performed.

The results of the room-temperature Raman and infrared absorption measurements on a variety of Mg-doped GaN samples are summarized in Fig. 1. Four Raman active vibrational modes were detected, which appear to comprise two pairs. One sample shows only the first pair at 2168 and 2219 $cm^{-1}$ [Fig. 1(a)]. In most samples studied, however, a second pair at about 2151 and 2185 is observed as shown in the Raman spectra of Fig. 1(b), the lower frequency peak being considerably broader than the other peaks observed here. Within a pair, the relative intensities of the peaks remain constant at around 1 to 2 for both pairs, while the intensities of the two pairs with respect to each other vary considerably as exhibited by the two Raman spectra shown. Both pairs show the same polarization dependence: By changing from the $z(xx)\bar{z}$ to the $z(xy)\bar{z}$ scattering configuration, the Raman intensity is reduced by a factor of 10, but the spectral shape remains unchanged. Both undoped and hydrogenated Si-doped ($4\times10^{20}$ $cm^{-3}$) control samples were investigated for similar vibrational modes both in this frequency region and near 3000 $cm^{-1}$. No Raman signal of a local vibrational mode was found in these samples.

In the IR absorption of all Mg-doped GaN films studied here, however, only the first pair is observed, with the high-frequency mode at 2219 $cm^{-1}$ barely detectable in the specific transmission geometry that was used. In fact, the IR spectrum shown in Fig. 1(c) was obtained on a

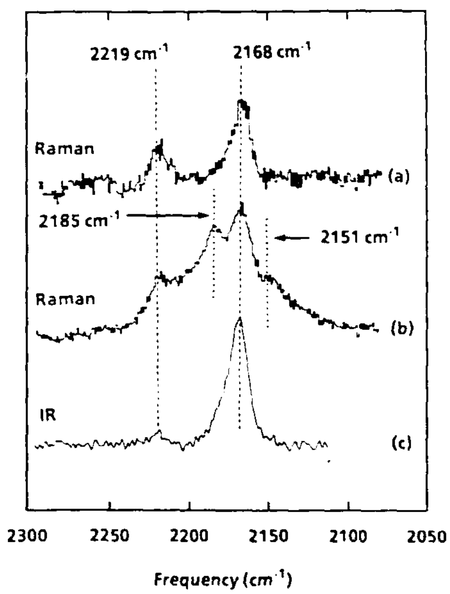


FIG. 1. Local vibrational modes in Mg-doped GaN. The Raman spectra (a) and (b) and the IR spectrum (c) were obtained from different samples. The Raman measurements were performed under ambient conditions in the $z(xx)\bar{z}$ polarization configuration. The IR measurements were performed with the sample in vacuum at room temperature. Two pairs of LVM are found, indicated by dashed and dotted lines. Only the pair at 2168 and 2219 $cm^{-1}$ is IR active. It is assigned to Mg-H complexes oriented either in the $c$ plane or parallel to the $c$ axis of the wurtzite lattice, respectively.

sample possessing a particularly strong Raman signal at 2185 $cm^{-1}$, which is a constituent of the second pair. The typical linewidth of the 2168 $cm^{-1}$ mode observed with both techniques is 15 $cm^{-1}$. This inhomogeneous broadening might be due to residual strain or the high concentration of vibrational centers.

Manabe and co-workers have studied local vibrational modes of Be in CdS and CdSe, which also have a wurtzite lattice.[10] While the wurtzite lattice has $C_{6v}$ point group symmetry, the defect with Be on the Cd site has $C_{3v}$ point group symmetry. The effect is a splitting of the local vibrational mode into two peaks with local symmetries $A_1$ (IR dipole parallel to $c$ axis) and $E_1$ (IR dipole perpendicular to $c$ axis). In the case of a hypothetical Mg-H local vibrational mode, the addition of the hydrogen changes the symmetry slightly. If the hydrogen atom is along the $c$ axis bonding direction (e.g., Conf. I in Fig. 2), the point symmetry is $C_{3v}$. If, on the other hand, the H is along a bonding direction in the plane (e.g., Conf. II), the symmetry is $C_s$: there is a single plane of symmetry containing the Ga atom in the next layer and the Mg-H bond. This gives rise to the selection rules for infrared and Raman spectroscopies listed in Table I. For the specific transmission and scattering geometries employed here, we therefore expect from group theory to observe only vibrations of Conf. II (H in $c$ plane) with IR, but both configurations in Raman.

Returning to the experimental results of Fig. 1, we find that the first pair at 2168 and 2219 $cm^{-1}$ indeed behaves as expected for an acceptor-hydrogen complex in a wurtzite material. From the selection rule exhibited by the IR spectrum, we therefore would assign the 2168 $cm^{-1}$ mode to the $A'$ vibration of Mg-H complexes oriented in the $c$ plane and the 2219 $cm^{-1}$ mode to the

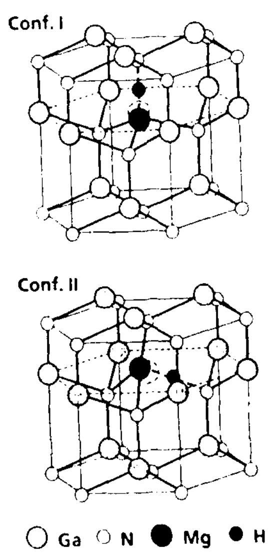


FIG. 2. Hypothetical structural configurations of the two inequivalent sites of the Mg-H complex in GaN. The hydrogen is assumed to be in a bond-center position, with the Mg atom relaxing to the plane formed by its nearest N neighbors. In Conf. I the Mg-H bond is in the $c$-axis direction, while in Conf. II the bond is in the $c$ plane. The dashed circles indicate substitutional lattice sites.

TABLE I. Selection rules for the vibrational spectroscopy of Mg-H complexes in wurtzite GaN.

| | Point symmetry | Vibration | IR | Raman |
|---|---|---|---|---|
| Conf. I | $C_{3v}$ | $A_1$ | $z$ | $xx = yy, zz$ |
| Conf. II | $C_s$ | $A'$ | $x, y$ | $xx, yy, xy, zz$ |

$A_1$ vibration of Mg-H parallel to the $c$ direction which is IR inactive for transmission experiments with the light propagating in the $c$ direction. (The weak IR signal at 2219 $cm^{-1}$ is indeed consistent with the slight off $c$ axis orientation of the sample during the IR measurements.) This assignment to a H complex is corroborated by the SIMS results which show that the local vibrational modes are observable only in samples with $[Mg] \geq 10^{20}$ $cm^{-3}$ and, avaraged over the sample thickness, $[H] \geq 10^{19}$ $cm^{-3}$. The participation of Mg in the complex is further supported by the absence of the modes discussed above in undoped or Si-doped GaN. Finally, the observed frequencies are in a spectral region where only stretching vibrations of hydrogen are expected. Indeed, the local vibrational modes of group-II acceptor hydrogen complexes in $p$ type GaAs and InP observed so far all lie between 2037 and 2287 $cm^{-1}$, very near to the modes reported here. However, there appears to be no previous report of vibrational modes related to Mg-H complexes in these materials.[11]

The exact microscopic configuration of the Mg-H complex in GaN cannot be established from the measurements reported here, although the observed selection rules are consistent with the hydrogen situated on a Mg-N bond axis. There are two sites available: (i) the H in the Mg-N bond (bonding or bond-center site) or (ii) the H opposite to this bond in the antibonding site. Total energy calculations have determined that for both group-III acceptors in Si and for group-II acceptors in GaAs the bond center site is the energetically more favorable. This specific configuration is shown in Fig. 2 for the complex in both the $c$ direction (Conf. I) and the $c$ plane (Conf. II). The introduction of the hydrogen may lead to a threefold coordination of the acceptor atom and a relaxation towards the plane formed by its three nearest N neighbors. Support for this assumption might be obtained from the comparison of the observed stretching frequencies around 2200 $cm^{-1}$ in GaN to those in corresponding molecules. One finds the stretching modes at 3444 $cm^{-1}$ in $NH_3$ and 1450 $cm^{-1}$ in MgH,[12] which could indeed indicate that both N and Mg participate in the bonding of the hydrogen atom. However, the corresponding argument fails in the case of B-doped Si, where the observed mode of the B-H complex has a lower frequency than both $SiH_4$ and $B_2H_6$. It should also be noted that the frequency of the proposed Mg-H local vibrational mode in GaN does not appear to be strongly influenced by the presence of nitrogen at the group-V lattice site, when compared, for example, to LVM's of group-II acceptor hydrogen complexes in GaAs. This might indicate that the hydrogen atom is in the antibonding site rather than in the bond center position. In addition, in silicon the H-Ga complex has a local vibrational mode[13] at 2171 $cm^{-1}$, which coincides with the strong IR-active mode shown in Fig. 1. Therefore, another possible candidate for the complex is a nitrogen vacancy with one or several of the adjacent Ga atoms passivated by hydrogen. Since the LVM's are observed only in Mg-doped material, such a hypothetical vacancy should correlate with a Mg atom. Total energy calculation will be invaluable to identify the microscopic configuration(s) of the Mg-H complex in GaN.

The assignment of the second pair at 2151 and 2185 $cm^{-1}$ in Mg-doped GaN films is considerably more difficult. The failure to observe absorption in IR spectroscopy would indicate that the microscopic structure does not exhibit a built-in dipole moment in the polarization direction of the IR used in the transmission experiments. (In fact, due to the limited signal-to-noise ratio, we can only conclude that the IR cross section is at least a factor of 20 smaller than that for the mode at 2168 $cm^{-1}$.) One possibility could be $Mg_2$ or Mg precipitates, although their vibrations are expected to occur at considerably lower frequencies. Another possibility are diatomics, however, $H_2$ and $N_2$ have stretching frequencies in the gas phase of 4395 and 2360 $cm^{-1}$, respectively. A definite assignment can once again only be made based on calculations. Although it is expected that the $H_2$ vibration in Si is considerably shifted downwards to about 2300 $cm^{-1}$,[14] preliminary calculations of $N_2$ in GaN show that this molecule can be incorporated into the crystal without significant changes in its vibrational frequency.[15] The suggestion that the second pair might originate from $N_2$ molecules, again oriented in two nonequivalent configurations parallel to the $c$ axis and in the $c$ plane, receives some corroboration from the growth conditions used, which as in the case of GaAs, employed an overpressure of the group-V constituent to avoid surface segregation of Ga. It however remains to be understood under this assumption why the hypothetical $N_2$ mode is not observed in undoped or Si-doped GaN, which are grown with the same overpressure of nitrogen. One possibility is that the incorporation or stability of $N_2$ in GaN might be dependent on the Fermi level position. A continuing systematic study of growth conditions by LVM spectroscopy is anticipated to yield new insights and fundamental information on native defects as well as dopant incorporation during growth of GaN.

The authors are pleased to thank C. Van de Walle, J. Neugebauer, and E. E. Haller for helpful discussions and B. Krusor for technical assistance. The work at Xerox PARC was supported by AFOSR under Contract No. F49620-91-C-0082 and at Boston University by ONR under Contract No. N0014-92-j-1436. The work at LBL was supported by the Director, Office of Energy Research, under Contract No. DE-AC03-76SC00098. Two of the authors (M.S.B. and W.G.) acknowledge partial support from the Alexander von Humboldt-Stiftung.

* Present address: Walter Schottky Institute, Technical University of Munich, D-85748 Garching, Germany.

† Permanent address: Solid State Electronics Laboratory, Stanford University, Stanford, CA 94305.

[1] *Hydrogen in Semiconductors*, edited by J. I. Pankove and N. M. Johnson (Academic, San Diego, 1991).

[2] M. Stavola and S. J. Pearton, in *Hydrogen in Semiconductors* (Ref. 1), p. 139, and references therein.

[3] J. Chevallier, B. Clerjaud, and B. Pajot, in *Hydrogen in Semiconductors* (Ref. 1), p. 447, and references therein.

[4] J. A. Wolk, J. W. Ager III, K. J. Duxstad, E. E. Haller, N. R. Taskar, D. R. Dorman, and D. J. Olego, Appl. Phys. Lett. **63**, 2756 (1993).

[5] A. Kamata, H. Mitsuhasi, and H. Fujita, Appl. Phys. Lett. **63**, 3353 (1993).

[6] M. S. Brandt, N. M. Johnson, R. J. Molnar, R. Singh, and T. D. Moustakas, Appl. Phys. Lett. (to be published).

[7] S. Nakamura, N. Iwasa, M. Senoh, and T. Mukai, Jpn. J. Appl. Phys. **31**, 1258 (1992).

[8] T. D. Moustakas and R. J. Molnar, in *Semiconductor Heterostructures for Photonic and Electronic Applications*, edited by C. W. Tu. D. C. Houghton, and R. T. Tung, MRS Symposia Proceedings No. 281 (Materials Research Society, Pittsburgh, 1993), p. 753.

[9] T. D. Moustakas, T. Lei, and R. J. Molnar, Physica B **185**, 36 (1993).

[10] A. Manabe, A. Mitsuishi, H. Komiya, and S. Ibuki, Solid State Commun. **12**, 337 (1973).

[11] R. Rahbi, B. Pajot, J. Chevallier, A. Marbeuf, R. C. Logan, and M. Gavand, J. Appl. Phys. **73**, 1723 (1993).

[12] A. Guntsch, Z. Phys. **104**, 587 (1937).

[13] M. Stavola, S. J. Pearton, J. Lopata, and W. C. Dautremont-Smith, Appl. Phys. Lett. **50**, 1086 (1987).

[14] C. G. Van de Walle, Phys. Rev. B **49**, 4579 (1994).

[15] J. Neugebauer and C. G. Van de Walle (private communication).

# Appendix M : "Reactive Ion Etching of GaN Thin Films"

# REACTIVE ION ETCHING OF GaN THIN FILMS

Michael Manfra[1], Stuart Berkowitz[1], Richard Molnar[2], Anna Clark[1], T.D. Moustakas[2] and W.J. Skocpol[1]

[1]Department of Physics, Boston University, Boston Ma 02215
[2]Department of Engineering. Boston University, Boston Ma 02215

## ABSTRACT

Reactive ion etching of GaN grown by electron-cyclotron-resonance, microwave plasma-assisted molecular beam epitaxy on (0001) sapphire substrates was investigated. A variety of reactive and inert gases such as $CCl_2F_2$, $SF_6$, $CF_4$, $H_2/CH_4$ mixtures, $CF_3Br$, $CF_3Br$/Argon mixtures and Ar were investigated. From these studies we conclude that of the halogen radicals investigated, Cl and Br etch GaN more effectively than F. The etching rate was found to increase with decreasing pressure at a constant cathode voltage. a result attributed to larger mean free path of the reactive species.

## INTRODUCTION

The family of refractory nitrides (InN, GaN, AlN), their solid solutions and heterojunctions are one of the most promising families of electronic materials. All three binary compounds are direct bandgap semiconductors with energy gaps covering the region from 1.95eV (InN) and 3.4eV (GaN) to 6.28eV (AlN). These materials should find applications in optical devices (LED's lasers, detectors) operating in the green-blue-UV parts of the electromagnetic spectrum. Due to their unique physical properties, the materials are also expected to find applications in high temperature, high power, and high frequency electronic devices. However, the fabrication of such devices requires the development of a number of device processing techniques, including reactive ion etching.

There are limited reports in the literature regarding etching of GaN [1-4]. Pankove [1] reported that GaN dissolves in hot alkali solutions at very slow rates, and thus, wet etching is not practical for this strongly bonded material. Foresi [2] reported the reactive ion etching of GaN grown on the R-plane of sapphire using $CCl_2F_2$, and Adesida [3] reported the etching of GaN using $SiCl_4$. Pearton [4] investigated ECR microwave discharges for the etching of GaN, InN and AlN.

In this paper we report on reactive ion etching studies of GaN grown on (0001) sapphire substrates using a variety of reactive and inert gases. The effect of plasma parameters on etch rate, morphology and selectivity were investigated.



Mat. Res. Soc. Symp. Proc. Vol. 324. ©1994 Materials Research Society

## EXPERIMENTAL METHODS

The GaN films were grown onto (0001) sapphire substrates by the method of electron-cyclotron-resonance microwave plasma-assisted molecular beam epitaxy (ECR-MBE) using a two temperature step growth process [5,6]. In this method a GaN buffer is grown first at low temperature (500°C) and the rest of the film is grown at higher temperatures. This process was shown [5.6] to lead to high lateral growth rate resulting in a layer by layer growth. The films have the wurtzite structure with the c-axis perpendicular to the substrate. Although the films were not intentionally doped they were found to be n-type with carrier concentrations in the order of $10^{18}cm^{-3}$, due presumably to nitrogen vacancies.

The ion etching of the GaN films was carried out in a parallel plate reactor supplied with 13.5 MHz RF power. Various patterns were formed on the top of the GaN films with AZ 1350 J photoresist. Various reactive and inert gases were employed. The depth of the profile of the etches was determined by a profilometer or by directly measuring the thickness by a cross-sectional SEM image. The quality of the etch morphology was also assessed by SEM imaging.

## EXPERIMENTAL RESULTS AND DISCUSSION

First the etching rate from different reactive and inert gases was investigated. To compare the results the etching was carried out at the same gas pressure (11mT) and the same cathode voltage (600V). The results are listed in Table I.

**Table I. Etching rates of GaN (11mT and 600V cathode voltage.)**

| Gas | Etching Rate (Å/min) |
|---|---|
| $CCl_2F_2$ | 185 |
| $CF_3Br$ | 150 |
| $CF_3Br/Ar$ (3:1) | 200 |
| $CF_4$ | 120 |
| $SF_6$ | 100 |
| $H_2/CH_4$ (2:1) | 30 |
| Ar | 65 |

From these results it is apparent that F is a less efficient etchant of GaN than the other halogen radicals Cl and Br. Etching by hydrogen radicals and physical sputtering are even less efficient processes. Nevertheless, the mixture of a certain percentage of Ar in $CF_3Br$ improves the etching rate of the reactive gas.

The effect of gas pressure on the etching rate of GaN was investigated by using $CF_3Br/Ar$ (3:1) and a constant cathode voltage of 600V. The results are shown in Figure 1.

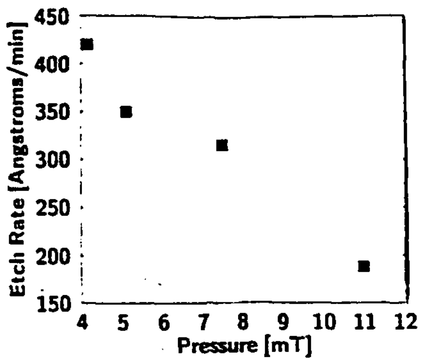


Fig. 1 Etch rate of GaN vs. the pressure of $CF_3Br/Ar$ (3:1) at a constant cathode bias of 600V.

The higher etching rate at lower pressures suggests that the limiting step in the etching process is the mean free path of the halogen radicals. A typical etching profile obtained at 11mT of $CF_3Br/Ar$ (3:1) and 600V of cathode voltage is shown in Figure 2.

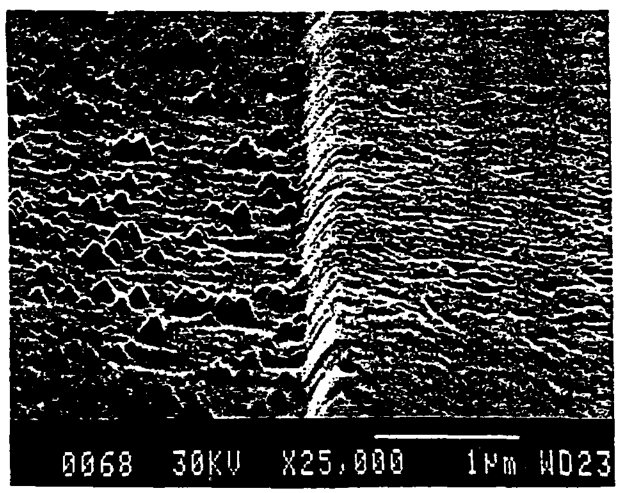


Fig. 2 A typical etch profile of GaN using $CF_3Br/Ar$ (3:1) made under conditions described in the text.

We observed that the pyramidal features in the etching pattern are not present when etching was carried out at 5mT. By measuring the thickness of the photoresist prior to and after etching the selectivity at 5mT was found to be greater than 3:1 GaN to photoresist.

## CONCLUSIONS

We report on reactive ion etching of GaN grown onto (0001) sapphire. Various reactive and inert gases were employed from which it was found that Cl and Br etch GaN more effectively than F. The effects of plasma parameters on etch rate and surface morphology were investigated using a $CF_3Br/Ar$ mixture in a 3:1 ratio. Etch rate and surface morphology were found to improve at lower plasma pressure, resulting in an etch rate in excess of 400 Å/min at 4.2 mT.

## ACKNOWLEDGEMENTS

This work was supported by the Office of Naval Research (grant no. N00014-92-J 1436).

## REFERENCES

1. J.I. Pankove, Electrochem. Soc. Vol **119**, 1110 (1972)

2. J. Foresi, M.S. Thesis (Boston University, 1991)

3. I. Adesida, A. Mahajan, E. Andideh, M. Asif Khan, D.T. Olsen and J.N. Kuzna Appl. Phy. Lett. **63**, 2777 (1993)

4. S.J. Pearton, C.P. Abernathy, F. Ren, J.R. Lothian, P.W. Wisk, A. Katz, and C. Constantine, Semicond. Sci. Technol. Vol **8** pg 310 (1993)

5. T.D. Moustakas, T. Lei and R. Molnar, Physica B 185 pg 36-49 (1993)

6. T.D. Moustakas and R. Molnar Mat. Res. Soc. Symp. Proc. Vol **281** (1993)

Appendix N : "The Growth of GaN by ECR-MBE; the role of charged species" submitted : *Journal of Applied Physics*

# The Growth of Gallium Nitride by Electron Cyclotron Resonance Plasma Assisted Molecular Beam Epitaxy; The Role of Charged Species

R. J. Molnar and T. D. Moustakas

*Molecular Beam Epitaxy Laboratory, Department of Electrical, Computer and Systems Engineering, Boston University, Boston, MA 02215*

## Abstract

The role of ionic and non-ionic excited species of nitrogen in the growth of GaN thin films by Electron Cyclotron Resonance Plasma Assisted Molecular Beam Epitaxy (ECR-MBE) has been investigated. It was found that the kinetics of film growth is significantly affected by the microwave power in the ECR discharge. Specifically, a transition from an island to a layer-by-layer and finally, to a three dimensional growth has been observed as a function of power. These morphological changes are accompanied by degradation of the electrical and luminescence properties, a result attributable to increased native defects and impurities. SIMS analysis indicates that impurity levels in the films increase with the plasma power levels used during the growth. To study the relative role of ion induced native defects in these films, strategies for charged species extraction were developed by using an off axis solenoid to modify the magnetic environment during growth. Films grown under a reduced ionic/excited neutral ratio environment show marked improvement in the electrical and luminescence properties. These data together with SIMS analysis, indicate that observed improvements in these films are due to a reduction of native defects and not impurities.

PACS # 68.55.-a, 68.55.Bd, 68.55.Ln, 72.80.Ey

## I. Introduction

Gallium nitride is a refractory semiconductor under intense study due to its direct bandgap at 3.4 eV as well as the ability to modify this value over an extremely wide range of the visible-UV part of the electromagnetic spectrum through the formation of ternary solutions with InN ($E_g$ = 1.9eV) and AlN ($E_g$ = 6.2eV). Difficulties in reproducible p-type doping as well as reducing background donors have proven formidable challenges that are just starting to be overcome. The background electron concentration in GaN has been ascribed to nitrogen vacancies, which is expected to be a shallow donor (~20-30 meV) in GaN[1,2]. In order to reduce nitrogen vacancies, a number of workers have developed plasma-enhanced, kinetically controlled processes, such as modified molecular beam epitaxy or sputtering, to achieve better control over the stoichiometry of the films [3-12]. These processes generally rely on plasmas of nitrogen to provide chemically active nitrogen species to allow film growth below the decomposition temperature of GaN[13]. These workers utilized a variety of plasma generating sources, which, in turn, can generate a variety of active nitrogen species. This raises a question as to what active nitrogen species are important for the growth of high quality GaN. Some important observations that can be made from these works is that 1.) GaN can be effectively grown without the presence of ionic species[9,10]. 2.) The plasma to substrate potential difference is critical in the formation of electrically active defects, either through bombardment effects[11] or through modulation of the defect formation energy for different surface potentials[14,15].

Electron cyclotron resonance (ECR) plasma sources are becoming popular for providing the activated nitrogen in the growth of the III-V nitrides as well as in the p-type doping of the II-VI family of semiconductors. The lower process pressures required for stable operation, the high ionization efficiency as well as the low energy of the excited species make them ideally suited for activating unreactive gas species such as nitrogen, thereby serving as a high density source for low pressure epitaxial growth processes. It has been widely observed that GaN films grown at higher microwave power levels exhibit degraded electrical and luminescent properties over films grown under lower microwave power, a result attributed to 'ion damage' [8,16,17].

Previously, workers have reported on various methods to control the ionic species in plasmas[11,18,19,20]. These techniques generally utilize an electric or magnetic field to guide/repel charged species through magnetic field confinement or Coulombic effects. Substrate or grid biasing is a popular technique due to the comparative ease of implementation[11]. However, in low pressure plasmas with ionic species having highly anisotropic kinetic energies, which lead to long range interactions, substrate biasing has been shown to strongly affect the plasma generation upstream in the source through electron extraction/reflection making the interpretation of such experiments difficult[18]. On axis solenoids have been extensively studied both in ECR as well as magnetron sputtering plasmas as a means of charged species control[19,20]. While this technique is very effective in charged species control, it is typically very difficult to introduce the required solenoids into the apparatus due to geometrical constraints.

In this paper, a comprehensive study of the growth of GaN by the method of ECR-assisted MBE (ECR-MBE) is reported. The mechanism by which ions affect the growth of the films has been studied. The degradation in film quality at elevated plasma power levels as well as the role of ionized species on film quality was investigated. In order to systematically study such phenomena, a new method of growth employing an off-axis external solenoid for charged species extraction was developed.

## II. Experimental Methods

### A. Film Growth

The films in this study were all deposited on (0001) $Al_2O_3$ substrates by a two-step growth technique described previously[3,21]. The growth apparatus (Figure 1) used in the current work, consists of an Intevac Gen II MBE unit with an AsTex compact ECR source mounted in one of the effusion cell ports. It is important to note that this source has an axial solenoid to generate the magnetic field required for ECR operation. The background pressure of the system before the introduction of the nitrogen gas was usually $<10^{-10}$ T. The gallium (99.99999% pure) flux is supplied by a conventional Knudsen effusion cell. The substrates were chemically etched in a hot $H_2SO_4$:$H_3PO_4$ (3:1) solution for 20 minutes to remove surface contaminates as well as damage from mechanical polishing. They were then fastened to an insulating BN plate with Mo wires and introduced into the MBE system where they were outgassed in the preparation chamber at850°C. Prior to growth the substrate was heated to about 850°C (as measured by a thermocouple behind the substrate) and exposed to a 35W nitrogen plasma to further clean the surface and form a thin AlN layer on the surface, as evidenced by a transformation in the RHEED diffraction pattern[3,21]. The substrate temperature was then lowered to 550°C for the growth of a thin GaN buffer layer (~300 Å). This step was typically done at low plasma power levels (~20W) in order to grow in a low active nitrogen overpressure environment which was shown to promote lateral growth (see Sec.III). After deposition the gallium shutter was closed and the substrate temperature was ramped to 800°C, while the gallium and nitrogen fluxes were adjusted for the growth of the rest of the film. The gallium shutter was then opened and the growth of a thick (1-2μm) GaN film proceeded at a rate of 0.22 μm/hr. The nitrogen gas (99.995% purity) was purified to >99.99999% by gettering with a Zr/Fe-based alloy. The nitrogen flow rate for all films grown in this study was 6.0 sccm which corresponded to a process pressure of $1.2 \times 10^{-4}$ T. Growth was terminated by interrupting the gallium beam and gradually cooling the substrate to <400°C in the presence of the nitrogen plasma to minimize surface decomposition of the film at elevated temperatures.

In order to study the effect of the extraction of charged species from the nitrogen plasma we grew a series of GaN films with the magnetic environment of the growth chamber modified utilizing the external solenoid indicated in Figure 1. The growth procedures are identical to those described above except for the inclusion of the external solenoid which is situated outside of the growth chamber at an angle of about 60° with respect to the axis of the ECR source. It consists of approximately 2300 turns of 18 gauge enameled copper magnet wire wound on an iron mandrel. The external magnet was powered by a DC power supply such that it induced a magnetic field *opposite* in sign to that of the ECR source's solenoid in relation to the substrate, as confirmed with a gaussmeter. Due to the relatively large separation between the external solenoid and the ECR source, there is negligible perturbation of the magnetic field inside the ECR solenoid due to this external field and it is expected that the species generation at the ECR condition would not be affected.

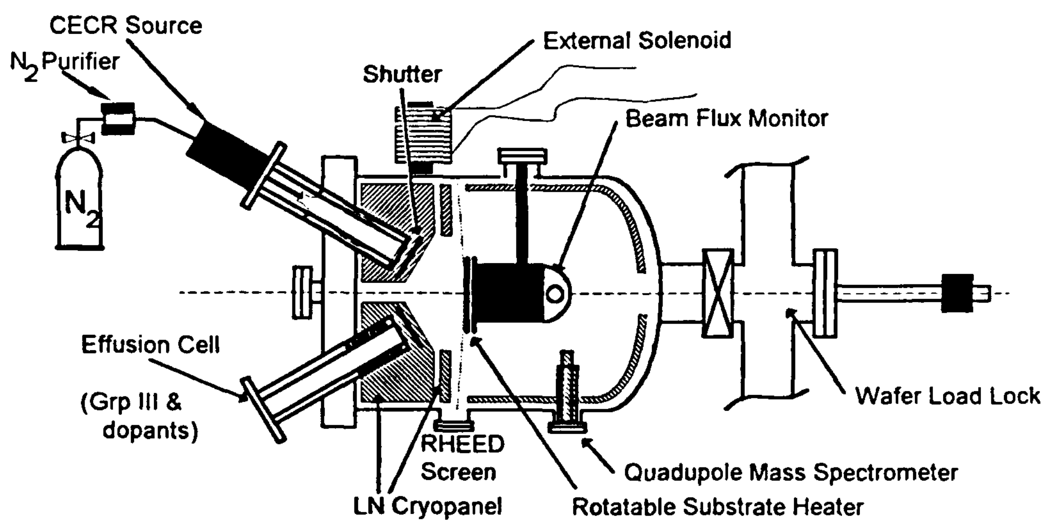


**Figure 1** - Modified ECR-MBE Growth Apparatus showing external solenoid used for the modification of the magnetic environment during growth.

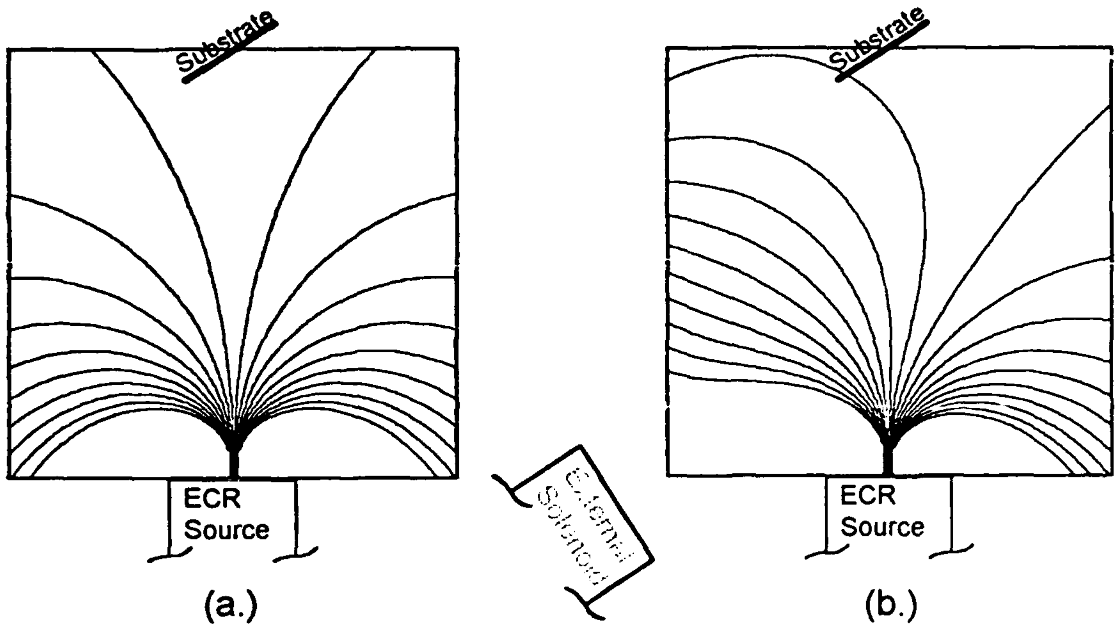


**Figure 2** - Magnetic field lines for (a.) no external solenoid and (b.) with external solenoid at 8 A. (Note: The external solenoid in (b.) is schematically represented as being closer to the ECR source than in the actual simulation and experiment.)

It is known that charged species in ECR plasmas are strongly guided along magnetic field lines or, equivalently, down the divergence of the magnetic field by ambipolar diffusion[20]. Magnetic field lines are drawn in figure 2 for the growth environment both without and with the external magnet at 8 Amperes. These were computed by plotting contours of vector potentials, calculated via linearly translated/rotated superimposed dipoles using an approximation that the radius of the solenoid is much smaller than the distance from the solenoid to the substrate. The vector potential for one dipole is given by Eq (1) [22]:

$$|\overline{A}| = \frac{\mu_o \pi}{4\pi}\frac{R^2 ni}{} \cdot \frac{x}{\left(z^2 + x^2\right)^{3/2}} \qquad (1)$$

Where R is the radius of the dipole, ni is the amp-turns associated with the dipole and z and x are the coordinate axes, normal to and in the plane of the dipole, respectively. As can be seen in Figure 2, the external solenoid serves to effectively divert the field lines away from the substrate area. By extracting the ions from the substrate area, the ratio of ions to excited neutral species could be systematically varied. The current to the external magnet was switched on to the specified value after the growth of the GaN buffer layer to avoid possible variations in the heteroepitaxial nucleation on the sapphire substrate which would be expected to affect the subsequent film growth. For the films grown with the external solenoid, the microwave power was kept constant at 30W which was deemed appropriately high enough to compensate for the extraction of the ions and maintain the stoichiometry of the films under the range of external solenoid currents used in this study.

### *B. Plasma Characterization*

Nitrogen plasmas have been shown to have a variety of excited nitrogen species, including $N_2^*$, $N_2^+$, N and $N^+$ [23]. The ECR plasmas used in our growth were characterized both by optical emission spectroscopy and Langmuir probe measurements. An optical emission spectra typical for our ECR nitrogen plasma source is shown in Figure 3. The measurement was performed using a UV fiber optic bundle to collect light from a viewport line-of-sight with the source. The light was dispersed through a 0.25m monochromeier.

These studies reveal the presence of $N_2^+$, as indicated by the emission at 391.4 nm associated with the first negative system of $N_2^+$ ($B\,^2\Sigma_u^+ \rightarrow X\,^2\Sigma_g^+$). The remainder of the dominant peaks in the region of the spectra at $\lambda <$ 500 nm are associated with the second positive system of $N_2^*$ ($C\,^3\Pi_u \rightarrow B\,^3\Pi_g$), such as the 337.1 nm line commonly utilized in nitrogen gas lasers. The banded emission in the visible part of the spectrum (500-700 nm) is due to the first positive system of $N_2^*$ ($B\,^3\Pi_g \rightarrow A\,^3\Sigma_u^+$) believed to result from the recombination of two ground state nitrogen ($^4S$) atoms. The emission band in the 700-800 nm range can be attributed either to the Y-bands of $N_2$ ($B'\,^3\Sigma_u^- \rightarrow B\,^3\Pi_g$) which are also thought to be due to recombination of ground state nitrogen atoms[24] or, as recently proposed by Vaudo et. al., attributable to atomic as opposed to molecular transitions[10,25].

In order to study the charged species extraction, we utilized the collector of a nude ionization gauge (Bayard-Alpert type), situated at the location of our substrate during the growth, as a Langmuir probe to measure the relative ion density as function of external magnet current. The probe current was directly measured with a Keithley 617

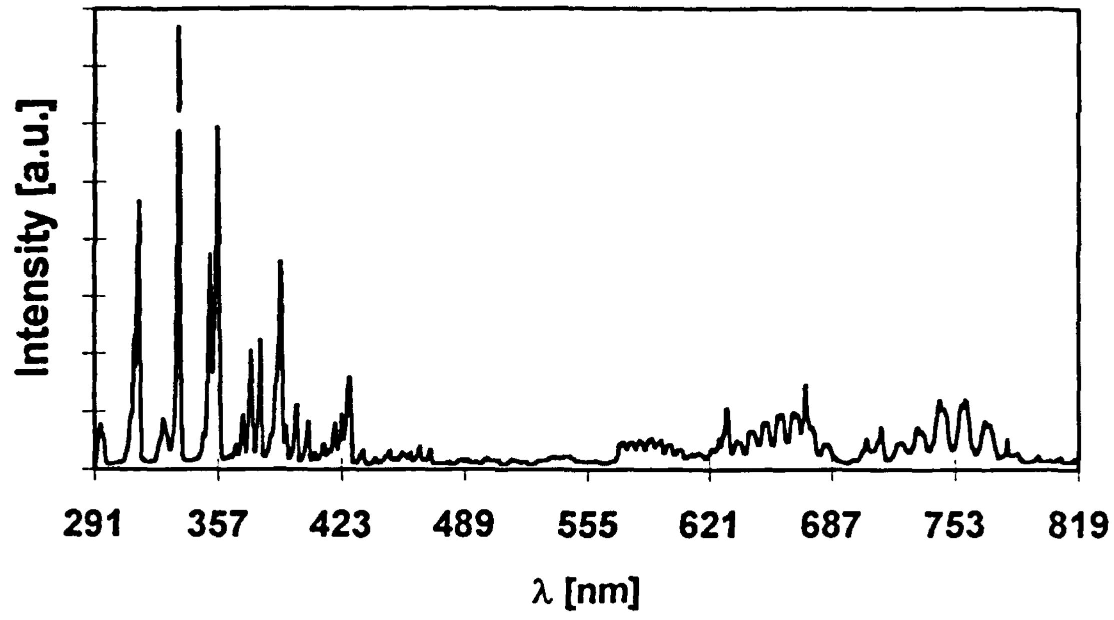


**Figure 3-** Typical optical emission spectra for ECR nitrogen plasma ($P_{microwave}$ = 35 W, nitrogen pressure = $1.2\times10^{-4}$ T).

electrometer connected in series with a DC power supply. The grid of the ionization gauge was left floating to minimize its effect on the plasma. Typical I-V characteristics of the probe both with and without the external solenoid are shown in Figure 4. It is apparent from these data that the activation of the external solenoid results in a reduction of both electron and ion densities at the substrate surface. Relative ion densities were determined by plotting $I^2$ vs. V and using the relation[26]:

$$\frac{\partial I_i^2}{\partial V_p} = -\frac{3A^2e^3N_i^2}{4\pi\ m_i} \qquad (2)$$

Where $I_i$ is the probe current in the saturated ion density (highly negative) regime, $V_p$ is the applied probe potential, A is the area of the probe, $N_i$ is the ion density and $m_i$ is the ion mass. Due to sheath effects of the grid *and surrounding* components at these low pressures ($10^{-4}$ T) quantitative determination of the plasma densities and other plasma parameters ($T_e$, $V_p$ and $V_f$) was not possible.

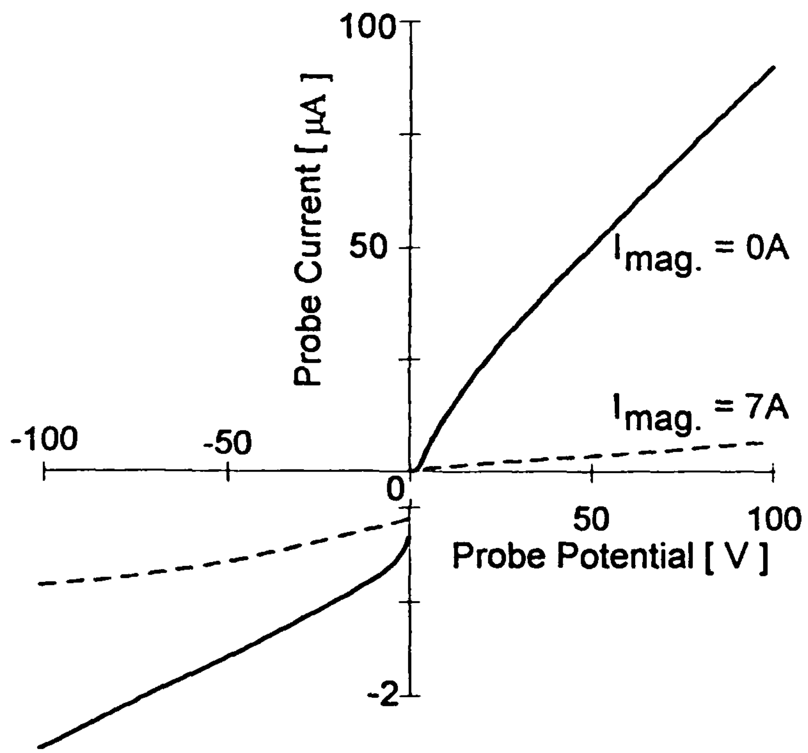


**Figure 4 -** I-V characteristics of Langmuir probe with the external solenoid current at 0A and 7A.

### *D. Sample Cl.aracterization*

To investigate the microstructure of the films we utilized a Jeol model JSM-6100 scanning electron microscope (SEM). The cross-sectional images presented in this study were all obtained at a tilt angle of 60° and a magnification of 25,000X. The crystallinity of all the films in this study was investigated by both *in situ* reflection high energy electron diffraction (RHEED) and post growth x-ray diffraction with a Huber four circle diffractometer. The RHEED patterns were generated with a 10 keV incident electron beam directed along the <11$\bar{2}$0> azimuth. The x-ray diffraction scans performed were in the $\theta/2\theta$ mode, which determines the film orientation along the film's surface normal and $\theta$-rocking curves about the main (0002) diffraction peak ($2\theta$=34.6°) which determines the spread of orientations along the surface normal. The source was a Cu sealed tube used in conjunction with a sagitally focused graphite (002) monochrometer crystal which resulted in a beam with both Cu $K\alpha_1$ and $K\alpha_2$ contributions ($\lambda$=1.54Å). The resolution of the system in this configuration is ~4 min.

To investigate impurity levels in the samples, Secondary Ion Mass Spectroscopy (SIMS) analysis was performed using a incident beam of Cs atoms. The sputter rate was modulated for a short period of time during the profiling to verify that the detected signals were not due to the background impurity levels of the analysis chamber. Due to a lack of calibration standards for impurities in GaN, calibration data obtained from implanted GaAs standards was utilized. Consequently, the data should be interpreted as a relative measure of impurities in the films.

The transport properties of the samples were studied by using the four probe Van der Pauw geometry. For samples grown with microwave power levels below ~19 W the sample was decorated with phase separated Ga droplets by the end of the run, and needed to be etched in concentrated HCl for several minutes to facilitate electrical measurements. The samples were first abrasively etched into cloverleaf lamilla ~5mm diameter and subsequently degreased in acetone and 2-propanol. Gold wires were then soldered to the four outer contact areas using indium solder. The samples were mounted in a closed loop helium cryostat which permitted measurements to be performed from 10K to 300K. Magnetic fields up to 0.7 T and test currents of $10^{-9}$-$10^{-4}$ A were used in these experiments.

The photoluminescence spectra of the samples were determined using a nitrogen pulsed laser as an excitation source. The laser line at 337.1 nm corresponded to a photon energy of 3.678 eV. The 10 ns pulses, at a repetition rate of 40 Hz were directed onto the sample which was mounted on a cold finger at 77K using a colloidal suspension of graphite. The resultant emission was dispersed through a 0.25 m spectrometer and detected with a Hamamatsu R-928 photomultiplier tube connected to a lock-in amplifier. The lock-in was fed an external trigger pulse from a photodiode which samples the incident beam. The spectra were not corrected for the response on the system.

## III. Experimental Results & Discussion

### *A. Films grown without the external solenoid*

#### 1. Film Structure/Morphology

We will first discuss the effect of the microwave power in the ECR discharge on the structure and surface morphology of the films. Figure 5 shows the RHEED diffraction patterns for the films grown at the indicated microwave power levels. The streakiness of the diffraction patterns for the films grown at microwave powers up to 20 W suggests that the surfaces of these films are atomically smooth. The spotty diffraction pattern of the film grown at 25 watts is consistent with a three dimensional diffraction pattern which indicates a rough surface morphology. Similar spotty diffraction patterns have been reported for samples grown at relatively high microwave power levels by other workers[27].

Post growth SEM studies of these films, shown in figure 6, are consistent with the RHEED diffraction data. The films grown at the lowest power (figure 6 (a.)) show a strong columnar morphology. The spaces between the columns are typically filled with phase separated gallium by the end of the growth which occludes the three dimensional diffraction which would be expected from such columnar surface morphologies. However, the top surface of the plateaus are atomically smooth, leading to the observed streaky RHEED pattern. The films grown at 19 and 2( W (figure 6 (b.) and (c.)) show a progressive coalescence of the islands with no columnar features discernible for the films grown at 20 W. On the other hand, for films grown at powers >20 W, we observe a characteristic roughening as shown in figure 6 (d.).

The data of figures 5 and 6 show the effect of ion assistance on the mode of growth in the transition from island growth (Volmer-Weber mode) (figure 6 (a.) and (b.)) to a layer by layer growth (Frank-Van der Merwe mode) (figure 6 (c.)) to a three dimensional growth which leads to rough surface morphologies(figure 6 (d.)). This roughening can be indicative of layer-by-layer followed by island growth (Stranski-Krastanov mode) which can be stress driven by either substrate/film lattice mismatch or structural defects. Alternatively, it can be the result of a kinetically induced roughening transition[28] due to the plasma's enhancement of surface adatom adsorption/desorption as has been observed in GaN epitaxial overlayers grown at high growth temperatures[29].

The crystallinity of the films was also examined by XRD studies. A typical $\theta/2\theta$ diffraction scan is indicated in figure 7, with inset showing the corresponding $\theta$-rocking curve scan. X-ray diffraction data corroborated with the RHEED data for the samples in this study indicate that all the films are single crystalline and of high quality with FWHM of $\theta$- rocking curve ~10-20 min. and not strongly correlated with the microwave plasma power used during the film growth

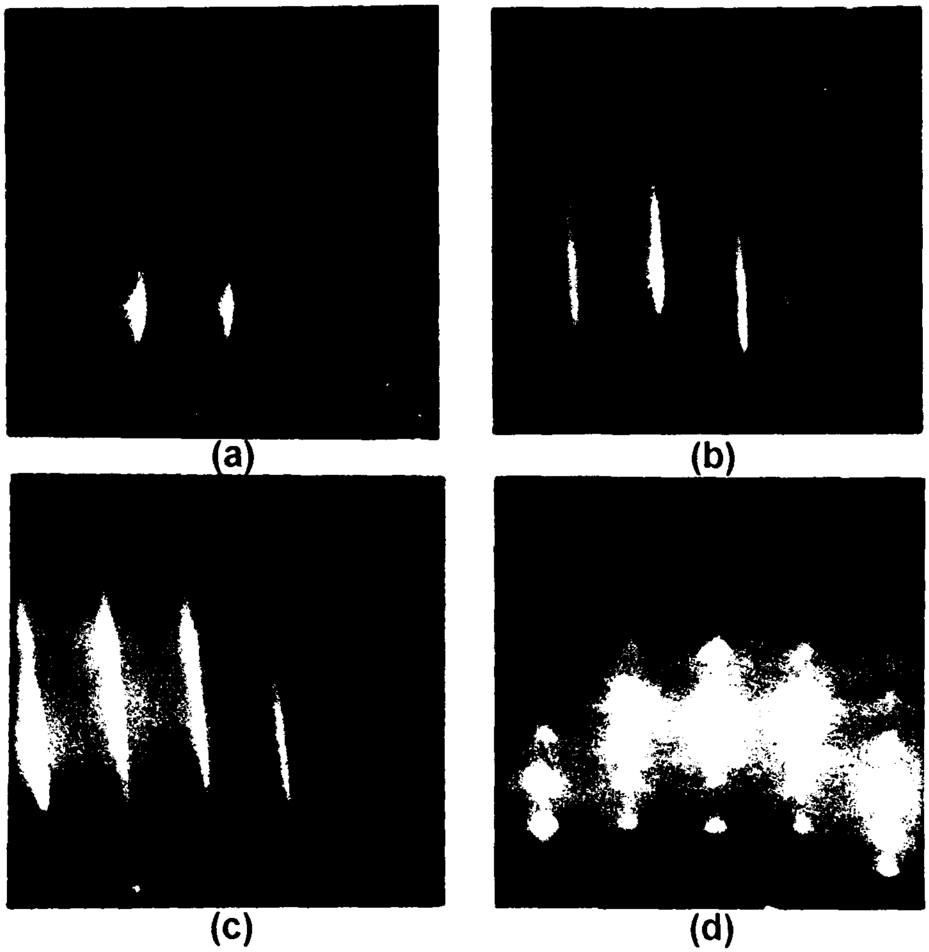


**Figure 5** - RHEED diffraction patterns for samples grown at various microwave power levels. (a) 18W, (b) 19W, (c) 20W and (d) 25W.

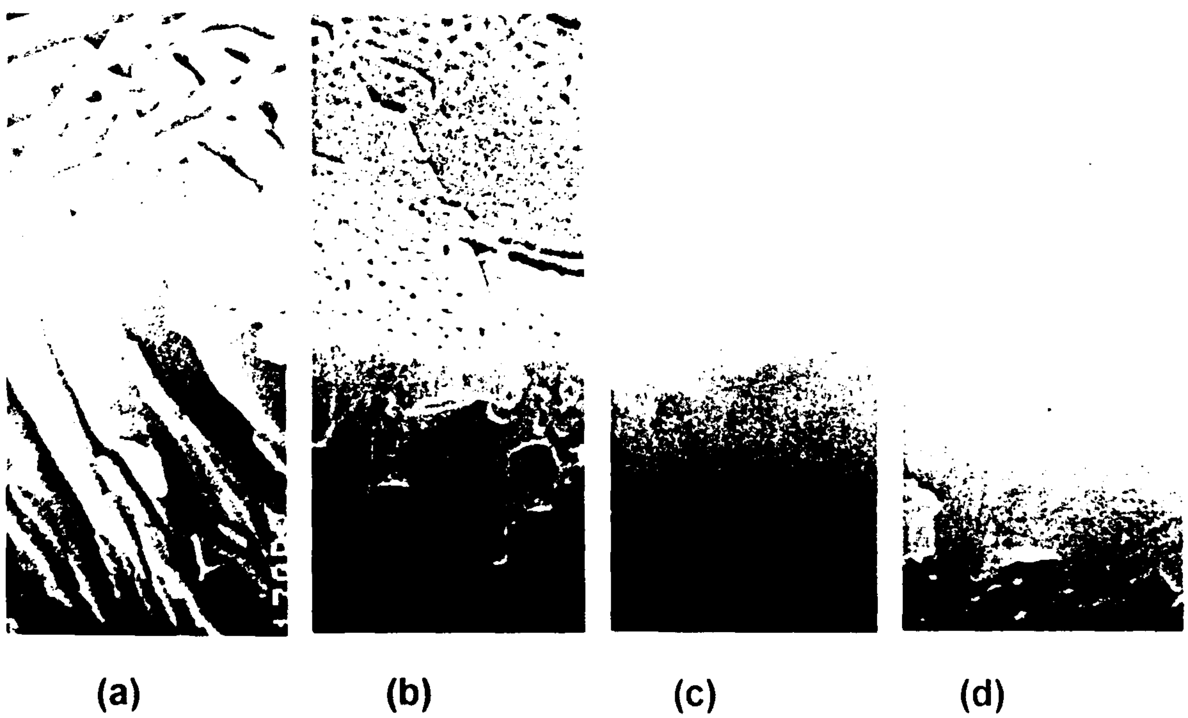


**Figure 6** - SEM micrographs of surface morphologies for films grown at various microwave power levels. (a) 18W, (b) 19W, (c) 20W and (d) 25W.

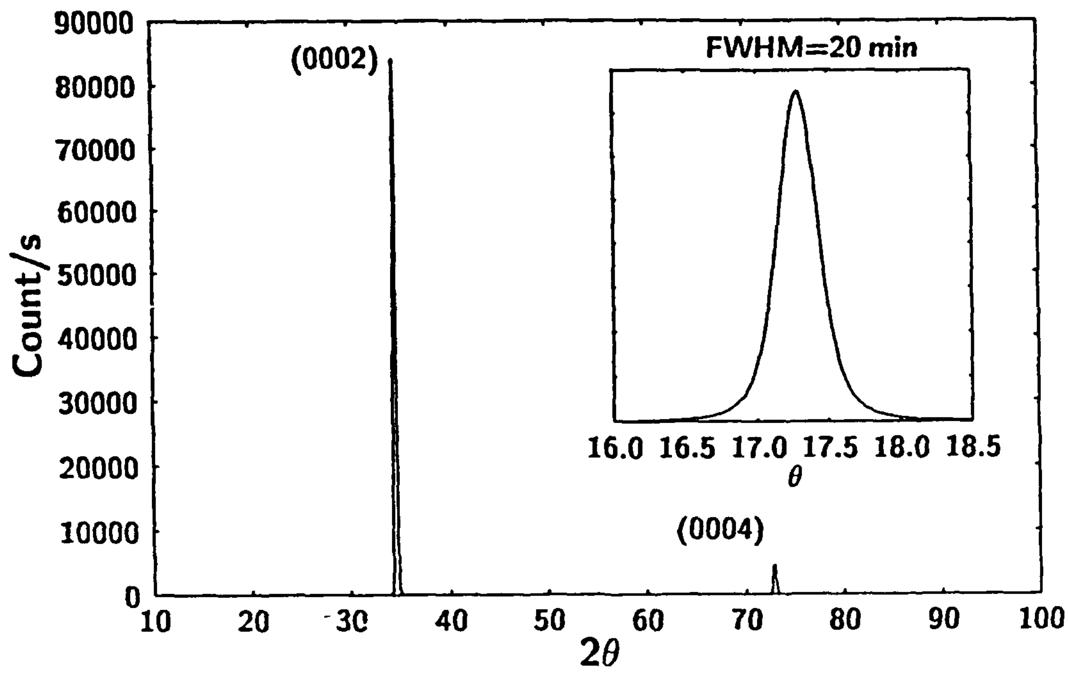


**Figure 7** - XRD θ/2θ scan with inset indicating corresponding θ-rocking curve.

**2. Impurities**

To investigate the role of the nitrogen plasma in the incorporation of impurities in the films, SIMS analysis was performed on samples grown at different microwave power levels. Figure 8 shows the dependence of the concentrations of hydrogen, oxygen, carbon and silicon as a function of microwave power in the ECR discharge. As discussed earlier, the absolute magnitude of these concentrations may be inaccurate due to the lack of proper calibration standards, however, their relative magnitudes and correlation with the microwave power in the plasma source is correct and points out that the plasma is responsible for the impurities in our films.

The exact origin of these impurities and their correlation with the plasma is currently under investigation. However, we do know that they do not originate from our source materials. Mass spectroscopy studies of the nitrogen source gas in the absence of the plasma indicate impurity levels too small to account for the observed results. Sputtering and thermal outgassing from the ECR source's quartz liner as well as spurious discharges observed in regions outside the quartz liner could be the source of these impurities, although one cannot rule out plasma activation of impurities from the

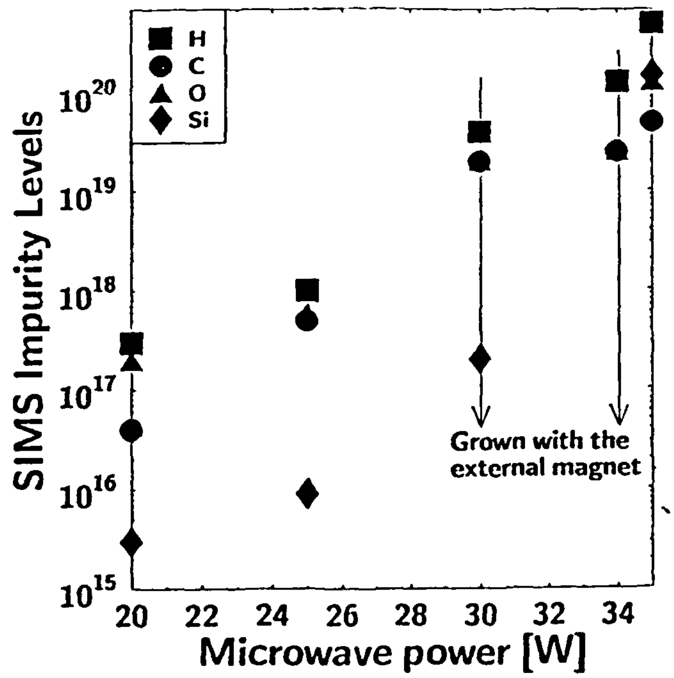


**Figure 8** - SIMS impurity levels vs. microwave power.

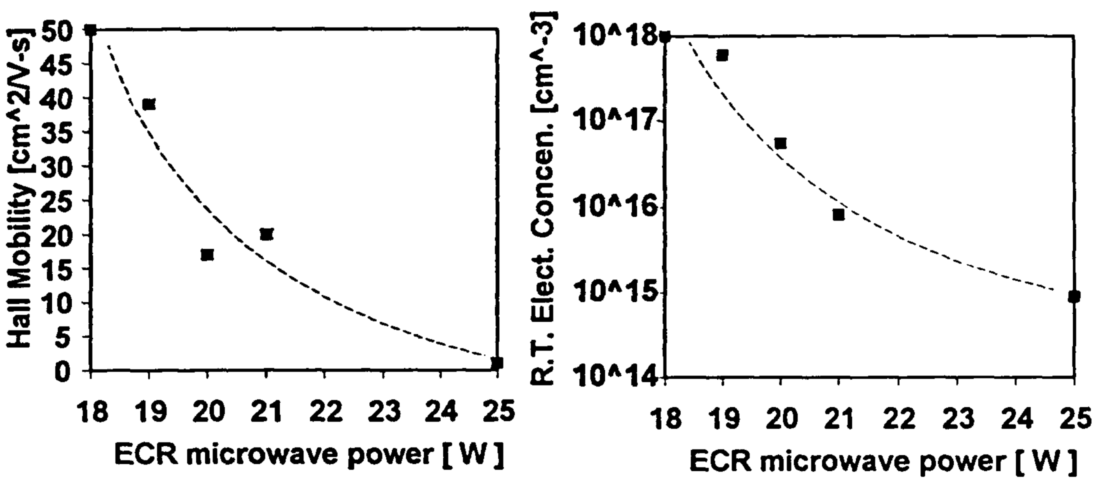


**Figure 9** - Transport properties vs. microwave power.

internal surfaces of our MBE system.

We will now discuss the potential role such impurities play in determining the electronic properties of the GaN films. SIMS analysis alone cannot differentiate between bonded and trapped impurities. In previous work[30] we reported evidence that intentionally introduced hydrogen in GaN films is bonded, and we interpreted new features in the photoluminescence spectra as suggesting that hydrogen may introduce deep donor-like states. Based on the size of tetrahedral atomic radii of silicon, carbon, gallium and nitrogen[31] one expects that silicon will incorporate in the Ga sublattice and act as a donor and carbon will incorporate in the N sublattice and act as an acceptor. By a similar argument oxygen will incorporate in the nitrogen sublattice and act as a donor. This is supported by empirical finding which show that intentional oxygen incorporation leads to n-type GaN films[32]. In the absence of exact theory regarding these impurities in GaN we can only speculate that their combined incorporation should lead to relatively compensated GaN films.

**2. Transport and recombination properties**

The dependence of the net carrier concentration and Hall mobility at 300K on the microwave power in the ECR discharge is shown in figure 9. Films grown at microwave power levels higher than 25 W were found to have unmeasurable room temperature conductivity similar to those reported by other workers[8,27]. Hall effect measurements indicate that all the investigated films are n-type. The transport coefficients were calculated by assuming that electron transport at 300K is dominated by conduction in the conduction band and thus carrier concentration was calculated from Equation 3,

$$n = \frac{1}{R_H e} \tag{3}$$

where $R_H$ is the measured Hall constant.

The decrease in carrier concentration with microwave power (figure 9 (a.)) is consistent with a reduction of nitrogen vacancies in the GaN which act as donors, since higher microwave power leads to higher concentrations of active nitrogen at the substrate. Such an interpretation is also consistent with the fact that the gallium droplets associated with the phase separation of gallium in films grown at low microwave power are absent in films grown at high microwave power. However, it cannot account for the reduction in electron mobility with microwave power indicated in figure 9(b.). The data of figures 9 (a.) and (b.) together suggest that films grown at high microwave power levels are highly compensated.

The dependence of photoluminescence on microwave power in the ECR discharge is shown in figure 10. These data indicate that recombination in films grown at low microwave power proceeds via a donor bound exciton at 3.47 eV[33]. Films grown at higher microwave power tend to show weaker photoluminescence with significant recombination occurring through states close to the middle of the bandgap at 2.2 eV. The recombination kinetics through these states was reported in another paper[17] and the origin of the states was attributed either to carbon in the films or ion damage[17,34,35,36]. The trend of the photoluminescence spectra with microwave power is also consistent with the notion that films grown at high microwave plasma power levels are highly compensated.

A possible mechanism for carrier compensation was suggested by the increase in impurities in the films discussed previously. Furthermore, films grown at high microwave power may have additional compensating centers due to various native defects (interstitials, Ga-vacancies, antisite defects) introduced either by ion bombardment or by modification of the kinetics of growth, since such films are grown at a higher ratio of active nitrogen/gallium.

### *B. Films grown in the presence of the external solenoid*

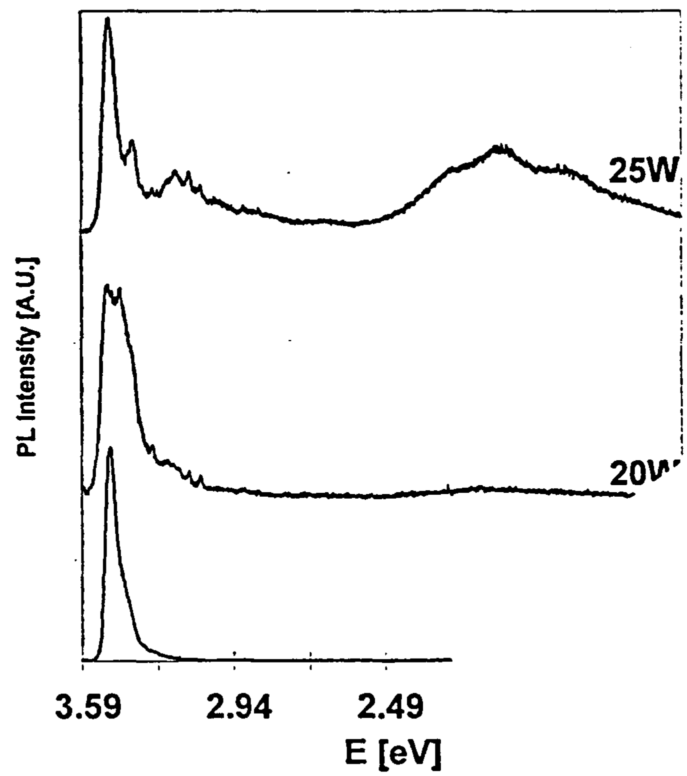


**Figure 10** - Photoluminescence spectra for films grown under various microwave power levels.

To study the relative roles of impurities versus ion damage as the mechanism for the observed compensation in our films, we also investigated the growth of GaN films in the presence of the external solenoid which allows for the extraction of ionic species from the growth area as discussed in Section II. A comprehensive study by Powell et al. on Reactive Ion Molecular Beam Epitaxy (RIMBE) grown GaN films[8], using a Kaufmann ion source to supply active nitrogen, shows a deterioration of the film quality, as evidenced by TEM cross-section, as the energy of the ions was varied from 35 to 90 eV. In sources with axial solenoids, such as the one used in this study, ionic species can gain significant translational kinetic energy through the ambipolar diffusion process associated with the divergent magnetic field. While it is expected that the energy of the ionic species in our plasma are somewhat lower than those associated with Kaufmann sources, studies of ion energetics in ECR plasmas[37,38] suggest ion energies of 25-40 eV are reasonable at the process pressures used for growth.

Langmuir probe studies, discussed in Section II, show a systematic decrease in the ion density at the substrate as a function of the current in the external solenoid. Figure 11 shows the normalized ion density versus external magnet current. It is worth noting that the number of amp-turns in the ECR source's solenoid and external magnet are approximately equivalent for an external magnet current of ~5A. This is roughly where substantial species extraction begins to occur. Thus, in the presence of the external magnet, the ion damage in our films should be minimized.

### 1. Impurities/film structure

The presence of the external magnet during the growth of the films did not appear to affect the impurity incorporation in the films as indicated in figure 8. In other words the observed impurity concentration in these films follows the same trend as a function of microwave power as in films grown without the external magnet. The structure of the films grown with the external magnet as revealed by RHEED and XRD studies are similar to those of films grown at approximately 19W microwave power without the external magnet.

An SEM micrograph of a film grown with the external magnet at 6 A and total microwave power in the ECR discharge of 30 W is shown in figure 12. These data indicate that the growth habit is island-like and thus the surface morphology of this film differs from that of figure 6 (d.) which was grown at high microwave power with no external magnet. This is significant as this correlates the surface roughening of the films grown at higher powers with the ions in the plasma.

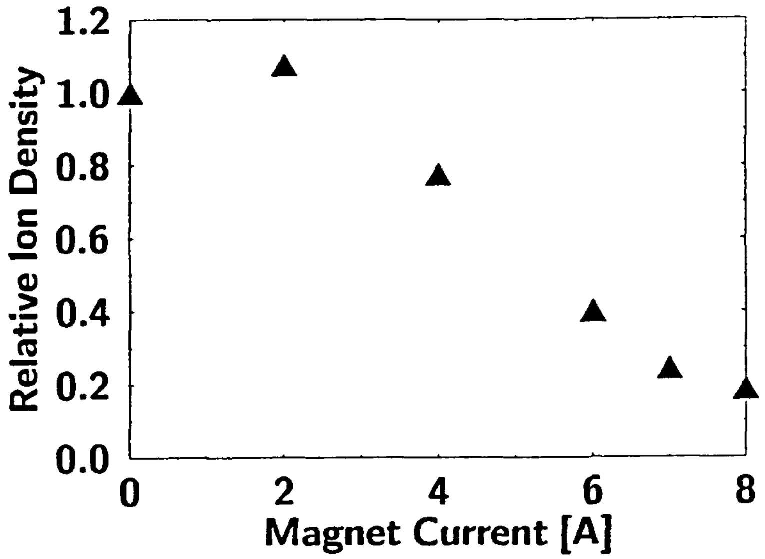


**Figure 12**- Relative ion saturation current vs. external magnet current.

**2. Transport and recombination properties**

Films produced at 30 W of microwave power in the presence of the external solenoid were found to be n-type and highly conductive. The room temperature net carrier concentration and Hall mobility for a number of films produced at various currents in the external magnet are shown in figure 13. These results indicate that the transport properties of these films are significantly different from those grown at high microwave power without the external magnet, which were found to be highly resistive. For the films grown at four amperes in the external magnet, room temperature Hall measurements indicate n-type conductivity with $\mu$ = ~40 $cm^2/V\cdot s$ and n=2-5 x $10^{18}$ $cm^{-3}$. Further increases in the magnet current result in higher mobilities and somewhat lower carrier concentrations as shown in Figure 13.

To study the electronic structure of the donors responsible for the n-type conductivity in these films, we measured the transport properties of these films as a function of temperature, as shown in figure 14. These results are consistent with the existence of shallow donors in the GaN films. Such temperature dependence was discussed in another paper[39], and is indicative of transport

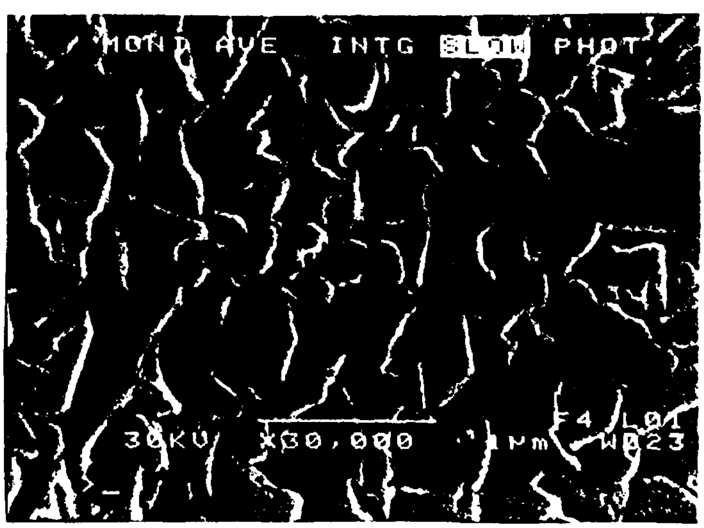

**Figure 11** - SEM micrograph of sample grown with external magnet at 6A

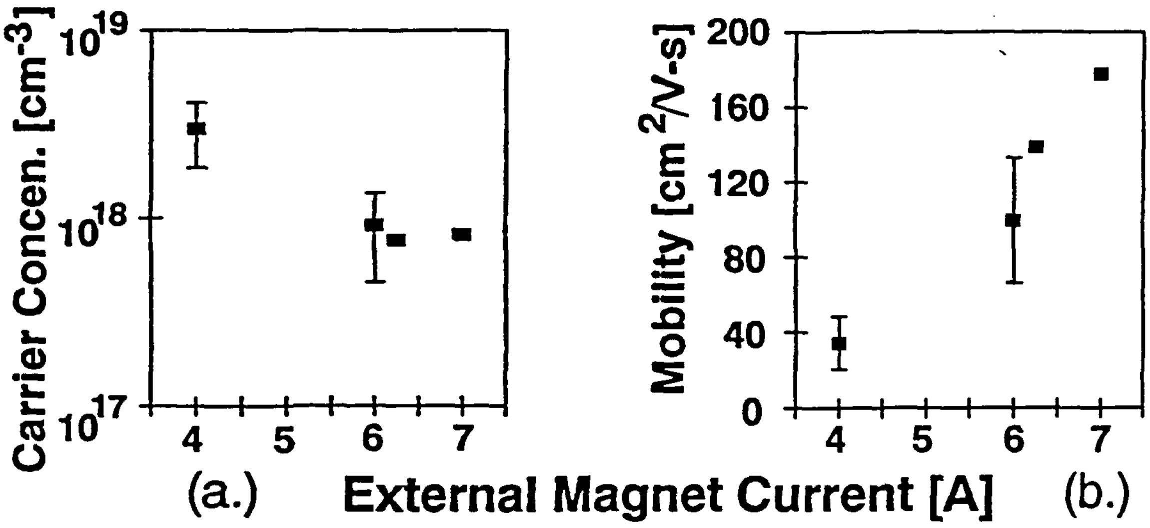


**Figure 13** - Transport properties of samples grown with various external magnet currents.

in both the conduction band and a shallow donor defect band. Regarding the nature of these shallow donors, we can speculate they are silicon and oxygen impurities which, as discussed earlier, were observed to exist with comparable concentrations in our films. However, based on this data alone, we cannot rule out nitrogen vacancies as potential donors. The fundamental difference between the transport properties of the GaN films grown at high microwave power with and without the external solenoid suggests that the films grown without the external solenoid have a high concentration of deep defects resulting from ionic species in our plasma.

Evidence that the films grown with the external magnet have a lower concentration of deep defects is also provided by photoluminescence studies on such films. Figure 15 shows the PL spectra for such a film measured at 77K. This spectra shows a sharp exitonic transition close to the bandgap of GaN and negligible luminescence at 2.2 eV, which was observed in films grown at high microwave power without the external magnet (Figure 10). In conclusion, films grown with the external magnet differ from the samples grown without the external magnet in their surface morphology, transport and photoluminescence properties. Furthermore, the data indicates that these differences result from ions in the plasma. Thus, films produced with the external magnet were found to be of substantially higher quality than films grown without the external magnet.

There are several roles ions may play in the formation of deep defects. The first and perhaps most obvious is through physical damage to the film through bombardment. It is also possible that the three dimensional growth observed at higher power levels results in a higher density of defects through the promotion of dislocation generation[40]. The nature of these native defects may be elucidated by high temperature conductivity

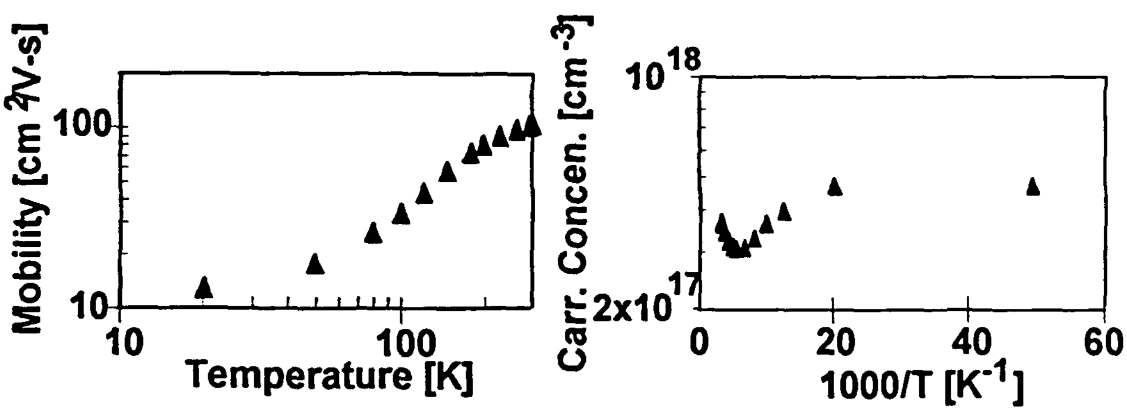


**Figure 14** -Transport properties vs. temperature for sample grown with external solenoid at 6A.

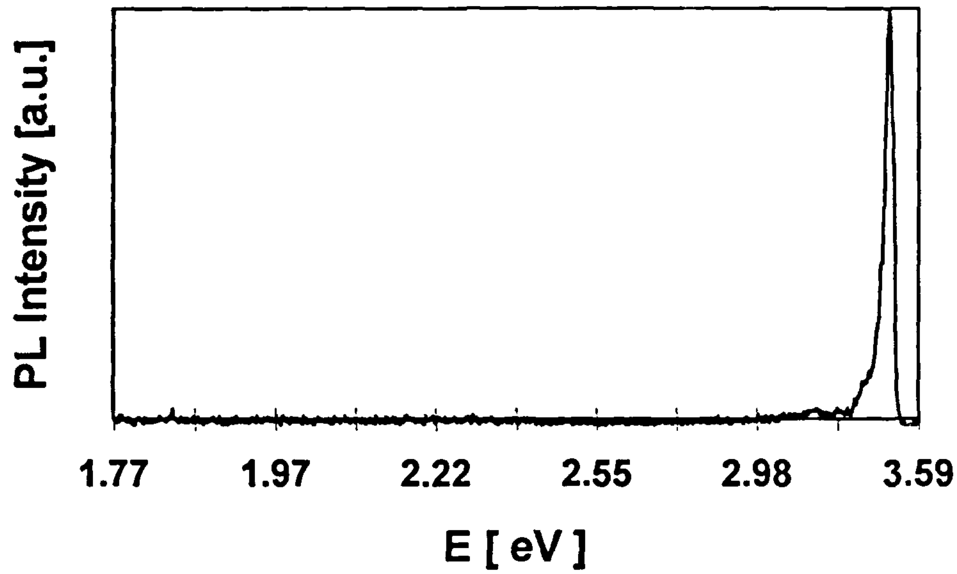


**Figure 15** - PL spectra at 77K of sample grown with external solenoid at 6 A.

measurements performed on the samples grown at 30W without the modified magnetic field environment. These measurements reveal the presence of a deep donor-like level approximately 0.7 eV below the conduction band, as has been reported previously for GaN films[41]. It is possible that this level is indicative of a native defect such as a dislocation, antisite, interstitial or complex (similar to the EL2 center in GaAs) acting as a donor-like trap, leading to the low residual conductivity.

## IV. Conclusions

The role of ionic plasma species in the growth of GaN films by the ECR-MBE method was investigated. Ion bombardment was found to have a profound effect on the mode of growth. The film growth was found to undergo a transition from an island mode to a layer-by-layer mode and finally to a three dimensional mode as a function of microwave power in the ECR source's discharge. The films exhibited a corresponding degradation in their electrical and optical properties. It was found that under the plasma conditions employed, the films had hydrogen, silicon, carbon and oxygen impurities whose concentrations increased with microwave power. It is likely that these impurities are the result of either sputtering or thermal outgassing of components in the ECR source. This is likely due to the extremely high plasma power densities generally present in these compact plasma sources.

To isolate the effect of the ionic species on the films growth, an external solenoid placed outside of the MBE unit was used to extract the charged species from the growth area. The difference between the surface morphologies, transport and photoluminescence properties of the films grown with and without this solenoid indicates that the charged species in the nitrogen plasma, besides affecting the mode of film growth, also affect the density of native defect states. We propose that these states are either point defects resulting from ion bombardment or dislocations whose formation is promoted by the ion induced three dimensional growth.

In addition, this modification of the magnetic field environment is demonstrated as being a simple, effective and unobtrusive method of extracting charged species, particularly where energetic anisotropies of the ionic species resulting from magnetic fields effects make biasing schemes difficult to interpret. This allows the growth of high quality GaN films with substantially improved electrical and luminescent properties.

## Acknowledgments

The authors would like to thank R. Singh for assistance with PL measurements as well as N. Johnson, M. Brandt and W. Götz from Xerox PARC for SIMS analysis. Many thanks are also due to W. Holber and L. Bourget of Astex, Inc.for helpful discussions. This work was supported by the Office of Naval Research (Grant No. N00014-92-J-1436).

## Bibliography

[1] J.I. Pankove, Non-Stoichiometry in Semiconductors, edited by K.J. Bachmann, H.L. Hwang and C. Schwab (Elsevier Science Publishers B.V., 1992).

[2] D.W. Jenkins and J.D. Dow, Phy. Rev. B **39**, 3317 (1989).
[3] T.D. Moustakas, T. Lei and R.J. Molnar, Physica B **185**, 36 (1993).
[4] T. Lei, M. Fanciulli, R.J. Molnar, T.D. Moustakas, R.J. Graham and J. Scanlon, Appl. Phys. Lett. **59**, 944 (1991).
[5] S. Strite, J. Ruan, Z. Li, N. Manning, A. Salvador, H. Chen, D.J. Smith, W.J. Choyke and H. Morkoç, J. Vac. Sci. Technol. B **9**, 1924 (1991).
[6] M.J. Paisley, Z. Sitar, J.B. Posthill and R.F. Davis, J. Vac. Sci. Technol. A **7**, 701 (1989).
[7] Z. Sitar, M.J. Paisley, B. Yan, J. Ruan, W.J. Choyke and R.F. Davis, J. Vac. Sci. Technol. B **8**, 316 (1990).
[8] R.C. Powell, N.E. Lee, Y.W. Kim and J.E. Greene, J. Appl. Phys. **73**, 189 (1993).
[9] W.E. Hoke, P.J. Lemonias and D.G. Weir, J. Crys. Growth **111**, 1024 (1991).
[10] H. Liu, A.C. Frenkel, J.G. Kim and R.M. Park, J. Appl. Phys. **74**, 6124 (1993).
[11] M. Rubin, N. Newman, J.S. Chen, T.C. Fu and J.T. Ross, Appl. Phys. Lett. **64**, 64 (1994).
[12] J. Ross and M. Rubin, Mater. Lett. **12**, 215 (1991).
[13] N. Newman, J. Ross and M. Rubin, Appl. Phys. Lett. **62**, 1242 (1993).
[14] Y. Bar Yam and T.D. Moustakas, Nature **342**, 786 (1989).
[15] G.F. Neumark, Ch.11 *Widegap II-VI Compounds for Opto-Electronic Applications*, edited by H.E. Rudo (1992).
[16] M.E. Lin, B. Sverdlov, G.L. Zhou and H. Morkoç, Appl. Phys. Lett. **62**, 3479 (1993).
[17] R. Singh, R.J. Molnar, M.S. Ünlü and T.D. Moustakas, Appl. Phys. Lett. **64**, 336 (1994).
[18] S.M. Rossnagel, K. Schatz, S.J. Whitehair, R.C. Guarnieri, D.N. Ruzic and J.J. Cuomo, J. Vac. Sci. Technol. A **9**, 702 (1991).
[19] I.Petrov, F. Adibi, J.E. Greene, W.D. Sproul and W.D. Münz, J.Vac. Sci. Technol.A **10**, 3283 (1992).
[20] M. Matsuoka and K. Ono, J. Vac. Sci. Technol. A **6**, 25 (1988).
[21] T.D. Moustakas and R.J. Molnar, Mat. Res. Soc. Symp. Proc. **281**, 753 (1993).
[22] H.A. Haus and J.R. Melcher, *Electromagnetic Fields and Energy* (Prentice Hall, Englewood Cliffs, NJ, 1989).
[23] A.N. Wright and C.A. Winkler, *Active Nitrogen* (Academic Press, New York, 1968).
[24] R.M. Park, J. Vac. Sci. Technol. A **10** 701 (1992).
[25] R.P. Vaudo, Z. Yu, J.W. Cook Jr. and J.F. Schetzina, Optics Lett. **18**, 1843 (1993).
[26] F.F. Chen, J. Appl. Phys. **36**, 675 (1964).
[27] C. Wang and R. Davis, Appl. Phys Lett. **63**, 990 (1993).
[28] J.D. Weeks, *Ordering in Strongly Fluctuating Condensed Matter Systems*, edited by T. Riste (Plenum Press, New York, 1980).
[29] T. Lei, T.D. Moustakas, R.J. Graham, Y. He and S.J. Berkowitz, J. Appl. Phys. **71**, 4933 (1992).
[30] M.S. Brandt, N.M. Johnson, R.J. Molnar, R. Singh and T.D. Moustakas, Appl. Phys. Lett. (accepted).
[31] C. Kittel, *Introduction to Solid State Physics, 6th Ed.* (John Wiley & Sons, New York, 1986).
[32] B-C. Chung and M. Gershenzon, J. Appl. Phys. **72**, 651 (1992).
[33] R. Dingle, D.D. Sell, S.E. Stokowski and M. Ilegems, Phy. Rev. B **3**, 1211 (1971).
[34] T. Ogino and M. Aoki, Jap. J. Appl. Phys. **19**, 2395 (1980).
[35] J.I. Pankove and J.A. Hutchby, J. Appl. Phys.,**47**, 5387 (1976).
[36] M.E. Lin, B.N. Sverdlov and H. Morkoç, Appl. Phys. Lett. **63**, 3625 (1993).
[37] W.M. Holber and J. Forster, J. Vac. Sci. Technol. A **8**, 3720 (1990).
[38] A.A. Shatas, Y.Z. Hu and E.A. Irene, J. Vac. Sci. Technol. A **10**, 3119 (1992).
[39] R.J. Molnar, T. Lei and T.D. Moustakas, Appl. Phys. Lett. **62**, 72 (1993).
[40] J.H. van der Merwe, Critical Reviews in Solid State and Material Sciences **17**, 187 (1991).
[41] T.L. Tansley and R.J. Egan, Mat. Res. Soc. Symp. Proc. **242**, 395 (1992).

# Appendix O : “Blue-violet Light Emitting GaN p-n Junctions grown by ECR-MBE”

submitted : *Applied Physics Letters*

# Blue-violet Light Emitting Gallium Nitride p-n Junctions Grown by Electron Cyclotron Resonance-assisted Molecular Beam Epitaxy

R.J. Molnar†, R. Singh and T.D. Moustakas
*Molecular Beam Epitaxy Laboratory, Department of Electrical, Computer and Systems Engineering, Boston University, Boston, MA 02215*

Blue-violet light emitting GaN p-n junctions were grown by the method of Electron Cyclotron Resonance-assisted Molecular Beam Epitaxy (ECR-MBE). This method has been modified to minimize plasma induced defects. Contrary to similar devices grown by Metallorganic Chemical Vapor Deposition, these devices do not require any post growth annealing to activate the Mg-acceptors in the p-layer. These devices turn-on at approximately 3 volts and have a spectral emission peaking at 430 nm.

† Current address: M.I.T. Lincoln Laboratory, Lexington, MA 02173

The III-V nitrides are rapidly becoming the material of choice for the fabrication of short wavelength light emitters and detectors due to the capability of obtaining a wide spectral region of direct band-to-band transitions (1.9-6.2 eV) as well as higher device stability than II-VI based devices. There have been a number of reports on the fabrication of p-n junction LED's by the MOCVD method[1-3]. These devices typically have turn-on voltages of approximately 3-10 volts. While a turn-on voltage of ~3V is expected based on the bandgap of the material, turn-on voltages >10V are not desirable in terms of device efficiency and may be related to difficulties in forming electrical contacts. More recently, substantial progress has been reported on MOCVD grown InGaN/AlGaN double heterostructures blue light emitting diodes with brightness levels larger than 1000 mcd[4]. However, all these MOCVD grown devices require a post growth annealing step[2,3] or low energy electron beam irradiation (LEEBI) treatment[1] to activate the dopants in the p-type material. This was correlated with the dissociation of H-Mg complexes[5] which have been identified by IR and Raman spectroscopies[6,7].

The use of ECR-plasma activated nitrogen gas reacted directly with Ga metal in kinetically controlled processes, such as molecular beam epitaxy, has been pursued as an alternative growth method to minimize incorporation of hydrogen during film growth. This has resulted in films which exhibit substantial p-type conductivity without post growth annealing[8].

In this letter we report the growth of p-n homojunction LED's by the ECR-assisted MBE method. These structures were found to emit light in the blue-violet part of the spectrum, characteristic of Mg-luminescent centers. These devices do not require a post growth treatment for efficient operation. Furthermore, by utilizing strategies to reduce ion-induced defects[9], devices with improved efficiency have been obtained.

The deposition system consists of an Intervac Gen II MBE unit with an ASTeX Compact ECR source to supply plasma activated nitrogen gas. To minimize plasma damage in the device layers, the kinetic energy of the ions, generated in the ECR source and guided towards the substrate along the magnetic field lines of the source's axial solenoid, was reduced through the utilization of an exit aperture, 1 cm in diameter, which promotes collisional relaxation of the ions due to the elevated pressure inside the source[10]. Furthermore, some device structures were also grown in an environment of a reduced ratio of ionic to neutral metastable and atomic species by using an external off-axis solenoid as described previously[9]. This technique was used to further reduce plasma induced defects.

The p-n junctions were deposited on a (0001) sapphire substrate in the following way. First the substrate was subjected to a nitridation process at 850°C to convert its surface to atomically smooth AlN as described previously[8,11,12]. The next step was the deposition of an undoped GaN-buffer approximately 300 Å thick deposited at 500°C. Following this deposition the substrate was heated to 800°C [8,11-13] and an autodoped n-type GaN film approximately 2 μm thick was deposited at a deposition rate of 0.2 μm/hr. Such films generally have a carrier concentration of about $5\times10^{18}$ $cm^{-3}$ and electron mobilities of about 80 $cm^2/V\cdot s$. Finally the Mg-doped p-layer approximately 0.5 μm thick was deposited by incorporating Mg, sublimated from a conventional knudsen cell at 230°C. Such Mg-doped films grown under identical conditions were found to be p-type with a net carrier concentration of $5\times10^{17}$ $cm^{-3}$ and a hole mobility of 6 $cm^2/V\cdot s$. The Mg flux was gradually raised by about an order of magnitude ($T_{Mg}$ = 270°C) near the end of the run to facilitate the electrical contacting of the top p-layer.

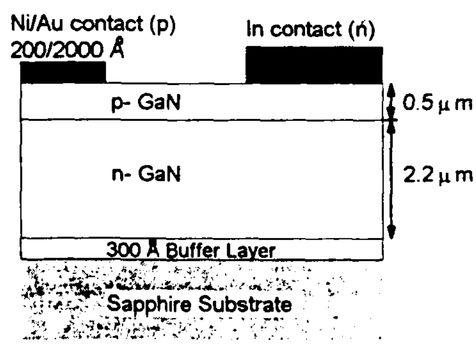


**Figure 1**- Schematic of investigated diode structure.

The top p-layer was electrically contacted by thermal evaporation of dots 300 μm in diameter consisting of 200 Å of Ni followed by 2000Å of Au . The bottom n-layer was contacted through the p-layer by soldering with indium metal. A schematic of the device is shown in Figure 1. In this structure the distance between the two contacts was of the order of 1-2 mm. The chip was then mounted in a chip carrier with silver paint and connected with an ultrasonic wire bonder. The devices' emission spectra was measured using a detector setup described previously for the measurement of PL emission[14]. The devices were driven with a pulse generator at ~40 Hz and 10% duty cycle to facilitate locked-in measurements. The spectra were measured at a drive current of 150 mA or a current density of 212 A/cm$^2$, which is comparable to those reported on AlGaN heterojunction diodes[15].

The I-V characteristics of one such device described in

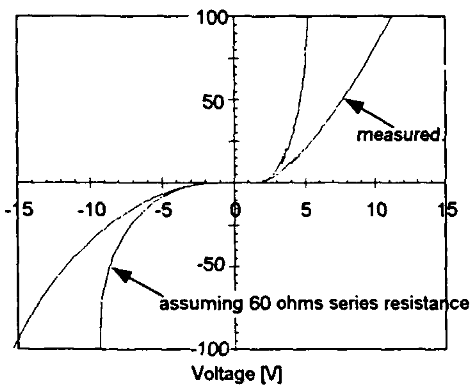


**Figure 2** - Room temperature I-V characteristics of typical GaN LED and calculated I-V characteristic after subtracting the effect of a 60 Ω series resistance.

Figure 1 is shown in Figure 2. Shown in the same figure is the I-V characteristics calculated from the experimental data after subtracted the effects of a 60 Ω series resistance. This series resistance is believed to be the result of the large separation of the two contacts of the device and are consistent with the sheet resistance of the n-layers. Devices with improved geometries as well as etched mesas are currently under development and will be detailed in another report. The reverse breakdown at ~-10 V is expected considering the high doping (>10$^{18}$ cm$^{-3}$) levels on both sides of the junction[16]. The rather large leakage current at lower voltages is probably due to defects in the material and has been found to be less significant in devices of reduced areas.

Due to the excess heat dissipation resulting from the parastic series resistance, the devices were first evaluated at 77K by immersing the chip in liquid $N_2$ during the measurement. Figure 3 shows the EL spectra of two devices fabricated from layers grown without and with the external solenoid driven at 7A. The peak emission at 430 nm is characteristic of Mg-doped GaN homojunction LED's. While this peak is in the violet part of the spectrum, the prominant tail which extends to longer wavelengths in the device grown without the external solenoid tends to dominate the apparent color of the device due to the

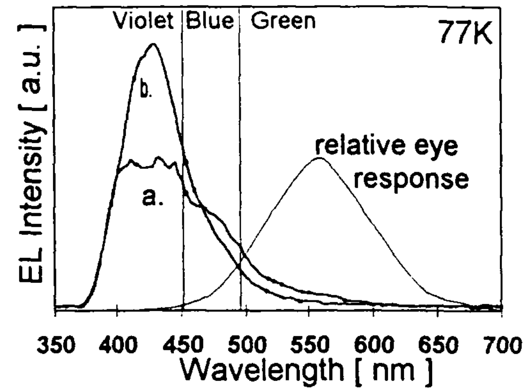


**Figure 3** - Low temperature (77K) EL spectra of L.E.D.'s grown (a.) without and (b.) with external solenoid driven at 7A. Relative eye response from Ref. 16.

enhanced eye response in this region[16]. By using the external solenoid to minimize ion damage in the film, a reduction in this tail as well as an enhancement of the peak at 430 nm is achieved resulting in a bluish-violet apparent color. The dependance of the total light intensity emission as a function of forward current for a typical LED is shown in Figure 4. The emission increases linearly with forward current up to about $I_F$ =175 mA. The sublinear dependance at higher currents is likely due to heating effects in the device.

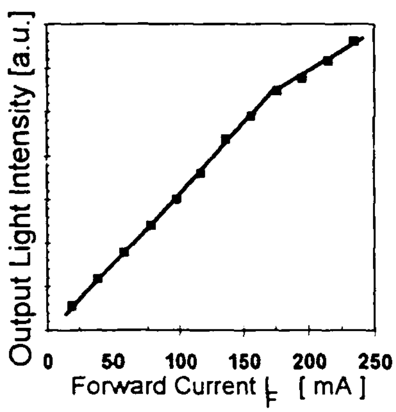


**Figure 4** - Output light intensity vs. $I_F$ for the diode of Figure 3a at 77K.

The spectral dependance was also evaluated at room temperature as shown in Figure 5. The peak wavelength of 470 nm is somewhat larger than what has been reported for

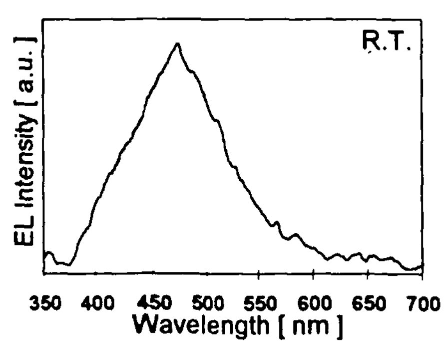


**Figure 5** - Room temperature EL spectra of a diode grown with the external solenoid at 7A.

GaN homojunction LED's and is believed to be related to the heating in these devices due to a.) the large drive current required for these large area diodes and b.) the parasitic series resistance decribed above, resulting in the chip and its carrier becoming quite hot during operation.

In conclusion, GaN blue-violet light emitting p-n junctions have been grown by MBE for the first time. These devices do not require a post growth thermal annealing or LEEBI treatment step to activate the Mg acceptors in the p-layer. Blue emissions characteristic of Mg luminescence centers are observed.

This work was supported by the Office of Naval Research (Grant No. N00014-92-J-1436).

1. I. Akasaki, H. Amano, M. Kito and K. Hiramatsu, J. of Luminescence **48 & 49**, 666 (1991).
2. S. Nakamura, T. Mukai and M. Senoh, Japan J. Appl. Phys. **30**, L1998 (1991).
3. B. Goldenberg, J.D. Zook and R.J. Ulmer, Appl. Phys. Lett. **62**, 381 (1993).
4. S. Nakamura, T. Mukai and M. Senoh, Appl. Phys. Lett. **64**, 1687 (1994).
5. S. Nakamura, N. Iwasa, M. Senoh and T. Mukai, Jpn. J. Appl. Phys. **31**, 1258 (1992).
6. M.S. Brandt, N.M. Johnson, R.J. Molnar, R. Singh and T.D. Moustakas, Appl. Phys. Lett. **64**, 2264 (1994).
7. M.S. Brandt, J.W. Ager III, W. Götz, N.M. Johnson, J.S. Harris Jr., R.J. Molnar and T.D. Moustakas, Phys. Rev. B **49**, 14 758 (1994).
8. T.D. Moustakas and R.J. Molnar, Mat. Res. Soc. Symp. Proc. **281**, 753 (1993).
9. R.J. Molnar and T.D. Moustakas, J. Appl. Phys. *(in press)*.
10. R. Singh, R.J. Molnar and T.D. Moustakas, J. of Elect. Mat. *(submitted)*.
11. T.D. Moustakas, R.J. Molnar, T. Lei, G. Menon and C. Eddy Jr., Mat. Res. Soc. Symp. Proc. **242**, 427 (1992).
12. T.D. Moustakas, T. Lei and R.J. Molnar, Physica B **185**, 36 (1993).
13. T. Lei, M. Fanciulli, R.J. Molnar, T.D. Moustakas, R.J. Graham and J. Scanlon, Appl. Phys. Lett. **59**, 944 (1991).
14. R. Singh, R.J. Molnar, M.S. Ünlü and T.D. Moustakas, Appl. Phys. Lett. **64**, 336 (1994).
15. I. Akasaki and H. Amano, Mat. Res. Soc. Symp. Proc. **242**, 383 (1992).
16. S.M. Sze, Physics of Semiconductor Devices, 2nd Ed., John Wiley & Sons, NY (1981).

Appendix P : "Temperature Dependence of the Energy-Gap in GaN Bulk single crystals and Epitaxial Layers."

# Temperature dependence of the energy gap in GaN bulk single crystals and epitaxial layer

H. Teisseyre, P. Perlin, T. Suski, I. Grzegory, S. Porowski, and J. Jun
*High Pressure Research Centre, Polish Academy of Sciences, Sokołowska 29, 01-142 Warszawa, Poland*

A. Pietraszko
*Institute of Low Temperature and Structural Research, Polish Academy of Sciences, Okólna 2, Wrocław, Poland*

T. D. Moustakas
*Boston University, Molecular Beam Epitaxy Laboratory, Department of Electrical, Computer and System Engineering, Boston, Massachusetts 02215*

(Received 28 January 1994; accepted for publication 20 April 1994)

We performed optical-absorption studies of the energy gap in various GaN samples in the temperature range from 10 up to 600 K. We investigated both bulk single crystals of GaN and an epitaxial layer grown on a sapphire substrate. The observed positions of the absorption edge vary for different samples of GaN (from 3.45 to 3.6 eV at $T=20$ K). We attribute this effect to different free-electron concentrations (Burstein–Moss effect) characterizing the employed samples. For the sample for which the Burstein shift is zero (low free-electron concentration) we could deduce the value of the energy gap as equal to 3.427 eV at 20 K. Samples with a different free-electron concentration exhibit differences in the temperature dependence of the absorption edge. We explain the origin of these differences by the temperature dependence of the Burstein–Moss effect.

## I. INTRODUCTION

GaN is a wide band-gap semiconductor, crystallizing in the hexagonal wurtzite structure. GaN is currently attracting a lot of interest which results from its possible applications in the field of optoelectronics and electronics. Because of the large, direct gap and its outstanding chemical and physical stability, this material is specially suited for the construction of short-wavelength light emitting devices (diodes and lasers) and transistors operating at high temperatures.[1,2] Concerning these applications, a fundamental problem consists in the determination of the energy-gap value $E_g$ and its variation with temperature, $dE_g/dT$. Measurements of the absorption edge position and its temperature evolution are usually employed for these purposes. Results of experimental studies of GaN have brought a wide spectrum of data from which different values of both $E_g$ and $dE_g/dT$ were deduced. The question of the origin of the reported dispersion has not been posed until now. A very likely explanation for the reported spread of the experimental data can be associated with the influence of the free-electron concentration on the position of experimentally determined $E_g$ (Burstein–Moss effect).

Moreover, since the majority of measurements of $E_g$ and all investigations of $dE_g/dT$ have been performed on epitaxial layers of GaN,[3–8] it might be expected that the quality of the used samples represents one of the effects responsible for the dispersion of the data. The perfection of epitaxially grown GaN layers is reduced by the lattice mismatch between the substrate and the layer of the nitride.[9]

Additionally, depending on the substrate used in epitaxial growth of GaN (and resulting differences in thermal-expansion coefficients between the substrate and layer), one can expect a different temperature dependence of the energy gap in various types of samples. Employing bulk single crystals of GaN may help to determine the role of a sample quality.

The purpose of this work was to examine critically the above listed contributions to the behavior of $E_g$ in gallium nitride.

## II. SAMPLES

We have studied two types of GaN samples. Besides using an epitaxial layer, we employed also bulk, single crystals of GaN. These crystals were grown by means of a high-pressure high-temperature method.[10,11] They represent high quality material characterized by a rocking curve halfwidth of a few arcseconds.[12] They have the shape of hexagonal plates of the thickness of about 10 $\mu$m and dimensions approximately $200\times200$ $\mu m^2$. These crystals are slightly yellowish. The free-electron concentration $n$, determined with the use of the Hall effect, for the high-pressure grown crystals is typically from $5\times10^{19}$ up to $1\times10^{20}$ $cm^{-3}$. These values were, however, obtained during the experiments performed on larger samples (typically of a 1–2 mm dimension. We will estimate the free-electron concentration of our samples in Sec. V. The second type of the sample was a 2-$\mu$m-thick epitaxial layer of GaN grown by the molecular-beam epitaxy method on a (0001) sapphire substrate with a free-electron concentration of $6\times10^{17}$ $cm^{-3}$.[13]

## III. EXPERIMENT

We used a 150-W tungsten halogen lamp as the light source. The signal was dispersed by a single grating Spex 500 M spectrometer and detected by a cooled GaAs photomultiplier equipped with a photon counting system. The sample was placed inside an Oxford Instruments continuous flow cryostat. After removing the sample, the lamp spectrum was measured. This spectrum was subsequently used to nor-

 0021-8979/94/76(4)/2429/6/$6.00  

malize obtained absorption spectra. The absorption spectra were not corrected for reflection and were calculated following the expression $\alpha=(1/d)\log[\tau(\lambda)/\tau_0(\lambda)]^{-1}$. Here $\tau$ and $\tau_0$ stand for the transmission of the optical system with and without the sample, respectively, and $d$ is the sample thickness. For high-temperature experiments the samples were placed on top of a copper finger of an electrical heater, which enabled us to stabilize the sample temperature with an accuracy $\pm 1$ K.

## IV. ANALYSIS OF ABSORPTION SPECTRA OF GaN

There is no unique procedure which allows the determination of an energy gap from the measured absorption spectrum. Generally two methods are employed. In the first one the value of the energy gap is determined by the wavelength of the light for which the absorption reaches some arbitrarily chosen level usually related to the experimental limit of the optical system. In the case when there is no visible change of the shape of the absorption edge with temperature, it can be used to determine the temperature shift of the gap. To obtain the absolute value of the energy gap we apply a second method. This consists in using a physical model of the energy gap $E_g$, which represents one of the parameters describing the behavior of the absorption coefficient $\alpha$. A comparison of the calculated and measured variation of $\alpha$ with energy makes it possible to extract the correct value of $E_g$.

In the interpretation of the results we have found it necessary to take into account the fact that optical transitions observed in the experiments are from the top of the valence band to the first unoccupied state in the conduction band, i.e., to a state located around the Fermi level $E_f$. The higher the concentration of carriers, the larger the increase in energy of the optical transitions. Though the displacement of the absorption edge with an increasing carrier concentration (Burstein shift, Burstein–Moss effect) has been observed for many semiconductors,[14,15] it has not been considered in case of GaN. This effect can play a significant role in this semiconductor, where the free-electron concentration is usually high. It is most probably due to the presence of a large number of nitrogen vacancies.[1,2,16] One should also remember that a high electron concentration changes the shape of the absorption edge.

In order to define our model, we assume that the absorption coefficient $\alpha$ is proportional to the square root of energy (parabolic conduction-band approximation)

$$\alpha=\alpha_0\sqrt{(E-E_g)}, \tag{1}$$

where $E$ is the photon energy and $\alpha_0$ is an energy independent parameter.[17]

## V. RESULTS

Figure 1 shows experimentally obtained absorption spectra of the epitaxial layer and the bulk single crystal of GaN. The presented spectra exhibit a sample dependent position of the absorption edge. The first hypothesis of a possible explanation of the above finding consists of an assumption that in

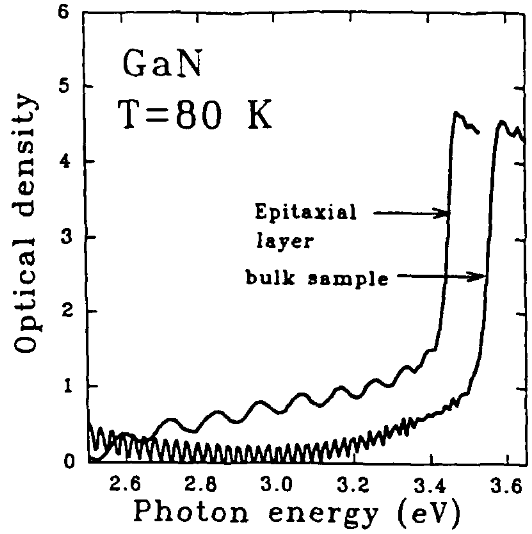


FIG. 1. Absorption spectrum of GaN samples: bulk and epitaxial layer at low temperature. The shift of the absorption edge is due to the Burstein–Moss effect.

the epitaxial layer, the strain induced changes of lattice constants (due to mismatch between the layer and the substrate) determine the observed shift of the absorption edge. To verify this suggestion, we have performed precise measurements of lattice constants of both the used samples. The test gives a negative answer. The samples have practically the same lattice parameters.[18]

The next step in our analysis was to associate the origin of such a large shift of the absorption edge with the Burstein–Moss effect,[14] which is related to different positions of the Fermi level. $E_f$ depends on the free-electron concentration of the sample under consideration. We know that the free-electron concentration in the epitaxially grown GaN is $6\times10^{17}$ cm$^{-3}$, which causes a negligible Burstein–Moss effect. The blue shift of the absorption edge for the bulk sample suggests that this crystal is characterized by higher $n$ with respect to the epitaxial layer. Below we estimate the contribution to the shift of the absorption edge related to the Burstein–Moss effect. Figure 2 illustrates the calculated Fermi energy dependence on the electron concentration for GaN samples. The parabolic band approximation with the electron effective mass $m_{eff}=0.15m_e$ (Ref.19) was used here. We used the following equations to calculate the Fermi energy:

$$n=N\frac{2}{\sqrt{\pi}}\int_0^\infty \frac{\sqrt{y}\,dy}{e^{(y-\eta)+1}}, \tag{2}$$

where $\eta$ is the reduced Fermi energy $E_f/kT$ and $y$ is equal to $E/kT$. $E$ is the electron energy above the conduction-band minimum, and $N$ is given by

$$N=2\left(\frac{m^*kT}{2\pi\hbar^2}\right)^{3/2}. \tag{3}$$

From Eqs. (2) and (3) we obtained the electron concentration as a function of the Fermi energy, which gave us $E_f(n)$.

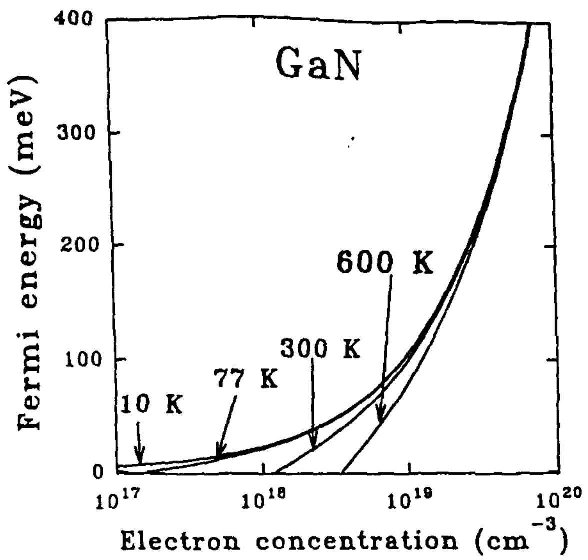


FIG. 2. Fermi energy in the function of electron concentration calculated in parabolic band approximation with $m^* = 0.15 m_e$.

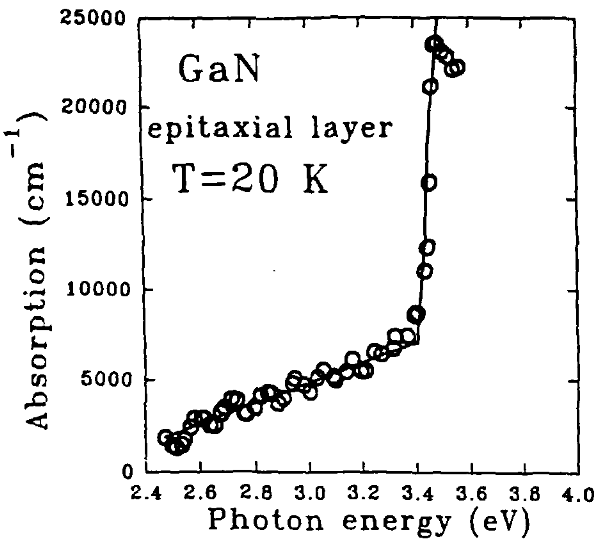


FIG. 3. Absorption edge of epitaxial layer of GaN at 20 K. Solid line represents a square-root-like theoretical shape of the absorption edge with the background line.

The parabolic conduction-band approximation should be adequate in the wide band-gap semiconductor like GaN. One can notice that for $n$ higher than about $5\times10^{18}$ $cm^{-3}$, the $E_f$ value increases considerably. In addition, for small $n$ a variation of $E_f$ is strongly temperature dependent. We apply the relation shown in Fig. 2 to evaluate $n$ for the GaN bulk sample. The shift of the absorption edge (Burstein shift) of the bulk sample related to the epitaxial layer ($E_f \cong 0$) is about 90 meV, from which we obtained $n = 8\times10^{18}$ $cm^{-3}$. The lower value of $n$, compared to the results obtained by means of the Hall effect on larger samples (between about $5\times10^{19}$ to $1\times10^{20}$ $cm^{-3}$), is probably related to the different electrical properties of the small and large samples. Absorption edge values determined for the other three single crystals of GaN are given by energies which differ from this deduced for the bulk sample illustrated in Fig. 1 (not more than $\pm15$ meV). Thus, an estimation of the electron concentration for the other bulk samples leads to values of $n$ between about $7\times10^{18}$ to $1.5\times10^{19}$ $cm^{-3}$.

In Fig. 3 we show the absorption edge of the epitaxial layer. As for this sample, the Burstein–Moss effect is not present; we could perform here the best fit to the model of the square-root dependence of the absorption edge [Eq. (1)]. In this model background absorption was also included as a straight line. We can see that actual absorption is very well reproduced by the theoretical model (solid line). Finally, we obtained $E_g = 3.427$ eV at 20 K.

In Fig. 4(a) we show the absorption spectra of GaN for various temperatures. We can observe the blue shift of the absorption edge with decreasing temperature. A very small change of the slope of the absorption edge can be observed for the bulk crystal [Fig. 4(a)] but there is no such effect in the case of the epitaxial layer [Fig. 4(b)]. The temperature dependence of the absorption edge for two different samples is represented in Fig. 5. This dependence is strongly nonlinear and slightly steeper for the bulk sample. We have also measured the temperature variation of the absorption spectra for the other three bulk samples of GaN between 10 and 300 K. In the considered temperature range they exhibit behavior identical with the single-crystal sample illustrated in Fig. 4(a).

## VI. DISCUSSION

The energy-gap temperature dependence is usually described by the equation

$$E_g = E_g(0) - \frac{\gamma T^2}{T+\beta}, \quad (4)$$

where $E_g(0)$ is the energy gap at 0 K; $\beta$ is sometimes associated with the Debye temperature; and $\gamma$ is an empirical constant. This form of the temperature dependence of the energy gap was proposed by Varshni[20] and this expression has been later successfully applied to describe $E_g(T)$ in many semiconductors. For example, in GaAs the experimental value of $\beta$ is 300 °K, which is very close to 344 °K which is the Debye temperature calculated from elastic constants.[21]

For GaN there were few measurements of the temperature dependence of the energy gap. We summarize them in Table I. Linear coefficients of $E_g(T)$ obtained by various authors differ considerably. Even more scattered are nonlinear parameters of the Varshni equation. For example, Monemar[4] obtained a negative value for $\beta$ in Eq. (4). In our experiment we obtain $\beta=745$ for bulk crystals and $\beta=772$ for the layer. Both these values are very close to 600 K, which is the estimated Debye temperature for GaN.[22]

In our experiment we observe a larger negative temperature coefficient for the bulk crystal than for the epitaxial layer. We believe that the main difference between these two samples lies in different free-electron concentrations. If for the bulk crystal we compare, using Fig. 6, temperature variations of the Burstein shift of the absorption edge and the Fermi energy, we see that hey behave qualitatively in the same way. Moreover, one should remember that at higher

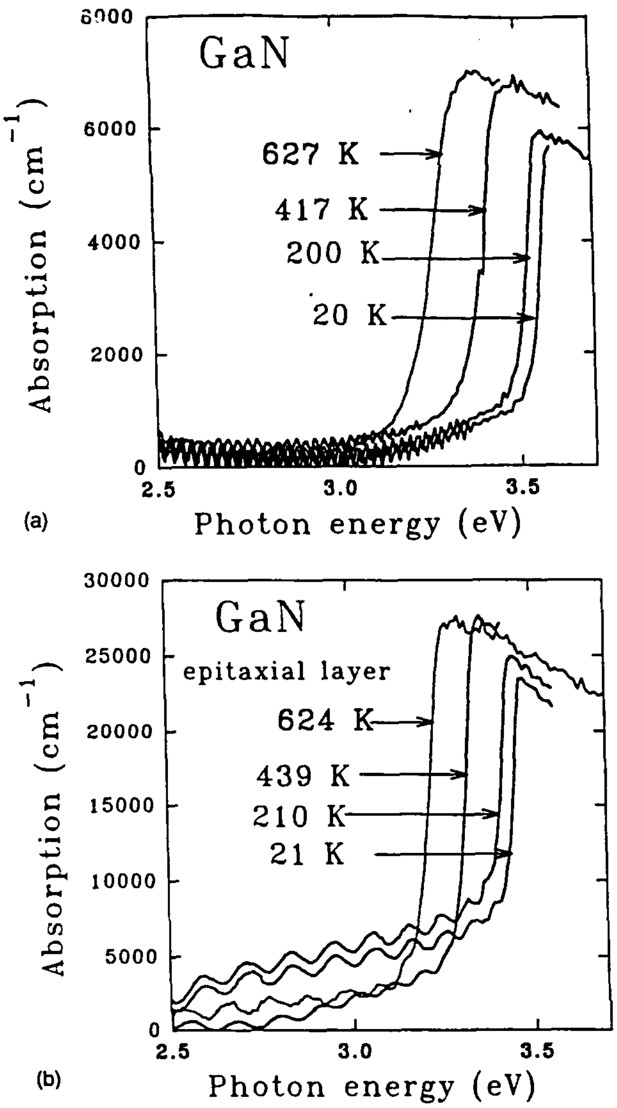


FIG. 4. (a) Absorption spectra of GaN bulk single crystal for various temperatures. Visible oscillations are due to the interference of light in the sample. (b) Absorption spectra of GaN (epitaxial layer) for various temperatures. Visible oscillations are due to the interference of light in the sample.

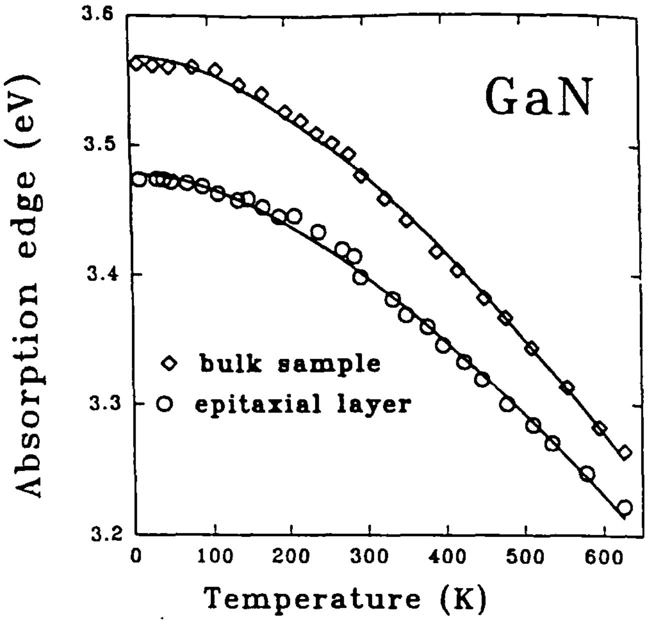


FIG. 5. Shift of energy gap as a function of temperature for two samples of GaN. Solid line represents the best fit to the model $E_g=\gamma T^2/(T+b)$.

temperatures there are more empty states available below the Fermi level. Thus, in the bulk GaN sample, rising temperature results in the additional red shift of the absorption edge. Since the latter effect was not taken into account in the calculations of $E_g$ versus temperature, it may explain discrepancies seen in Fig. 6. We should stress here that for the bulk samples which have a high free-electron concentration ($1\times10^{19}$ $cm^{-3}$), the Burstein shift is also observed at low temperature (4 K). (This fact is additionally confirmed by our electron-transport experiments.) This indicates that the sample is above the Mott transition.

There is a substantial disagreement between the data on $dE_g/dT$ given by several authors. It seems that one reason for this can be the different electron concentrations in studied samples and consequently, the influence of the Burstein shift on the interpretation of the experimental results. Determination of the nonlinear term in Eq. (4) requires measurements in a wide temperature range. Otherwise, a precision of its determination is rather poor. There is also another problem which should be mentioned here, namely, a difference between thermal-expansion coefficients of the GaN layer on a sapphire substrate with respect to the bulk crystal. There are no experimental data which would make it possible to accept or eliminate this possibility. The assumption that the layer experiences the same thermal expansion as a sapphire substrate (which is about 10% larger than that measured for GaN[22]) gives for the epitaxial layer a stronger variation of $E_g$ with temperature than that obtained for the bulk crystals. The experimentally observed effect is opposite. Moreover, one should remember that all studied layer of GaN have thicknesses larger then the critical one and thus they are relaxed by dislocations. Therefore, the change of the lattice constant of the substrate does not have to change the lattice constant of the layer in an identical manner.

Finally we would like to discuss the problem of the contribution of different mechanisms to the temperature dependence of the energy gap. One of them is a simple change of lattice parameters which also occurs when pressure is applied to the sample. The second mechanism is related to the phonon-electron interaction. Both these mechanisms should lead to a linear dependence of the energy gap with temperature for sufficiently high temperatures, i.e., above the Debye temperature.[23] This relation can be expressed as follows:

$$\Delta E = a\alpha_T T - \beta_T \cdot T. \tag{5}$$

Here $a$ is the deformation potential of the gap, $\alpha_T$ the volume expansion coefficient, and $\beta_T$ the thermal coefficient resulting from the electron-phonon interaction.

At high temperatures, Eq. (5) is equal to $\gamma T$ as defined in Eq. (4). Thus, applying values of $a=-11.51$ eV[24] determined for the bulk GaN and $\alpha_T=11.5\times10^{-6}$ $K^{-1}$ (Ref. 22) measured by the x-ray powder diffraction method, we obtain $\beta_T=8.07\times10^{-4}$ eV $K^{-1}$. We can see that the thermal expansion is responsible for only about 14% of the observed effect.

TABLE I. Energy gap of GaN and its temperature dependence.

| Sample type | Exp. method | Linear temperature coefficient $\frac{dE_g}{dT}$ ($T$ = 300 K) ($10^{-4}$ eV/K) | Nonlinear temperature coefficients of Eq. (2) $\gamma$ ($10^{-4}$ eV/K) | $\beta$ (K) | Reference |
|---|---|---|---|---|---|
| epitaxial on sapphire | luminescence | −5.32 | +5.08 | −996 | Monemar[a] |
| epitaxial on sapphire | absorption | −4.8 | not determined | not determined | Pankove[b] |
| epitaxial on sapphire | absorption | −6.7 | not determined | not determined | Camphausen[c] |
| epitaxial on sapphire | luminescence | −4.0 | −7.2 | +600[e] | Ilegems[d] |
| epitaxial on sapphire | absorption | −4.5 | −9.39 | +772 | present work |
| bulk samples | absorption | −5.3 | −10.8 | +745 | present work |

[a]Reference 4.
[b]Reference 5.
[c]Reference 3.
[d]Reference 6.
[e]Fitted with Eq. (4) with the $\beta$ parameter fixed at 600 K.

## VII. SUMMARY

The performed measurements of the optical absorption in different samples of GaN have enabled us to point out the importance of the free-carrier contribution to the observed positions of the absorption edges. This represents the Burstein–Moss effect, which is well known from studies of other semiconductors. This effect gives the main contribution to the scatter of values of $E_g$ estimated by different authors. We have also determined the temperature dependence of the absorption edge of GaN in a wide temperature range (10–600 K). This dependence is sample dependent and a decrease of $E_g$ with temperature is stronger for the sample with a higher electron concentration. The latter behavior can be qualitatively explained by the temperature dependence of the Burstein–Moss effect. For the sample with a negligible contribution due to free electrons, the linear temperature coefficient of the gap is $-4.5\times10^{-4}$ eV/K at 300 K.

In addition, we observed a strongly nonlinear change of $dE_g$ with temperature even at relatively high temperatures. This occurs in the range where, for example, the GaAs crystal shows a practically constant $dE_g/dT$. The observed effect can be correlated with the high Debye temperature of GaN (about 600 K, in comparison with 300 K for GaAs).

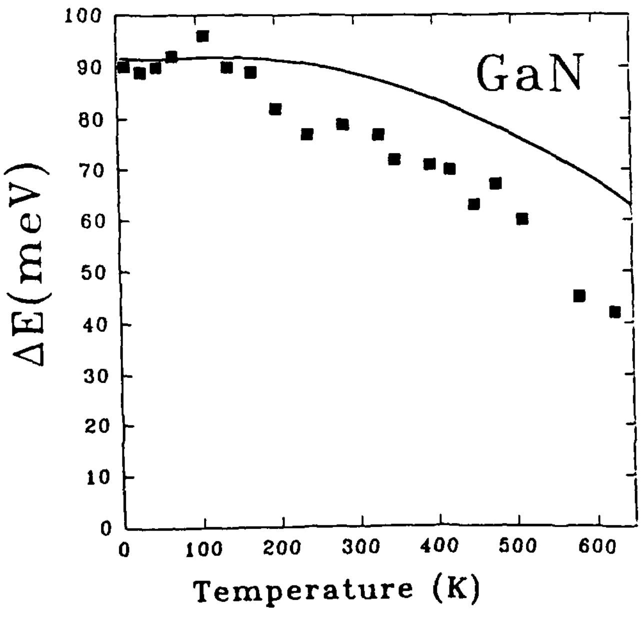


FIG. 6. Calculated temperature dependence of the Fermi energy in the bulk crystal of GaN (solid line) in comparison with the experimentally determined shift of the absorption edge (filled squares).

## ACKNOWLEDGMENTS

The authors (H.T., P.P., T.S., I.G.) would like to acknowledge financial support from the Polish Committee of Scientific Research (Grant No. 30068 91 01 and Grant No. 066949305). Work at Boston University was supported by the Office of Naval Research (Grant No. N00014-92-J-1436).

[1] R. F. Davis, Proc. IEEE 79, 702 (1991).
[2] J. H. Edgar, J. Mater. Res. 7, 235 (1992).
[3] D. L. Camphausen and G. A. N. Connell, J. Appl. Phys. 42, 4438 (1971).
[4] B. Monemar, Phys. Rev. B 10, 676 (1974).
[5] J. I. Pankove, J. Lumin. 7, 114 (1973).
[6] M. Illegems, R. Dingle, and R. A. Cogan, J. Appl. Phys. 43, 3797 (1972).
[7] M. Illegems and R. Dingle, J. Appl. Phys. 44, 4234 (1973).
[8] O. Lagerstedt and B. Monemar, J. Appl. Phys. 45, 2266 (1973).
[9] K. Itoh, T. Kawamoto, H. Amano, K. Hiramatsu, and I. Akasaki, Jpn. J. Appl. Phys. 30, 1924 (1991).
[10] S. Porowski, I. Grzegory, and J. Jun, in *High Pressure Chemical Synthesis*, edited by J. Jurczak and B. Baranowski (Elsevier, Amsterdam, 1989), p. 21.
[11] I. Grzegory, J. Jun, St. Krukowski, M. Bockowski, and S. Porowski, Physica B 185, 99 (1993).

[12] M. Leszczynski, I. Grzegory, and M. Bockowski, J. Cryst. Growth **126**, 601 (1993).
[13] T. Moustakas, T. Lei, and R. J. Molnar, Physica B **185**, 36 (1993).
[14] E. Burstein, Phys. Rev. **93**, 632 (1954).
[15] M. Bugajski and W. Lewandowski, J. Appl. Phys. **57**, 521 (1985).
[16] D. W. Jenkins, J. D. Dow, and M.-H. Tsai, J. Appl. Phys. **72**, 4130 (1992).
[17] J. I. Pankove, in *Optical processes in semiconductors* (Prentice-Hall, Englewood Cliffs, NJ, 1971).
[18] From our measurements we obtained $a=3.18942\pm0.00010$ and $c=5.18564\pm0.00008$ for the bulk crystal and for the epitaxial layer we obtained $a=3.18709\pm0.00026$ and $c=5.18574\pm0.00013$ ($T=300$ K).
[19] M. Fanciulli, T. Lei, and T. D. Moustakas, Phys. Rev. B **48**, 15144 (1993).
[20] Y. P. Varshni, Physica **34**, 149 (1967).
[21] *Numerical Data and Functional Relationship in Science and Technology*, edited by O. Madelung, M. Schulz, and H. Weiss, Landolt-Börnstein, New Series, Vol. 17 (Springer, Berlin, 1982).
[22] M. Leszczynski, T. Suski, H. Teisseyre, P. Perlin, I. Grzegory, J. Jun, S. Porowski, and T. D. Moustakas (unpublished).
[23] A. Haug, in *Theoretical Solid State Physics* (Pergamon, New York, 1972), p. 52.
[24] P. Perlin, I. Gorczyca, N. E. Christensen, I. Grzegory, H. Teisseyre, and T. Suski, Phys. Rev. B **45**, 13307 (1992).